THE BEHAVIOUR OF A BED OF PARTICLES UNDER THE INFLUENCE OF SHEAR STRESS

by

A.C. TODD

Submitted for the Degree

of

Doctor of Philosophy

of

Loughborough University of Technology

Supervisor:

B. Scarlett

Director of Research:

Professor D.C. Freshwater

Department of Chemical Engineering

September 1969

CONTENTS

(A detailed contents list is given at the beginning of each chapter).

SUMMARY

The four characterisation groups of microscopic, state, macroscopic and behavioural properties are discussed for a packed system of particles, with particular reference to the shear strength and flow behaviour of particulate material. The relationships between the behavioural and macroscopic and between the behavioural and microscopic properties have been shown to be deficient in describing what actually happens with a material under shear stress.

It is postulated that a clearer understanding of the flow behaviour of particulate material will be obtained when the relationships have been obtained between the microscopic, state and macroscopic properties. The present links between these groups are reviewed and discussed.

The difficulties of defining the size and shape of a particle are discussed, and the more fundamental units of laminae and filaments of a particle system are proposed. The use of the science of the study of sections, Stereology, to predict three dimensional microscopic properties is reviewed, and the definition of Stereology extended to predict three dimensional behaviour.

A statistical model is proposed using the filament size distribution of a bed of random isotropic particles. The model predicts the separation of two layers of sectioned filaments during flow at the steady state condition; and so determines the critical porosity of the packed particle system as a function of a microscopic property. Further applications to the strength behaviour of particulate materials are discussed.

A Split Ring Annular Shear Cell is designed to overcome the basic limitations of a conventional annular shear cell, namely wall friction and large changes in shear strain with radius. The cell is used for measurements at different normal stresses and shear rates on a dry free-flowing sand, at the steady state flowing condition. The porosity of the particulate bed in the cell is determined using a gamma ray attenuation technique. An examination is also made of the shear behaviour in a direct shear cell for different initial porosities.

The chord size distribution, which is equivalent to the filament size distribution, is determined by an automatic system which scans photographs of particle sections.

The theoretical values of the critical porosity, determined from the measured chord size distributions, are compared with the measured values from the shear cell experiments. It is shown that the theoretical and measured values compare well.

Finally, suggestions for further work are given.

"I lift up my eyes to the hills,
From whence does my help come?
My help comes from the Lord,
Who made heaven and earth".

Psalm 121:1,2.

ACKNOWLEDGEMENTS

I would like to express my gratitude to my supervisor, Mr. B. Scarlett, for his persistant encouragement and guidance; to Professor D.C. Freshwater for providing the research facilities; and to the Science Research Council for the award of a research scholarship, under which the work was carried out. Also, I would like to express my thanks to the following groups and individuals:-

The academic staff of the Department of Chemical Engineering, in particular Mr. P.J. Lloyd, Dr. P. Allen and Dr. R.J. Akers for valuable discussion.

Mr. G. Oldham and Mr. E. Miller for advice given in using the gamma attenuation equipment.

Mr. L. Aldred of I.C.I. Dyestuffs Division for co-operation in comparing the "Portishead" and Split Ring Annular Shear Cells.

Dr. A.J. Evans and the Library staff for co-operative service.

Mr. D. Hogg and his staff for the use of the University's computing services.

Messrs. K. Betts and L. Moore in the construction of the Split Ring Annular Shear Cell and other experimental equipment.

Mrs. M. Warren and Miss C. Bostock for laboratory services.

Mr. G. Bordon for photographic services.

Mr. B.F.W. Powell, my father-in-law, for reading the manuscript.

My wife, Valerie, for her continued support, help and encouragement, and for typing the manuscript.

ERRATA

p iii line 2 for "persistant" read "persistent".

p 18 line 11 add "if the behaviour is plastic".

p 41 line 13 add "and" thus:- "to a fixed direction and which".

p 83 line 25 for "principle" read "principal".

p 119 figure 4.14 reverse captions.

p 137 line 25 for "scafold" read "scaffold".

p 160 second equation should read:- $\rho_i = \frac{m_i}{2\, l_{i,i}}$

p 189 line 5 delete "not".

p 201 line 6 for "effected" read "affected".

p 204 line 13 for "applied" read "applies".

p 217 line 2 for"siutable" read "suitable".

p 220 line 4 delete "the" thus:- "to overcome this, new . . ".

p 221 line 8 for "existance" read "existence".

CHAPTER 1

GENERAL INTRODUCTION

CHAPTER 1:- GENERAL INTRODUCTION

1.1. The Characterisation of Particulate Systems

Particle systems can be characterised by the consideration of the four concepts; microscopic, state, macroscopic and behavioural properties. In table 1.1. below, under these four headings, are some of the important properties relating to packed systems of particles.

Table 1.1.

Characterisation of Packed Particle Systems

Microscopic Property	State Property	Macroscopic Property	Behavioural Property
Particle Size Distribution	Homogeneity	Conductivity	Conduction
Surface Properties	Porosity	Permeability	Flow of Fluid
Properties of Solid & Interstitial Fluid	Moisture Content	Shear Strength	Flow of Powder

A full understanding of the flow characteristics of particulate material will only be obtained when the relationships between all these four divisions have been evolved.

The specific interest in this thesis centres around the flow of powders and its relation to shear strength and particle size. It is disconcerting to find that a modern factory, equipped with all the latest automatic controls, must depend, in varying degrees, upon manual poke holes or rapping devices to assist the flow of such materials as ores, grain and bulk chemicals. The extrapolation of inadequate empirical data in this field cannot assure safe limits in the design of storage bunkers and other systems where particulate material is in

flow; nor can precautions in design, with all its additional capital investment of uncertain need, be considered an acceptable substitute for sound engineering procedure. Such sound procedure can only be founded on a clear understanding of the bulk behaviour of materials during storage and flow. In the 1930's safety factors were cut down, resulting in many structural failures, some classic examples of which have been given recently by Theimer.[173]*

Considering figure 1.1., the previous work can best be understood in the links between the characterisation groups. Before considering in detail the relationships between the macroscopic, state and primary properties, the macroscopic and behaviour link and the behaviour and primary link will be briefly discussed in turn.

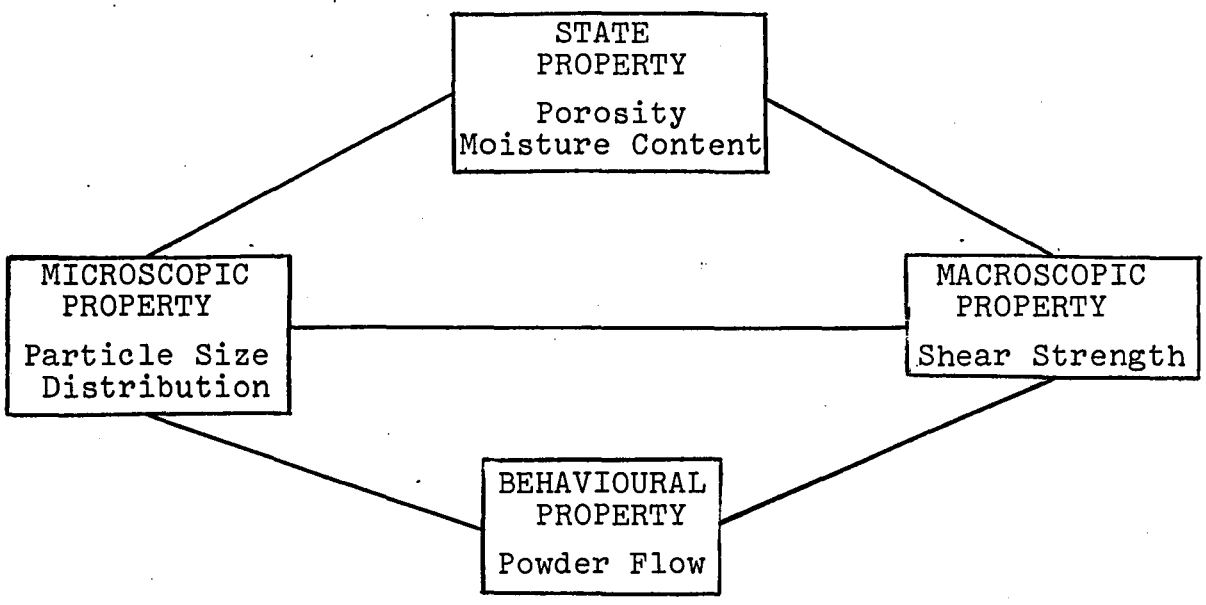

Figure 1.1. Block diagram of representation of the links between the characterisation groups for packed particle systems with reference to powder flow.

1.2. The Behavioural and Macroscopic Property Relationship

Stimulated by the lack of reliable design techniques for the design of storage bunkers to handle particulate material,

*Numbers designate references in the Bibliography, pp. 263-275

Jenike[87–92] has studied the flow behaviour of such material from the concept of characterising the material by its strength. His experience of handling material in bulk made him aware of the following irritating problems:-

i. cessation of flow due to the formation of "arches" or "pipes" within the material in a hopper.

ii. erratic flow due to the temporary formation of "arches" and "pipes" which then collapse.

iii. ineffective design capacity due to substantial quantities of the stored material remaining static and hence becoming degraded.

iv. segregation of the material into its fractions which flow out from the hopper at different times.

v. inaccuracy of measurement of quantity in a hopper (other than by weighing) due to the effect on level control of material flow into the centre and the formation of "pipes".

Jenike simultaneously worked from both the behaviour standpoint in examining the pressures exerted in a storage hopper and the frictional characteristics of hopper materials and stored material; and from the macroscopic viewpoint by analysing the shear strength of particulate material at different consolidating pressures. He has defined the strength of a bulk solid by a term called "the flow-function".

At a free surface (figure 1.2.) of a mass of solid, the minor pressure normal to the surface is equal to zero, and the largest pressure which the solid can support in the tangential direction to the surface is the major pressure, f_c, which is referred to as the unconfined yield pressure. This is a function of the major consolidation pressure, $\bar{\sigma}_1$, and this function:

$$f_c = f(\bar{\sigma}_1)$$

expresses the flow property of a bulk solid and this is what Jenike terms the "flow-function" (Figure 1.3.).

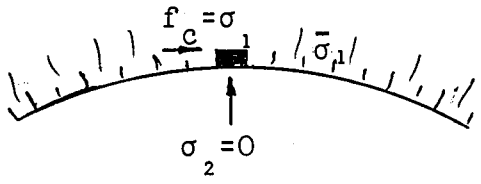

Figure 1.2. Pressures at a free surface

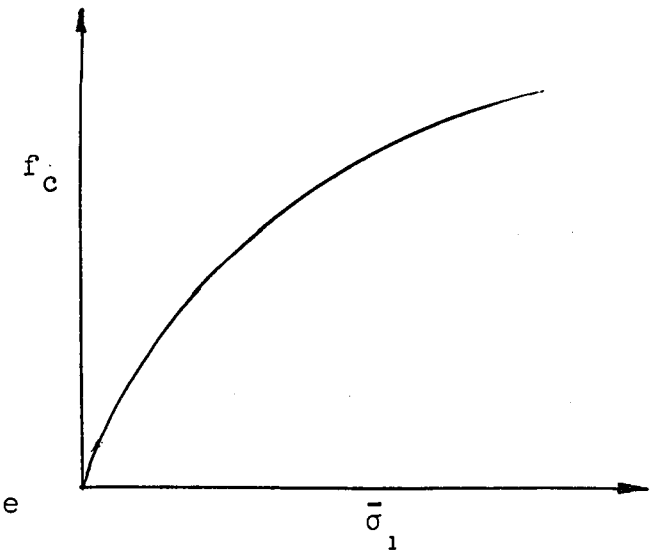

Figure 1.3. Flow-Function

f_c = unconfined yield pressure

σ_1 = major pressure

σ_2 = minor pressure

$\bar{\sigma}_1$ = major consolidation pressure

Considering now a material of a particular strength. Depending on the hopper geometry and material of construction, a bulk material of a particular strength will set up a pressure at an arch (assuming one has formed) according to the depth of the arch and hence to the consolidation pressure. This function is termed the hopper/material flow-factor.

Jenike has computed these hopper/material flow-factors from an assumed radial stress field existing in a hopper. By comparing the material's flow-function with the hopper/material flow-factor a position can be obtained where the material strength is equivalent to the force acting at an arch. Jenike has termed this the "flow-no-flow" criterion.

The flow-factor and flow-function are plotted together, using the same co-ordinates, and the situation with regard to

one another is noted. If the flow-factor lies above the flow-function, then the pressure exerted at an arch is always greater than the unconfined yield strength of the material; and the material is unable to support an arch. If the flow-factor lies below the flow-function then the material will always arch in that particular hopper. If an intersection is obtained, then the flow-no-flow situation has been determined.

The flow-no-flow criterion as postulated by Jenike is as follows: "gravity flow of a solid in a channel will prevail provided the yield strength which the solid develops as a result of the consolidating pressures is everywhere within the channel insufficient to support an obstruction to flow".

From these considerations Jenike has proposed a design procedure for storage bunkers to ensure the elimination of arching and piping.

The stability of a cohesive arch in a hopper has also been considered by Walker[108], Richmond and Gardner[133], Gardner[54], and Richmond[113]. The basic assumption, as for Jenike's work, is the approximation of the material to the Coulomb solid, which is discussed further in chapter 2. A table of the solutions for the minimum linear dimensions of a stable arch has been given in a review on the literature pertaining to the storage and handling of solids, edited by Richards[131].

Previous to the work of Jenike, the strength characteristics were largely based on the angular characteristics of the material, that is the various angles formed by the material in particular situations. These angular measurements have then been used to predict material behaviour in hoppers.

The angle of repose is the most commonly observed and measured property of granular solids. It is often regarded as

providing a measure of the internal friction of the material and hence as an important influence on the flow behaviour of materials. Brown[19] has given a number of definitions for the angle and Train[179] has compared the angles of repose obtained from four different techniques. The observations of Train indicate the dependence of the value of the angle of repose on the packing of the material, causing difficulty in comparing different techniques. His overall conclusion on the use of the angle of repose is that it is a useful measurement in providing data for comparisons between samples during quality control studies. He emphasises, however, the need to ensure reproducability by defining practical experimental conditions.

His observations also point to the greatest limitation of this approach which is due to the fact (which has largely been ignored) that the strength of a material is also dependent on its state and, in particular, on its packing.

Jenike[89] criticises the use of the angle of repose as a measurement of the flow properties of particulate materials, pointing out the different density regions which can occur in a pile of material; and suggests that its wide use as a means of characterisation stems from its ease of measurement rather than its practical significance.

Other angular properties measured have been the angle of rupture[202], angle of slide[50], and angle of internal friction. The angle of internal friction is probably the most relevant of the interparticulate angles as a fundamental property of the behaviour of a granular material. The simplest method of determining this angle is by measuring the angle, with the horizontal, taken up by the moving core of solids in a hopper section which is provided with a central opening in the bottom

through which the contents can flow in free fall. Again, however, as with all the angular measurements the value is dependent upon the state of the material.

Although these angular measurements may be of interest and use for specific situations, they do not reveal (apart from the angle of internal friction) what is happening within the material. It is evident from the literature that, although an angular characterisation gives some indication of flowability and of the stress within a powder bed, it is difficult to use and interpret the results in terms of flow behaviour.

The pressures exerted by granular material have attracted much attention but it is only recently that improved pressure measuring devices have made possible a clearer understanding of the pressures existing in storage bunkers during filling and emptying.

Jenike and Johanson[92], in a study of the behaviour of bulk solids in storage and their pressure effects, have given an excellent review on the work in connection with pressures in bunkers.

The bunker pressure studies, however, have been limited, in general, to a broad continuum approach rather than from a particulate approach. When descriptions are available on how individual particles transmit stress, and on how this is affected by particle size and state of the material, a clearer understanding of the pressure distribution in bunkers will be obtained. It may then be possible to predict the pressure distribution by a measurement of the microscopic properties of the material.

1.3. The Behavioural and Microscopic Relationship

The study of the rate of flow of granular materials through orifices has attracted much attention and many correlations have been given to show the effect of the various system variables on the flow rate. Ketchum[96], an early investigator, published a simple basis for the rate of flow as the cube of the orifice diameter. This is, indeed, an over simplification.

There have been three types of approach to this study; and the equations developed can be divided into those which have been derived from dimensional analysis, those of an empirical nature and those which have been proposed from considerations of the energy of a moving column of powder. These equations cover a wide range of materials of various sizes, size distributions, shapes and surface roughness.

The general form of most of the empirical correlations, as Shinohara et al[156] found is:-

$$\frac{F_0}{\rho_p \sqrt{g} d_p^{2.5}} = i\left(\frac{D_0}{d_p}\right)^j$$

F_0 = flow rate of particles

ρ_p = particle density

g = acceleration due to gravity

d_p = particle size

D_0 = diameter of outlet

i,j = coefficients

The particle diameters used have been almost as numerous as the investigators. A more thorough discussion of these diameters is given in chapter 2.

White et al[192], on examination of the literature pertaining

to flow through orifices noticed that many workers had found that the flow rate was directly proportional to the orifice diameter to the power of approximately 2.6. Again, many workers have found that the mass flow rate is directly proportional to the bulk density, again showing the relationship between the "state" of the material and the other characterisation groups. However, controversy has arisen as to whether bulk density or particle density should be used in such correlations.

Shinohara et al[156] have pointed out what they feel to be the inadequacy of flow rate equations based on dimensional analysis and experimental results. They indicate that the flow rate equations should be derived in connection with the basic mechanism of gravity flow of particles. They base their concept on the dynamic arch. Arching phenomena can be classified into either the so-called static arch, which completely stops the flow; or the dynamic arch which involves the continuous formation and collapse of a bridge without blocking the flow. From the analysis of the dynamic arch, and the theoretical location of it, they derive an equation for the flow rate which compares well with the equations derived from other approaches.

These correlations have been of little use except in particular situations where the size and type of material used in the practical applications have been very similar to those used in developing the particular correlations. The correlations also fail to describe what is actually happening within the material during flow.

1.4. Relationship between Microscopic, State and Macroscopic Properties

Sections 1.2 and 1.3 above indicate that the

relationships, so far developed, between the behavioural properties and the macroscopic and microscopic properties, respectively, are unsuitable to describe what really happens during the flow of particulate material.

This full description will only be possible when the relationships between the microscopic, state and macroscopic properties have been developed. One of the most useful applications of this development will be the prediction of a material's behavioural property from a knowledge of its particle size distribution. From a knowledge of the strength and behaviour relationships a particular material may be found unsuitable for storage with unassisted gravity flow. However, when the relationships between the strength and the particle size distribution have been derived, the comparatively inexpensive process of changing the material's particle size distribution, and hence its bulk strength could replace the present use of expensive capital equipment and of undesirable flow additives in dealing with "difficult" materials.

This thesis sets out in the following chapters, therefore, to show the existing links between the microscopic, state and macroscopic properties; to propose a statistical model to predict a macroscopic from a microscopic property; and to examine this model with experimentally determined values using a dry, non-cohesive sand.

CHAPTER 2

INTRODUCTORY LITERATURE

CHAPTER 2:- INTRODUCTORY LITERATURE

In chapter 1 the relationships have been described between the four characterisation groups of a particulate system. It is the purpose of this chapter to review the literature applying to the macroscopic, state and microscopic properties, for it is in the consideration of these three aspects that the fundamental characteristics pertaining to the flow behaviour of powders will be understood.

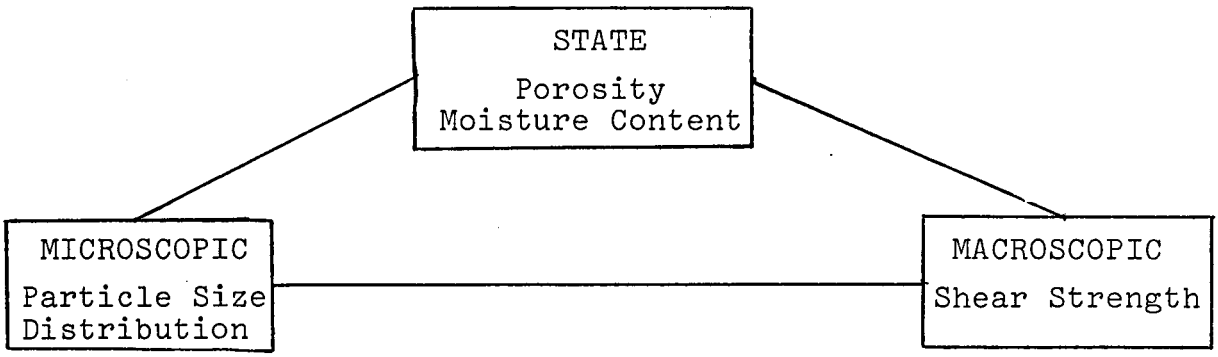

The four properties to be considered are the particle size, porosity and moisture content and the shear strength.

2.1. The Shear Strength of Granular Material

2.1.1. Particle and Surface Mechanics

Before considering what happens in the bulk behaviour of particulate materials consideration will first be given to the laws governing the friction between particle surfaces.

According to MacCurdy[111], Leonardo da Vinci, in the sixteenth century, was the first known commentator on the nature of the laws that govern the phenomenon of friction. He suggested that friction was directly proportional to the normal force between sliding surfaces and that it was independent of the area of contact between the surfaces.

In 1699 Amontons[3] formulated the laws relating frictional resistance and normal force acting on a body sliding on a surface. He stated that the shear force, S, is proportional to the normal load, N, that is:-

$$S = fN$$

where f is a constant of proportionality called the coefficient of friction. Amontons's laws gained little favour until Coulomb[35], in 1781, confirmed and again proposed them. He also distinguished between static and kinetic friction and he found that the coefficient of kinetic friction was independent of the velocity of sliding between the surfaces.

In the twentieth century the mechanism of friction between solids has been clarified. Terzaghi[171] proposed that the frictional force developed between two unlubricated surfaces was the result of molecular bonds developed at the real contact area. His assumptions were that the real contact area was directly proportional to the normal load; and that the shear strength at the contact was independent of the normal load, that is:-

$$S = A's'$$

$$f = s'/_p$$

where S = frictional resistance

A'= real area of contact

s'= shear strength per unit area of molecular bond

f = coefficient of friction

p = normal pressure per unit area of real contact

Working with metals, Bowden and Tabor[18] have clarified many of the laws of friction. They found that, under any level of applied normal load, plastic yielding takes place at the contact between asperities. Thus, the real contact area

becomes directly proportional to the applied load, confirming Terzaghi's assumption. The tangential force necessary to shear the junctions at the real contact is then proportional to the area of real contact. Thus:-

$$A' = \frac{N}{p}$$

$$S = A's'$$

$$S = \frac{N.s'}{p} = N.f$$

$$\therefore \quad f = \frac{s'}{p}$$

where p is the yield pressure at the real contact. Hence the coefficient of friction depends on the nature or composition of the sliding surfaces in contact.

Tabor[166] derived the term "junction growth" to explain another mechanism between solids. He showed that as the tangential force was gradually increased from zero, the area of real contact increased reaching a maximum when slip was imminent. The maximum area was several times the initial area with no change in normal force. The ratio of final to initial contact area was found, however, to be a constant, thus maintaining the proportionality between tangential and normal forces when slip occurred.

Eyring and Powell[45] also working with metals, have given the following mechanism of friction for unlubricated surfaces. For "smooth" metals, they found that, in addition to the irregular "hills and valleys" in these surfaces, there were other smaller irregularities due to the basic nature of the material. They suggest, therefore, that the force necessary to cause sliding has three components:- one component to supply the work to raise one surface over the gross irregularities; the second component to raise the surface over the "atom"

irregularities; and the third component to break the bonds produced by plastic deformation of the surface.

Yong and Warkentin[201] attribute sliding friction to the first two of the above components. This surface roughness they term "microscopic interlocking" and they note that there is no significant volume change associated with this action.

2.1.2. The Frictional Characteristics of Bulk Material

2.1.2.1. The Yield Locus

Coulomb's[34] Law, first put forward in 1773, has been used for many years in soil mechanics. It states that:-

$$\tau = \sigma \tan \phi + C$$

where C = cohesion

ϕ = angle of internal friction

σ = normal stress

τ = shear stress

To work out a solution for the continuous plastic flow of solids with an angle of friction greater than zero, Jenike and Shield[94] proposed a yield surface from which they were able to overcome the original difficulties arising from previous plastic flow solutions. These difficulties centred largely around the assumption of continuous dilation.

Jenike[91] has pointed out that bulk solids exhibit elastic, plastic and viscous properties, as well as time effect, similar to Bingham materials. However, he suggests that a simpler analysis can be based on the assumption that a bulk solid is sufficiently closely approximated by a modified rigid-plastic Coulomb solid. Jenike defines a Coulomb solid in the following way: "A rigid-plastic solid is one for which there exists a

limiting stress function such that stresses lower than those determined by the function cause no deformation, whereas stresses equal to the limiting stress cause either failure or plastic flow. Stress conditions exceeding the limiting stresses are not possible".

In σ,τ co-ordinates, where τ is the shear stress and σ is the normal stress, the limiting stress function is represented by a yield locus. For a Coulomb solid the yield locus is straight, inclined at an angle ϕ to the σ axis, and intersects the τ axis at a value of τ equal to C, which is called the cohesion of the solid. The Coulomb equation is represented in graphical form in figure 2.1.

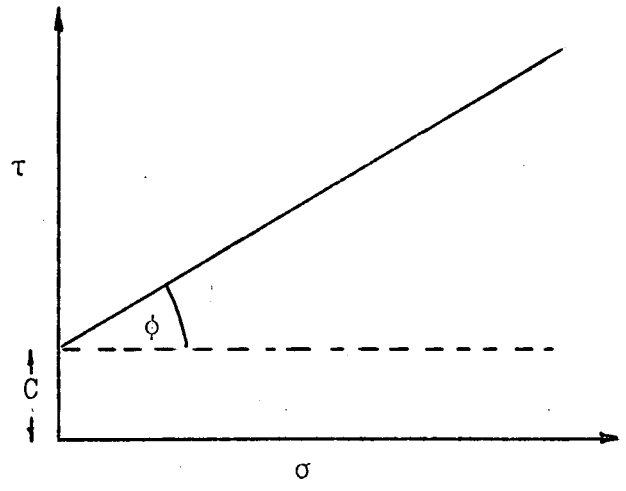

Figure 2.1. A Coulomb Solid

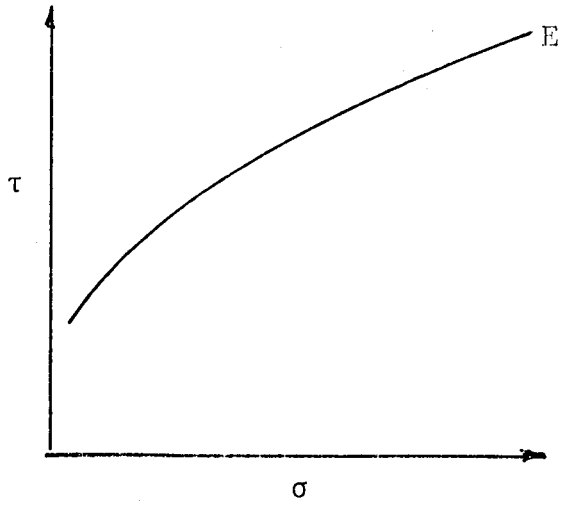

Figure 2.2. Yield locus for a Cohesive solid

According to Jenike, a bulk solid differs from a Coulomb solid in three ways. Firstly, for small values of normal pressure, the yield locus deviates significantly from a straight line. Its usual shape for a cohesive bulk solid is convex upward. (Figure 2.2.). Secondly, the yield locus does not extend indefinitely with increasing σ but terminates at a point E. Thirdly, the position of the yield locus is not constant but

is a function of the degree of consolidation of the solid. This indicates the effect of state, in the form of packing, on the yield locus. A series of consolidations gives, therefore, a family of yield loci. (Figure 2.3.).

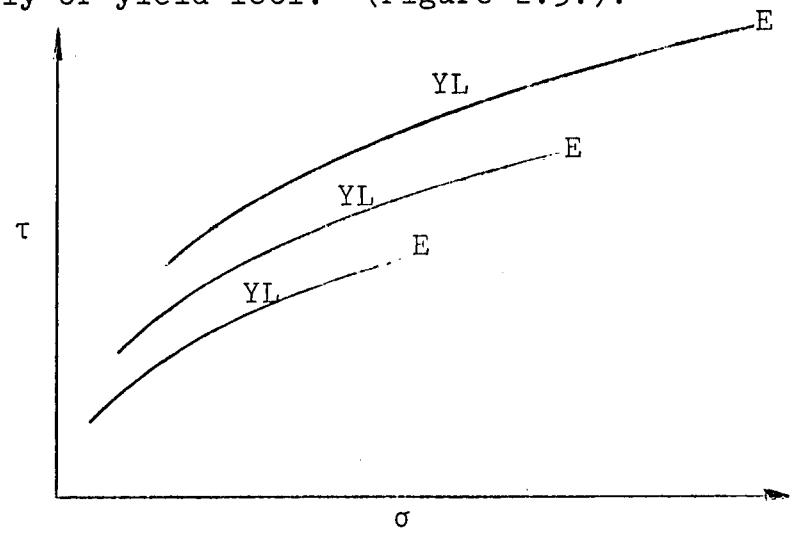

Figure 2.3 Family of yield loci for a cohesive solid

The yield locus determines not only the stress conditions for which flow occurs but also the direction of the strain rate vector $\bar{\varepsilon}$ during flow. Considering figure 2.4. for any limiting stress condition determined by a Mohr semicircle, A', the direction of the strain rate vector $\bar{\varepsilon}$ is normal to the yield locus at the point of tangency, if the behaviour is plastic. The direction of the vector $\bar{\varepsilon}$ is measured by the angle ϕ_v which the vector forms with the γ axis.

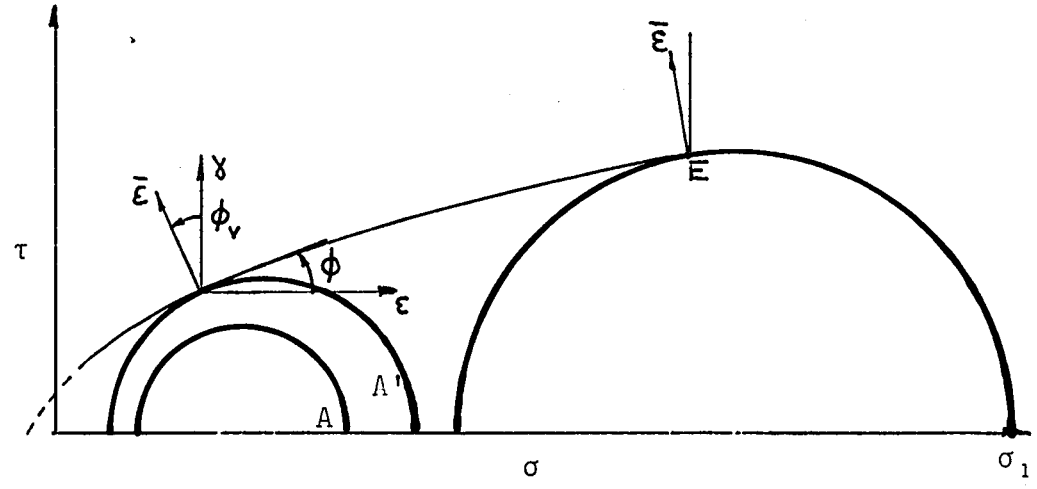

Figure 2.4.

For negative values of ϕ_v the strain rate vector has a positive compression strain rate component ε. This implies consolidation and an increase of yield strength signified by an expansion of the yield locus. Positive values of ϕ_v imply expansion of the solid, which is opposite to consolidation, and therefore a shrinking of the yield locus.

The yield locus is formed by consolidation, with shear, measured by the major pressure σ_1. The Mohr circle through σ_1 and tangential to the yield locus determines the terminus E of the locus. The bulk solid is rigid for any stress condition represented by a Mohr semicircle not touching the yield locus. When the stress condition A changes to A' so as to touch the yield locus the solid shears. When the solid shears the direction of the strain rate vector $\bar{\varepsilon}$ is normal to the yield locus, ϕ_v is equal to ϕ and is positive, the solid expands, the density decreases and the yield locus decreases until it assumes the shape corresponding to the new pressure which establishes a new degree of consolidation. As the terminus E is approached, the difference in the value of failure and flow diminishes until, at E, there is no difference and plastic flow occurs. The solid then flows with no change in density and no change of the yield locus. When the pressure increases continuously consolidation progresses, the density of the solid increases and the yield locus expands.

From measurements of the principal pressures during flow, Jenike has observed that the ratio σ_1/σ_2 is practically constant for wide ranges of pressures. The ratio is expressed by the relationship:-

$$\frac{\sigma_1}{\sigma_2} = \frac{1 + \sin \delta}{1 - \sin \delta}$$

where σ_1, σ_2 are the major and minor principal stresses and δ is the angle subtended to the σ axis by a line drawn through the origin tangential to the Mohr circle representing the consolidation conditions. δ is called the effective angle of friction and is considered to be a significant flow property of bulk solids. Jenike points out that if a line is formed tangential to all the consolidation Mohr circles, then this line, in general, approximates to a straight line, which he terms the effective yield locus. (Figure 2.5.).

The yield loci as obtained from measurements in a Jenike direct shear tester (section 4.1.1.1.) do not allow the complete yield loci to be determined. (Figure 2.6.).

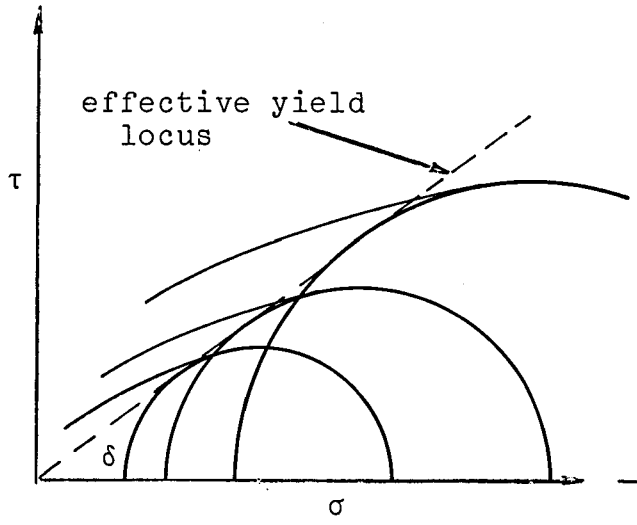

Figure 2.5. Effective Yield Locus

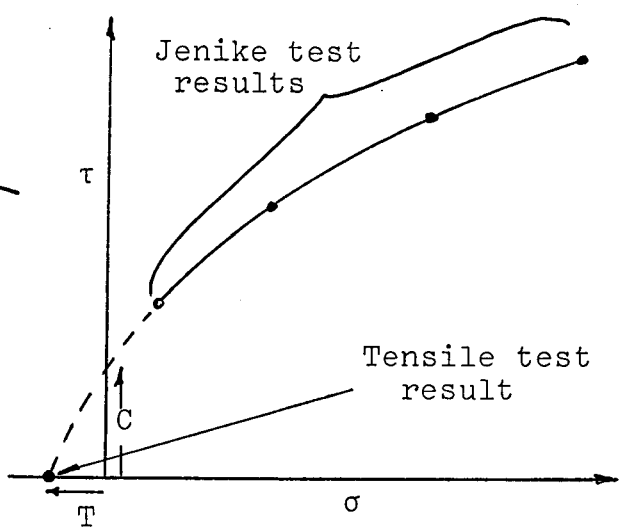

Figure 2.6. Extension of yield locus.

Using a tensile tester (section 4.1.1.4.) Ashton et al[6] have extended the yield loci to the low normal stress regions difficult to obtain in the Jenike shear test. Another property of a bulk material is that it may fail in tension, that is the negative normal force necessary to separate the material at zero shear stress. The tensile stress plotted on the τ, σ axes enables the yield locus to be extrapolated to zero normal load.

Ashton et al[7] have carried out tests in conjunction with the Jenike tester and have shown that for a very large number of powders, the yield loci fit the equation:-

$$\left(\frac{\tau}{C}\right)^n = \frac{\sigma + T}{T}$$

where τ = shear stress

σ = normal stress

C = cohesion

T = tensile stress

n = constant

They suggest that the value of n, which they call the "flowability index", is constant for each particular material sample and increases from 1, for free flowing materials, to approximately 3 for the very cohesive materials. The factor n is, therefore, an indication, and useful scale, for classifying the flow properties. Previously, Sokolowski[164], suggested that the yield locus for a cohesive soil could be defined by the power law:-

$$\left(\frac{\tau}{C}\right)^n = \frac{\sigma + T}{C}$$

When $\sigma = 0$, $\tau = C$ this equation reduces to $\frac{T}{C} = 1$ which, in practice has been found not to be true for powders.

Williams and Birks[196], using an analogy between the sliding of two metal surfaces with magnetic attraction and the shearing of powder with a tensile stress, point out that, in considering the shear stress to cause failure, the normal stress to be taken into account is $(\sigma + T)$ and not σ. $(\sigma + T)$ is called the <u>compound stress</u>.

They have plotted a series of yield loci for titanium dioxide, against σ and against $(\sigma + T)$, finding that the end points of the yield loci in both cases lie on a straight line

through the origin. (Figure 2.7.). This straight line, formed when plotting τ against compound stress, is termed the internal friction yield locus, as, according to Williams and Birks, along this line the shear force is used only in overcoming internal friction of the powder, and not in doing work due to volume change.

Williams and Birks have proposed a method for the linearising of the yield locus of a cohesive powder, based on the equation developed by Ashton et al.[7]

By plotting log τ against log compound stress each yield locus will be a straight line of slope $\frac{1}{n}$; and, since n has been found to be constant for a powder, the yield loci for different consolidations become a series of parallel straight lines. They further simplify the data by using reduced dimensionless stresses, by plotting with axes log $\frac{\tau}{\sigma_L}$ and log $\frac{\sigma + T}{\sigma_L}$, where σ_L is the consolidation normal stress. For titanium dioxide data they found that the results lay within 10% of the straight line through the points. (Figure 2.8.).

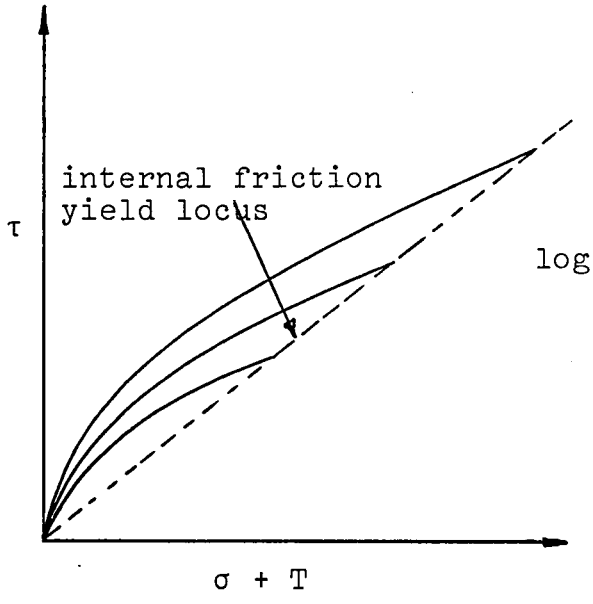

Figure 2.7. Internal friction yield locus

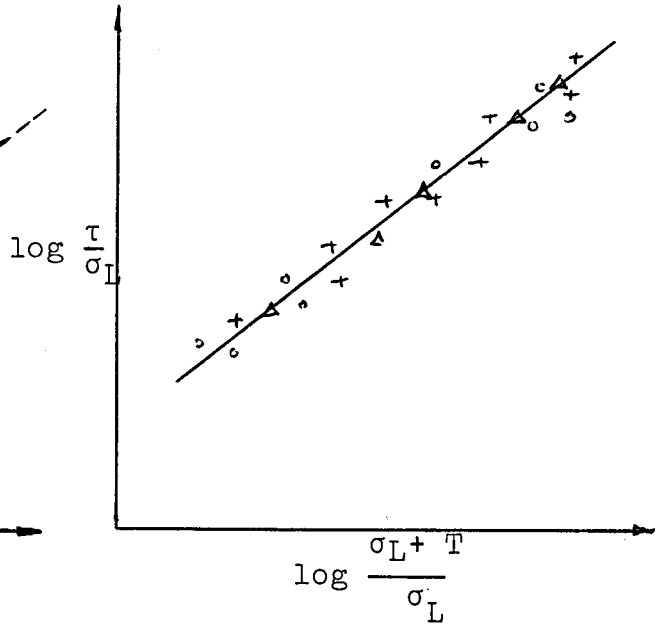

Figure 2.8. Linearisation of yield loci

2.1.2.2. Dependence of Shear Strength on Initial Density

In 1885 Reynolds[130] presented his classic paper on dilatancy. He pointed out that ideal rigid particles had been used to build a fundamental dynamical hypothesis of matter; and that the particles had generally been assumed smooth while actual media were influenced by friction between the particles. He found that dense sands expand during shear failure and that loose sands contract during failure. This property, he realised, was fundamental to granular material but not possessed by known fluids or solids. To quote Reynolds:

"On perceiving something which resembles nothing within the limit of one's knowledge, a name is a matter of great difficulty. I have called this unique property of granular masses "dilatancy"; because the property consists in a definite change of bulk, consequent on a definite change of shape or distortional strain, any disturbance whatever causing a change of volume and generally dilation".

Dilatancy is due to the interlocking of particles. When particles are lodged in the depressions between other particles, it is necessary for them to be lifted out before shear displacement can occur. To quote Reynolds again:-

"So long as the grains are held in mutual equilibrium by stresses transmitted through the mass, every change of relative position of the grains is attended by a consequent change of volume, and if in any way the volume be fixed, then all the change of shape is prevented".

Roscoe[136] has indicated that the equation used by Coulomb is a simple development of the equation of solid body sliding; the assumption being made that the element of soil, when subjected to shear, will fail on a plane through the element

thus forming two pieces which slide as if they were solid bodies. Also, according to Roscoe, the equation implies that the surface of sliding is of negligible thickness. Granular materials however, do not behave like solid bodies in that when shear is applied they tend to dilate and, as they do so, the values of C and ϕ change. He suggests that the equation can only be applied provided the following conditions are satisfied:

i. failure surfaces have fully developed right through the material.

ii. no part of the material is still dilating.

iii. the stresses at all points of the failure surfaces are known.

iv. the intermediate principle stresses have no effect on the mechanical behaviour of the material.

Roscoe[135] has shown that, when flow has started, conditions i. and ii. are likely to be satisfied. Due, however, to the great change of packing at the point of peak stress, the equation cannot be used with great confidence to predict the peak stress conditions.

It was not until the 1930's that the real significance of Reynold's ideas on dilatancy were applied to the shearing behaviour of soils. Hvorslev[83], in 1937, showed that the shear stress at failure was a function of the voids ratio in the plane of failure, as well as of the effective normal stress across the plane.

Hvorslev's failure equation, as reported by Roscoe et al[140], is:-

$$\tau_f = \mu_o \sigma_f + \nu \exp(-B e_f)$$

where μ_o, ν and B are constants of the particular soil,

τ_f = peak shearing resistance

σ_f = effective normal stress

e_f = void ratio at failure

Just previously, in 1936, Casagrande[24] had made comments on the importance of volume changes associated with the deformation of soil, particularly of cohesionless materials.

Burmister[21], in a review of studies on shearing resistance for cohesive and cohesionless materials, reports three characteristic features of the effect of the initial density of sand and soil samples when subjected to shear.

i. The first feature concerns the stress/strain relationship. In the loose state, with gradually increasing horizontal strain, the shear stress increases gradually and continuously to a maximum which is reached at a rather large horizontal deformation. In the dense state, the shear stress increases rapidly to a much higher maximum than for the loose state; and the stress then decreases until, if sufficient strain is permitted, an ultimate shear strain is reached. Taylor and Leps[169] have shown that the ultimate shear strength is very little affected by change in density.

ii. The second feature is the volume change. In the loose state, the material decreases in volume, as a result of deformation, and assumes a more dense state. A point is reached where continuous shear deformation occurs at constant shear stress and at constant volume. Casagrande[24] defined this state as the "critical density". In the dense state, the material rapidly dilates at the maximum stress point, thus bringing the material to the state of flow at constant stress.

iii. The third feature is the effect of the initial density upon the value of the peak angle of friction. In the loose state tan ϕ, as reported by Burmister[21] for Ottawa sand, was $33\frac{1}{2}^{\circ}$,

while for the dense state it was $43\frac{1}{2}^{o}$.

Figure 2.9. shows the stress strain plots for a loose packed material and a dense packed material, illustrating the influence of the "state" of the material on its shear strength.

Burmister[21] also noted that the "critical density" was a function of the normal pressure N decreasing from .74 at a normal stress of .25kg/cm^2 to .63 at 2kg/cm.^{2}

Bjerrum et al[15] examined the effect of the initial density for sand samples on the angle of friction and dilation during a triaxial test. The sand tested had a maximum and minimum porosity of 46.2% and 39.2%, respectively. One of the most significant points raised by their work was that the angle of friction varied over a wider range than had been previously supposed; and that, when the porosity exceeded a certain value, the friction angle decreased very rapidly, as shown in figure 2.10.

2.1.2.3. The Failure Surface Concept

For some time the soil mechanics group at Cambridge University has been studying the behaviour of soils, to understand the stress/strain relationships of real soil so that reliable predictions can be made concerning its behaviour in particular situations.

Roscoe[136] has written a review of their work pointing out the anomalies that exist in present shear strength theories. The review also gives a bibliography containing much of the work which has been published by the group. The group has studied both cohesive clays and free flowing sands.

A continuum approach has been the basis of the studies rather than a particulate approach. Roscoe suggests that the

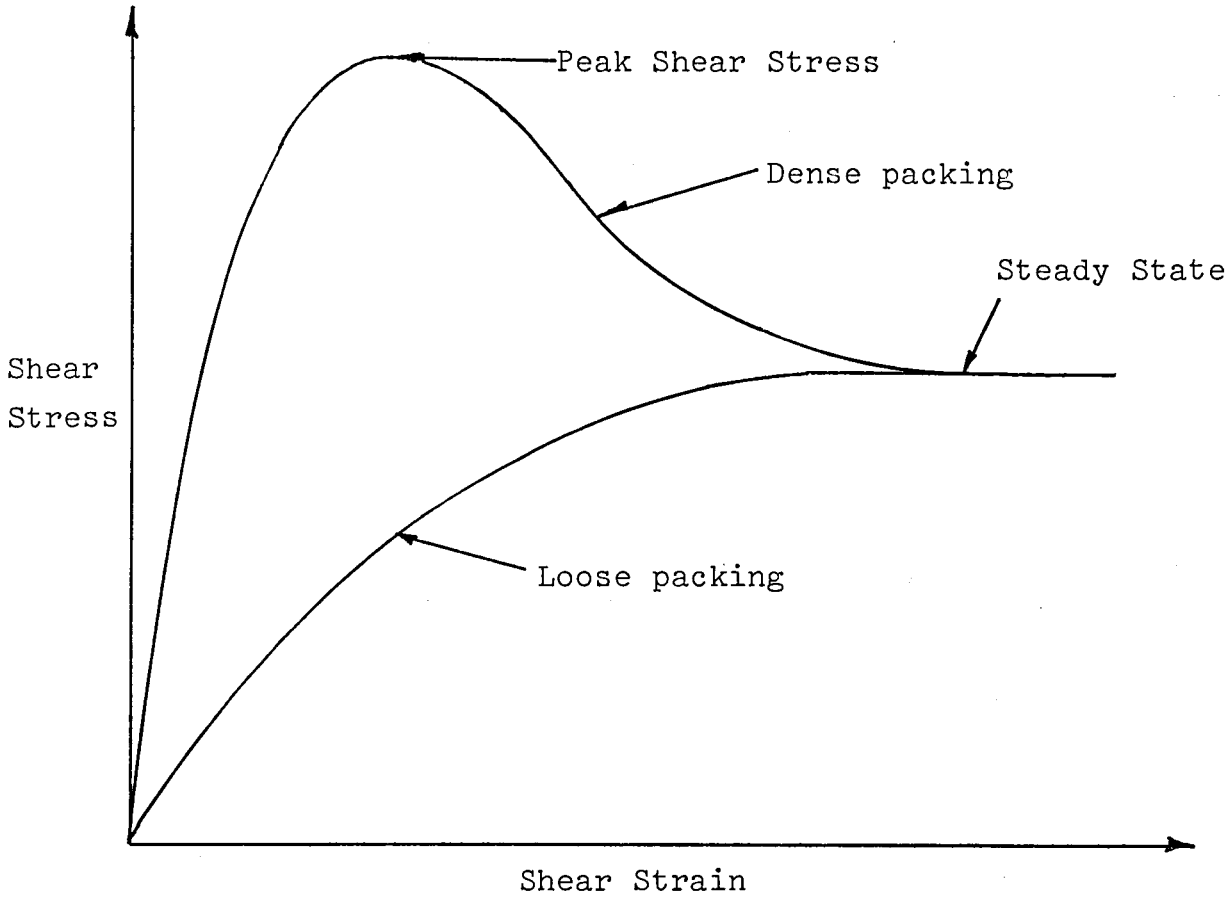

Figure 2.9. Stress / Strain plots for loose and dense packings

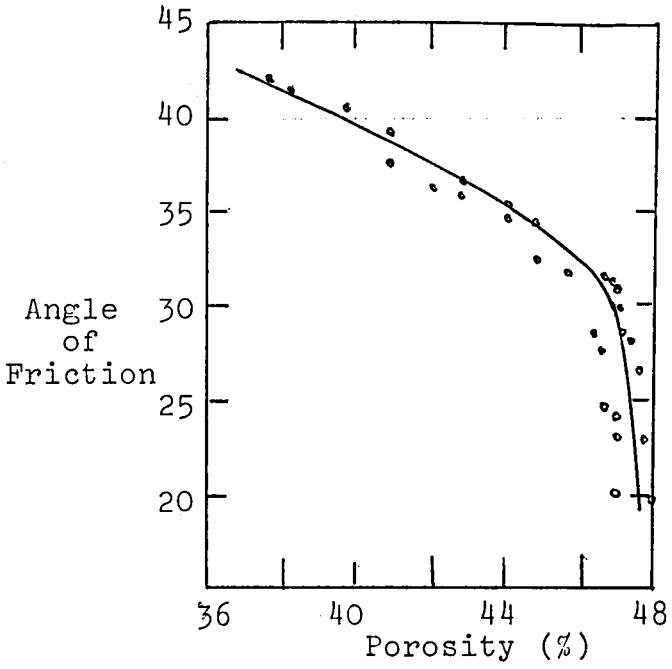

Figure 2.10. Angle of friction versus initial porosity for sand. (Bjerrum[15])

continuum approach lends itself to mathematical analysis more than does the interparticulate approach. In the development of their work useful experimental techniques have been developed, notably the design of a Simple Shear Apparatus to give uniform strain during shear. (This is described in section 4.1.1.1.) It was designed so that an examination of the voids ratio at failure could be examined and the "Hvorslev failure surface" could be investigated. A diagram of this surface, obtained from their studies, is given in figure 2.11.

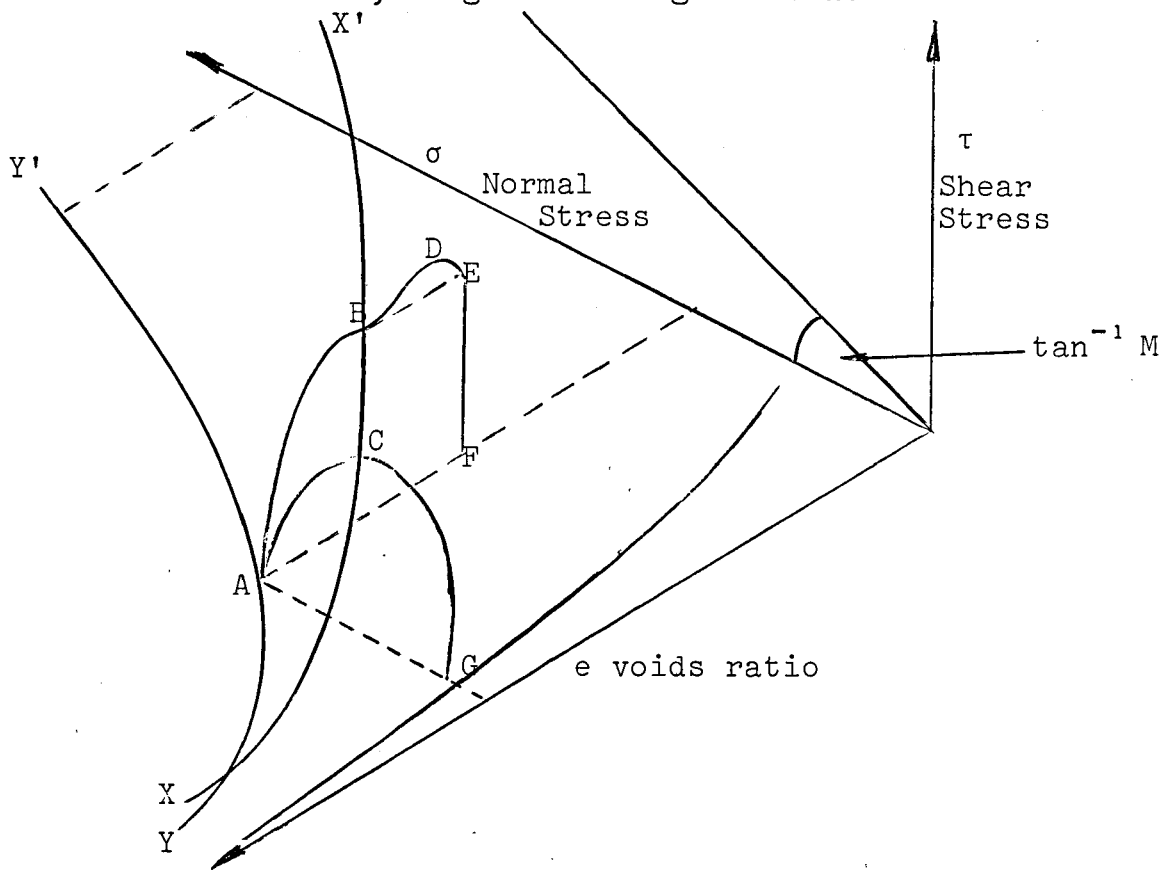

Figure 2.11. Hvorslev Failure Surface

The line YY' drawn in the σ, e plane is termed the "virgin consolidation line" and represents the lowest state of packing that the sample can achieve under a given normal load.

Consider a sample at point A, in the loosest possible initial state. In a drained test (that is in a test which is

carried out at constant normal load) as shear is applied the sample reduces in volume until it reaches B, which is termed the "critical state", when shear takes place at constant volume and constant stress. If on the other hand, in an undrained test (that is the voids ratio is kept constant) then the path is represented by AC, C being the critical state point.

If the sample were compacted to a state greater than the virgin consolidation line, different stress paths would be formed when shear is applied. For the drained test (constant σ) consider an initial condition as represented by the point F. In the region FE, there is no change in volume as shear is applied, but at point E, the sample begins to dilate. At point D, on the failure surface, failure takes place and the dilation rate is at its maximum. Having passed the peak condition at D, the sample proceeds along the path DB until, at B, the critical state is reached and this is where shear takes place at constant volume and constant stress. In the same way, in the undrained test, at constant volume, the stress path is given by the line GC. Thus, by carrying out a whole series of tests at different initial conditions the researchers at Cambridge have been able to define the failure surface and critical state line for a number of materials. A significant feature of the critical state line is that, when projected on to the σ, τ plane, a straight line of slope M is formed, that is:-

$$\tau = \sigma M$$

$$\tau = \sigma \tan \phi_{crit.}$$

Roscoe suggests that $\phi_{crit.}$ can be thought of as the angle of internal friction at the critical state.

2.1.2.4. Explanation of Yield Loci in Terms of Failure Surface

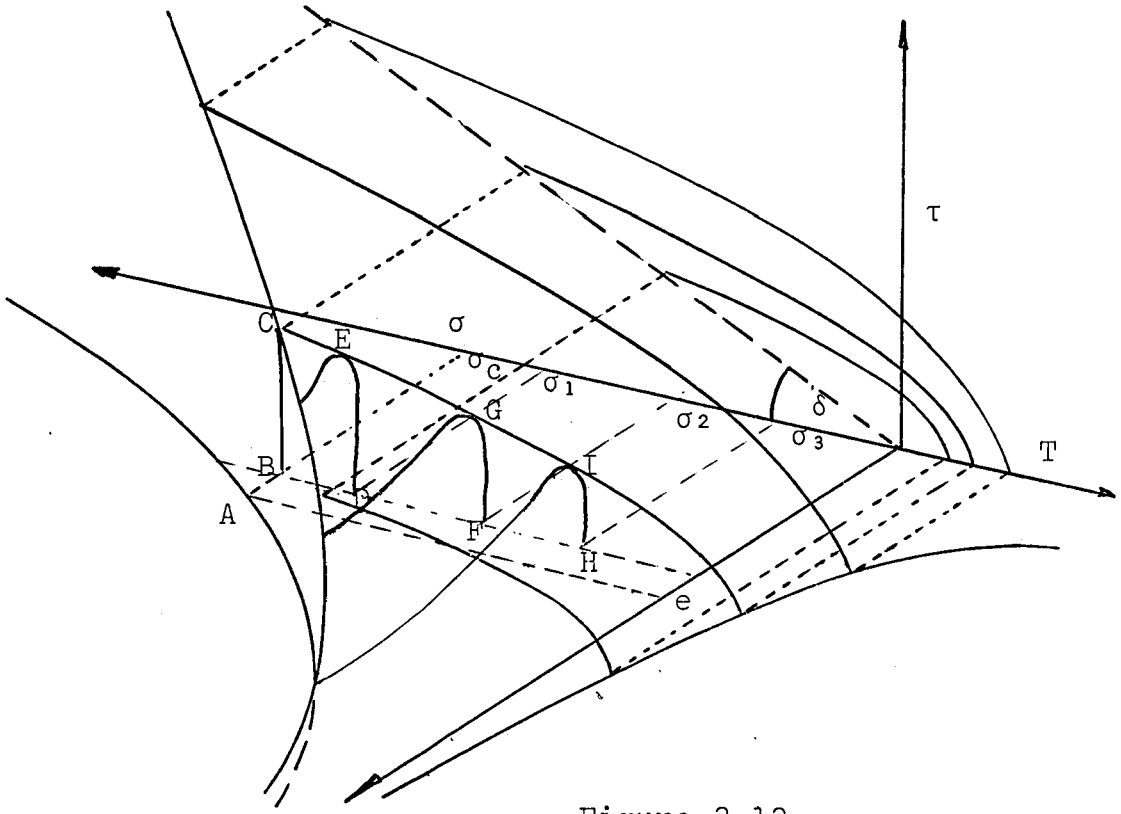

Figure 2.12.

The yield loci obtained using the Jenike Flow Factor tester can now be understood more clearly in terms of the Hvorslev surface. Williams and Birks[196] have discussed this on two occasions. With reference to figure 2.12., which shows three yield loci drawn on the failure surface, consider a sample at point A, which has then been compacted to a point B. If then the sample is sheared at the compaction load, σ_c, point C is reached without change in volume or a peak stress. If compaction to condition B is followed by shearing at a normal load, σ_1, the stress path is DE, E being the peak failure stress. Having reached E, the sample reduces in its dilation rate until the critical state is attained. However, in the Jenike test, after point E is reached the test is terminated. The yield loci are formed by measuring this peak value for the consolidation condition at different normal loads. The end points of the

yield loci are the points on the critical state line, making the straight line in τ, σ co-ordinates only.

2.1.2.5. The Critical State and Free Flowing Materials

Roscoe et al[140] have reported some work by Wroth[199] on the behaviour of cohesionless materials, sand, glass beads and steel balls in the Simple Shear Apparatus. For the tests random packings were prepared at different initial porosities. Figure 2.13. shows the void ratio plotted against the horizontal displacement for one normal stress. Roscoe[140] showed that the voids ratio reached a final condition with a mean of .646, that is a porosity of ≃ 39.5%.

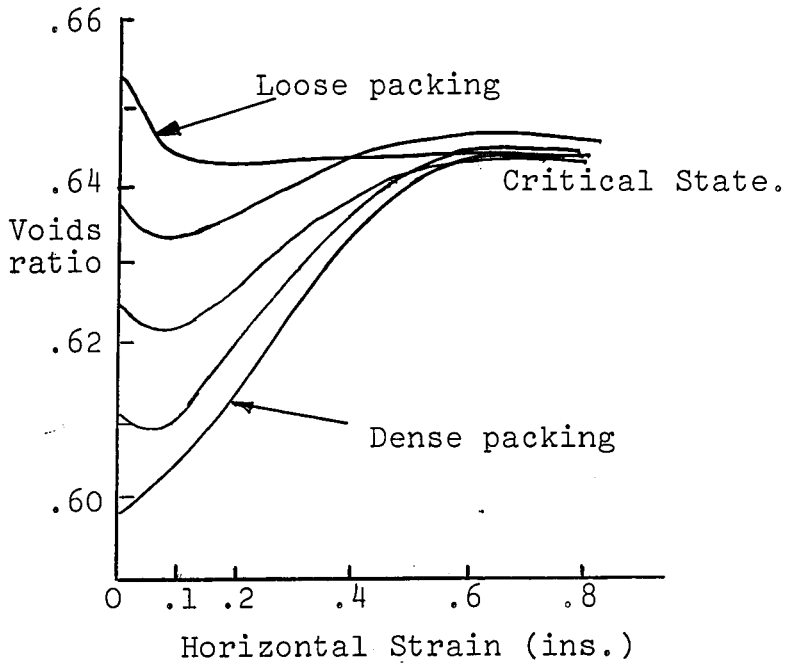

Figure 2.13. Results of simple shear tests on steel balls. (Roscoe[140])

The work on the cohesionless spheres and sands showed that there was a well defined yield surface with a critical voids ratio line. The tests were conducted over a normal load range of 0 to 100lb/in^2. The critical voids ratio, CVR, for glass spheres had a small range .67>CVR>.63, that is 40.27>CP>38.7; and for steel balls .71>CVR>.69, that is 41.6>CP>40.8.

CP is the critical porosity. The steel balls were mono-size and the glass beads were between .75-.8mm in diameter. Apparently the results from the sands behaved similarly but with greater scatter.

Wroth and Bassett[200] have noted that the critical state line is defined by the equation:-

$$e = \Gamma - \lambda \log_e \sigma'$$

$$\tau = M\sigma'$$

where M, Γ and λ represent basic soil material properties. They note the importance of the line, for when plotted in e, $\log_e \sigma$ co-ordinates, the line divides all samples into two distinct categories. The samples with initial states on the far side of the critical state line, termed the "wet" side, contract when sheared at constant normal stress; whereas the samples on the near, "dry", side expand.

2.1.2.6. The Triple State Concept

Cheng and Valentin[31] point out that the phenomenological approach, which originated from the Coulomb yield equation, is a useful approach in the design and interpretation of experiments in powder behaviour, although not an ultimate in giving a fundamental explanation of the phenomena. They suggest that only a particulate approach, using statistical methods, will achieve this aim. They have developed a phenomenological approach and a theory which suggests that powders can exist in three states:- elastic, consolidating or flowing, depending on the stresses acting on it. When stress values are less than critical they say that the powder is elastic, indicating that in some cases this elastic region is small. When the critical stresses are exceeded, permanent deformation takes place

resulting in either consolidation or flow. They suggest that the critical stresses for yield form an incipient yield surface in the (ρ,σ,τ) space, where ρ = density, σ = normal stress and τ = shear stress. In like manner, the critical stresses for consolidation form an incipient consolidation surface. The incipient consolidation and incipient yield surfaces intersect in a curve which is termed the "triple state line". Others[135,140] have called this the "critical state line", but Cheng and Valentin suggest that a steady flow surface exists which meets in the one line, hence the term "triple state". The existance of this surface had not been indicated by Roscoe et al[138], in that experiments were not conducted beyond the critical state line. Again, however, Cheng and Valentin point out that more experimental evidence is required to resolve the conflict between a steady flow curve and the triple state line.

2.1.2.7. The Separation of the Components of Shear Stress

Taylor[168] was the first to attempt the separation of the strength component due to friction and that due to dilation, suggesting that the difference between peak and ultimate stresses could be accounted for by this separation. Taylor's derived expression for the expansion component of shear stress was:-

$$\tau_e = \sigma_n \frac{dh}{dx}$$

where τ_e = shear stress required to provide energy for expansion

σ_n = normal stress

dx = increment of shear deformation

dh = corresponding increment in thickness of sample

In 1950, Skempton and Bishop[159] also attempted this separation. In both cases the work done in expanding a sample, in a direct

shear box by an amount δV per unit area against a vertical pressure σ_n, was equated with the equivalent shear component τ_d, acting horizontally through a distance of $\delta\Delta$, equal to the relative displacement of the box. A residual angle ϕ_r was used to express the difference between the maximum applied shear and τ_d.

$$\tan \phi_r = \frac{\tau - \tau_d}{\sigma_n} = \tan \phi_{max} - \frac{\delta V}{\delta \Delta}$$

that is, $$\tan \phi_{max} = \tan \phi_r + \frac{\delta V}{\delta \Delta}$$

From an analysis of particle movement during shear and the resultant direction of movement during dilation, Newland and Allely[119] have derived an equation relating the angle of internal friction, ϕ_f, to tan θ where

$$\tan \theta = \left(\frac{\delta V}{\delta \Delta}\right)_{max}$$

their equation is:-

$$\phi_{max} = \phi_f + \theta$$

They noted that there were differences between the angle of sliding friction ϕ_μ and the angle of internal friction ϕ_f. They attributed the difference to the "mode of failure taking place during shear". When $\phi_f \rightarrow \phi_\mu$ they suggest that the mode of failure is that particle contacts have been "bridged", transferring the normal stress to the sliding contacts. When $\phi_f > \phi_\mu$, the mode of failure is such that the "bridges" collapse resulting in a smaller overall volume change.

From this mode of failure concept they suggest that for high values of ϕ_μ, the mode of failure will tend to be of the type in which the "bridges" do not collapse, hence ϕ_f will approximate to ϕ_μ; while for lower values of ϕ_μ collapse of

"bridges" may increase so that there is increasing divergence between ϕ_f and ϕ_μ.

The value of ϕ_f from Newland and Allely[119] and of ϕ_r from Bishop,[159] were derived to measure the same physical quantity. Newland and Allely suggest that the difference found between the two values is due to the fact that Bishop assumes that the work done in overcoming friction is the same at both the peak and residual states. They, themselves, suggest that the shear stress has a component normal to the plane of sliding which contributes to the frictional strength but which decreases in magnitude as expansion occurs. That is, the work done in overcoming friction forces is greater at the point of maximum stress than at the residual stress.

Wroth and Bassett[200] using an idealised soil propose mathematical equations to describe the shear stress/strain characteristics of a sand. The equations fit accurately experimental results obtained from tests on steel balls and on a sand. The three equations are:-

$$(e-e_o) = \alpha \log_e(\sigma'/\sigma_o') \quad . \quad . \quad . \quad . \quad (a)$$

$$\tau = M\sigma' + \sigma'\frac{\delta e}{\delta z} + \kappa\frac{\delta \sigma'}{\delta z} \quad . \quad . \quad . \quad . \quad (b)$$

$$\frac{(e-e_x) + \lambda \log(\sigma'/\sigma'_x)}{D_o} = (1+bz)\exp(-az) \quad . \quad (c)$$

where σ' = effective normal stress

e = voids ratio

σ'_x, e_x = critical state condition

α = ∞ when σ' is constant through the test

α = 0 when e is constant through the test

z = dimensionless strain parameter

D_o = vector distance from critical state line

λ, κ, are constants for the material

$\sigma'_o, e_o, \alpha, a, b$, and D_o constants for the particular test.

Equation (a) is the equation relating the "degree of volume change" α to σ', and e

when $$\alpha = \frac{\Delta e}{\Delta(\log_e \sigma')}$$

Equation (b) is the energy equation comprising a frictional component, which is irrecoverable energy dissipated within the system directly proportional to σ'; a volume change component which is recoverable energy crossing the system boundary; and a pressure change component which is stored "elastically" within the system.

Using Wroth and Bassett's notation, considering figure 2.14:-

$$\text{Frictional} = (M\sigma' A)\delta x$$

$$\text{Volume change} = (\sigma' A)\delta y$$

$$\text{Pressure change} = \kappa V_s \delta\sigma'$$

$$\text{Applied energy} = (\tau A)\delta x$$

Equation (c) is an expression of the degree to which the test has been completed.

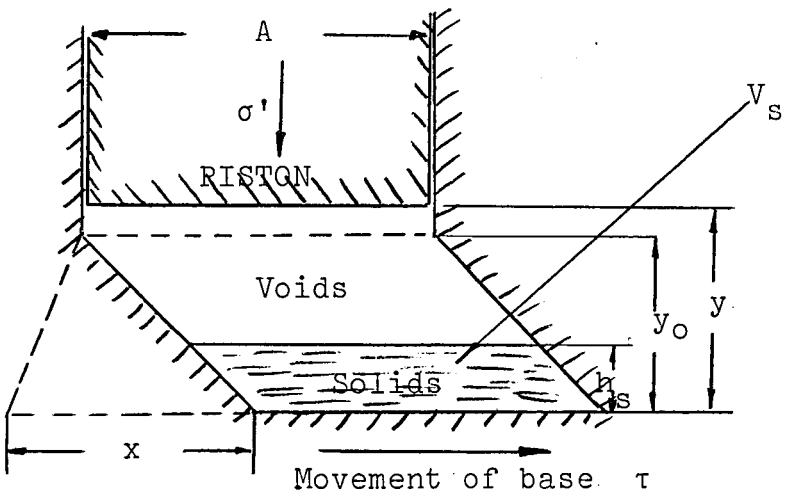

Figure 2.14. Representation of sample in simple shear (Wroth and Bassett[200])

Owing to the difference in maximum shear resistance and ultimate shear resistance, which he has attributed to particle interlocking, Hough[80] has suggested that the standard practice, when reporting the angle of friction data, should be to report the ultimate friction. This would avoid confusion due to interlocking effects.

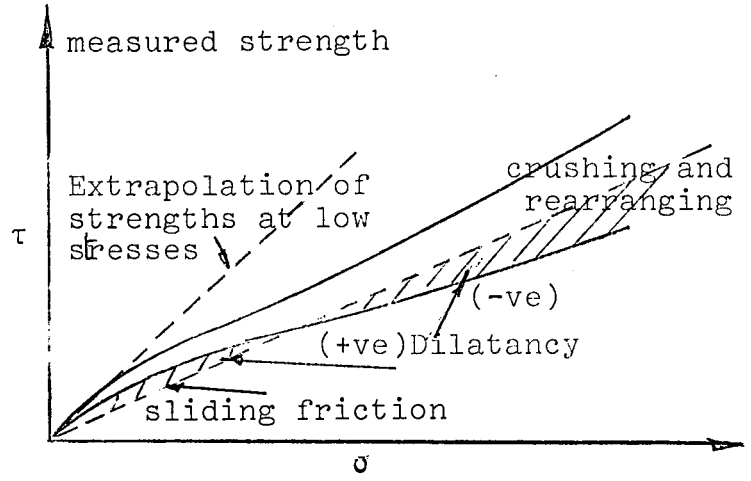

Figure 2.15. Contribution of sliding friction, dilatancy and crushing to shear strength. (Lee[107])

Lee,[107] considering the incompressibility of sand, has suggested that, at high pressures, there can be considerable volume changes due to crushing of the grains. He says that for tests at high confining pressures the influence of particle crushing must be considered. At high pressures the crushing will absorb energy, similar to that of rearranging grains in loose sands, causing the angle of friction corrected for dilatancy effects, to be greater than ϕ_μ, the angle of sliding friction. Also, since the failure strain becomes large in tests at high confining pressures, there will be an increase in the energy required for rearranging the grains. Thus the shear stress of a cohesionless soil, according to Lee, can be expressed as:-

measured shear strength = strength due to sliding friction

+ dilatancy effects

+ crushing and rearranging effects

Figure 2.15. shows Lee's diagram of the contribution of dilatancy, crushing and sliding friction to the measured shear strength for sand.

2.1.2.8. The Shear Strength and the Rate of Shear

According to Clayton[32] the frictional characteristics of many minerals are functions of the rate of sliding. However, Horn[75] has concluded that between sliding rates of .7 and 6.0in/min. for massive-structured minerals such as quartz, there is no effect on the frictional characteristics.

For the bulk material Whitman[194] has shown that tan ϕ is independent of the rate of strain in the triaxial test when the failure time is varied from 5m.sec. to 5min.

Jenike[89] has also increased the rate of shear, by a factor of two, in his direct shear apparatus on the assumption that there is no influence of the rate of shear.

2.1.2.9. Moisture Content and Shear Strength

Having considered the effect of the state as far as packing is concerned on the strength behaviour of particulate materials, it is realised that the moisture content state has a significant effect on the shear strength of a material. However, in this present work, the effect of moisture has been neglected and consideration restricted to a dry system.

2.2. Particle Characterisation

The basic difference in the behaviour of a subdivided solid and a homogeneous solid is in the interaction of the

constituent particles; and this is dependent on the particle size distribution of the system.

Section 2.1.2., in dealing with the shear strength of particulate material and its relationship to the state of the system, has considered particularly those researchers who have worked from a continuum basis. However, a number of authors have approached the problem from a particulate basis in an attempt to relate the microscopic properties to the macroscopic properties.

One of the soil mechanics masters, Terzaghi[170], published the following statement in 1920. "The fundamental assumptions of the traditional earth-pressure theories cannot, in fact, stand superficial examination. The fundamental error was introduced by Coulomb, who purposely ignored the fact, that sand consists of individual grains, and who dealt with the sand as if it were a homogeneous mass with certain mechanical properties. Coulomb's idea proved very useful as a working hypothesis for the solution of one special problem of the earth pressure theory, but it developed into an obstacle against further progress as soon as its hypothetical character came to be forgotten by Coulomb's successors.

The way out of the difficulty lies in dropping the old fundamental principles and starting again from the elementary fact that the sand consists of individual grains".

Before considering the particulate approach an examination of the particle size and shape will be considered.

2.2.1. Particle Size

It has been pointed out by Hausner[64] that the factors which characterise an individual particle making up a powder

are difficult to determine, mainly because the characteristic features are hard to define. Heywood[70] has indicated that an irregularly shaped particle has no unique dimension and because of this the size of particles has been expressed in terms of the diameter of a sphere that is equivalent to the particle with regard to some property.

2.2.1.1. Equivalent Sphere Diameters

The traditional method of defining particle size is as the size of a sphere, equivalent in some geometrical property or in behaviour.

Allen[2], in a review of the measurement of particle size, has listed some of these equivalent diameters. His list is given in table 2.1. below:-

Table 2.1. Definitions of Particle Size

Symbol	Name	Definition
d_s	Surface diameter	The diameter of a sphere having the same surface area as the particle
d_v	Volume diameter	The diameter of a sphere having the same volume as the particle
d_d	Drag diameter	The diameter of a sphere having the same resistance to motion as the particle in a fluid of the same viscosity and at the same velocity
d_a	Projected area diameter	The diameter of a sphere having the same projected area as the particle when viewed in a direction perpendicular to a plane of stability
d_f	Free-falling diameter	The diameter of a sphere having the same density and the same free-falling speed as the particle in a fluid of the same density and viscosity
d_{St}	Stokes' diameter $d_{St}=\sqrt{(d_v^3/d_d)}$	The free-falling diameter in the lamina flow region (Re<0.2)
d_A	Sieve diameter	The width of the minimum square aperture through which the particle will pass
d_{vs}	Specific surface diameter $d_{vs}=d_v^3/d_s^2$	The diameter of a sphere having the same ratio of surface area to volume as the particle

Another equivalent diameter, as given by Heywood[70], is the Perimeter diameter, which is the diameter of the sphere having the same projected perimeter as the particle when it is in its position of greatest stability. Heywood has stated, also, that for an irregular particle resting on a plane so that its minimum dimension is perpendicular to the plane, there are limiting dimensions for its thickness, breadth and length.

2.2.1.2. Statistical Diameters

The alternative definition of particle size is a statistical diameter. The two statistical diameters often used to describe the size of an irregular particle are (i) the Martin's diameter which is the length of the line through the particle profile, parallel to a fixed direction and which divides the particle into two equal areas and, (ii) the Feret's diameter which is the projected length of the particle profile with respect to a fixed direction. As indicated by Kaye[95], in a discussion on the efficiency of statistical methods of particle size analysis, for both of these sizes a single value does not uniquely define the particle profile. If, however, the particle is measured more than once, that is in other orientations, then the average value can be a physical property of the profile.

A graphical representation of some of the statistical and equivalent diameters is given below in figure 2.16. The limiting dimensions of a particle and a particle resting on a plane of maximum stability are also shown.

Another statistical diameter is the image shearing diameter obtained by using an image shearing eyepiece in a microscope. The one image is displaced so that the two images

of the particle just touch and the displacement is measured.

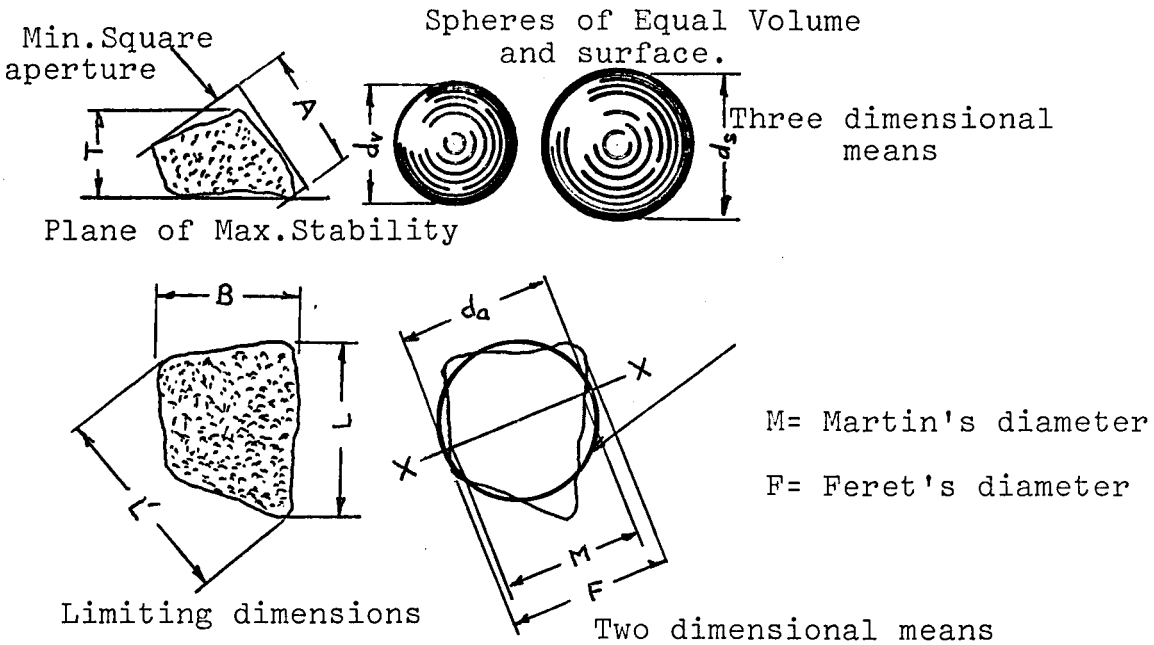

Figure 2.16. Equivalent Particle Diameters. (Heywood [70])

2.2.1.3. The Mean Size of a System of Particles

In addition to the problem of defining the size of an individual particle there is the further problem of expressing the distribution of particle size, for example by a number or by weight. Mathematical expressions for the mean diameter can be derived if the complete size range is subdivided into small groupings of size range δx and with assumed diameters of $x_1, x_2 \ldots$ The number of particles in the groupings is δN_1, $\delta N_2, \ldots$ The length, surface area and volume of the particles in each group are represented by the expressions $x_1 \delta N$, $x_1^2 \delta N$, and $x_1^3 \delta N$, respectively; and the totals for the whole of the powder by the summations $(x_1 \delta N_1 + x_2 \delta N_2 + \ldots) = \Sigma x \delta N$, and similarly for terms with higher powers of x. The expression $\Sigma x^3 \delta N$ may be replaced by $\Sigma \delta V$, and the expression $\Sigma x^2 \delta N$ by $\Sigma \delta V / x$, where δV represents the volume of particles in a grouping. Heywood's [70] table 2.2. showing

the mathematical expressions and nomenclature for the various mean diameters is given below:-

Table 2.2. Derivation of Mean Diameters

Nomenclature and properties	Expressions for means	Symbols
Number length mean diameter	$\Sigma x\delta N/\Sigma\delta N$	x_{nl}
Number surface mean diameter	$\sqrt{\Sigma x^2\delta N/\Sigma\delta N}$	x_{ns}
Number volume mean diameter	$\sqrt[3]{\Sigma x^3\delta N/\Sigma\delta N}$	x_{nv}
Length surface mean diameter	$\Sigma x^2\delta N/\Sigma x\delta N$	x_{ls}
Surface volume mean diameter	$\Sigma x^3\delta N/\Sigma x^2\delta N$ $=\Sigma\delta V/\Sigma\delta V/x$	x_{sv}
Volume moment mean diameter	$\Sigma x^4\delta N/\Sigma x^3\delta N$ $=\Sigma x\delta V/\Sigma\delta V$	x_{vm}
Weight moment mean diameter	or $\Sigma x\delta W/\Sigma\delta W$	x_{wm}

The particle size distribution of a system of particles can be expressed, therefore, by a mean size and standard deviation.

2.2.2. Particle Shape

The definition of a particle's shape is important because this shape greatly influences the behaviour of a powder. A number of authors have discussed shape factors:- Herdan[68], Heywood[70], Hausner[64], Orr and Dallavalle[122]. B.S. 2955 has defined various particle shapes, such as Acicular, Angular, Crystalline, Dendritic, Fibrous, Flaky, Granular, Irregular, Nodular and Spherical. However, as pointed out by Heywood, these are inadequate for the purposes of calculating particle properties which incorporate the effect of shape. Shape factors are obtained by relating the bulk property of a system, say its surface area, to one of the equivalent diameters.

The surface and volume of a particle are related to spherical particles by the equations:-

$$\text{Surface:} \quad S = \alpha_s d_a^2 = \pi d_s^2$$

$$\text{Volume:} \quad V = \alpha_v d_a^3 = \frac{\pi}{6} d_v^3$$

where α_s and α_v are the surface projected area and volume projected area shape factors.

2.3. The Packing of Particles

Having considered particle characterisation, the relationship between it and the packing of particles will now be discussed, thus linking the microscopic and state properties.

2.3.1. The Packing of Spheres

Many studies on the packing of particles have been based on spherical or near spherical particles. The systematic arrangement of spheres in connection with the flow of water through soil was first studied by Slichter[160] in 1899.

Graton and Fraser[58] have discussed various systematic assemblages of spheres. In each assemblage every sphere was packed in an identical manner to every other sphere and every sphere had the same co-ordination. The table 2.3. below has four such systematic packings, their porosities and co-ordination numbers.

Table 2.3. Properties of Regular Packings of Uniform Spheres

Type	Void Ratio	Porosity	Co-ordination Number
Cubic	.91	47.64	6
Orthorhombic	.65	39.54	8
Tetragonal Spheroidal	.44	30.19	10
Rhombohedral	.35	25.95	12

The stability of the system increases as the porosity

decreases. The cubical system is the least stable because each sphere is delicately supported at one point from below and is only prevented from toppling by lateral support provided by four neighbouring spheres in the same layer. The orthorhombic and tetragonal spheroidal systems have more stability because each sphere has two points of support from below as it rests in the cusp formed by two adjacent spheres. A force having a component perpendicular to the plane of this cusp will tend to topple it. The rhombohedral system has complete stability.

Other researchers, Furnas[53], Fraser[52], Horsfield[79], White and Walton[193] have examined the systematic packing of spheres of different sizes. By considering a system of successive spheres just large enough to fill the voids, they have determined the porosity for particular systems. In practice, of course, it is impossible to attain a system packed in such a way.

Table 2.4. below gives the results of Horsfield[79] for the decrease in porosity resulting from the insertion into voids of the rhombohedral system.

Table 2.4. Effect on Porosity of Spheres Inserted in Voids of a Rhombohedral System

Sphere Type	Radius	No. of Spheres	Porosity
Primary	1	1	25.95
Secondary	.4142	1	20.69
Tertiary	.2247	2	19.01
Quaternary	.1766	8	15.74
Quinary	.1163	8	14.81
Filler	-	-	3.84

A system which was more representative of a real system was studied mathematically by Wise[198], who examined statistically the dense random packing of unequal spheres. The random packing is obtained in the following manner.

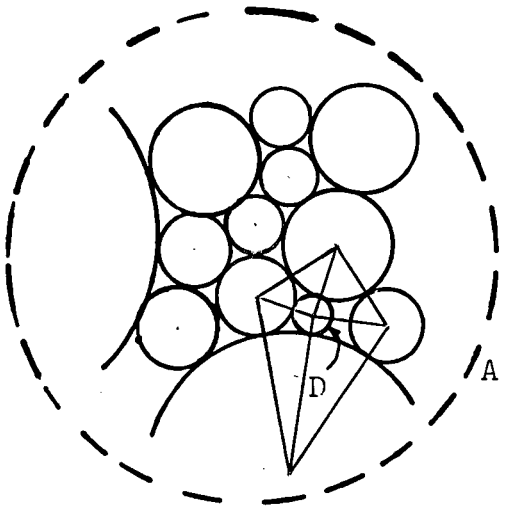

Figure 2.17. Random Packing of Spheres (Wise[198])

Considering figure 2.17, a large sphere A is taken and other smaller spheres are placed on its surface. The first and second sphere must touch each other and also A. Every new sphere must touch A and at least two others that touch each other. Figure 2.17 shows what is seen looking from A. If the centre of a sphere D is joined to the centres of the spheres around it, a network of triangles is formed, each of which lies in a different plane. These triangles are the faces of a polyhedron with the centres of the spheres as its vertices. If these vertices are joined to the centre of A, the whole space enclosed by the polyhedron is partitioned into tetrahedra associated with the given sphere D. Wise sets up a probability distribution function w for the four radii in each tetrahedron and deduces general equations for w. The properties of the packing are expressed in terms of w.

2.3.2. The Packing of Real Granular Systems

In a real granular system, the co-ordination numbers of spheres vary according to the position of each sphere. Smith[162]

has suggested a simple method to determine the average co-ordination number, N, of a system having a porosity n. N is considered to decrease linearly as the porosity increases from the rhombohedral system to the cubic system. Later, after some experiments on the packing of lead shot, Smith et al[163] determined experimentally the co-ordination numbers of well packed aggregate of lead shot for various porosities; and found that the co-ordination number varied according to a Gaussian distribution. They formed an expression for the average co-ordination number in terms of the porosity:

$$N = 26.4858 - \frac{10.7262}{n}$$

Kolbuszewski[100] examined the limiting porosities for sands. The loose packings were obtained by pouring in air, while dense packings were obtained by vibrating in layers in water. He emphasised that it was important to ensure that, for reproduction of the packing, the technique should be exactly repeated.

Burmister[20] has also taken interest in the maximum and minimum porosities of materials and has termed the expression "relative density".

$$\text{Relative density (\%)} = \frac{(e_L - e_n)}{e_L - e_D} \times 100$$

where e = voids ratio

Subscript L = minimum density state

" D = maximum density state

" n = state being considered

He set out to show that he considered the relative density as a fundamental concept, in soil mechanics, in bringing

together complex phenomena of soil behaviour on a common basis.

2.4. The Macroscopic Behaviour/Microscopic Property Relationship

In relating the macroscopic property of shear strength to the microscopic property of particle size, in relation to the state, there are a number of approaches shown in the diagram below.

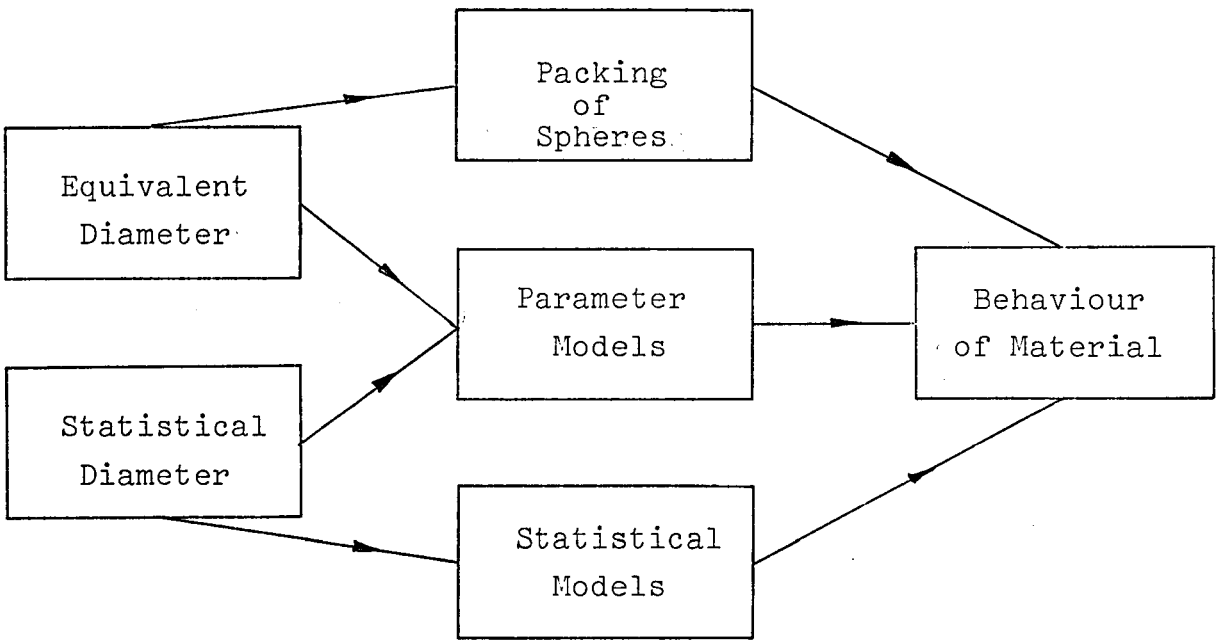

2.4.1. The Stress-Dilatancy Theory

Rowe[142], in 1962, presented his "stress-dilatancy theory for soils".

He discussed the behaviour of ideal packing of spherical particles subjected to a major effective principal stress σ'_1 and equal minor effective stresses $\sigma'_2 = \sigma'_3$, with associated strain rates as $\dot{\varepsilon}_1$, $\dot{\varepsilon}_2$ and $\dot{\varepsilon}_3$ where $\dot{\varepsilon}_2 = \dot{\varepsilon}_3$. He found that for a close packed regular array, deforming with $\dot{\varepsilon}$ negative, groups of particles slide relative to each other, the planes of contact being at any angle β. The angle characterising the packing he termed α.

He derived a stress-dilatancy relation for these packings given by:-

$$\frac{\sigma_1}{\sigma_3} = \tan\alpha \tan(\phi_\mu + \beta)$$

where ϕ_μ = angle of friction between the particles and

$$\frac{\dot{\varepsilon}_3}{\dot{\varepsilon}_1} = \tfrac{1}{2} \tan\alpha \tan\beta$$

He also derived an energy ratio given by:-

$$\dot{E} = \frac{\sigma'_1 \dot{\varepsilon}_1}{2\sigma'_3 \dot{\varepsilon}_3} = \frac{\sigma'_1}{\sigma'_3 \left(1+\frac{\dot{dv}}{V\dot{\varepsilon}}\right)} = \frac{\tan(\phi_\mu+\beta)}{\tan\beta}$$

Observing that the angle α, characteristic of the particular packing, has disappeared from the energy ratio equation, Rowe suggests that the equation applies to random assemblies of particles as well as regular arrays. He proceeded to derive the critical angle of sliding between particles in a random assembly by postulating that the ratio of energy absorbed in internal friction to energy supplied namely, $\dot{E}$, was a minimum. The minimization of $\dot{E}$ with respect to β gives $\beta = \frac{1}{4}\pi - \frac{1}{2}\phi_\mu$, that is:-

$$\dot{E} = \frac{\sigma'_1 \dot{\varepsilon}_1}{2\sigma'_3 \dot{\varepsilon}_3} = \frac{\sigma'_1}{\sigma'_3 \left(1+\frac{\dot{dv}}{V\dot{\varepsilon}_1}\right)} = \tan^2(45+\tfrac{1}{2}\phi_\mu)$$

Rowe tested his theory using the triaxial test on randomly packed masses of steel, glass and quartz particles. He found the true friction, ϕ_μ, by measuring the shear force necessary to move the bulk material over a solid block of the same material, the test being conducted with water covering the material. He showed that the minimum energy ratio criterion was closely obeyed by highly dilatant, dense, over-consolidated assemblies throughout deformation to failure; but that the value

of ϕ, to satisfy the theory, increased to ϕ_f when loose packings were considered because of the additional energy losses due to rearranging of the loose particles. Rowe found that $\phi_\mu \leq \phi_f \leq \phi_{cv}$ where ϕ_{cv} was the calculated value of ϕ when the sample reached the stage of zero rate of volume change.

Figure 2.19. from Rowe's paper shows the various values of ϕ for various porosities for a medium fine sand.

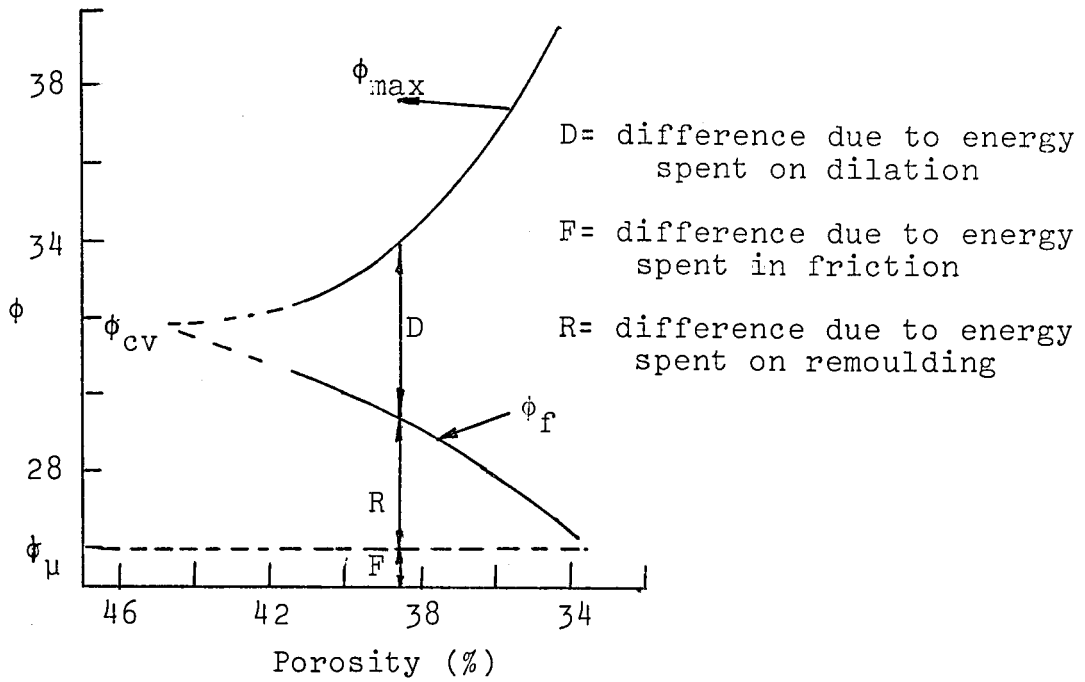

Figure 2.19. Components of strength of sand (Rowe[142])

In the discussion on Rowe's[143] 1963 paper, Gibson and Morgenstein[56], Trollope and Parkin[180], Roscoe and Schofield[139], and Scott[152] discussed the stress-dilatancy theory and their criticisms have been directed mainly towards; (i) the assumed mechanism of deformation; (ii) the assumed absence of rolling; (iii) the assumption that the energy ratio $\dot{E}$ is a minimum in a random assembly of particles and (iv) the meaning of "α planes" in a random assembly of particles.

Roscoe[139] suggests that the method of measuring the true friction is suspect, pointing out that in the method used by Rowe it was possible that loose particles formed rolling contacts

so that the value of ϕ_μ is underestimated. Roscoe also criticises the direct application of the theory from regular particle arrays to irregular particles in random orientation, although he was impressed by the apparent experimental justification. In Roscoe's[139] discussion of microscopic behaviour, he mentions the rejection of using regular packings as a means of characterising parameters relevant to random packings. The findings of Wroth[199] showed that, for regular packings of spheres, the shear strength decreased as the density of packing increased. This is the opposite of what occurs with random packings.

In closing the discussion Rowe[141] concludes with four advantages of a particulate treatment of soils. Firstly, that the prediction of ultimate friction values from true friction measurements places soil science on a firmer base than does the use of empirical correlations. Secondly, all the solutions, being applied at the time, to earth pressures and slopes are retained when using particulate mechanics. Thirdly, fundamental expressions for relations between principal strains in an element may be derived in terms of interparticulate friction and soil structures. Lastly, the use of soil structures rather than the arbitrary statement that soil is isotropic, is the most compelling advantage.

Rowe's theory has been substantiated by Horne[76], who did not restrict his analysis to an idealized packing. Horne analysed a randomly packed particulate assembly assuming: (i) the particles were rotund and rigid with a constant coefficient of solid friction and (ii) deformation occurred as a result of relative motion between groups of particles, but rolling was not allowed between the groups of particles. Horne obtained the expression for $\dot{E}$ by writing a virtual work equation for the

input of $\sigma'_1\dot{\varepsilon}_1$. He then minimised this ratio to obtain the value of $\beta_c = 45 - \frac{1}{2}\phi_\mu$ which then led to:-

$$E = \tan^2(45+\tfrac{1}{2}\phi_\mu)$$

Horne established the limitations of the stress-dilatancy theory and concluded that the equation of the energy ratio $\dot{E}$ that provided a relationship between $\sigma'_1\dot{\varepsilon}_1$, $\sigma'_2\dot{\varepsilon}_2$ and $\sigma_3\dot{\varepsilon}_3$ does not provide a relationship between stresses or strain rates separately. He suggested that the packing characteristics of random assemblies must also be considered before stress or strain ratios can be derived. Also he concluded that the relationship may not apply to a highly compact assembly with a high degree of interlocking.

2.4.2. Powder Strength and Particle Size and Shape Parameter Models

Although, according to the tan ϕ expressions, no consideration has been given to the effects of particle size and shape, a number of investigators have considered if and what contribution size and shape make to the strength characteristics.

2.4.2.1. Size Effects

From a study conducted by Holtz and Gibbs[74], of the effect of maximum particle size on the shearing resistance, they found that for a 4:1 mixture of sand and gravel, the shear strength increased slightly with increasing maximum particle size; whereas with a 1:1 mixture there was essentially no difference Holtz' size range studied, however, was from $\frac{3}{4}$" to 3". Hennes[66] studied narrower size distributions of rounded gravel and found

that tan ϕ increased appreciably with grain size up to $\frac{1}{4}$"; but beyond this there was little variation. However, apparently the grain shapes varied considerably within each sample and from sample to sample.

On the other hand Parsons[124] found that tan ϕ had a minimum value at a grain size of $\frac{3}{4}$" but again the results are inconclusive because particle shapes varied within the size ranges.

Kolbuszewski and Frederick[101], using glass beads from .48mm. to .86mm., again found that there was a minimum shear resistance reached.

Kirkpatrick[98] made sure that the sand used for his investigations was uniform in shape and mineralogy. He measured two values of the shear strength, one not corrected for dilation and one from the steady state situation. From the peak value he found that there was a decrease in the angle of friction with increasing size; but with the steady state value of ϕ, he concluded that there was no effect of particle size or grading. The difference implies that the effect of size is to modify the stress-strain characteristics rather than the frictional characteristics. Idel[86] also found no size effect when using glass beads and quartz sand, although he found considerable scatter in tan ϕ.

It appears, then, that although some authors give evidence indicating an increase of tan ϕ with size, there exists more and better evidence to suggest that tan ϕ is independent of particle size.

In the field of powder technology little emphasis seems to have been laid on the effect of particle size on the shear strength and tensile strength measurements. However, Cheng, Farley and Valentin[30] have made an attempt to correlate particle

size to the bulk properties of shear strength, cohesion and tensile strength. The materials examined were in the 0-10 micron range considerably smaller than for the studies reported earlier.

Using an empirical approach, a correlation was obtained relating the particle size of the material to the shear index n from the equation on page 21. The correlation is:-

$$n = 1 + \frac{B}{(d)^{\frac{2}{3}}}$$

where B = constant

d = volume/surface mean diameter

Cheng[29] has obtained a correlation for the theoretical effect of particle size on tensile strength. Cheng's particulate approach showed that the tensile strength was related to particle size parameters by the equation:-

$$T = abc\ \tfrac{1}{2}\ \frac{s}{\nu}\frac{\rho}{\rho_s}\ h(t)$$

a = ratio of the number of pairs of particles that are in contact per unit area

b = ratio of contact area to surface area

c = co-ordination number

s = mean effective surface area per particle

ν = mean volume per particle

ρ_s = density of powder particle

ρ = density of powder compact

h(t) = interparticulate force per unit area of contact

where $$t = t_o - \frac{d}{3}\frac{\rho}{\rho_o} - 1$$

t = mean surface separation

t_o = length parameter of interparticulate force

d = mean effective diameter per particle

ρ_o = density at which tensile strength vanishes

2.4.2.2. Shape Effects

It has long been recognised that the shape of individual particles has influenced the shear resistance. The constant B in Cheng, Farley and Valentin[30]'s equation is dependent on particle shape and would be about .7 for spherical particles and .4 for elongated particles.

Terzaghi and Peck[172] and Chen[27] have reported that angular sands give higher values of tan ϕ than rounded sands. Holtz[73] has stated that a reasonable range of angle of internal friction might be 22° to 45° for rounded sandy soils at low and high relative densities; and 27° to 52° for angular gravelly materials at low and high relative densities, respectively.

Morris[116] has attempted to separate shape effect from surface texture effects. By rounding the shape without altering the texture there is an increase in shear strength; and smoothing the texture without altering the shape results in a reduction in shear strength.

Mackey[112], also, notes that the shape of particles exercises a considerable influence on the limiting porosities of sand, in that spherical particles can also be compacted to a considerably greater degree than can angular particles.

In dealing with the flow through orifices many parameter models have been used to equate the equivalent and statistical diameters of particle systems to the mass flow rate through hopper outlets.

2.4.3. Statistical Models in the Strength Behaviour of Bulk Materials

Statistical approaches to the mechanics of granular materials have been used by Mogami[115] and his co-workers.

Expressions have been derived calculating the void ratio and the angle of internal friction. The probability approach to problems of soil mechanics was first suggested in the U.S.S.R. by Pokrovsky[126] in 1933. His fundamental principles were that the stress distribution in a soil is controlled by the laws of probability; and that the strength of soil is determined by the maximum local stress coinciding with the weakest points of the material, and statistically distributed over the whole sample of soil. However, in the process of this present survey statistical models have not been found to relate a statistical particle size measurement to the strength of the bulk material.

2.5. Other Approaches to the Mechanical Behaviour of Soils and Granular Materials

Winterkorn[197] has suggested that in shear, granular systems behave as macromeritic liquids. He has listed the main characteristics of the three principal states of matter alongside those of an assembly of sand or gravel particles; and shows how a large number of the characteristics for liquids and grain assemblies are similar. He also mentions the known fact of matter changing to a different state at the "critical conditions". At these critical values the volumes occupied by a certain amount can be expressed in proportions that are approximately the same for many different materials. Using spheres he sets out to show that the void ratio for tetrahedral packing, the most stable for uniform spheres, is identical to the boiling state of tetrahedral packing, and that the critical void ratio and melting point void ratio are also similar, thus showing that in shear, granular systems behave as macromeritic liquids. The comparison with ordinary molecular liquids gave rise to the

following equation:-

$$\tan \phi = \frac{C'}{V-V_{min}}$$

which is equivalent to:-

$$\tan \phi = \frac{C}{e-e_{min}}$$

C', C = constants

e = void ratio

V = volume of the system in the given state

e_{min}, V_{min} = the corresponding values with the system in the densest state

Winterkorn found that the value of C was approximately constant provided the same type of test was used.

Mitchell[114] has suggested that the shear resistance of a soil at a fixed void ratio is a function of frictional and cohesive properties, effective stress, rate of strain and temperature. Using the theory of rate processes he has derived an equation relating these factors to shear stress.

Having considered in this chapter the existing links between the macroscopic, state and microscopic properties, in chapter 3 a statistical model is proposed to relate a statistical particle size measurement to a macroscopic property.

CHAPTER 3

THEORY

CHAPTER 3:- THEORY

In chapter 2 the various particle size diameters have been discussed with special reference to their relevance and limitations in characterising a particulate material. The two basic types of diameter are an equivalent sphere diameter and a statistical diameter.

In general these diameter distributions have been described by a mean size and a standard deviation; and, then, related to macroscopic behaviour by experimentally determined constants.

In this present chapter, however, consideration is given to the possibility of getting a direct relationship between the macroscopic property of the porosity at the critical state and a statistical size distribution.

Up to the present, the primary unit of a particle system has been considered, in general, to be a particle, with all its added complications of size and shape. However, a particle can be, itself, characterised by two further subdivisions. Firstly, it can be considered to consist of laminae; and, secondly, to consist of filaments. The concept of considering laminae and filaments of matter, belongs to the science of Stereology. Before considering the specific application of Stereological principles to the behaviour of particulate matter, a review of its general principles and applications will be given.

3.1. Review of the General Principles and Application of Stereology

3.1.1. Definition of Stereology

"Stereology[43] is the three dimensional interpretation of

flat images or the extrapolation from two to three dimensional space". That is, it is the science of relating dimensional sections of matter to the total dimensions of the system.

Weibel[188] has pointed out, however, that there are several degrees of sectioning. For a solid structure the following can be obtained:-

i. a three dimensional section

ii. a two dimensional section, which is a true section

iii. a one dimensional section, when a line intersects the solid

iv. a zero dimensional section, represented by a set of points

The effects of these four degrees of sectioning are shown in figure 3.1. for a volume, V, of surface, S; for a lineal element, L; and for a number of points, P.

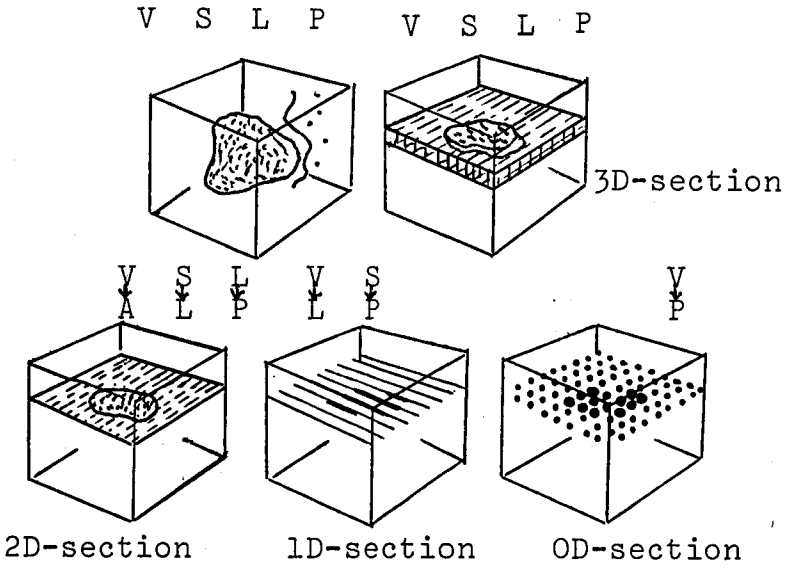

Figure 3.1. Effect of sectioning on structures (Weibel[188])

For the volume, the stages of sectioning go from volume to area to length and, finally, to points; that is from 3D sectioning to zero D sectioning.

It is interesting to note that Stereology has been used in the arts for forming decorative sectioned textures,[161]

Before considering the application of Stereology to Powder Technology, we shall consider its use in Morphometry which is the detailed quantitative study of the structure of organs and tissue systems, and also in the geological field.

Weibel[187] has given an excellent review of the principles and methods of Morphometry and the use of Stereology. In general, Morphometry makes use of statistical procedures; and, although statistics demand random conditions for analysis, biological structures have a high degree of organisation.

Weibel justifies the use of statistical procedures by the consideration of the following aspects regarding randomness. Firstly, random distribution of structures in space can be assumed if the units under investigation do not exhibit any stratified array in a particular volume, even though they may well be organised into units of higher order. Secondly, the randomness only refers to a specified part of the structure; and, thirdly, it is necessary to specify the degree of randomness.

The question arises, in the first instance, of how a two dimensional sample of a three dimensional system can be quantitatively representative of the composition of the structure. In 1847 Delesse,[41] a geologist, answered the question by proving that the mean surface fraction of a component present in a representative slice is an estimate of the volume fraction in the whole system.

Rosiwal[144], in 1898, extended the principle by demonstrating that the fraction of any line passing through one component of a randomly distributed system is an estimate of the volume fraction occupied by that component.

Weibel[187] further extended the principle to the section case and showed that, if a set of points was distributed over a tissue plane, the fraction of points lying on one component was an estimate of the volume fraction of that component.

The proofs are given in appendix A.1.

The measurement of fractions of length is an easier task than the determination of surface fractions; and developments in the geological field have been along the former lines. Mechanical computing devices developed by Shand[155], Wentworth[190], and Schumann[154] have enabled this type of Stereological analysis of the mineral composition of rocks; and in 1948, Gerstal[55], used these devices to analyse histological sections. These devices lacked accuracy and in 1954 Schuchardt[153] devised an integrating eyepiece, later manufactured by Weitz, which consisted of the movements of a cross wire, mounted in the eyepiece, being recorded on a set of micrometer heads.

The point-counting principle was first applied to a volumetric analysis of a three dimensional system by Glagoleff[57], a geologist, in 1933. In 1943 it was used histologically by Chalkley[25] but, at that stage, it was rather cumbersome. Haug[63] and Hennig[67] made efficient point-counting more feasible by using, respectively, a square grid of 121 points and a triangular lattice of 25 points on an eyepiece graticule.

It can be said that values of the transection fraction and point fraction are estimates of the volume fraction. With small volume fractions the precision is lowered rather than

increased.

When the thickness of the section is significant compared to the size of the object, the transection fraction measurements are subject to an error described by Holmes[72] and quoted by Weibel.[187]

Weibel and Gomez[189] have further developed the principle to show that the number of transections of objects found in a unit area of a random slice is related to the number of objects contained in a unit volume. They showed that this relationship depended on the volume fraction and the shape of the objects.

Measurements obtained on random sections generally do not correspond directly to a characteristic dimension. Equal sized spheres will give a distribution of chords and it is possible to relate the set mean chord length to the true radius. The more complex relationship of a size distribution has been studied by Wicksell[195] and by Lenz.[108]

Application of chord size measurements to the determining of the total surface of a component has been used by Tomkieff,[178] Hennig[67] and Chalkley et al[26] using a combination of the point-counting principle and surface determination by "mean chord length". If a line of known length is thrown on a random section, the surface-to-volume ratio can be estimated from the number of "hits" of the bodies under consideration by the end-points of the line and from the number of intercepts of the line with their surface.

In considering the sampling of material for statistical analysis in quantitative Stereology, DeHoff[40] has indicated that there can be two basic kinds of structural inhomogeneity in a system, which can effect the sampling of the population: variation of geometric properties with orientation, that is

anisotropy, and variation of geometric properties with position, that is structural gradients. The basic relationships of quantitative Stereology assume that the population which is to be sampled is uniformly distributed in both position and orientation. Considering figure 3.2. of an isotropic structure containing a one dimensional gradient. Depending on the direction of the section, the section contains the direction of the gradient or, on the other hand, the area fraction can vary from 0 to 1.00 depending on the position of the sectioning plane. With more complicated gradients, for example a three dimensional twisting pattern of properties, the volume must be sampled by a set of planes uniformly distributed in position in order to obtain a representative sample.

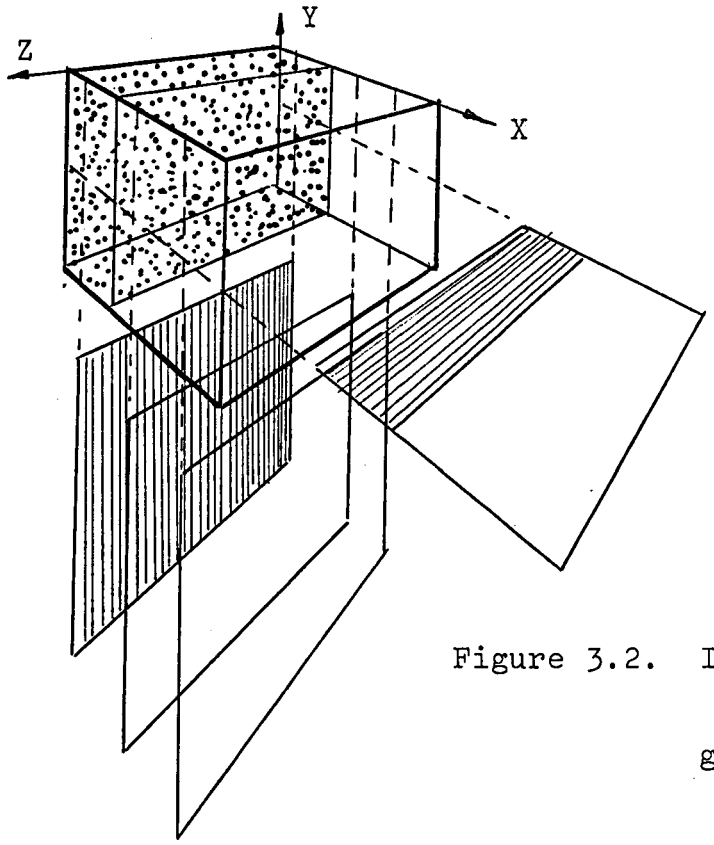

Figure 3.2. Illustration of a structure with a one-dimensional gradient in volume fraction.

Considering now figure 3.3. which shows an illustration of anisotropy in particle size. A system may be relatively uniform in the distribution of its geometrical properties with position, but the particles in such a system may be elongated or

flattened in a preferred direction. Again, therefore, to obtain a representative sample it is necessary to obtain a set of sectioning planes which have orientations that are uniformly distributed in space. DeHoff[40] has also given an indication of the number of points, lines or sections it is necessary to measure to seek a desired accuracy; but he points out that it is necessary to seek an optimum between the accuracy desired and the effort expended in terms of the number of observations deemed practical.

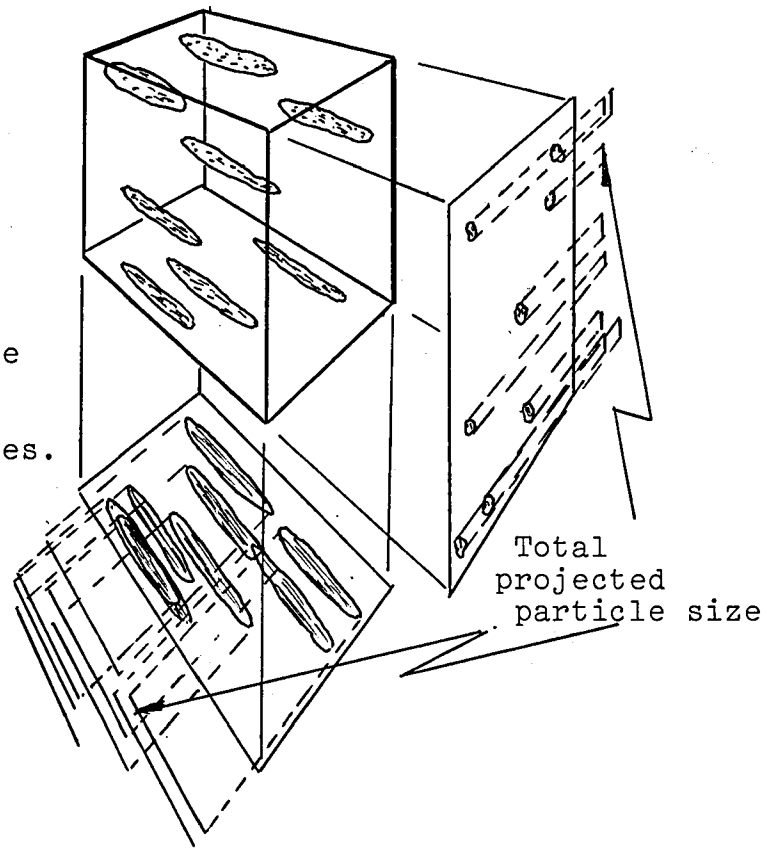

Figure 3.3.
Illustration of anisotropy in particle size in an sample of non-spherical particles.

Hilliard[71] has described methods for specifying and measuring the degree of anisotropy in two and three dimensional arrays. He uses distribution functions and describes the methods for determining these functions from measurements on sections through structures. He points out that the analysis of anisotropy in the third dimensional case is too tedious to be feasible unless an automatic scanning instrument is used.

3.1.2. Application of Stereology to Particle Technology

In a quantitative evaluation of sectioned material, Underwood[181] has outlined the basic symbols and equations used in Stereology; and has compared the length to area and surface to volume relationships derived by Saltikov[148], Tomkieff[178] and Chalkley[25], including those for a system of particles. Saltikov[147] uses a Stereological method for measuring the specific surface of metallic powders and points out the advantage over the indirect methods such as gas adsorption. Saltikov[146], Bach[8] and Myers[117] have determined the size distribution of particles from studies of their sections. However, in most cases, the sizes considered are those of regular particles.

Many attempts[58,198,16,160] have been made to calculate the properties of packed particle systems from a knowledge of the particle size distribution of the system. Recently Rumpf and Debas[145] have used a Stereological approach and have shown that some properties of a packed system of spheres can be derived by considering the distribution of random, cross-sectional areas. To verify their ideas experimentally, they packed the system under investigation into cylinders and filled the voids of the packing with an epoxy resin under vacuum. When these had cured, sections were machined. Rumpf and Debas' analysis for random cross-sectional areas of irregular particles still has to overcome the problem of defining their size to account for their shape.

The basic limitation of the definition of Stereology is that it restricts the application of the science to the microscopic properties of the system, such as the measurement of specific surface. However, the present study seeks to show that Stereology has a much wider definition in that, from an analysis of dimensional sections of a material, the bulk and

behavioural properties can be directly determined.

3.2. Application of Stereology to the Flow Behaviour of Particles

3.2.1. Introduction

The primary units of a system of particles are here considered to be laminae and filaments. A lamina of a particle is defined as a lamina lying on and having the area of a randomly orientated plane, lying within and cutting through the particle. Similarly, a filament is defined as that part of a particle lying on the chord bounded by the particle on a line passing through the particle in a random direction. These definitions are illustrated below in figure 3.4.

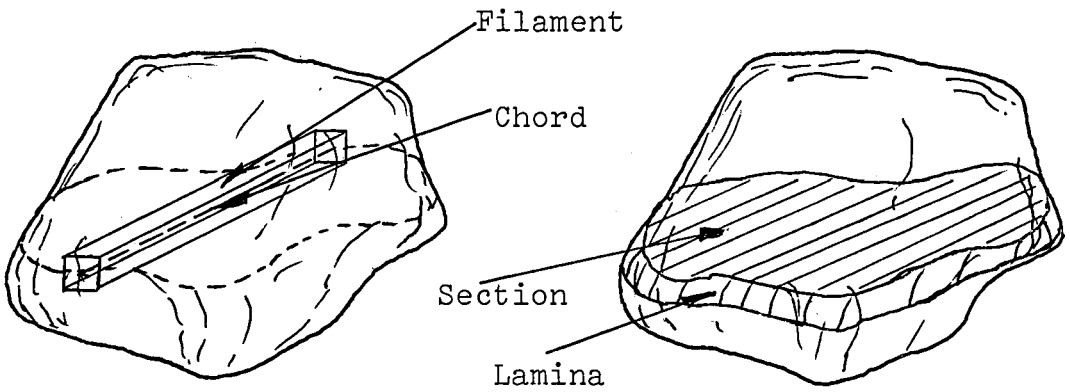

Figure 3.4. Primary Units of a Particle

A lamina has dimensions of volume, while a section has dimensions of area; but when the thickness of the lamina tends to zero, the lamina tends to a section. In the same way a filament has the dimensions of volume, with a length l and cross-sectional area dz. As dz tends to zero, then a filament tends to a chord with only dimensions of length.

Through one particle an infinite number of sections can be drawn, each particle having a lamina size distribution; and

therefore, for a total bed of particles there is a total lamina size distribution. The number size distribution of the lamina is, therefore, a unique characteristic of the bed of particles. In a similar way, through one particle an infinite number of chords can be drawn in all directions, each particle thus having a filament size distribution. For a total bed of particles there is, therefore, a total filament size distribution. The number size distribution of the filaments is, therefore, also a unique characteristic of the bed of particles.

From these distributions it is possible to calculate many macroscopic and behavioural properties of a packed system; because, being one and two dimensional bodies respectively, these laminae and filaments are more amenable to statistical treatment than are the particles themselves.

An example of the use of the filament distribution is in the description of the phenomena of flow through packed beds.[17] Recently, also, Scarlett and Eastham[149] have used it to describe the propagation of stress due to vibration. Similarly, an example of the use of the lamina distribution is that of Scarlett et al[150] who have applied it to the electrical and thermal conductivities of powders.

The description of other behavioural properties of a material may well require the use of a particle volume distribution; while, in some cases, all three distributions may be necessary. It is suggested, therefore, that for the complete characterisation of a system the following distributions are required:-

number : filament (as a chordal measurement)

number : lamina (as a sectional area measurement)

number : particle volume.

The following theory shows how the number filament distribution of a bed of particles can be used to predict the macroscopic property of critical porosity, thus relating the state of packing in the steady state condition to a microscopic property of the system.

When referring to the actual particles, the fundamental elements are here termed filaments; but when referring to their measurements the elements are termed chords.

3.2.2. Relation of Filament Size to Critical Porosity

Consider a three dimensional bed of particles. It is unimportant whether the particles are touching or widely spaced but the array must be isotropic, that is, completely random as to the position and orientation of the particles. Considering figure 3.5., if this array of particles is cut by a straight line then the line will consist of a number of chords and spaces.

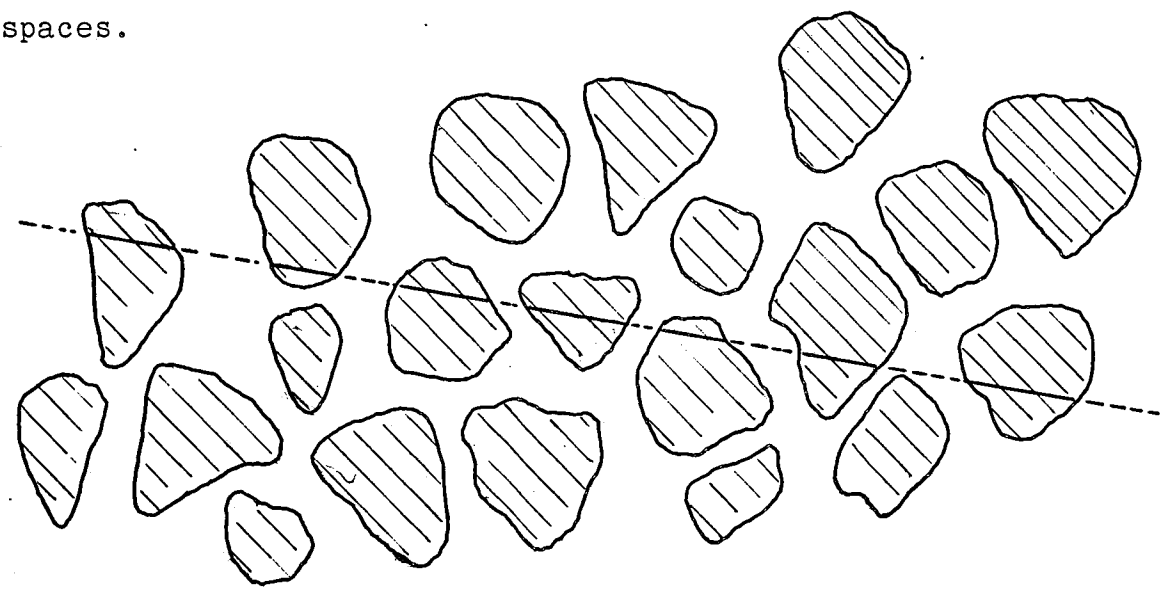

Figure 3.5. Random Chord Distribution

If a sufficient number of lines are passed through the array then the size distribution of the chords thus produced characterises the system. It is also equal to the filament size distribution because, although the chord has dimensions of length only and the filament has dimensions length^3, as dz tends to zero the filament tends to a chord. Therefore, filaments are considered with respect to the particles and chords to the actual measured parameter, the two being of equivalent length. As the number filament distribution of the particles characterises the particles, so the number distribution of the chords passing through the pores characterises the pores. However, when the packing of a particle bed changes, although the pore chord size distribution changes, the particle filament size distribution remains constant. In other words, the particle filament distribution is independent of the state of packing of the material.

Consider, now, the particles in a zone of shear in a shear cell. The bed of particles can be pictured, not as an array of particles, but as an array of filaments, lying in all directions. The absolute number of filaments is not important although their size distribution must be the size obtained from a statistically representative sample of chords.

If, now, only the filaments lying in a vertical position are considered, the critical porosity can be considered by predicting the porosity at which the vertical filaments move relative to each other. This situation is represented in figure 3.6.

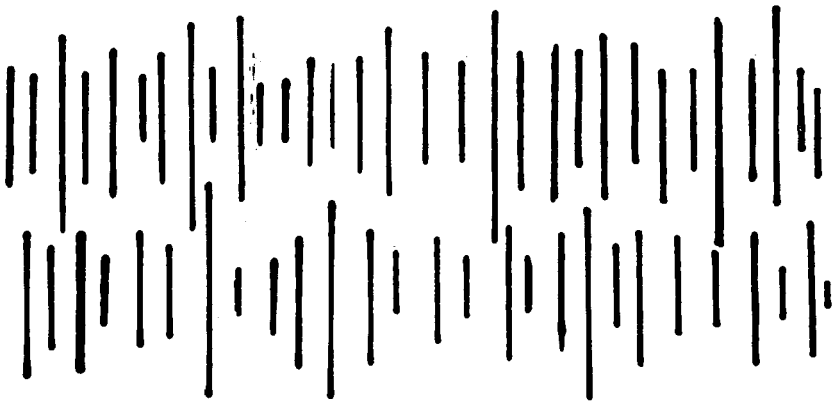

Figure 3.6. Representation of a bed of particles by random filaments.

The following assumptions are made in the calculation:

i. The bed is completely random. That is there is no regular packing of the bed, any particle has equal chance of being at any point within the bed and there is no particle segregation.

ii. The bed is isotropic which means that, if a sufficiently long line is taken, the same chord size distribution is obtained from different directions in the bed. The total chord length to total length of line is independent of the direction of the line; and this ratio, as shown by Rosiwal[144] and given in appendix A.1., is equal to the ratio of solids volume to total volume of the bed.

Let f(x) represent the number distribution of the filaments of length x. If this distribution is normalised then:

$$\int_{0}^{x_{max}} f(x)dx = 1$$

If the bed is isotropic:

$$\int_{0}^{x_{max}} f(x)xdx = 1 - \varepsilon$$

where ε is the porosity of the bed.

When a shear force is applied to a bed of particles, and the shear force is sufficient to overcome the sliding friction of the particles, the particles move relative to one another in a complicated fashion as a function of depth. (Figure 3.7.).

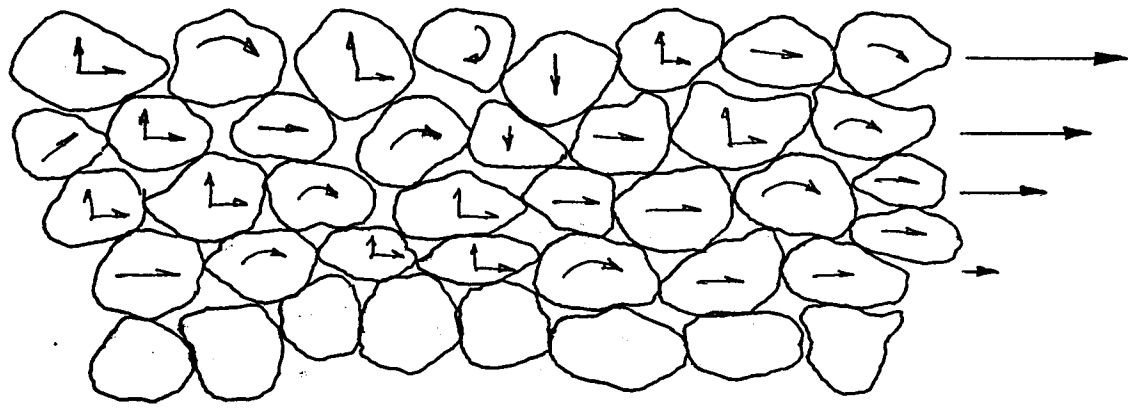

Figure 3.7. Representation of complicated particle movement in a region of shear.

Considering figure 3.7., the particles have three possible movements as follows:-

i. They may move at right angles to the direction of shear in order that they may pass.

ii. They may have relative motion in the direction of shear simply because they do not overlap.

iii. They may roll in order to present a smaller dimension at right angles to the plane of shear. Alternatively, the particles may rotate in the plane of shear such that the maximum dimensions of the particles effectively side-step each other.

The equivalent filament movements are:-

i. Figure 3.8. is a representation of the layers of filaments in a region of shear. Before calculating the

separation of the layers at the flowing condition, it is necessary to allow for the fact of vertical filament motion due to overlap. As one filament can contribute to two separation volumes a further sectioning of the filaments is required.

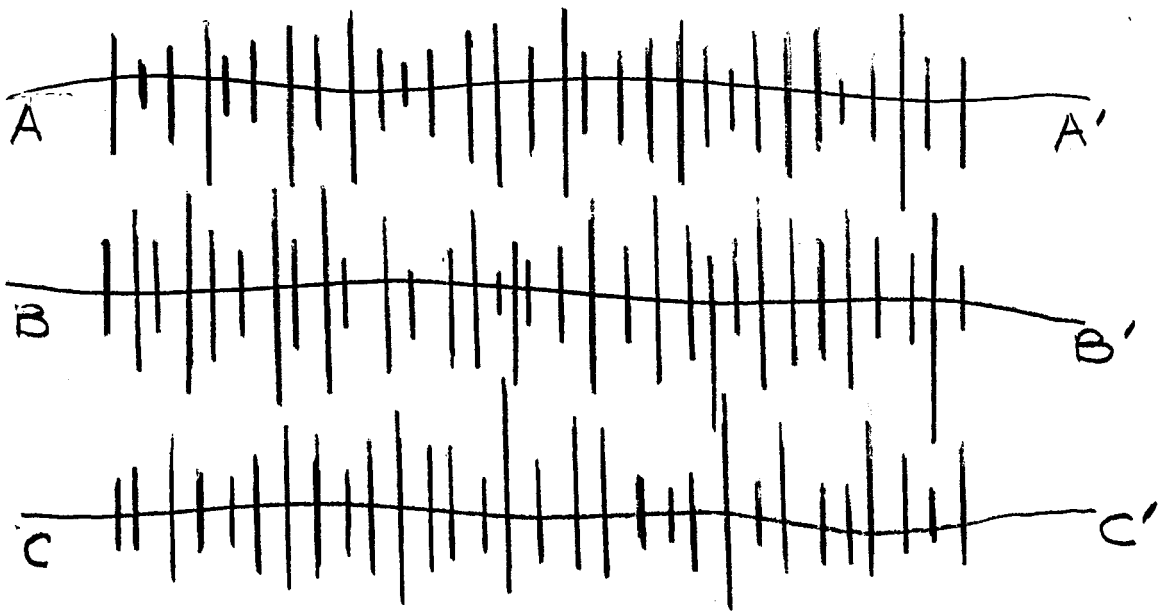

Figure 3.8. Representation of sectioned filaments contained in a critical volume.

The diagram shows three typical layers of filaments and that the centre layer contributes to the separation of both AA' from BB' and BB' from CC'. For this reason the size distribution of the chords cannot be used directly to calculate the critical porosity. Instead, the size distribution of chords which have again been sectioned by a random line must be considered. The motion may be considered to be the relative movement of two sets of sectioned filaments contained within the distance AA' and BB'. The filaments are sectioned so that the size distribution of the filaments is the same on both sides of each line; and the volume of the bed considered contains the random sectioned filament distribution.

Considering the figure 3.9. below:-

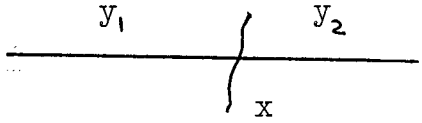

Figure 3.9.

A filament of length x can contribute to the two volumes 1 and 2 forming the sectioned filaments of length y_1 and y_2.

The probability of sectioning a filament between 0 and x/2 is $\frac{1}{2}$. (Figure 3.10.)

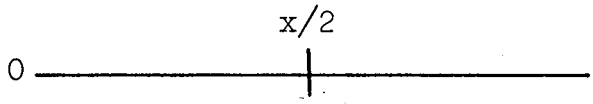

Figure 3.10.

The probability of sectioning a filament between a position y and y+dy is: (Figure 3.11.)

$$p(y)dy = \frac{dy}{x} \quad \text{if } 0<y<x$$

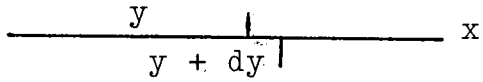

Figure 3.11.

Obviously no sectioned filament can be formed of greater length from a filament of smaller length, that is:-

$$p(y) = 0 \quad \text{if} \quad y>x$$

Let g(y) be the number distribution of sectioned filaments of length y. Therefore, the total probability of a sectioned filament y is given by:-

(probability of y from x) × (the probability of x)

that is:

$$g(y)dy = \int_{x=y}^{x=x_{max}} p(y)dy.f(x)dx$$

therefore:

$$g(y)dy = \int_{x=y}^{x=x_{max}} \frac{f(x)dx.}{x}dy \quad . \quad . \quad . \quad . \quad (1)$$

This equation represents the distribution of the sectioned filaments.

ii. The filament size distribution and the sectioned filament size distribution must span a range of sizes from 0 to x_{max}. Considering then the criterion that the particles may have relative motion because they do not overlap. Clearly, if the two sectioned filament layers were separated by $2.x_{max}$, then the system could flow. However, in such a situation the bed would be unstable, and it is not necessary for the separation to be so large because the filaments can change position, as postulated above, either by vertical movement of the particles, or by their rotation so that the fouling longer filaments become horizontal.

As often observed, even if the bed starts to flow at any open spacing the movement of the particles will produce an average spacing of the sectioned filaments which is less than x_{max}. At such a condition, the smaller filaments are undisturbed and pass without interference; while the large ones pass by either lateral movement or by change of position with smaller filaments. This latter corresponds to particle rolling.

iii. The fact that the particles may roll in order to present smaller dimensions at right angles to the plane of shear is considered to be that which determines the critical distance between two layers of sectioned filaments if the filaments which overlap are able to become horizontal or to side-step in order to pass.

When however, a change of position takes place, because the overall porosity and size distribution of the filaments must remain constant, then a vertical filament changing its position to a horizontal position, must be replaced by another filament from the horizontal. Considering this change of position to represent particle rotation, because the total volume of

particles in an element of the bed must remain constant, then the same total length of filaments must interchange locally. This is so if the particles are irregular and do not have a preferential orientation.

Thus the criterion for flow is that the total length of the sectioned filament lengths which are less than the critical value of the separation, must be equal to the total length of those which are greater. This critical value is the median value of the sectioned filament distribution. So then if a filament overlaps another filament a longer filament may be replaced by the same length in smaller filaments. On rotation the particle volume remains constant so then the total length of filament must remain constant. Because of this, since the sectioned filament distribution remains constant on both sides of the sectioning line, the sectioned filaments will be replaced on a total length basis.

If now the sectioned filaments in one vertical plane of width dz are arranged in order of size, the new arrangement of the sectioned filament size distribution is equivalent to a cumulative percentage curve. (Figure 3.12.).

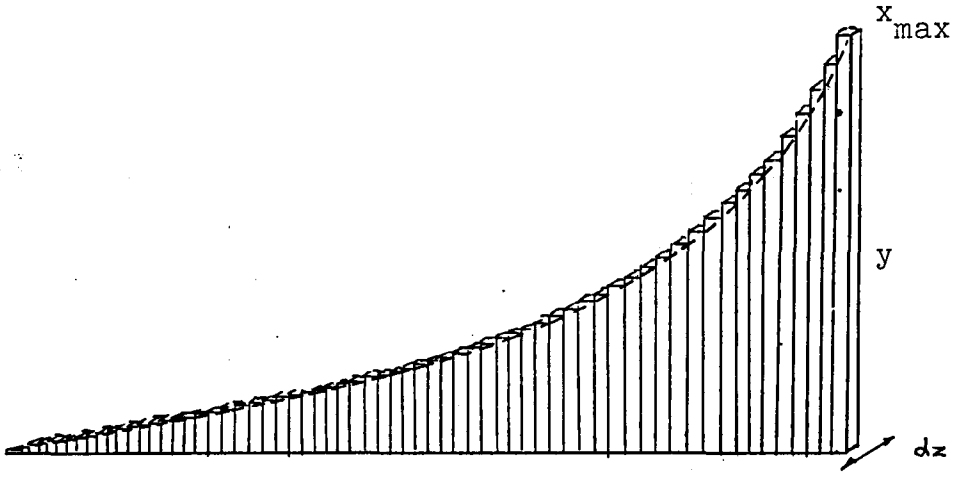

Figure 3.12. Sectioned filaments arranged in order of size.

The critical porosity can now be considered from the separation of two layers of sectioned filaments, arranged on a cumulative basis. (Figure 3.13.).

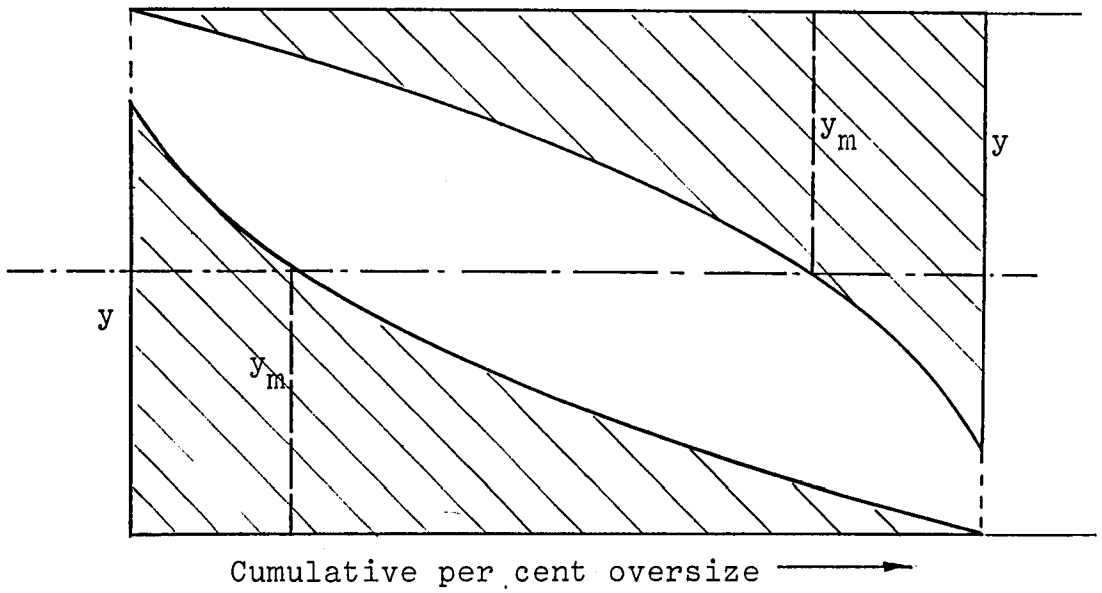

Figure 3.13. Condition for Flow

y_m is termed the median value and the two curves may move relative to one another when separated by $2.y_m$. The total length of sectioned filament greater than y_m is equal to the total length of sectioned filament less than y_m, that is:-

$$\int_{o}^{y_m} g(y)ydy = \int_{y_m}^{x_{max}} g(y)ydy \quad . \quad . \quad . \quad (2)$$

So then, considering figure 3.13, the critical porosity is given by the ratio of free area in the diagram to the ratio of the total area in the diagram, since the fractional length occupied by the chords in a random plane has been shown (appendix A.1) to be the same as the fractional volume occupied by the particles.

The area occupied by the filaments in the diagram is simply the first moment of the distribution:

$$A_{sc} = 2.\int_{o}^{x_{max}} g(y)ydy \quad . \quad . \quad . \quad . \quad (3)$$

The total area occupied by the diagram is given by:-

$$A_T = 2.y_m \int_{o}^{x_{max}} g(y)dy \quad . \quad . \quad . \quad . \quad (4)$$

assuming that the sectioned filament distribution is normalised such that:

$$\int_{o}^{x_{max}} g(y)dy = 1$$

therefore:

$$A_T = 2.y_m$$

then the critical porosity is now given by:

$$1 - \varepsilon_c = \frac{A_{sc}}{A_T}$$

where ε_c = critical porosity at which the system will flow.

Therefore:

$$1 - \varepsilon_c = \frac{2.\int_{o}^{x_{max}} g(y)ydy}{2.y_m}$$

that is:

$$1 - \varepsilon_c = \frac{\int_{o}^{x_{max}} g(y)ydy}{y_m} \quad . \quad . \quad . \quad . \quad (5)$$

The theory just proposed assumes three basic assumptions:

i. The bed is random

ii. The bed is isotropic

iii. There is no segregation

The application of the theory to the conditions where these assumptions are not adhered to will be considered below.

3.2.3. Systems not Adhering to the Basic Assumptions

3.2.3.1. The Critical Porosity of Monosize Spheres

It is known that monosize spheres will arrange themselves into an ordered array rather than an irregular random pattern. The application of the proposed theory will now be considered for monosize spheres.

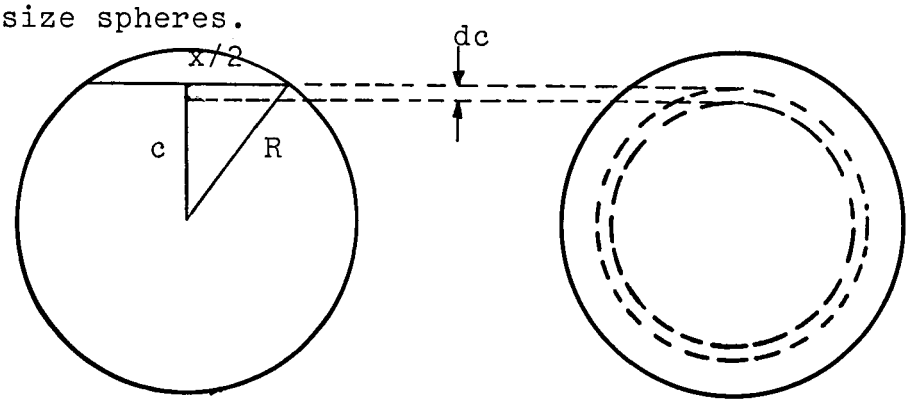

Figure 3.14. Chord Size Distribution for Spheres

The calculation is considered in five parts:-

i. The calculation of the chord size distribution for monosize spheres f(x):- Consider the projected area of a sphere at right angles to the direction of the random line forming the chord. If the line passes through the projected area at distance c from the centre, the length of the chord produced is given by:-

$$\frac{x^2}{4} + c^2 = R^2 \quad . \quad . \quad . \quad . \quad (6)$$

This is illustrated above in figure 3.14. From this diagram considering a small element dc, the probability of a chord of length x is given by the ratio of the area enclosed by the annulus of radius c and width dc to the total projected area of the sphere.

That is:- $$f(x)dx = \frac{2\pi c dc}{\pi r^2}$$

From equation (6):-

$$xdx = -4cdc$$

Therefore:

$$f(x)dx = -\frac{xdx}{2R^2} \quad . \quad . \quad . \quad . \quad (7)$$

The negative sign indicates that x is decreasing as c increases and can be dropped if dx is considered to be positive.

Integrating equation (7) between the limits 2R and 0 gives:-

$$\int_0^{2R} f(x)dx = \int_0^{2R} \frac{xdx}{2R^2}$$

$$= \left[\frac{x^2}{4R^2}\right]_0^{2R}$$

$$= 1$$

ii. To calculate the sectioned filament size distribution represented by g(y):- From equation (1)

$$g(y) = \int_{y=x}^{y=x_{max}} \frac{f(x)dx}{x}$$

Now from equation (7):

$$f(x)dx = \frac{xdx}{2R^2}$$

therefore:

$$g(y) = \int_{y=x}^{y=x_{max}} \frac{dx}{2R^2}$$

therefore:

$$g(y) = \left[\frac{x}{2R^2}\right]_y^{y=x_{max}}$$

therefore:

$$g(y) = \frac{1}{2R^2}\left(2R - y\right) \quad . \quad . \quad . \quad . \quad (8)$$

Therefore the total sectioned filament distribution is given by:-

$$\int_0^{2R} g(y)dy$$

$$= \frac{1}{2R^2}\int_0^{2R}(2R - y)dy$$

$$= \frac{1}{2R^2}\left[2Ry - \frac{y^2}{2}\right]_0^{2R}$$

$$= \frac{1}{2R^2}\left[4R^2 - \frac{4R^2}{2}\right] - 0$$

$$= 1$$

Therefore:-

$$\int_0^{2R} g(y)dy = 1$$

iii. The area enclosed by the cumulative distribution of y:-

The area enclosed by the cumulative distribution curve is as given in equation (3):-

$$A_{sc} = \int_0^{x_{max}} g(y)ydy$$

Substituting equation (8):-

$$A_{sc} = \frac{1}{2R^2}\int_0^{2R}(2Ry - y^2)dy$$

$$= \frac{1}{2R^2}\left[Ry^2 - \frac{y^3}{3}\right]_0^{2R} \quad . \quad . \quad . \quad (9)$$

$$= \frac{1}{2R^2}\left[4R^3 - \frac{8R^3}{3}\right] = \frac{2R}{3} \quad . \quad (10)$$

iv. To calculate the median value of g(y) which is represented by y_m:- From equation (2)

$$\int_0^{y_m} g(y)ydy = \int_{y_m}^{x_{max}} g(y)ydy$$

Therefore for monosized spheres using equation (9):-

$$\left[Ry^2 - \frac{y^3}{3}\right]_0^{y_m} = \left[Ry^2 - \frac{y^3}{3}\right]_{y_m}^{2R}$$

$$2\left(Ry_m^2 - \frac{y_m^3}{3}\right) = \frac{4R^3}{3}$$

Thus:-

$$\frac{2y_m^3}{3} - 2Ry_m^2 + \frac{4R^3}{3} = 0$$

Therefore:-

$$\left(\frac{y_m}{R}\right)^3 - 3\left(\frac{y_m}{R}\right)^2 + 2 = 0$$

The real solution to this equation is:-

$$y_m = R$$

v. To calculate the critical porosity of a bed of monosized spheres which will be represented by ε_c:- The critical porosity is given by:

$$1 - \varepsilon_c = \frac{A_{sc}}{y_m}$$

From equation (10):

$$A_{sc} = \frac{2R}{3}$$

Therefore:

$$1 - \varepsilon_c = \frac{2}{3}$$

Therefore:

$$\varepsilon_c = \frac{1}{3} \simeq 33\%$$

3.2.3.2. The Critical Porosity of an Anisotropic Bed

Although the basic model assumes the bed is isotropic, the model will be adjusted to account for anisotropy. However, before considering this adjustment a review of the literature on anisotropy will be discussed.

In reply to the discussion on a paper of his, Rowe[141] has said that soils, in general, are anisotropic, the anisotropy resulting from the stress system during deposition.

Housel[81], in 1936, while discussing some inconsistencies in internal friction theory, states that the assumption of isotropy had been violated because of the equivalent introduction of preferential planes of weakness. His opinion was that the assumption of isotropy must be given up when dealing with materials exhibiting granular characteristics.

Rowe[141] stated that according to Horne[76] it is incorrect to make the assumption that a particular anisotropic condition can be assigned to a granular mass. The property is a function of the void ratio and particle shape, but also according to Horn[75], depends on the shear stress system imposed.

One of the basic assumptions of most continuum theories is that at all times the material is isotropic. Rowe considers this a big criticism for the continuum approach; and he indicates that, from the work of his group, sands are initially anisotropic, and that interparticulate slides occur during an increase in mean principle stress even under isotropic stress conditions. One of the Cambridge group, Arthur[4], however has postulated that some form of anisotropy developes during tests on granular media. However, the group avoided introducing the complication caused by anisotropy into their theoretical work until they had reliable evidence that it should be taken into

account.

Roscoe[139] suggests that the particulate or microscopic approach is useful when thinking of anisotropy, especially with respect to two types:- (i) the development of preferred orientation of contacts, during yield with respect to the principle stress directions, such as can occur in uniform spheres and, (ii) the preferential orientation of the longer axes of non-spherical particles. The preferential orientation entails rotation of particles, which Roscoe et al have observed to be up to 15^{o} for dense sands.

Rowe[141] agrees with Arthur's comment but says that he will not try to avoid anisotropy, because it is a fundamental result of placing particulate matter under a stress system.

Horne[77], confining himself to uniform spherical particles, has described the state of anisotropy in an irregular assembly. He considers the MPSP, or mean projected solid path, through a particle in the three co-ordinate directions. The MPSP is the ratio of the length of solid line through the particulate contacts to the number of particles. The ratio he defines as m_1, m_2 and m_3 for the three OX, OY and OZ directions. For isotropy $m_1 = m_2 = m_3$, but, for anisotropy the ratios are not necessarily identical. Hence the ratios m_2/m_1 and m_3/m_1 can be regarded as packing characteristics for anisotropic assemblies. He derives expressions for the rates of strain in the principle directions in terms of the frequency and intensity of sliding between particles.

The state of anisotropy is derived by considering the formation of new contacts and a strain rate ratio is deduced:-

$$\frac{\sigma'_1}{\sigma_3} = \frac{4}{\pi}\frac{m}{m_2}^{1}\tan\left(\tfrac{1}{4}\pi+\tfrac{1}{2}\phi_\mu\right)$$

thus relating the degree of anisotropy as measured by the ratio m_1/m_3 to the stress ratio σ'_1/σ_3. The anisotropy is caused by the preferential directions of slidings, such that when sliding moves from the critical direction, the ratio m_1/m_3 decreases causing a decrease in the ratio σ_1/σ'_3.

Horne suggests that the complete behaviour in a triaxial test, on which his work is based, can be explained in terms of the degree of induced anisotropy.

It is suggested that for a bed of particles in which anisotropy occurs due to particle shape, the maximum filament is greater than twice the median value of the sectioned filament size distribution. The condition is illustrated in figure 3.15. below.

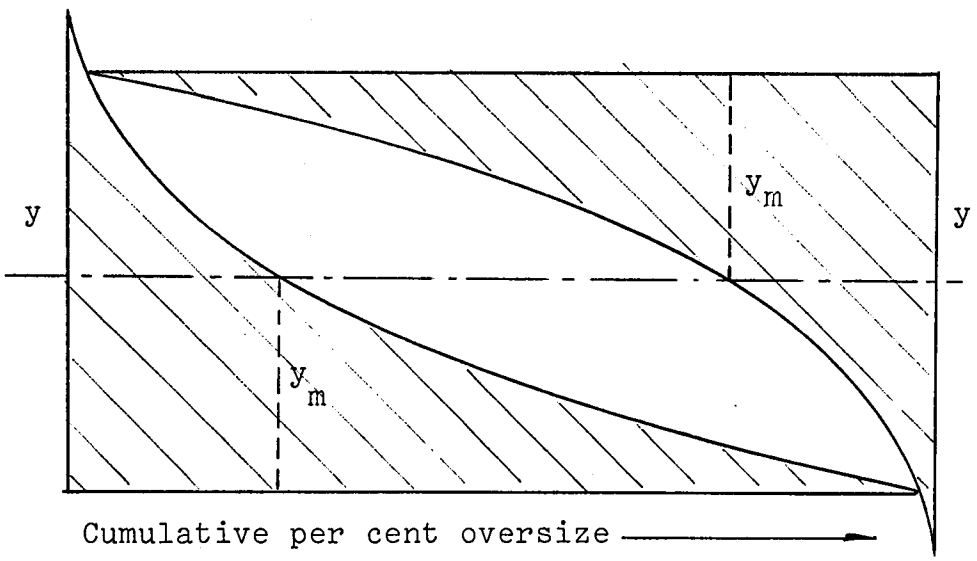

Figure 3.15. Condition for Preferential Particle Alignment

It is suggested that in this case the tendency will be for the particles to preferentially orientate themselves such that the longest filaments will lie in the direction of shear, that is the bed will become anisotropic.

Consider a bed in which the particles are preferentially orientated with their longest axes in the plane of shear. The sectioned filament size distribution obtained from measuring the chords, obtained by drawing a line in the plane of shear, is "skewed" towards x_{max} when compared to the distribution for an isotropic bed; and vice versa for the distribution of filaments perpendicular to the plane of shear.

Let $g_1(y)$ be the number distribution of sectioned filaments perpendicular to the plane of shear. Let $g_2(y)$ be the number distribution of sectioned filaments parallel to the plane of shear.

If the bed is anisotropic, considering equation (2):-

$$\int_{y_{m_1}}^{x_{max}} g_1(y)ydy \quad < \quad \int_{o}^{y_{m_2}} g_2(y)ydy$$

where y_{m_1} and y_{m_2} are the respective median values.

The critical porosity is not given by either y_{m_1} or by y_{m_2}. The critical separation is given when the long filaments of the perpendicular distribution can be replaced by the same total length of shorter filaments from the parallel distribution. (Figure 3.16.)

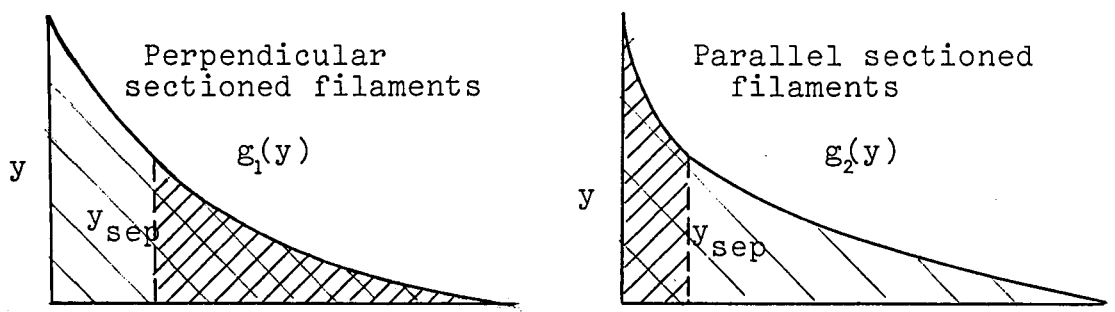

Figure 3.16. Condition for Flow with Anisotropy

If y_{sep} is the critical separation for the anisotropic case, y_{sep} is given by:-

$$\int_{o}^{y_{sep}} g_2(y)ydy = \int_{y_{sep}}^{x_{max}} g_1(y)ydy \quad . \quad . \quad . \quad (11)$$

Clearly: $$y_{m_1} < y_{sep} < y_{m_2}$$

The critical porosity, then, for an anisotropic bed will be given by the separation y_{sep} of the perpendicular sectioned filaments. That is:-

$$1 - \varepsilon_c = \frac{\int_{o}^{x_{max}} g(y)ydy}{y_{sep}} \quad . \quad . \quad . \quad . \quad (12)$$

Eventually it may be found that a filament analysis could be used in defining the degree of anisotropy in a bed of particles by the ratio of:-

$$\frac{\int_{o}^{x_{max}} f_1(x)xdx}{\int_{o}^{x_{max}} f_2(x)xdx}$$

and

$$\frac{\int_{o}^{x_{max}} f_1(x)xdx}{\int_{o}^{x_{max}} f_3(x)xdx}$$

where $f_3(x)$ is the filament distribution in the parallel plane at right angles to the direction of shear.

This is similar to the MPSP of Horne, but using irregular particles instead of spherical ones. Unlike Horne's analysis it takes into consideration not only structural gradients, which would be the case for spherical particles in an anisotropic state, but also anisotropy due to variation of

particle length with orientation.

3.2.3.3. The Critical Porosity and Segregation

It is known that in certain flowing conditions, such as the flow of materials in a hopper[183], in a drum mixer[110] and during vibration[106], certain particle size distributions segregate.

It is suggested that, if, when the sectioned filament distributions are separated by twice the median value, obtained from the isotropic condition, the distributions overlap and the particles will tend to segregate during shear. This may occur when the distribution is convex, which is unlikely with particles which are reasonably angular, or if the distribution is bimodal. This is illustrated in figure 3.17. below.

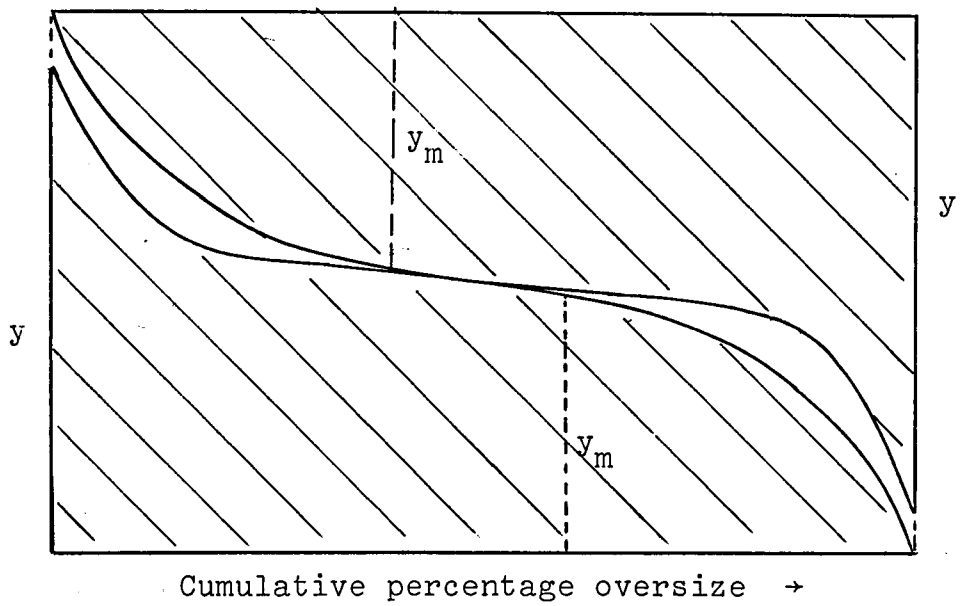

Figure 3.17 Condition for Size Segregation

3.2.4. The Difference between the Bulk Angle of Friction and the Coefficient of Friction

From the work of a number of authors it has been shown that the angle of friction, having taken into consideration dilatancy effects, is still larger than the angle of friction

between two flat surfaces of the material.

As stated in a review by Farouki and Winterkorn[47] a number of expressions have been derived relating the angle of friction ϕ to the coefficient of friction between grains μ.

Caquot[22] found that:-

$$\tan \phi = (\frac{\pi}{2})\mu$$

having considered an irregular system composed of various shapes and sizes. Bishop,[12] from energy considerations, obtained the expression:-

$$\sin \phi = \frac{3}{2}\mu$$

In both cases $\tan \phi = 0$ when $\mu = 0$ which is not true for porosities below the critical state, as a finite amount of work is necessary to dilate the material. Dantu[38] considered a sphere and the normal reactions acting on it, and found the relation:-

$$\sin \phi = 3\,\frac{\sqrt{2} + 2\mu}{5\sqrt{2} + 2\mu}$$

From statistical considerations Idel[86] obtained the following expression:-

$$\sin \phi = \frac{1.5 \tan(\psi-\theta)-1}{1.5 \tan(\psi+\theta)+1}$$

where $\tan \psi = \mu$

where $$n = 1 - \frac{\pi}{9\sqrt{3}} \frac{1}{\sin \theta \cos^2\theta}$$

n = fractional porosity

θ = contact angle

Scott,[151] using some of the theoretical calculations of Thurston and Dereisiewicz[175] obtained:-

$$\tan \phi = \frac{\sqrt{3}+(4\sqrt{2})\mu}{2(\sqrt{6}-\mu)}$$

Sjaastad[157] considered both the static and the kinetic case, the kinetic case existing after a very small displacement.

Farouki and Winterkorn[47] have plotted the different theoretical solutions for tan ϕ of regular systems of spheres in terms of the coefficient of friction of spheres; and have discussed the solutions.

Although Rowe's work takes the assumption of no rotation between particles, others have considered it. Osterman[123] shows the relation between shear and normal stress schematically in figure 3.18., pointing out that the difference between the apparent angle of friction and the true angle of friction can be explained by the rotation of the grains; and that the rotation must be dependent on the grain shape.

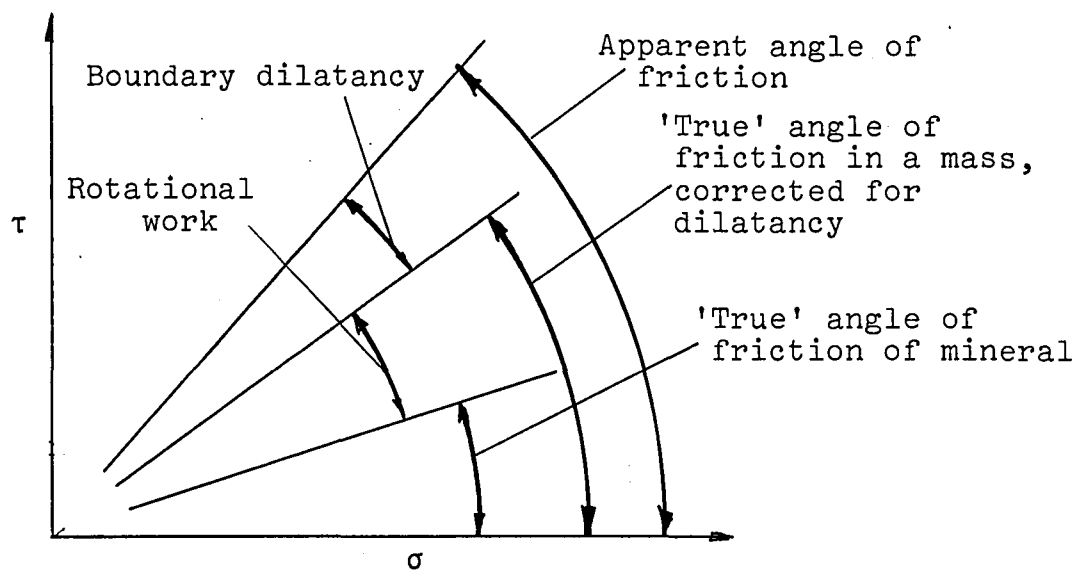

Figure 3.18. Energy analysis of granular mass subjected to shear (Osterman[123])

Tinoco[177] has also discussed the separation of the two mechanisms of sliding and rotation, but concluded that, from an energy study of the failure mechanism, resistance to sliding was the principle factor in the frictional resistance.

It is suggested that a filament analysis could be used

to predict the difference between the bulk friction and the mineral friction, the difference being assumed to include that due to rotation of the particles.

Considering figure 3.19 below, which isolates a particle rotating in the plane of shear.

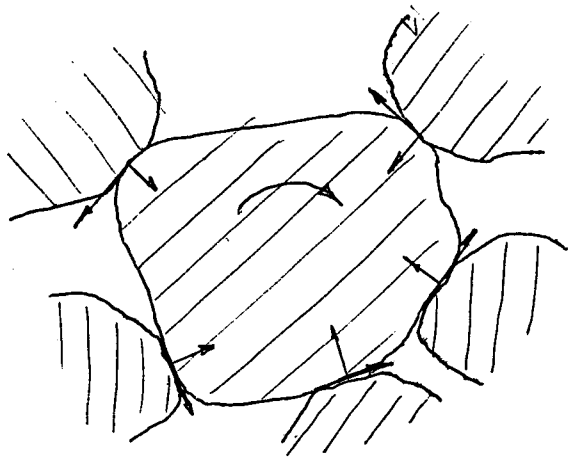

Figure 3.19. Point contacts on an irregular particle rotating in a plane of shear

If sliding occurs without rotation then the distance travelled by the contacts in the horizontal direction is almost equal to the horizontal distance moved by the particle. However, if at the sliding contacts rotation is also taking place, then the sliding distance at the contact will be greater than the horizontal distance moved by the particle. Thus the work done in rotating the sliding contacts will be greater than the work done in sliding the contacts assuming only horizontal sliding movement.

Thus if F_i is the sliding force per contact and d_{s_i} is the sliding distance; for rotation the sliding work done per particle will be:-

$$W_r = \sum_{i=1}^{n} F_i d_{s_i}$$

(where n is the number of contacts), and for sliding alone:-

$$W_s = \sum_{i=1}^{n} F_i d_s$$

(where d_s is the horizontal displacement of the particle)

Therefore:-

$$W_r > W_s \quad \text{if} \quad \frac{\sum_{i=1}^{n} d_{s_i}}{n} > d_s$$

It is possible that filament or lamina movement models could be applied to this situation so that the bulk friction in the steady state could be obtained from a Stereological measurement of the system.

3.2.5. The Propagation of Shear Stress

As pointed out by Novosad[120], when using free flowing materials in his annular shear cell, the material was flowing up to 3mm. above and below the predetermined plane of shear. This indicates a shear force gradient with the material. (Figure 3.20.)

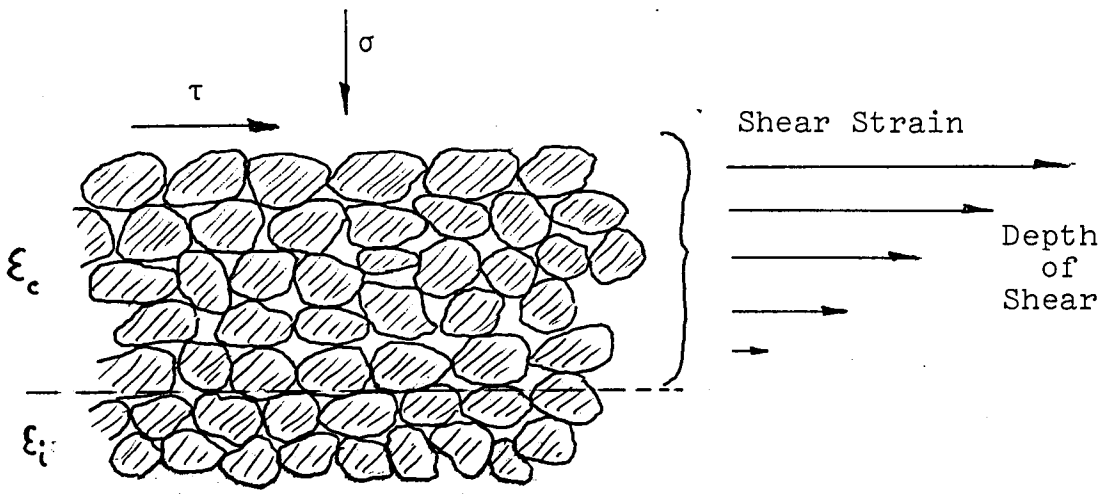

Figure 3.20. Shear Gradient in a Region of Shear

The number of effective particle layers disturbed in shear can be calculated using the concept of filament distributions.

Let f(x) be the number distribution of filaments of length x, as before. Then:-

$$\int_0^{x_{max}} f(x)dx = 1$$

The number of chords lying on a line of unit length is equal to the number of particles cut by the line. This is equal, in turn, to the number of spaces, it being understood that a space will have zero length when two particles touch on the line. If this number is represented by N then the effective average depth of a layer of particles is simply N^{-1}. However, since the fractional length of the line occupied by the chords is the same as the fractional volume occupied by the particles:-

$$N.\bar{x} = 1 - \varepsilon_c$$

where $\bar{x}$ is the mean chord length

ε_c is the porosity at the critical state

Therefore:-

$$\bar{x} = \frac{\int_0^{x_{max}} f(x)xdx}{\int_0^{x_{max}} f(x)dx}$$

$$\bar{x} = \int_0^{x_{max}} f(x)xdx \quad . \quad . \quad . \quad . \quad (13)$$

Therefore, if the depth of shear at the critical state is represented by H, the number of particle layers in this depth is given by:-

$$HN = \frac{H.(1 - \varepsilon_c)}{\int_0^{x_{max}} f(x)xdx} \quad . \quad . \quad . \quad . \quad (14)$$

It may be possible from the filament size distribution of the particles to predict the depth of shear as a function of

the stress conditions applied and of the packing of the material. However, in this case, rather than use the distribution of filaments obtained from a random chord measurement, the filaments connecting particle contacts may have to be considered, that is the contact filament distribution. (Figure 3.21.)

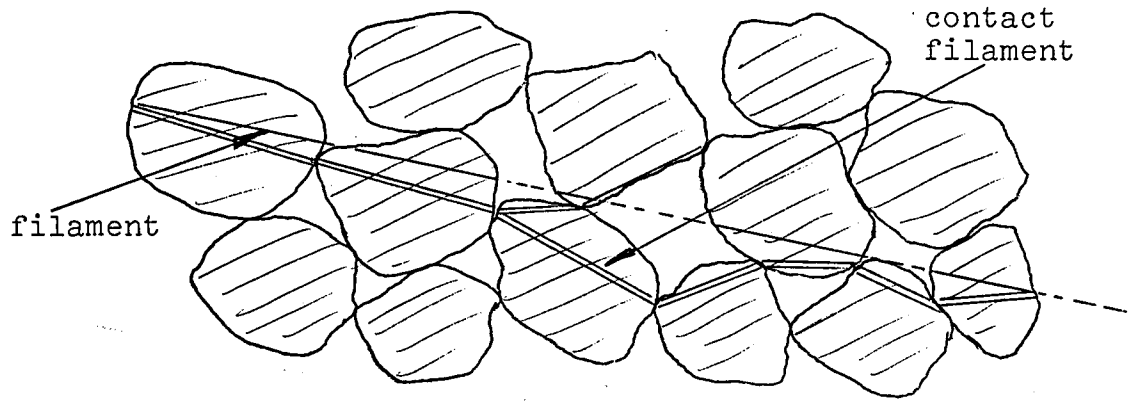

Figure 3.21. Filaments and Contact Filaments

By consideration of the force lost at a contact and the force transmitted through a contact, the depth of shear could be predicted. This type of analysis would require a measurement or prediction of the number of contacts per unit area or volume. This may also apply to the prediction of the angle of friction.

The following chapters describe and discuss measurements made on dry free-flowing sand under shear stress; and the comparison of the results with those predicted from Stereological examinations of the material.

CHAPTER 4

EXPERIMENTAL APPARATUS

CHAPTER 4:- EXPERIMENTAL APPARATUS

In chapter 1 the relationships are set out between the four characterisation groups of particulate systems:- primary properties, state, macroscopic properties and material behaviour.

In chapter 2 the macroscopic property of shear strength is shown to be particularly dependent on the state of the system; and chiefly on its moisture content and its porosity (or consolidation).

In chapter 3 the proposed theory considers the particulate system in the dry state and in the critical state. The latter is reached when an applied shear force causes rearrangement of the particles such that, when this force has become constant, the state of packing of the bed of the material has become constant also.

The present chapter now deals, in turn, with the measurement of the shear strength and of the porosity under this steady state condition. In both cases the details of the apparatus used for the present work are preceeded by a review of existing literature.

4.1. Measurement of Shear Strength

4.1.1. Review of Methods of Measuring the Shear Strength of Particulate Material

Earlier reviews include those by Skempton and Bishop[158] and by Hvorslev.[84 85] The former is not critical but it is useful in explaining the parameters measured in the most

popular shear tests. Hvorslev's publications include more thorough and critical reviews as he sets out to discuss the practical advantages and disadvantages of torsion shear tests. To make his discussions more useful he includes brief details of other conventional shear tests. The criteria (to which reference is made in the following sub-sections) he uses as the basis for his examination of each test include:-

i. its ability to furnish the value of the maximum shear resistance of the material, that is the shear stress at which failure or rapid plastic flow starts.

ii. its ability to display the temporary or permanent degree of shear resistance after failure. (Because very large displacements are often required to produce the ultimate shear resistance many types of tests are unable to give this information).

iii. its ability to demonstrate the stress-strain relationships and volume changes due to the shear stress.

iv. its simplicity in construction and operation.

v. its requirements in sample preparation.

vi. its duration.

4.1.1.1. Direct Shear Tests

These were used as some of the earliest methods of measuring the shear strength of soils and were described by Krey[102] in 1912. They have the advantage, in general, of being simple in construction and operation; and sample preparation is comparatively easy.

In general, most of the tests used for the determination of the strength of powders, for design purposes

or for purely analytical investigations, are similar to those used in the field of soil mechanics.

In the Direct Transverse Shear Test (figure 4.1a) the soil is confined between three vertically superimposed rings and the centre ring is displaced horizontally. It has two disadvantages; it requires more time for consolidation due to the height of the sample contained and the effective cross-section of the test specimen decreases with increasing deformation. This latter makes the test unsuitable for investigation of the shear resistance after failure.

The Direct Shear Box Tester (figure 4.1b) is the most commonly used direct shear test. Details of the shear box have been given by Bishop.[13] A relatively thin soil sample is confined between two rigid frames. The shear forces are transmitted in part as normal pressure between soil and frames, but primarily as tangential forces. It has the advantage of being simple in construction and operation but it, too, suffers from the fact that the effective cross section decreases with increasing displacements.

Roscoe[134] has shown the type of deformation which occurs in a direct shear test by fixing a bed of material with dyed tracer after shear and has shown that the deformation within the cell is not uniform. (Figure 4.2)

The Jenike Flow Factor Tester[87-91] (figure 4.3) was developed directly for use with powders as opposed to soils but it is basically a direct shear box tester. The equipment consists essentially of a shear cell, circular in cross section (instead of square as in the soil mechanics direct shear box test), a gravity loading system and a constant rate shearing device. The force necessary to maintain the constant rate of

shear is recorded via a pneumatic transducer on a chart recorder.

The base and the ring are filled with the powder to be tested. The vertical compressive force N, is applied to the cover and the horizontal shear force S is applied by means of a stem which acts on a bracket attached to the cover.

In conjunction with the equipment just described, a 'consolidation' bench can be used, which enables the material to be consolidated under load for any amount of time. This enables any investigation of the strength of powders under time storage. Jenike[91] has given a detailed description of the apparatus and its use.

The Swedish Direct Shear Tester (figure 4.1c) was developed by the Royal Swedish Geotechnical Institute[97] to overcome the non-uniformity of the deformations in conventional direct shear testers. The sample is confined by a rubber membrane and a series of thin, evenly spaced rings. The main advantage of the cell is that the horizontal cross-section remains constant throughout the test. Hvorslev[84] pointed out several limitations including the setting up procedure for the test and the fact that the shear resistance after failure can only be investigated to a limited extent. Roscoe[134] has pointed out other disadvantages, mainly that the test cross-section is cylindrical so that across a horizontal circular cross-section the shear stresses cannot be uniform. Furthermore the use of rubber membranes allowing the sides to stretch and to be undisturbed by the action of the contact stresses with the soil seem incompatible; while volume changes of the actual soil sample are not likely to be recorded correctly owing to the yield of the rubber membrane under pressure.

Figure 4.1.

Direct Shear Tests

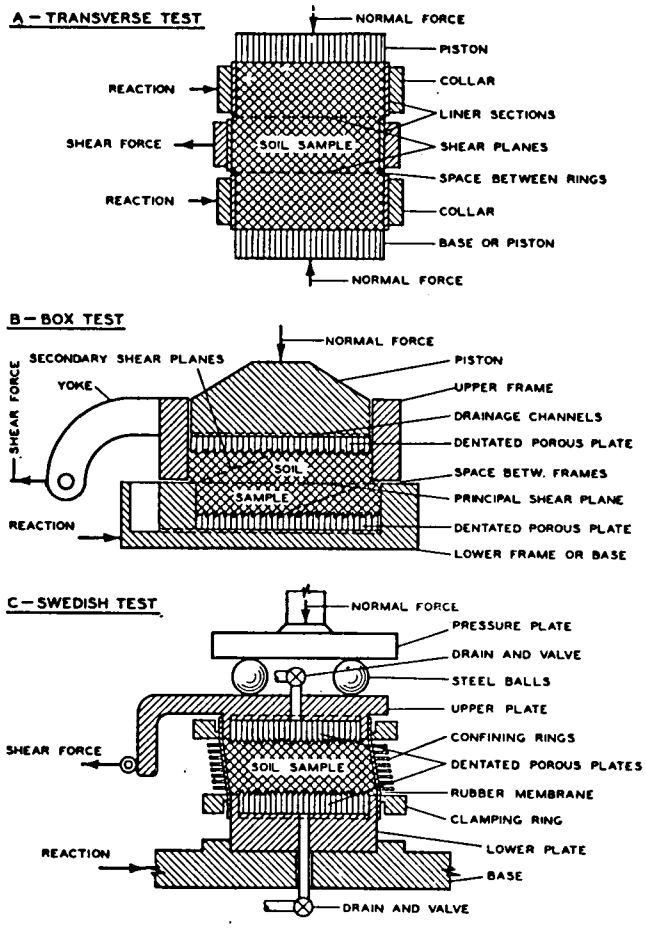

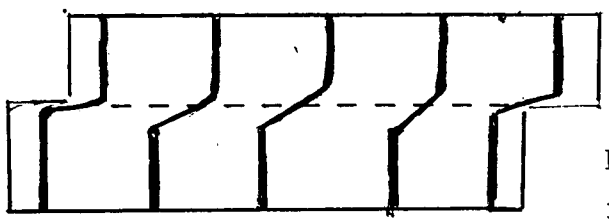

Figure 4.2.

Deformation due to shear in direct shear test.

Figure 4.3.

Jenike Flow-Factor Tester Shear Cell

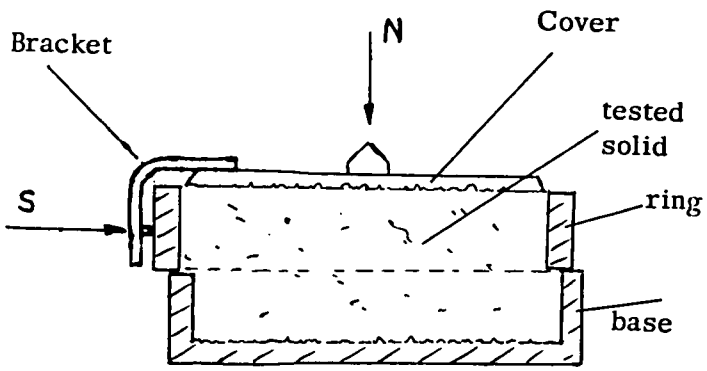

The Simple Shear Apparatus developed by Roscoe is similar to the Swedish tester without suffering from its faults. Even so, he indicated that, despite the inherent disadvantages, the usual direct shear test is viable due to its ease of use and simple sample preparation. The cell is rectangular in cross-section and, by a system of hinges, uniform strain throughout is applied to the sample contained. Comparing the strain produced in the Simple Shear Apparatus using the dyed tracer technique with the strain produced in the direct shear tester, Roscoe showed how his apparatus overcame the problem of uniform deformation produced in the direct shear tester. (Figure 4.4).

The Roscoe simple shear cell has progressed through six versions and Mark 6 is a very much improved piece of equipment from Mark 1. Sketches are shown in figure 4.5a & b. The sample is surrounded by a number of load cells and the hinged system is so arranged that there is no dead zone when dilation occurs as was found with earlier models. The latest version enables a complete set of stress/strain measurements to be made.

Three other examples of direct shear test apparatus are those described respectively by Nash et al[118], Okada and Abe[121], and Pilpel[125].

Although not directly a direct shear test in the conventional form, Nash et al[118] used an apparatus for measuring the shear strength of powders where the material was not contained in a cell, but was only confined by a plate lying on the surface of the powder. The force necessary to move the roughened plate, on which various loads were placed, over the powder, gave a measure of the shear strength.

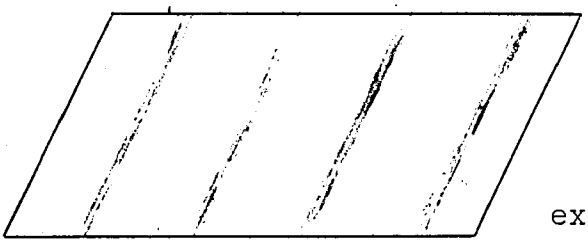

Figure 4.4.

Uniform deformation experienced in Simple Shear Apparatus

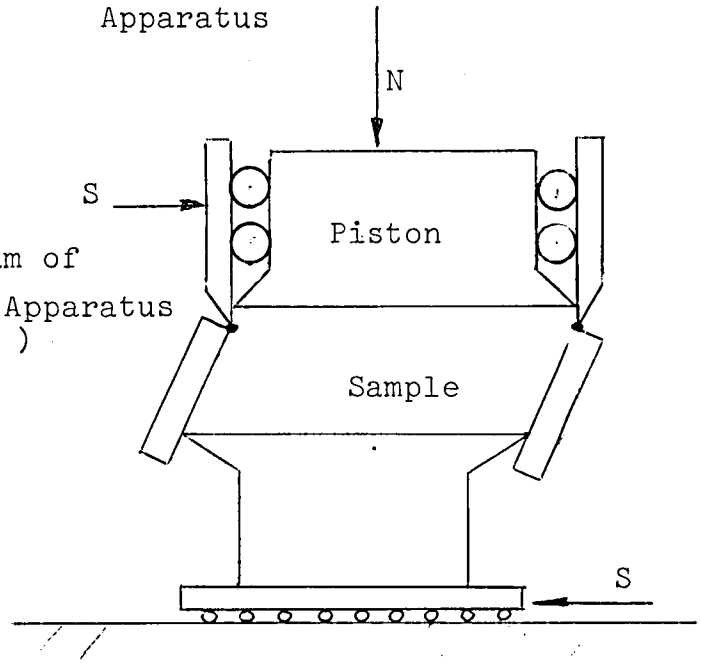

Figure 4.5a.

Schematic diagram of Mks.1-4 Simple Shear Apparatus (Roscoe[106])

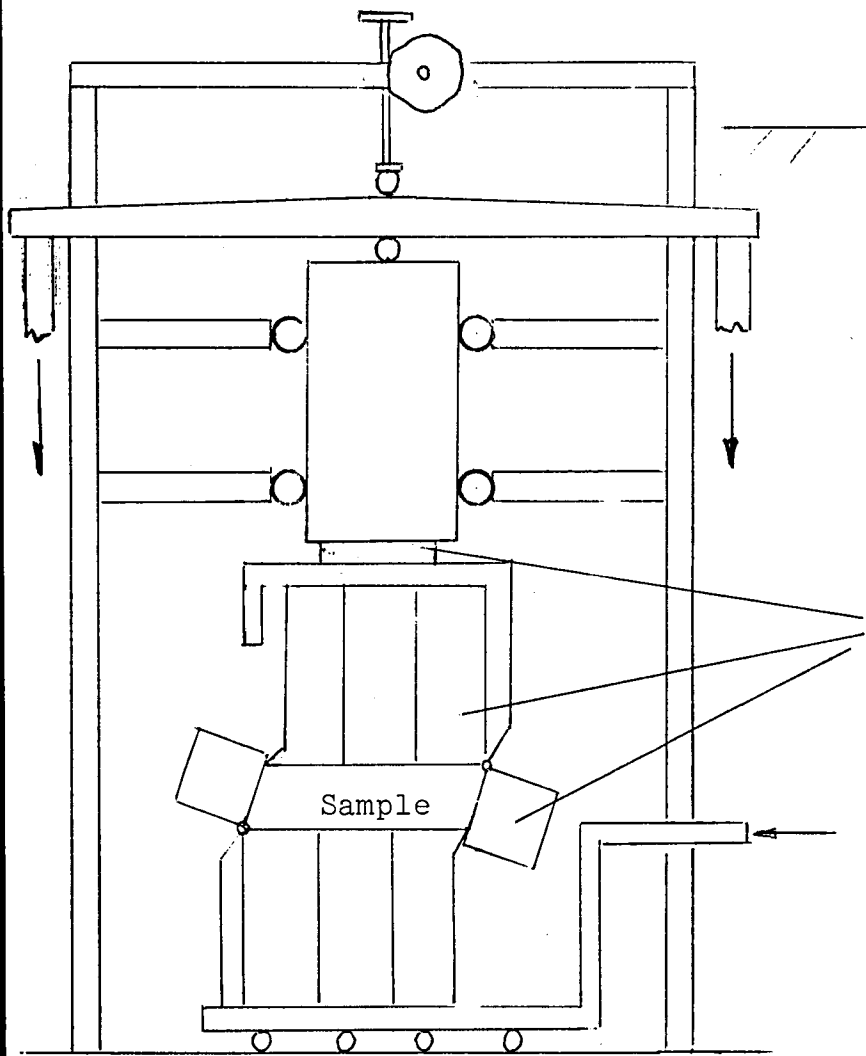

Figure 4.5b.

Schematic diagram of Mk.6 Simple Shear Apparatus. (Roscoe[106])

A study was made by Nash of the effect of the rate of shear and the depth of powder on the shear strength. It was found that there was no effect on the shear strength and for depths above 1.66mm there was no effect due to the powder depth. It was pointed out that below this depth an effect was noted; and it was suggested that this was due, probably, to the asperities of the roughened surface of the top plate and base plate rubbing together!

For examining the coefficient of friction and the adhesion power of drug powder, Okada and Abe[121] used an apparatus which was essentially a transverse direct shear tester. Shear was applied to the centre section by a pulley mechanism, on the end of which was a little bottle into which mercury was slowly poured. When shear took place the weight of mercury in the bottle was noted. Okada and Abe used the Coulomb equation for their work in comparing various drugs and dry constituents.

Pilpel[125] used an apparatus which was essentially a Jenike Tester in that it included a circular cross section cell; and a soil mechanics direct shear box in that it employed the same type of drive and shear measuring mechanism. It was cheaper than the complete Jenike system but suffered in that a continuous recording of the shear force was not possible. It was used in the same manner as prescribed by Jenike, so that the lack of this continuous measurement was not too great a handicap.

4.1.1.2. Torsion Shear Tests

Torsion shear tests are made on cylindrical samples with either an annular or solid circular cross-section. For both types the major advantage over the direct shear and

triaxial tests is that the cross-section of the sample is constant throughout the duration of the test and that there is no limit to the amount of angular displacement.

According to Hvorslev[84], the first torsion shear apparatus was developed in 1916 by the American Society of Civil Engineers.[5] Similar devices were developed by the Institute of Technology in Hanover[51] in 1929, and by Langer[105] in 1938. All these types had a solid circular cross-section.

With solid cylindrical samples the variation of shear stresses and strains goes from zero at the centre to a maximum at the outer surface. Also, since dilation is likely to occur and will be a function of the shear strain, a non-uniform distribution of the normal stress will be set up. Hvorslev also points out that at the outer and inner edges of the cell a concentration of shear stress will be set up due to the material in contact with the walls. This may have an undesirable influence on the results.

In 1933, the first attempt to overcome the problem of zero to maximum shear strains and stresses was made by Tiedemann.[176] Though using a solid circular cross-section of sample, the part through which the shear stress was transmitted was annular in shape and was fitted in the base of the apparatus. As pointed out by Hvorslev, there is a danger that the material could arch over the shearing ring, giving difficulties of determining the normal stress distribution on the failure plane. Tiedemann replaced his solid cross-section apparatus with an annular shear apparatus in 1937. Annular shear apparatus was developed, independently, by Hvorslev[82] in 1934, by Gruner and Haefeli[60] in 1934, and by Cooling and Smith[33] in 1937. Hvorslev's work was directed by Terzaghi, who was largely responsible for

the triaxial shear test. Fuller details of all these types of annular shear cells are given in the reference by Hvorslev.[84]

The major disadvantage of a cell of annular cross-section compared to one of solid circular cross-section, as far as soils are concerned, is that samples are more difficult to prepare, although a more uniform stress and strain distribution is obtained. Again, however, the influence of friction between wall and sample can be significant.

As pointed out by Hvorslev in connection with soil strength measurements, torsional or annular shear cells allow one to measure the steady state flowing condition. This is due to the unlimited amount of displacement which can occur and, also, to the constant cross sectional area with shear strain (unlike the many direct shear tests). For these reasons the application of torsion shear tests has been made to the study of flowing powders.

Novosad[120] modified the Hvorslev shear apparatus for measuring the angles of friction of materials at high shearing speeds and low normal stresses. He indicated that in the chemical industry, granular materials are usually subjected to high shear strains at small shear stresses. A diagram of the apparatus used is shown in figure 4.6a. The torque was measured using a pulley system and weights. (Figure 4.6b.)

Novosad's analysis was the same as that of Walker[23,186] for determining the shear stress of the material.

Considering figure 4.7. The differential torque dM is equal to the product of the shearing stress τ, the annular area of width dr, and the radius r of this area. That is:-

$$dM = 2\pi\tau r^2 dr$$

Therefore, the torque M over the whole annulus between r_2 and

Figure 4.6.a

Annular Shear Cell
used by Novosad

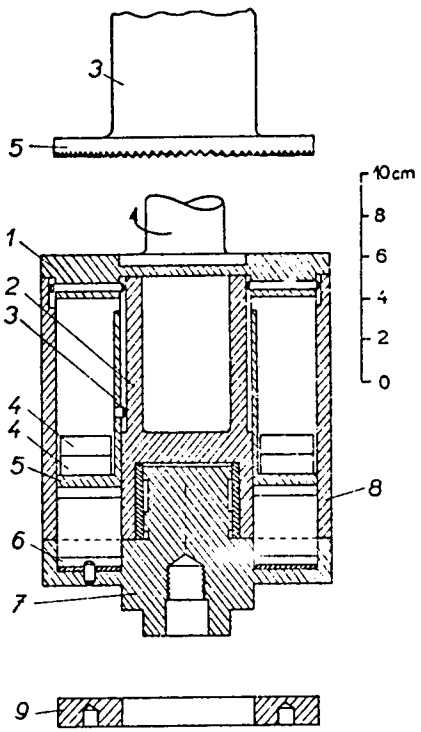

Schematic Drawing of Shearing Apparatus *1* **Lid,** *2* **hub,** *3* **guide tube,** *4* **weights,** *5* **pressure plate,** *6* **grooved inner piece,** *7* **bottom,** *8* **shell,** *9* **annular plate for the measurement of the angle of external friction.**

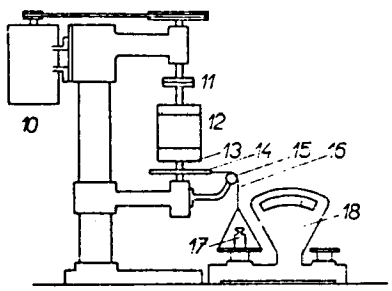

Figure 4.6.b

Method of Torque Measurement
10 **Electric motor,** *11* **coupling,** *12* **shearing apparatus,** *13* **turn table,** *14* **pulley,** *15* **roller,** *16* **cable,** *17* **weights,** *18* **balance.**

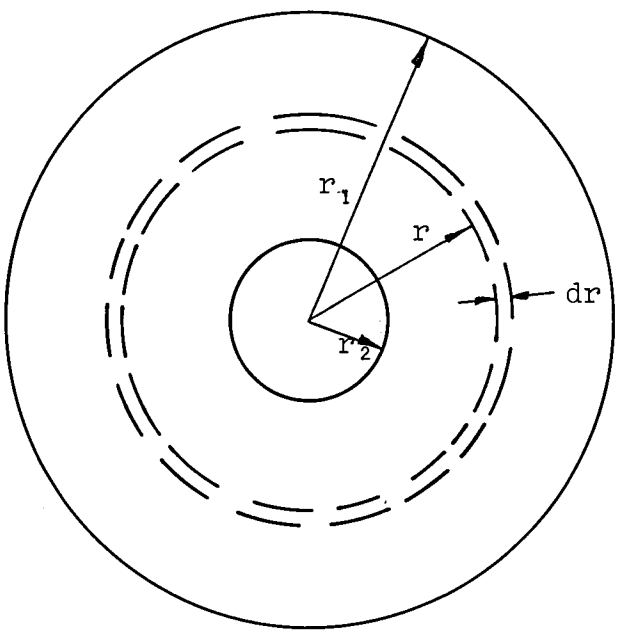

< Figure 4.7.

r_1, is given by:-

$$M = 2\pi\tau \int_{r_1}^{r_2} r^2 dr$$

It is assumed that τ is independent of the shear rate and hence independent of the radius. Therefore:-

$$M = \frac{2\pi\tau}{3}\left(r_2^3 - r_1^3\right)$$

Novosad, using ideal granular materials without cohesion, determined their dynamic angle of friction. The materials he used were sand, sugar and glass spheres. His results showed considerable dispersion which discouraged further work. He also noted that the free flowing material did not shear in a very narrow region but was in motion 3mm. above and below the shear plane predetermined by the construction of the apparatus.

Carr and Walker[23] saw in the torsional or annular shear cell a way of overcoming two of the inherent disadvantages in the Jenike type shear cell. Firstly, the limited shear displacement in the Jenike shear cell makes it necessary for a tedious preparation of the sample prior to shear and consolidation. Secondly, the Jenike cell does not allow for normal stresses below 1 lb/in^2.

Carr and Walker have designed what they call the "Portishead" shear cell for use in hopper design; and a cross-sectional diagram of the apparatus is shown in figure 4.8. The base of the cell is rotated and the torque measured by allowing the radial torque arm to rest against a load cell. The recessed underside of the top plate through which the shear strain is transmitted has vertical radial vanes to grip the sample. Normal loads are placed on top of the shearing plate and for low loads the shearing plate is counterbalanced.

Carr and Walker used their apparatus not for its advantage of reading steady state conditions but to measure the peak values. It is possible to measure the whole series of shear stresses at various consolidational and normal loads without preparing fresh samples. This makes it very advantageous when handling unpleasant materials. Walker suggests that the apparatus is also useful when measuring the tensile strength, by measuring the force necessary to lift the top shearing plate from off of the powder bed. It is wondered, however, if this technique is very accurate in that the tensile force necessary to separate the top plate from the powder would be small in comparison to that necessary just to lift the plate with no powder present. The wall friction can be determined by replacing the top plate with an annulus made up in the material to be used in the construction of the hopper. The flow functions Walker has obtained from his cell have been lower than those from the Jenike cell. His analysis, he suggests, is more accurate than the Jenike analysis in that he does not allow for such a large safety margin as Jenike.

In the view of Hvorslev, the torsion shear on ring shaped samples were the best for determining shear resistance after failure, although for the determination of the maximum shear resistance he favoured the triaxial shear test.

Cheng[31], having theoretically discussed powder behaviour, comments on the need to investigate the elastic and flow properties of powders and the need for measuring the steady state flow condition. He has designed a torsional shear cell[28] to measure these properties. Use was made of the Weissenberg Rheogoniometer, which was adapted so that a shear cell and

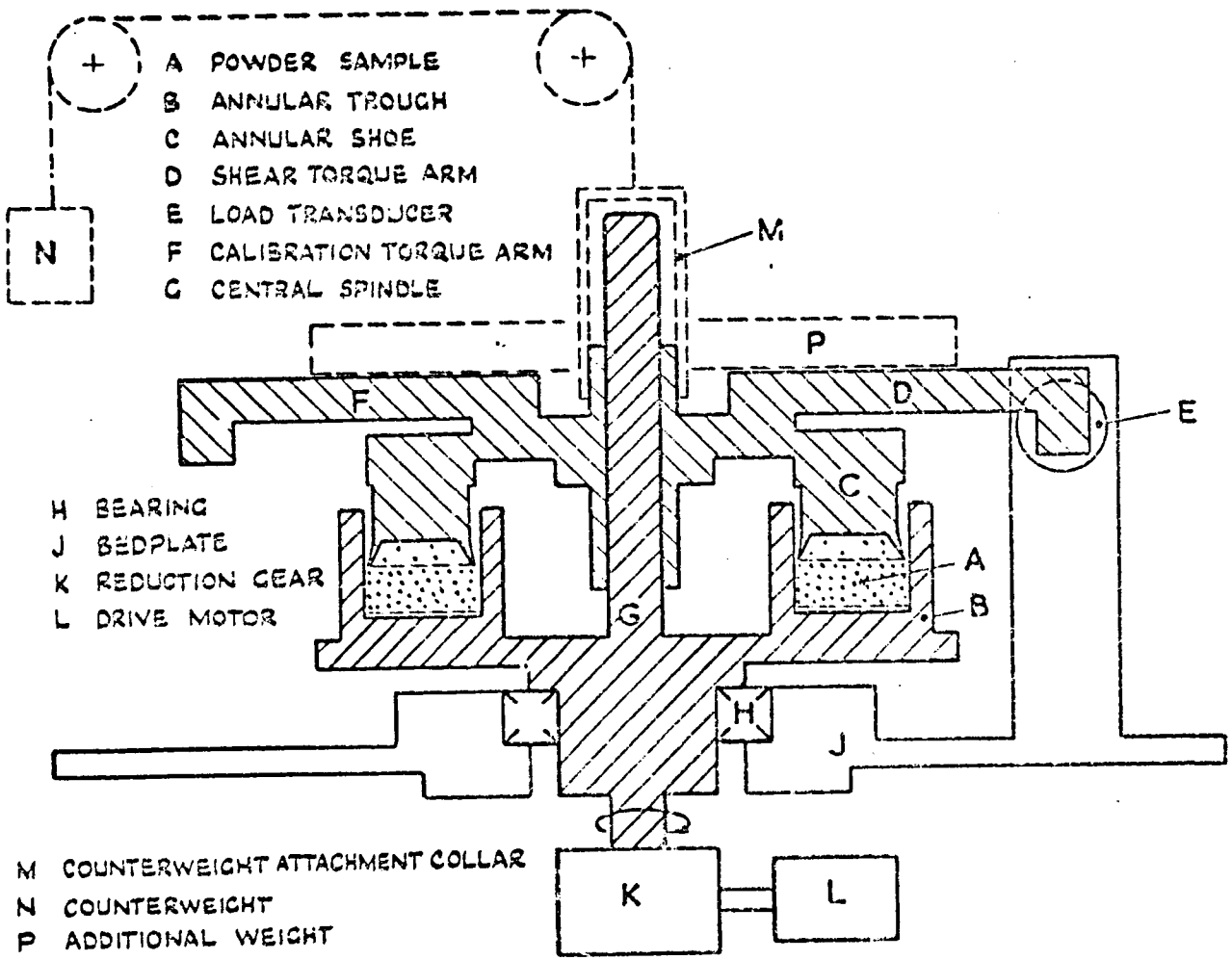

Figure 4.8. Schematic diagram of Portishead Annular Shear Cell

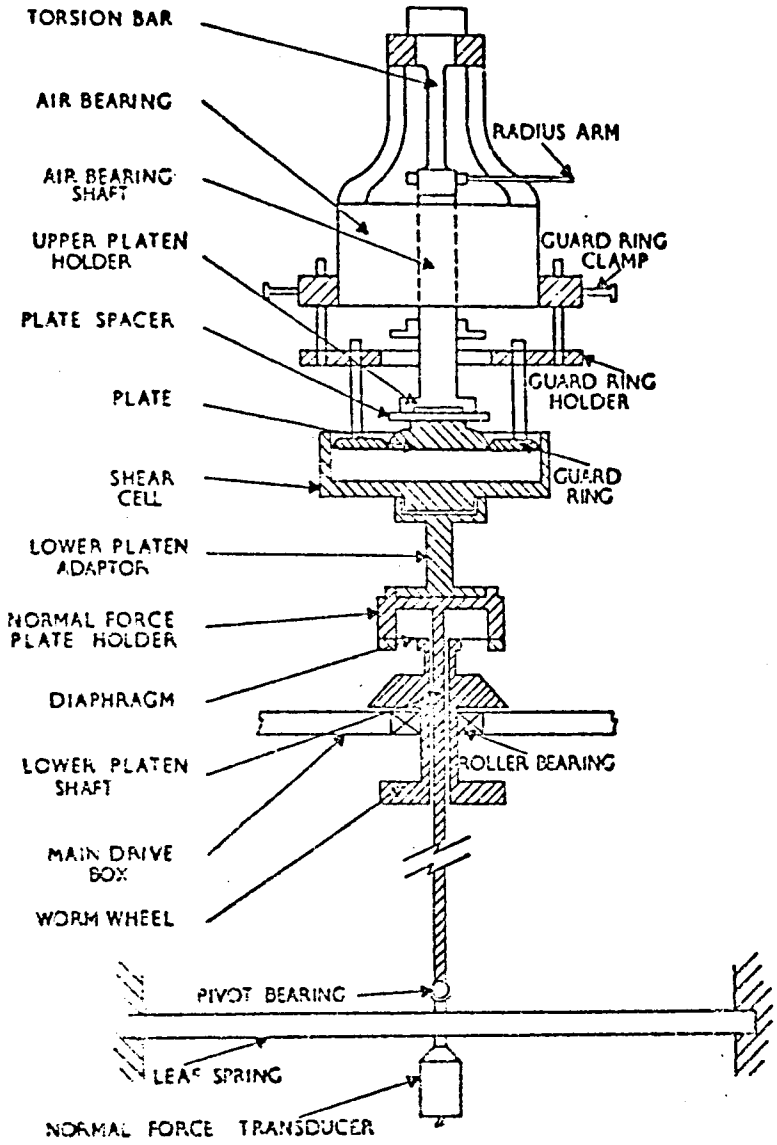

Figure 4.9. Cheng's Torsional Shear Cell (Crown Copyright, reproduced by permission of the Controller H.M.S.O.)

plate assembly could be fitted to it. A diagram of the unit is shown in figure 4.9. A full description of the unit is given by Cheng.

The essential features of the instrument are the outer guard ring to overcome the problem of stress concentration pick up at the walls of the cell; and the ability to vary the normal load on the cell during the test. Again, the speed of rotation of the cell is variable and Cheng found (as have other investigators) that the rate of shear did not significantly effect the measured torque.

Viscometer Type Torsional Shear Units have been used by a number of investigators including Benarie[10], Taneya[167], Kuno and Kunihara[103], Herwood and Pilpel[69]. These units are all of the same basic design and vary according to the method of measuring the torque and the method used to ensure a good powder to powder contact. Figure 4.10 gives a general indication of their operation. Vanes or roughened surfaces are used to ensure that, where slip occurs, it occurs between the powder surfaces and not between powder and metal. In some cases the outer cylinder is rotated and the torque necessary to shear the powder is measured on the centre cylinder. In the other types the force is measured on the outer cylinder whilst the centre is rotated. In most cases the speed of rotation can be varied.

Benarie used a number of different cylindrical surfaces and found that the torque for dynamic flow was independent of the angular velocity. In the analysis of the torque, use is made of the Rankine formula for the relationship of horizontal pressure to vertical pressure. This is probably a weakness in the analysis, as there is some doubt as to the accuracy of the Rankine formula, especially from the findings of Handley and

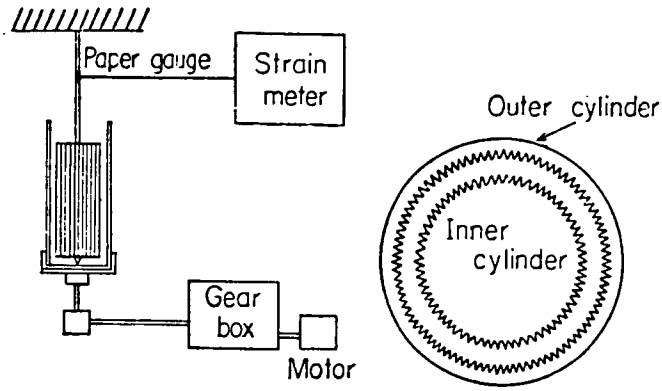

Figure 4.10. Schematic diagram of viscometer used by Taneya[167] for measuring the strength of powders.

Figure 4.11.

Triaxial Test

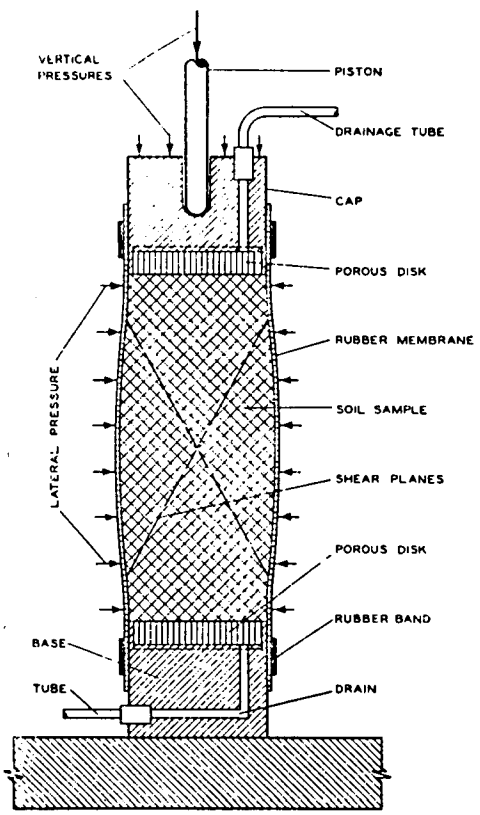

Perry[61], who used a radio pill pressure measurement in a model hopper.

A number of difficulties arise with this type of measurement. Firstly, as dilation occurs a ridge is formed between the flowing and stationary material, making the measurement of the height of the material difficult. Secondly, the pressure over the cylinder is a function of the bed depth, again making the shear stress analysis complicated.

Vane Shear Tests which are used in the determining of the strength of clays are similar in principle to the viscometer type shear unit. Although they are not an ideal way of measuring the strength of clays, they have the advantage that they can be used "in situ". The force necessary to turn the vanes at the end of a shaft embedded in the clay gives an indication of the strength of the clay.

4.1.1.3. Triaxial Shear Tests (Figure 4.11)

The method that is now used in most soil mechanics laboratories throughout the world is the triaxial apparatus. It was described, first of all, by Westerberg[191], in 1921, and was further developed by Rendulic[129], in 1935 and Housel[81], in 1936. Since that time the method has been the subject of intensive research. A detailed account of the triaxial test has been presented by Bishop and Henkel[14].

The triaxial shear or compression test consists of a cylindrical sample of material subjected to definitely known external vertical and horizontal normal pressures. Unlike the previously described direct shear tests, the resistance is not determined directly. By using the Mohr's circles of stress, it is obtained from the corresponding values of the vertical

and horizontal normal pressures at failure. The term "triaxial" comes from the fact that the apparatus is designed to impose only axially symmetrical stress and strain conditions to the sample. The vertical and horizontal stresses can be varied independently of each other (unlike the direct shear test). The plane of failure is not predetermined by the geometry of the apparatus but the material fails along the weakest point.

The main disadvantages are that long samples are required and for loose silts and sands sample preparation can be difficult. Furthermore, it does not lend itself to the determination of the decrease of shear resistance after failure. On the other hand, the apparatus can be totally enclosed, and the amount of drainage of moisture can be controlled and measured, enabling the stress-strain relationships and volume changes to be determined with the apparatus.

Haythornthwaite[65] has analysed the test against the normal plastic theory, from the basis of a particular stress-strain relationship that would ensure stability of the material and the uniqueness of failure loads.

The tendency has been not to use the triaxial test in the study of the strength characteristics of powder, probably due to the delicacy required in the preparation of the samples and the large number of tests required for a rigorous investigation.

However, some tests have been carried out using the test on unconfined stress determinations, by compacting specimens to various consolidations and measuring the force required to fail the specimens in the unconfined state.

4.1.1.4. Tensile Tests

The use of the Jenike Tester for direct measurement of the tensile strength or cohesion of the material is difficult in that it requires extrapolation of the data to determine a value of the shear stress at zero normal stress.

Ashton et al[6], have attempted to overcome this problem by developing a tensile measuring device. The shear cell which is used for the test is of the same shape as the Jenike cell, but, whereas the Jenike cell has a horizontal predetermined plane of shear, the tensile cell has a vertical plane of shear. The material in the cell is consolidated by precompacting the material under various normal stresses, and the force necessary to separate the two halves of the cell (that is the tensile strength) is measured. The tensile force T, is combined with the data from the Jenike test and a more accurate yield locus can be drawn giving a value for the cohesion.

Other tensile testers have been developed by Dawes[39], Thauzeau and Taylor[174], Eisner, Fogg and Taylor[44]. These are of the tilting table type, where a split cell similar to the Warren Spring cell[199] is used but the force required to split the sample is obtained by tilting the table on which the split cell is mounted. The tilting table makes control and accurate measurements difficult. Also, there must be an influence on the plane of rupture by the angle of tilt.

Nash et al[118] have measured the tensile strength by compacting material contained in a cylinder, split across the centre, and measuring the force necessary to separate the two halves of the cylinder. This test, however, must suffer from the fact that the sample is rather long and thin, probably

giving uneven compaction of the sample.

4.1.2. Design of the Split Ring Annular Shear Cell

From the review given in section 4.1.1. the test best suited for the present work on the determination of the shear resistance after failure and at the steady state condition is the annular shear cell. This apparatus provides strain at constant cross-sectional area.

An annular shear cell was chosen as a basic design in preference to the Simple Shear Apparatus for the following reasons. Firstly, an annular shear cell can be subjected to shear strain for an unlimited time, thus enabling not only the steady state to be reached but also any time degradation effects to be investigated. Secondly, in the Simple Shear Apparatus the shear strain throughout the sample is dictated by the change of geometry of the cell, producing uniform strain during the test. However, with an annular cell the shear stress is propagated through the particle contacts, thus forming a vertical shear strain profile in the cell, so that an investigation of the depth of shear can be conducted.

As pointed out in section 4.1.1. there are two basic disadvantages in the conventional annular shear cell. Firstly, there exists at the walls of the shear cell a concentration of shear stress, caused by the material under shear moving against the walls of the cell. This concentration can be appreciable and so it is not possible to form a simple flow profile which is due only to the vertical stress. The second disadvantage is that the shear strain increases with radius, making the annular cell unsuitable for the measurement of the peak stress value. The shear stress is a function of strain

until the steady state is reached. It follows that the peak stress condition at the outer walls of the cell, in an annular shear cell, is reached before the peak stress condition at the inner wall of the cell. The overall effect is to reduce the measured peak stress value and prolong its effect. (Figure 4.12.) The difference in strain rate can be reduced by decreasing the width of the annulus; but this, in turn, increases the significance of the wall friction.

To overcome these difficulties, and still keep the major advantages of constant cross sectional area and unlimited shear strain, a new type of shear cell was designed utilising the "guard ring" principle.

The principle is demonstrated in figure 4.13, which shows the horizontal flow profile developed during shear in the material. The dotted line across the cell indicates the stress concentration at the walls of the cell.

By forming the top annular shearing plate of three independent annuli, the problems of stress concentration at the walls and of large shear strain variation can be overcome. The dimensions of the annuli were so chosen that the inner and outer annuli cover the regions affected by this stress concentration, so that the centre annulus does not detect any friction at the walls.

There immerged six main criteria to be satisfied by the final design and these are set out below with supporting comments.

4.1.2.1. <u>Each annulus was to be loaded independently and in such a way that the normal stress was evenly distributed over each annulus and over the cell as a whole</u>.

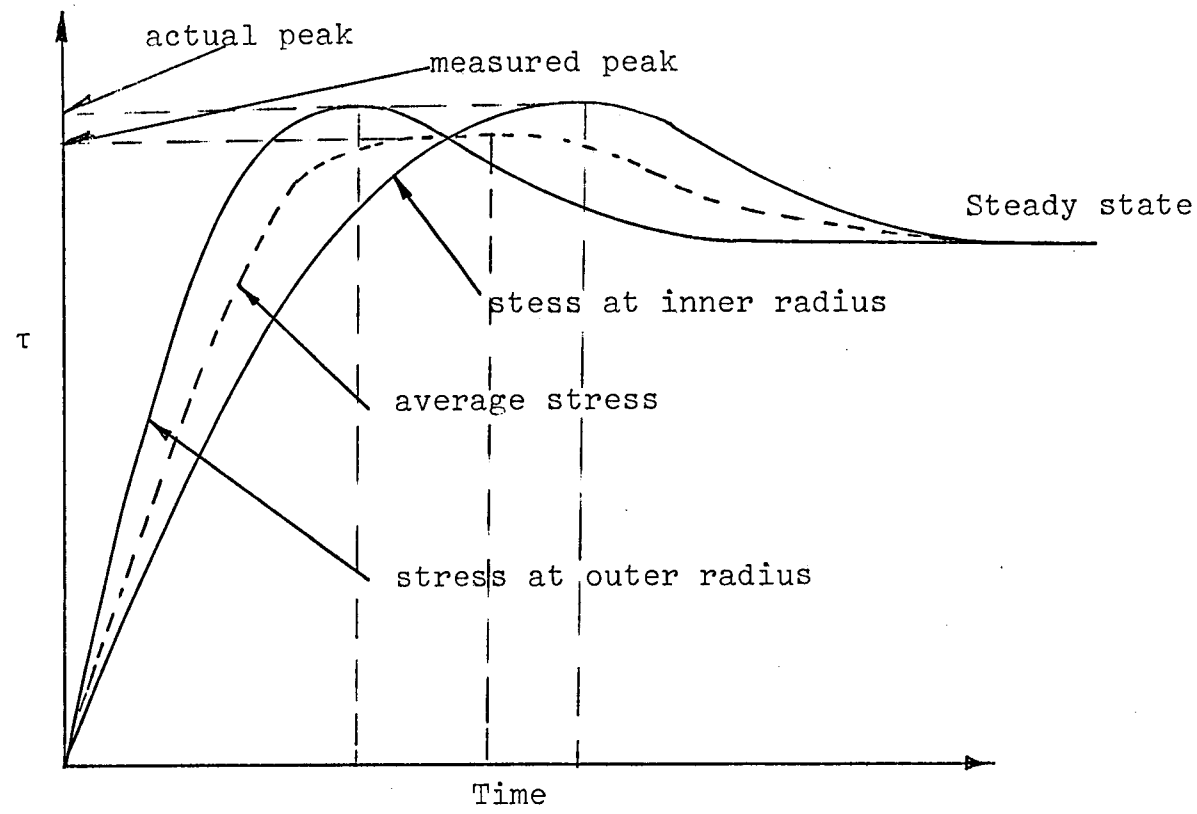

Figure 4.12. Diagram showing the error in the peak stress measurement in an annular shear cell.

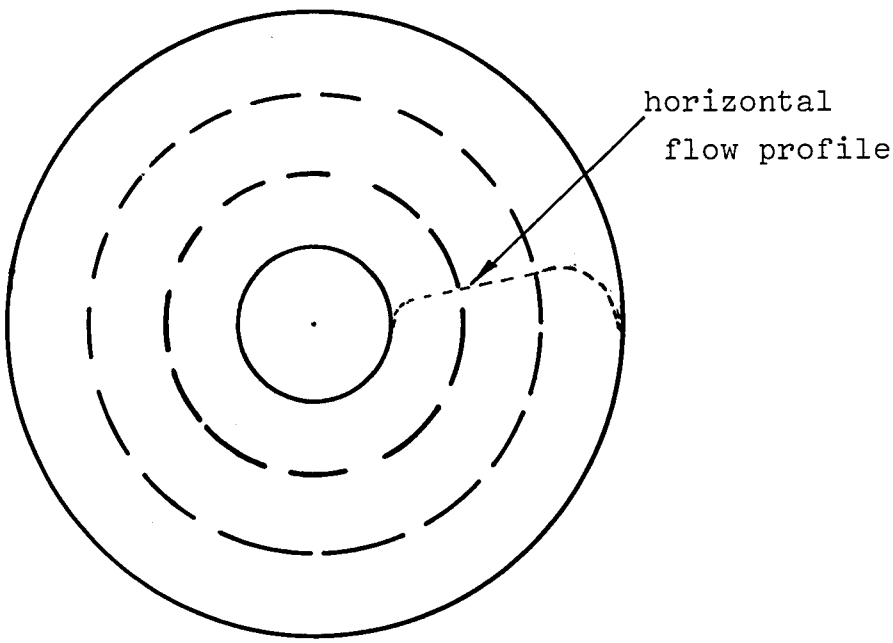

Figure 4.13. Horizontal flow profile created in an annular shear cell, showing the stress concentation at the walls

This was achieved by means of weights suspended below the shear plate on narrow concentric stainless steel tubes, themselves supported on a system of discs and pillars, so that the centre of gravity of each load passed through the centre of the cell. (The layout is shown in figure 4.14, together with an alternative method, which was discarded due to practical difficulties of manufacture and assembly, whereby the weights would be above the annuli shear plate). Each load carrying tube was eventually fitted with a universal joint system to facilitate the even distribution of normal stress. The loading of each annulus was proportional to its area, the dimensions of which were such that the radial flow profile was linear over the area of the centre annulus without giving too large a change in strain with radius.

4.1.2.2. <u>The three annuli were to retain their concentricity while being deliberately separated to prevent the transmission of torque from one to another</u>.

This was achieved by the insertion of a ring of $\frac{1}{8}$" diameter ball bearings between the inner and centre annuli; and between the centre and outer annuli. These bearings also allowed the annuli to move independently in a vertical direction when the material dilated. (Figure 4.15). The dilation of the sample in the cell was measured by the vertical movement of the centre annulus using an "S.E." inductive type displacement transducer, fitted above the annulus.

Felt was fitted between the three annuli to prevent the material from "binding" the plates; and between the annulus and the inner and outer walls of the cell to prevent loss of material during shear.

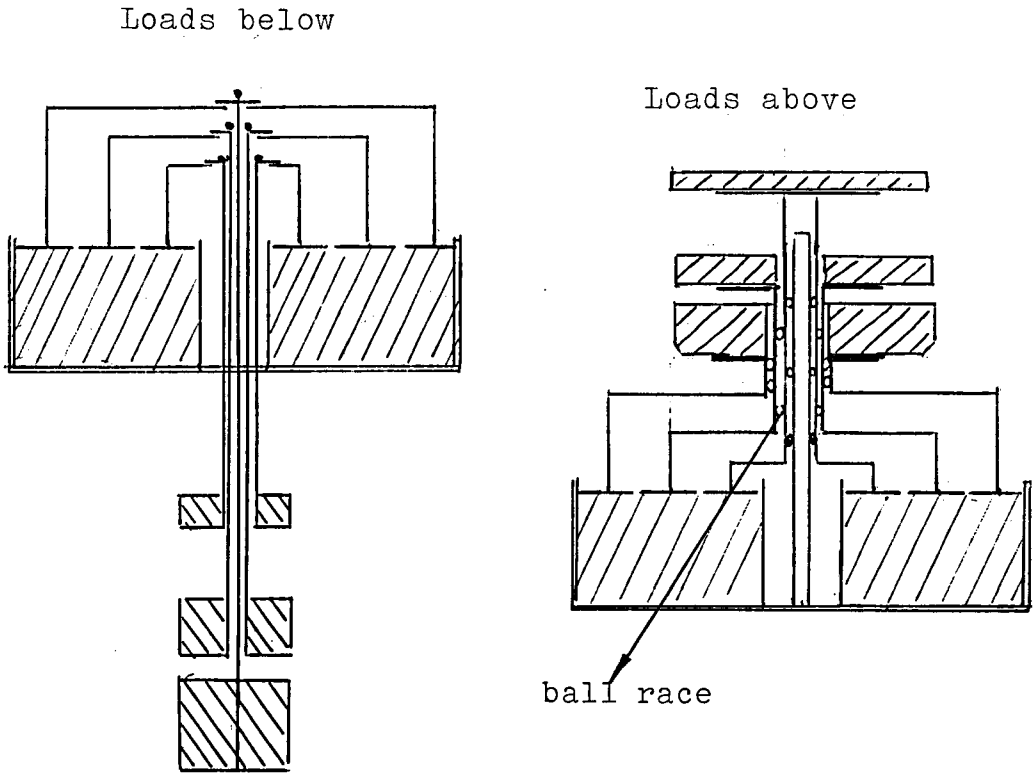

Figure 4.14. Possible loading arrangements for Split Ring Annular Shear Cell

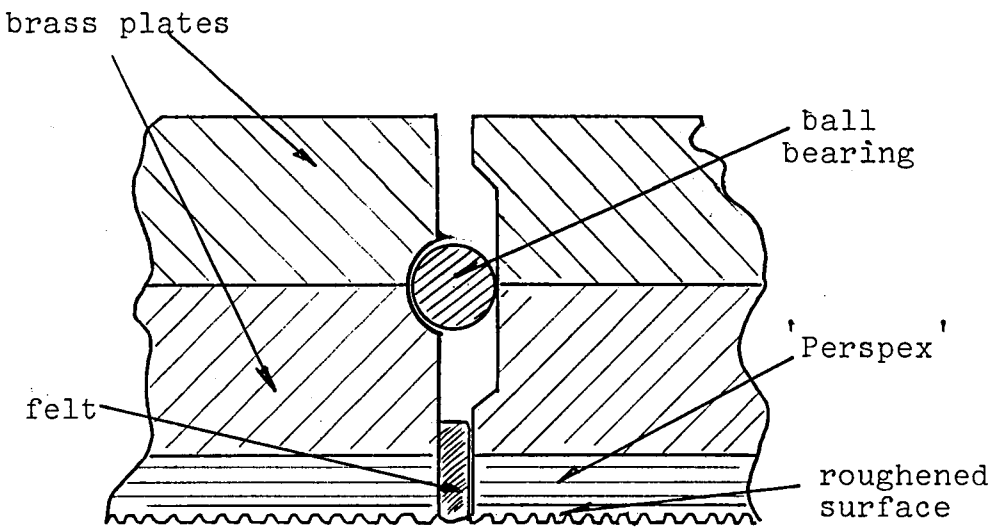

Figure 4.15. Cross-section diagram through a section of the Split Ring Annulus

4.1.2.3. It was necessary to have a predetermined plane of shear or to shear adjacent to the top shearing plate (as in the "Portishead" Cell).

In fact it was decided to shear adjacent to the top shear plate but the design was such that it could be easily adapted to give a predetermined plane of shear.

The material under examination was contained in the annular base of the cell which was approximately 22cm. in diameter. This base was rotated while the split annulus shearing plate above the material was constrained against rotation, thus causing a shear gradient over the sample in a vertical direction. The constraint was applied by three rods which slotted into the shearing plate, one rod to each of the three annuli, with the centre rod bearing against the "Kistler" piezo-electric force transducer which had a sensitivity of 0.1gm. and a range of ±50kg.

A set of spacers was provided so that different depths of material could be used.

To ensure good contact between the top surface of the material and the shearing plate the latter was roughened on its underside by fixing to each of the three annuli a mono-layer of sand particles (the material to be studied) using an epoxy resin. This method, which proved satisfactory in practice, was preferred to other possibilities such as the cutting of radial slots in the shearing plate or the fitting of vanes below the plate, which would "bite" into the material under test.

4.1.2.4. The apparatus was to be suitable for the application of a gamma attenuation technique for the measurement of the

bulk density of the material in the cell.

This was achieved by the use of aluminium (which has a low absorption of gamma rays) for the construction of the outer wall of the cell.

4.1.2.5. The drive was to be capable of speed variation to allow for the study of shear rates.

As the loading system was to pass through the centre of the cell, the drive unit was placed off centre below the shear cell unit. A variable speed reversible electric motor was chosen to facilitate quick release of the shear force.

Fitted below the cell was a brass collar, which located on the drive unit by a system of three spring loaded pins, to prevent disturbing the sample when placing the cell into position on the unit.

4.1.2.6. Constant recording apparatus was required.

The output from the force transducer was fed, via a charge amplifier, to one channel of a two channel spark chart recorder. On the other channel of the recorder the output from the displacement transducer was recorded, which again had been amplified previously.

The whole equipment is fully illustrated in the following diagrams and photographs:-

Figure 4.16. Schematic cross-section diagram of the Split Ring Annular Shear Cell, showing normal load assembly.

Figure 4.17. Top view of the cell showing torque measuring system and the displacement transducer.

Figure 4.18. Close-up of the cell showing the split ring annulus.

Figure 4.19. View of the base of the cell containing powdered material, and the underside of the split ring annulus showing roughened surface.

4.1.2.7. Calibration

Although the calibration factor for the force transducer was supplied with the instrument, the calibration was checked using the Jenike Flow Factor Tester. A photograph of the unit is shown in figure 4.20. A series of loads were placed on the calibration frame and the output from the force transducer was recorded. The calibration was checked for different settings on the transducer charge amplifier.

A calibration factor was not provided with the inductive displacement transducer. To determine this factor the transducer was set up above a depth gauge, both fixed rigidly. The micrometer adjustment on the depth gauge was moved at fixed intervals and the output from the transducer recorded.

4.2. Measurement of the Critical Porosity

The Split Ring Annular Shear Cell described in section 4.1.2. was designed such that a zone of flowing material was formed adjacent to the roughened surface of the split annulus.

Reference has been made (4.1.2.4.) to the use of a gamma attenuation technique to measure the bulk density of the material in the shear cell. The porosity is related to the bulk density by the equation:-

$$1-\varepsilon=\frac{\rho}{\rho_s}$$

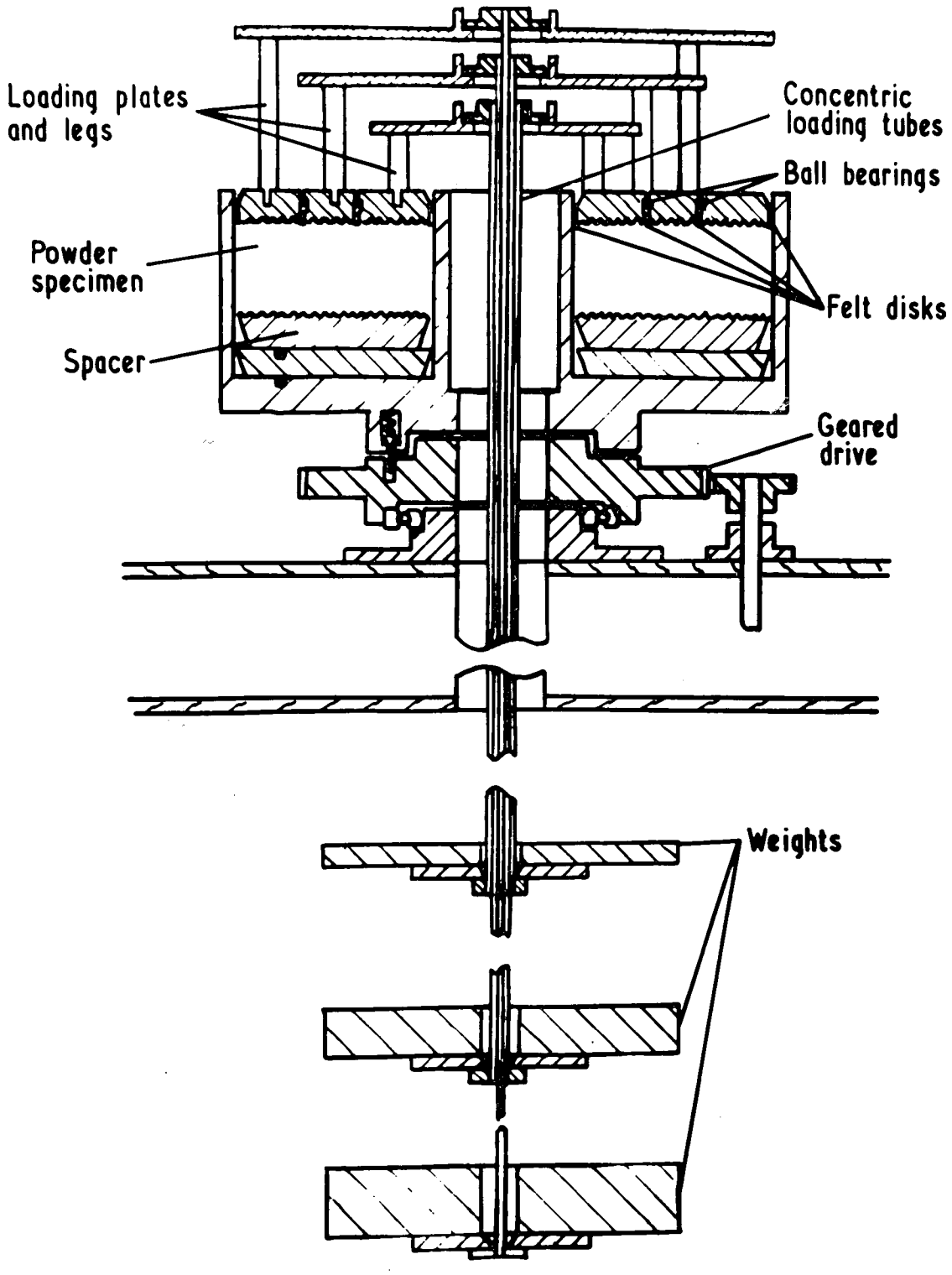

Figure 4.16. Schematic diagram of the Split Ring Annular Shear Cell, showing the normal load assembly

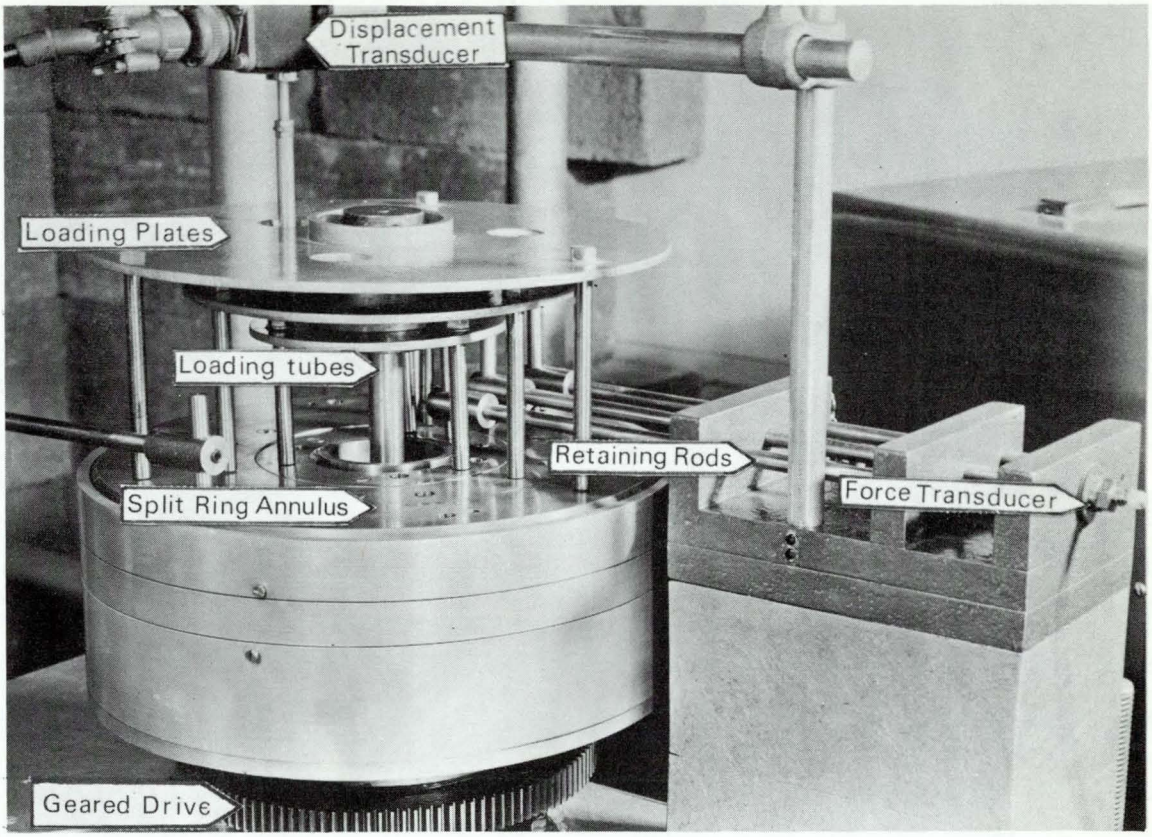

Figure 4.17. Top view of the Split Ring Annular Shear Cell showing torque measuring system and displacement transducer

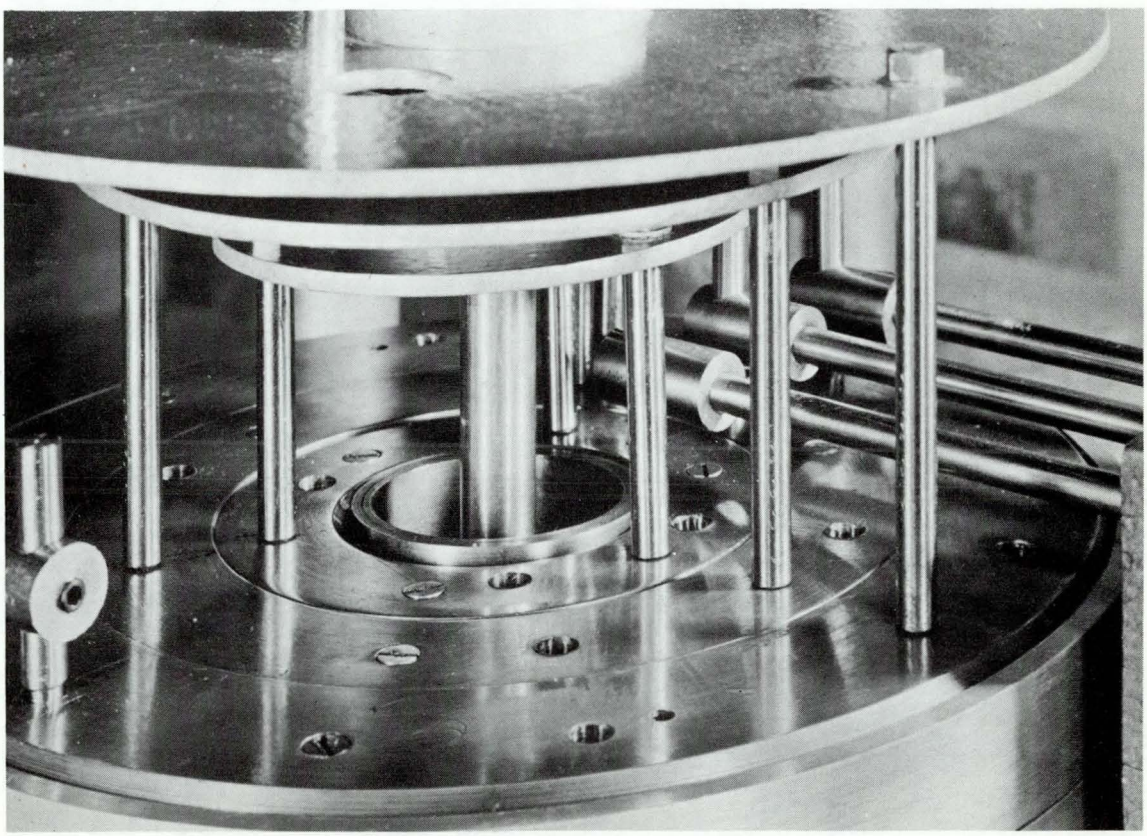

Figure 4.18. Close-up view of the cell showing the Split Ring Annulus

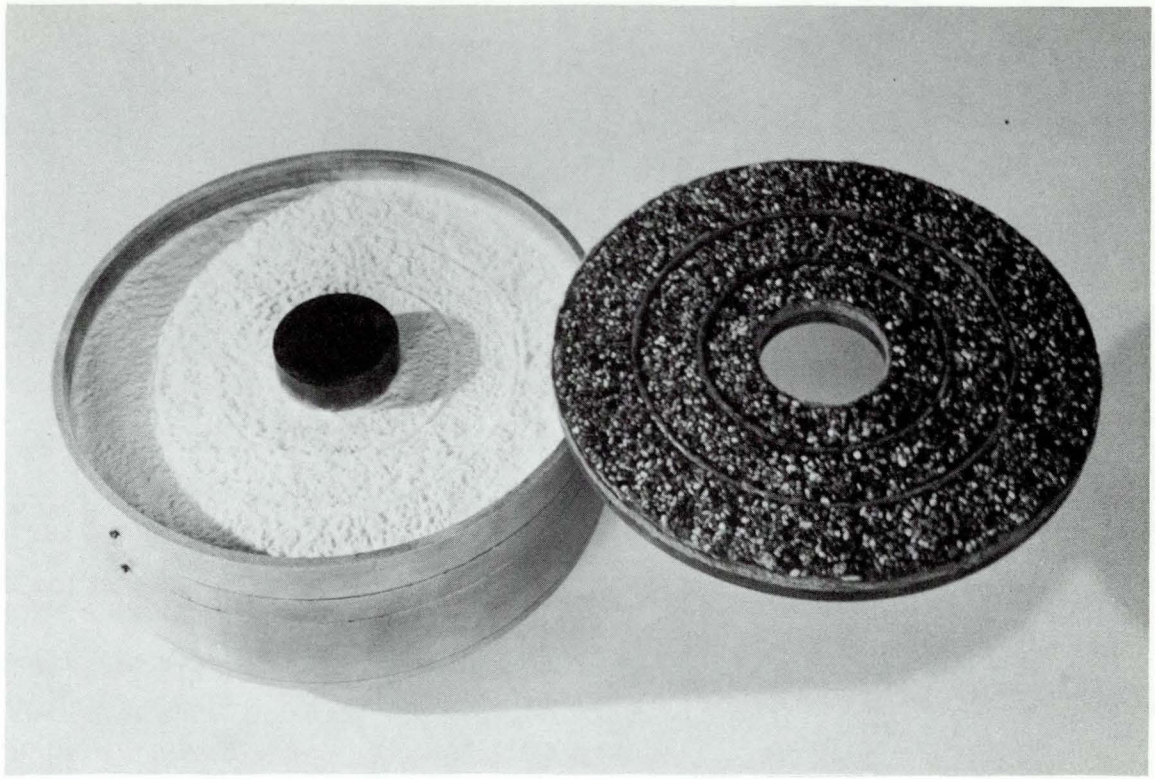

Figure 4.19. View of the base of the cell containing powdered material, and the underside of the Split Ring annulus showing roughened surface.

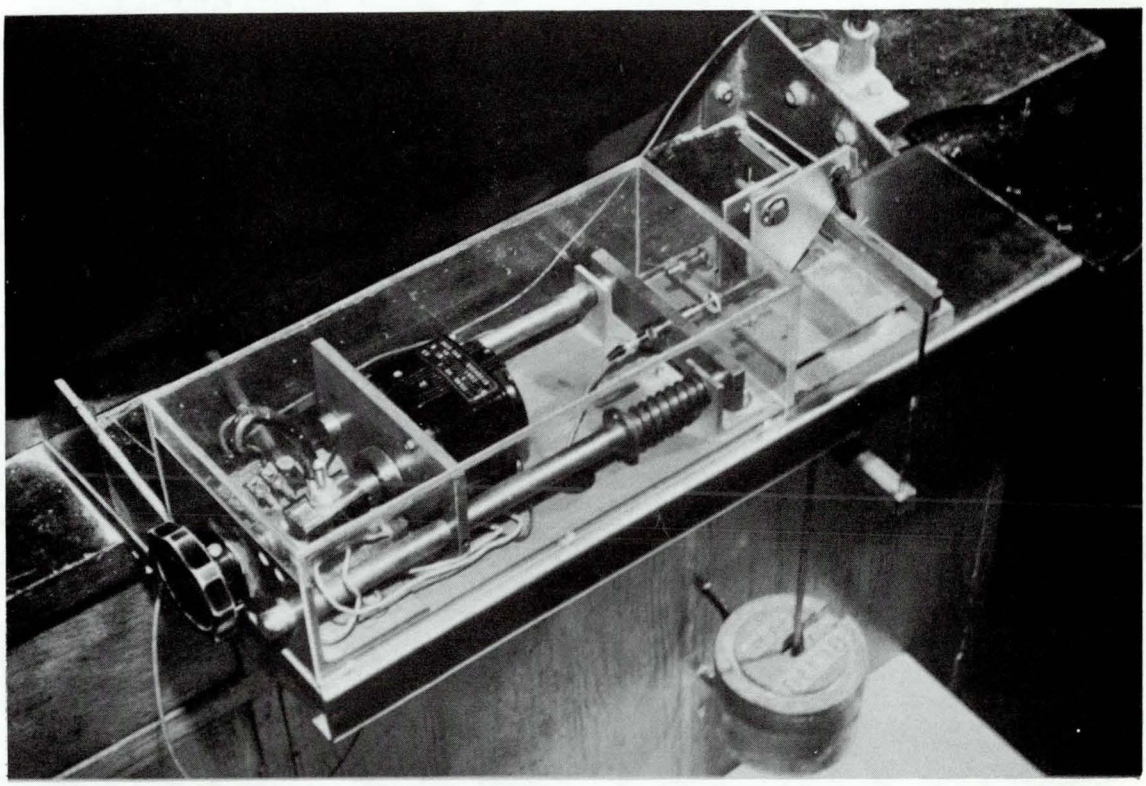

Figure 4.20. Jenike Flow-Factor Tester as used for calibration of force transducer

where ε = porosity

ρ = bulk density

ρ_s = specific density

This section now deals with the design considerations for the application of this technique.

4.2.1. Possible Methods of Measuring the Critical Porosity

There are four basic possibilities for the measurement of the critical porosity as follows:-

i. Assuming the porosity in the shearing zone is constant and the depth of the shearing zone is known, the simplest method is to measure the vertical dilation of the bed as recorded by the displacement transducer. The original packed density can be determined by weighing the sample contained in the cell and measuring the depth before shear. Then by a simple mass balance:-

$$\rho_c = \rho_i \frac{(H-h)}{H}$$

where ρ_c = bulk density at critical state

ρ_i = initial bulk density

H = depth of sheared region

h = dilation

ii. If a wet system was being used, a liquid penetration technique would be a suitable way of measuring the density via the volume of liquid necessary to fill the increase in pore space created by shear. This method, however, has many practical drawbacks and is unsuitable for a dry system.

iii. The material in the bed could be fixed in a resin after shear. When the resin had cured, examined sections of the bed would reveal not only the porosity but also the extent of the

sheared region. This technique has limitations chiefly due to the possibility of disturbing the bed when introducing the resin.

iv. A radiation technique could be used and the following three possibilities were considered:-

a. Using lead shot as a tracer, radiography taken through the shear cell before, during and after shear will indicate the extent and the amount of strain taking place within the shear cell and so give an indication of the porosity in the packed region and the zone of shear. Roscoe et al[137] have used this technique to study the strains in a soil mass subjected to plain strain. They have developed the technique to such an extent that they scan a radiograph automatically and the co-ordinates of the images of the lead shot are punched on to tape. This technique was not chosen for use with the annular shear cell as it was felt that the placing of the lead shot was not only tedious but also that there was the possible disturbance of the bed by the lead shot tracer.

b. The measuring of the intensity of a radiograph taken through the shear cell is the technique used by Cuttress and Pulfer[37] who have used cine X-ray film to examine the slip planes occurring when material is flowing out of a hopper. It has been used, also, by the soil mechanics group at Cambridge and discussed by Roscoe[187]. However, it was felt that this system was unsuitable for the present work, in that a circular cross-section was being studied rather than a plane cross-section as in the Cambridge investigation.

c. A gamma attenuation technique was, in fact, adopted as it was felt it obviates the problems of the disturbance of the bed, as in a., and the difficulty in analysing the data, as in b.

There follows a review of the technique, a preliminary investigation into its suitability and details of the final design of the system.

4.2.2. Gamma Attenuation as a Method of Measuring the Bulk Density of Particulate Materials.

4.2.2.1. History

The use of gamma radiation to measure soil density and moisture content belongs to the science of geophysics; and, according to Meigh and Skipp,[113] was first applied in 1941 by Pontecorvo.[127] In the latter years of the 1940 decade the use of the radio-isotope techniques for measuring accurately soil moisture and density were developed by Belcher.[9] Other early papers on the technique are those of Lane, Torchinsky and Spinks;[104] Stone, Kirkham and Read;[165] Underwood, van Bavel and Swanson;[182] Horojeff and Goldberg;[78] Bernhard and Chasek;[11] Vomocil;[184] Kodocikov and Jurjev.[99]

4.2.2.2. Gamma Ray Spectrometry

The nuclear method of determining density is based on the absorption of gamma rays through the Compton scattering effect. Gamma rays interact with matter in three ways, depending on their energy, giving rise to:-

i. The photo-electric effect (low energy gammas)

ii. The Compton scattering effect (intermediate energy gammas)

iii. Pair production (high energy gammas)

The photo-electric effect consists of the ejection from an atom by the gamma photon of an orbital electron. The

resulting pulse spectrum produces a single peak with a statistical spread.

The Compton scattering effect is a process in which only part of the energy is transferred to an electron giving a recoil electron together with a gamma photon of lower energy. The pulse spectrum thus obtained is continuous up to the photopeak. Compton scattering may also occur from the surroundings, giving rise to what is known as the "backscatter peak".

Pair production occurs where the energy of the gamma ray is greater than 1.02 MeV and absorption may occur with the production of a positron and an electron. The spectrum produced is a series of three peaks.

A diagram of the gamma spectrum expected with Caesium 137 is given in figure 4.21.

The radioactive source must provide an energy level in the range where the Compton effect is the only operative mechanism of absorption. Through this mechanism, when the source emits gamma rays (photons) into the soil, they collide with the electrons of the constituents of the material, for example sand, the density of which is required. The photons lose part of their energy and continue their travel along slightly deflected paths.

Considering the transmission of gamma rays as a simple wave motion, the simple exponential attenuation function common to all radiation may be used. This is the Beer-Lambert Law of exponential absorption in an homogeneous medium; and for mono-energetic radiation this can be expressed as:-

$$I = I_o e^{-\mu m}$$

I = transmitted intensity

I_o = incident intensity

μ = mass absorption coefficient

m = mass of material per unit cross section of the gamma ray beam

Thus, by considering a collimated beam and cutting out all low energy scattered radiation, the bulk density of the material can be determined.

4.2.2.3. Attenuation Coefficient

From the above equation, the semilogarithmic plot of transmitted intensity, I, versus the mass per square centimetre of absorber follows a straight line (figure 4.22.), the slope of which represents the probability that a photon will be removed from the incident beam per unit mass of the material. The attenuation coefficient, μ, is often expressed in cm^2/gm.

Harland and Urkan[62] investigated the effect of soil type on the transmission of gamma rays through soils and sands and they gave figures obtained from Grodstein's[59] tables for the mass absorption coefficients for clays and a well graded sand. These are given in table 4.1. below:-

Table 4.1. Soil mass absorption coefficients (cm^2/gm).

	Gamma Ray Energies (MeV.)					
	0.03	0.06	0.10	0.20	0.40	0.60
Heavy Clay	1.1909	0.2886	0.1765	0.1257	0.0953	0.0800
Sandy Clay	1.2247	0.2929	0.1777	0.1262	0.0956	0.0802
Well Graded Clay	1.0343	0.2688	0.1726	0.1257	0.0957	0.0803
Gravel Sand Clay	1.0402	0.2697	0.1728	0.1258	0.0957	0.0804

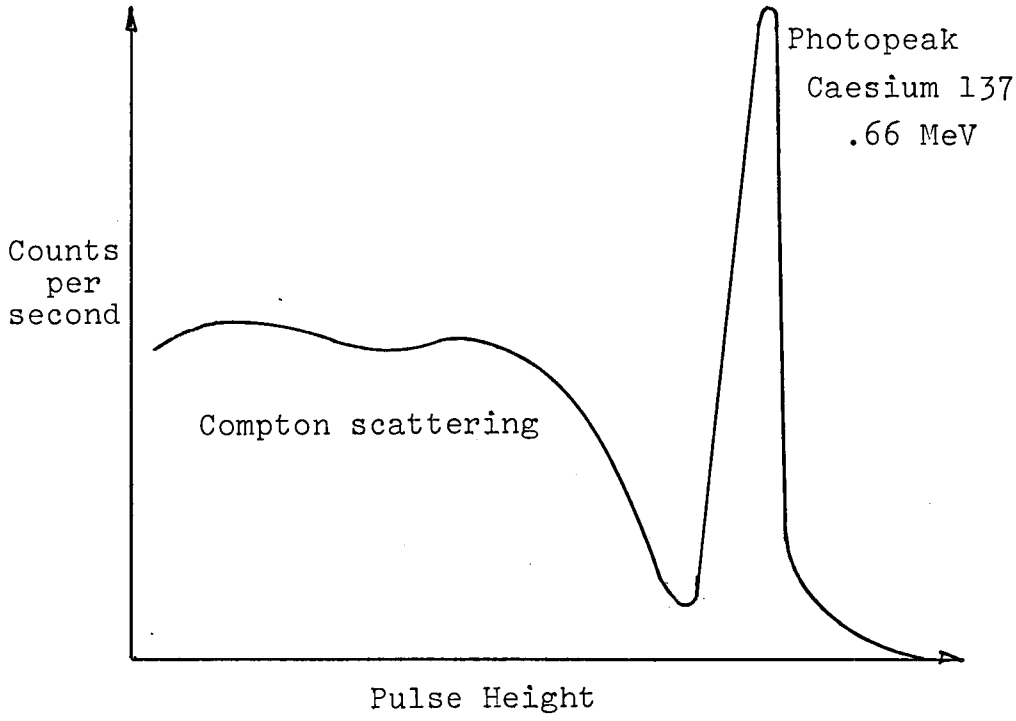

Figure 4.21. Gamma spectrum for Caesium 137

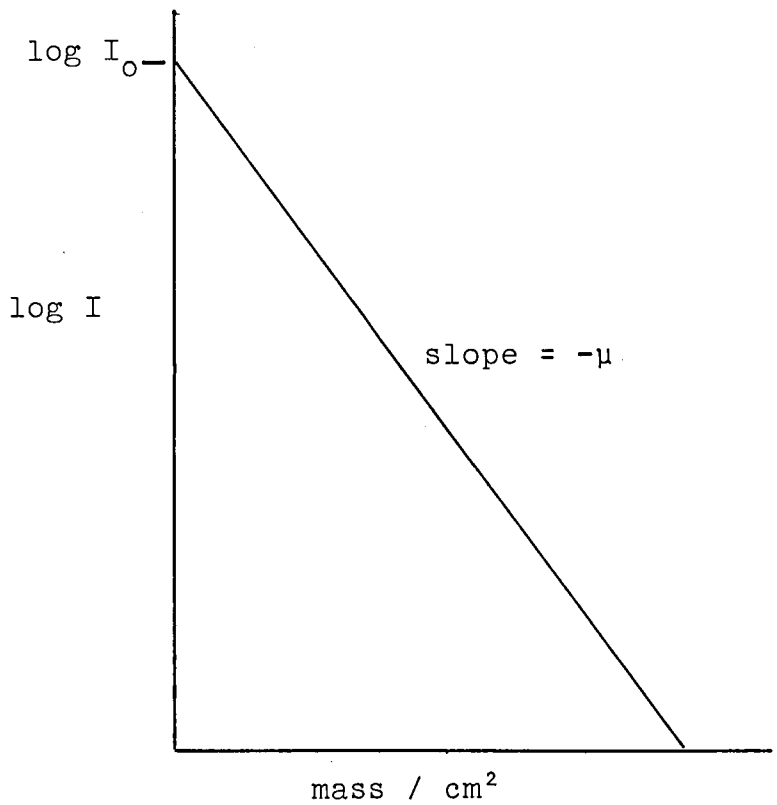

Figure 4.22. Semi-log. plot of transmitted radiation, I , versus mass per square centimetre of absorber

A number of authors, including Ralston and Anday[128], have emphasised the need for good calibration of the device used, to ensure a good value for the mass absorption coefficient.

4.2.2.4. Effect of Particle Size Distribution

Lewis[109] showed that coarse non-cohesive soils are poorer absorbers of gamma rays than cohesive clays, indicating a possible correlation between material and grading. Harland and Urkan[62] studied the absorption for coarse and fine fractions of a gravel sand clay; and found that there appeared to be a somewhat greater absorption with the fine than with the coarse fraction. However, it is reported in their studies that the difference could have been due to differences of moisture content. Their experiments included backscatter measurements as well as direct transmission measurements and it was seen from these that the effect of "soil type" was more significant in backscatter measurements.

4.2.2.5. Scintillation Counting

Gamma rays are forms of electromagnetic radiation produced by transition between nuclear states. Certain substances fluoresce when bombarded with ionising radiation, each "particle" causing a tiny flash of light (scintillation). A scintillation counter consists of a number of intermediate electrodes or dynodes to which steadily increasing voltages are applied. The photoelectrons, which are emitted from the light sensitive surface of the photomultiplier face, are multiplied through the tube and the current pulses are converted to voltage pulses which are again amplified and counted by a scaler or ratemeter.

For gamma rays a sodium iodide crystal is generally used as a scintillant. It is essential to have good contact between this and the face of the photomultiplier tube. To protect the crystal and to absorb any beta radiation the crystal is enclosed on its face by a thin aluminium cover.

The pulse height from the gamma ray is dependent upon the energy of the radiation; and in a scintillation counter the pulse produced is proportional to the energy lost by the gamma ray in the crystal.

4.2.3. Preliminary Investigation into the Use of Gamma Ray Attenuation Technique for the Measurement of the Porosity of Sand

Before obtaining the expensive equipment necessary in the use of gamma ray spectrometry, a study was made of the possibility of using the technique for the measurement of the bulk density of free flowing sand and its accuracy in detecting density changes.

4.2.3.1. Radio-active Source

From an estimation of the total thickness of sand through which the gamma beam would have to pass, and the necessary collimation required, a suitable radio-active source was selected. This was Caesium 137. The 132 milli-curie source of Caesium 137 had a half life of thirty years and an energy of 0.66 MeV. The source, supplied by the Radiochemical Centre at Amersham, was in the form of a 3mm. bead enclosed in an aluminium capsule.

For these preliminary studies a "mock-up" version of the base of the proposed annular cell was made, the outer walls

being constructed of aluminium. The Caesium source was contained in a collimated tube which fitted into a lead vessel used for storing sources.

The intensity of the gamma radiation was detected by a scintillation counter with a sodium iodide crystal. An arrangement of the apparatus used for this investigation is shown in figure 4.23.

4.2.3.2. Caesium Spectrum

The pulse spectrum obtained from the Caesium source was obtained by passing the output pulses from a scintillation counter through an amplifier and then a pulse height analyser to a ratemeter or scaler.

The single channel pulse height analyser, as used, contains two discriminators, the separation between which may be varied. The lower value is called the "threshold" and the separation is termed the "gate width". An output pulse is obtained when the lower discriminator fires without the upper one firing. It was therefore possible to scan the whole pulse spectrum manually by gradually raising the lower discriminator setting and recording the count for each setting.

4.2.3.3. Pulse Spectra with and without Sand

For the initial studies a series of collimators could be fitted to the scintillation counter. The need for the collimators and the shielding around the counter was to cut out, as far as possible, any scattered energy.

½", ¼" and 2mm. collimators were used in turn to obtain the pulse spectra for the Caesium source. Sufficient room was left between the source and the counter to place the annular

shear cell base between them. A spectrum for each collimator was obtained first with the cell base empty and, then, with it filled with sand. The spectra obtained were as expected and are given in figure 4.24.

4.2.3.4. Effect of Different Sand Packings

Having determined the photopeak and its width, the "threshold" was set so as not to detect any backscatter, but just to measure the photopeak.

Using the ¼" collimator on the counting end, the following test was conducted. Sand of size 8-14 B.S.S. mesh was loosely poured into the cell and thirty counts each of a hundred seconds duration were taken with the cell between the source and the counter. More sand was added into the cell, packed tighter and again scanned. The results were statistically examined to see if the distribution followed a Poisson distribution, to check whether a true record of disintegrations was given. Another set of results was obtained by passing the beam through a region of tight and loose sand in the cell base. The experiments were repeated with a 36-52 B.S.S. mesh sample.

4.2.3.5. Conclusion from Gamma Attenuation Experiments

From these preliminary experiments, the use of gamma attenuation for the measurement of bulk density was found to be possible. The results showed that it was a suitable method of detecting the density changes within the shear cell.

On the basis of this work and the literature, a scintillation counter, H.V. unit, pulse height analyser and ratemeter were obtained.

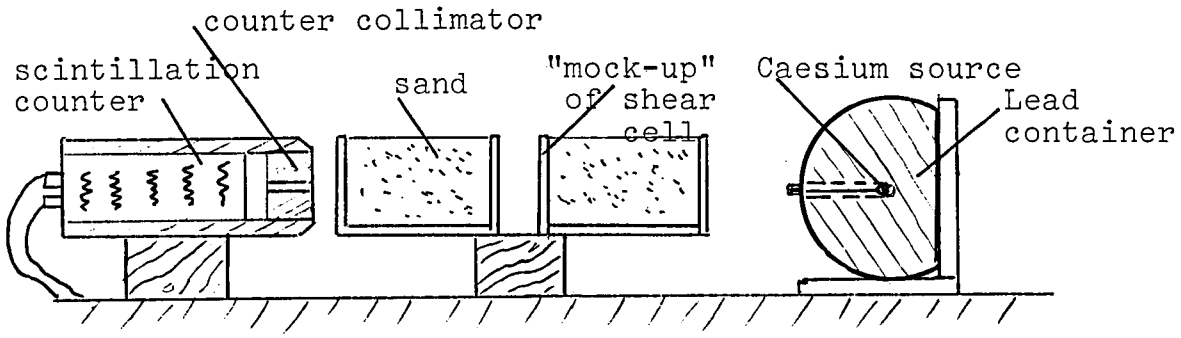

Figure 4.23. Arrangement of apparatus used in preliminary gamma attenuation investigation

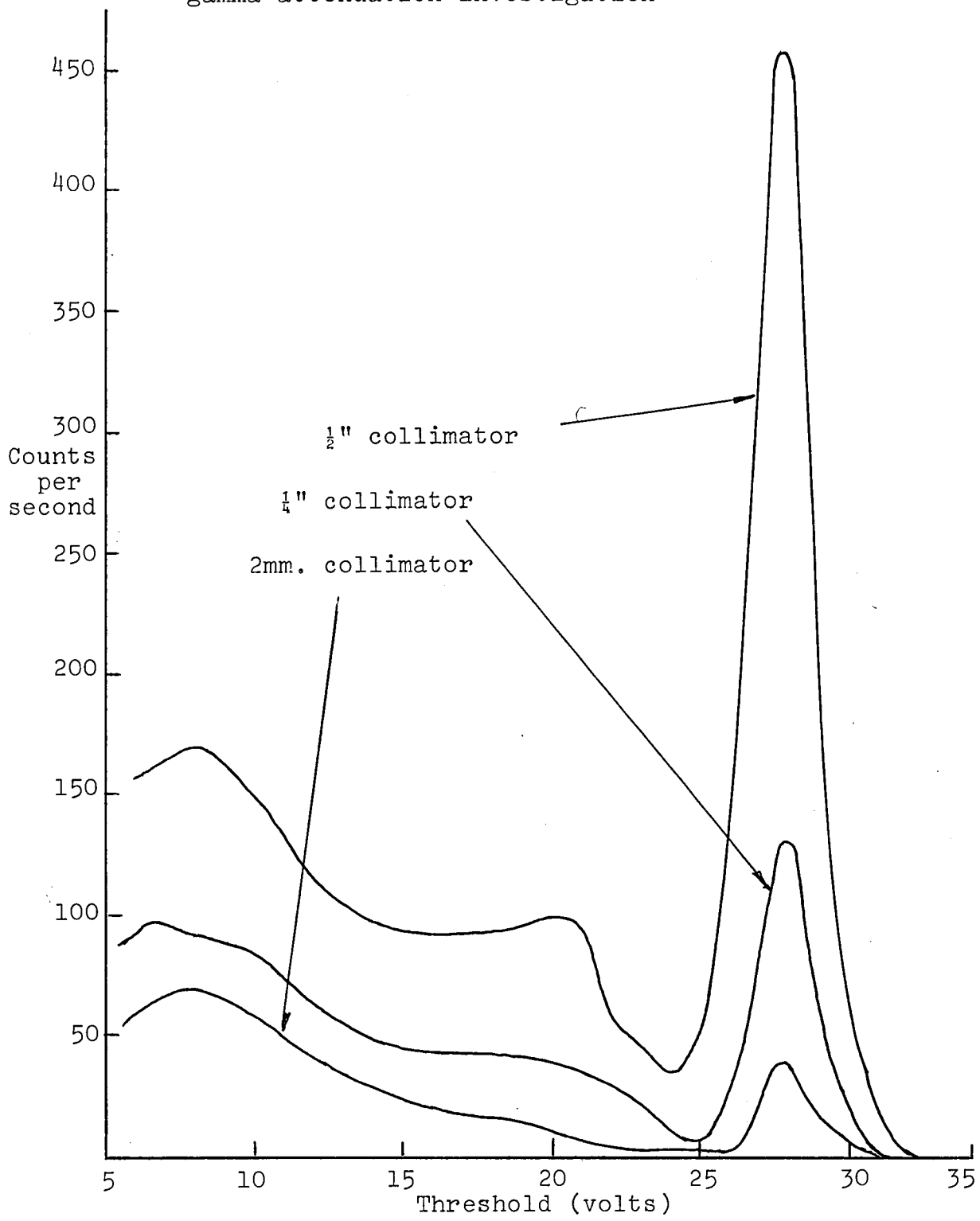

Figure 4.24. Caesium spectrum obtained with sand for different collimators.

4.2.4. Design of Gamma Attenuation Unit for Use with the Split Ring Annular Shear Cell

The system to measure the absorption of gamma rays from a source, through the shear cell, had to be such that it was able to scan the cell horizontally and vertically with a horizontal narrow beam of radiation.

A diagnostic scintillation counter was obtained as this was already a shielded and suitable collimated unit. The counter was mounted so that it could be directed in all directions.

From the considerations of the strength of the Caesium 137 source and the allowable limits of radiation, the source was enclosed in a spherical lead container giving approximately four inches of lead shielding. A cross section diagram and photograph of the container are shown in figures 4.25 and 4.26 respectively. The collimation for the source was 2mm. and the source (A) could be isolated within the lead container by turning the rear knob (B) so taking the source out of the line of collimation.

Since the total mass of the lead surrounding the source and counter was considerable and to ensure that the two were constantly in line, it was decided to design a system where the shear cell unit was moved in the gamma beam, rather than the beam moved over the cell.

A scafold frame was constructed to hold both the lead container and the counter rigidly in place. A trolley was fitted between the container and the counter to hold the shear cell unit. This trolley could be racked into the path of the beam in a vertical and horizontal direction. A photograph and a block diagram of the shear cell unit on the trolley, the

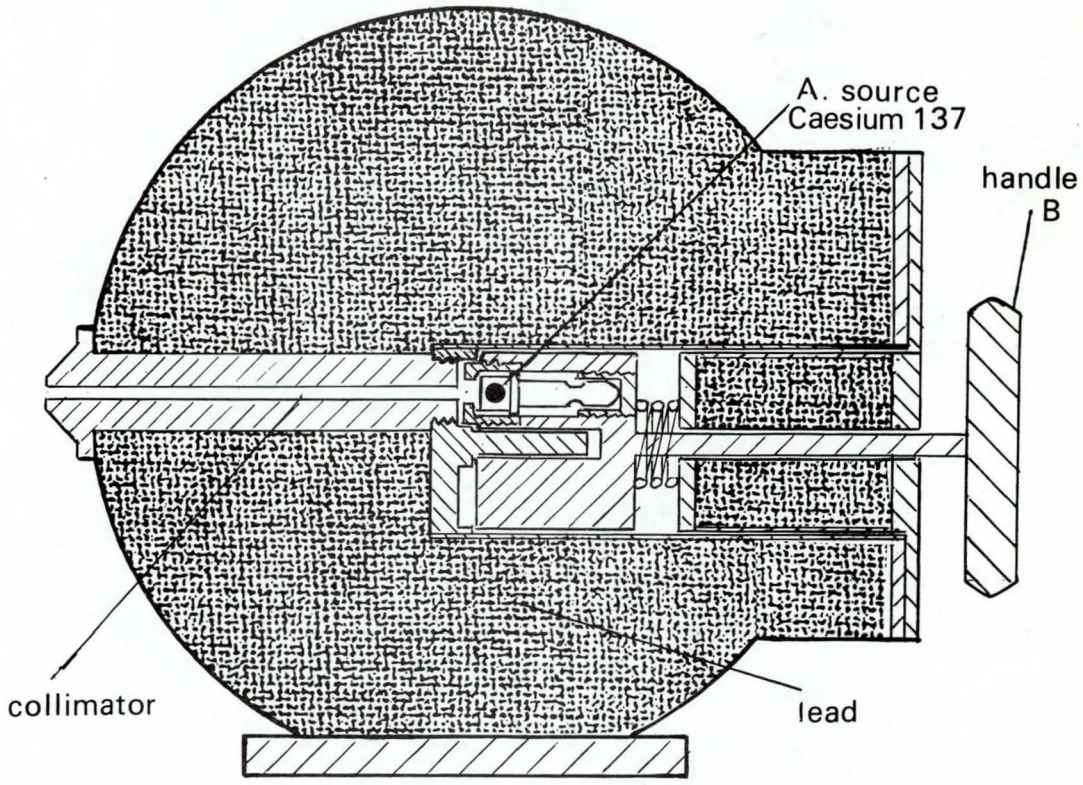

Figure 4.25. Cross-section diagram of lead container for Caesium 137 source.

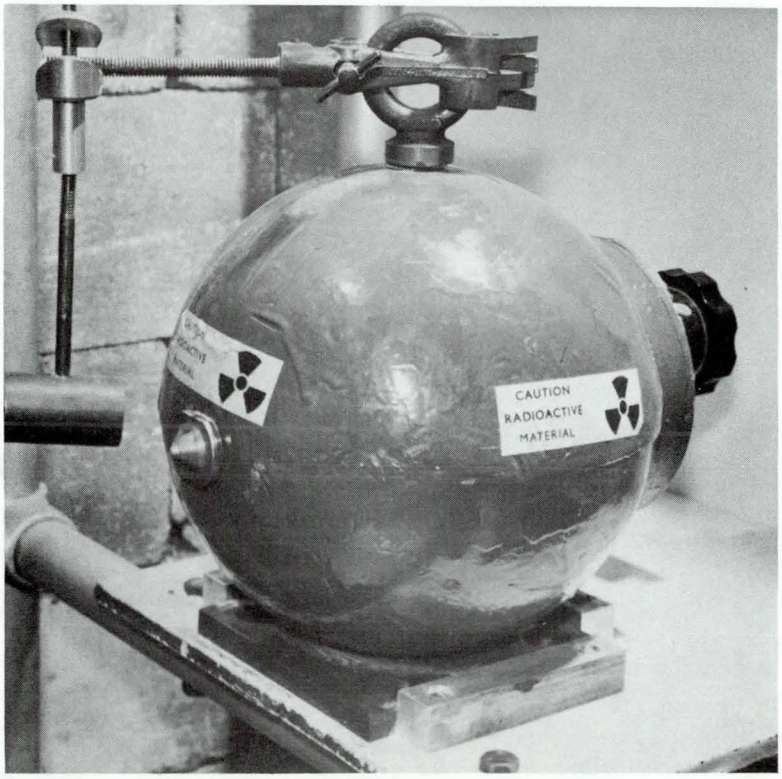

Figure 4.26. Photograph of lead container for Caesium 137 source.

counter and the lead container are shown in figures 4.28 and 4.29, respectively.

Due to the narrow collimation used, perfect alignment of the source and the counter was necessary. The container without its source and rear attachments and the counter without the photomultiplier tube and crystal were located in an approximate position. A light was inserted into the container in line with the collimator and the units moved until the beam of light located on to the centre of a screen fixed at the rear of the counter. (Figure 4.27). The units were then fixed rigidly.

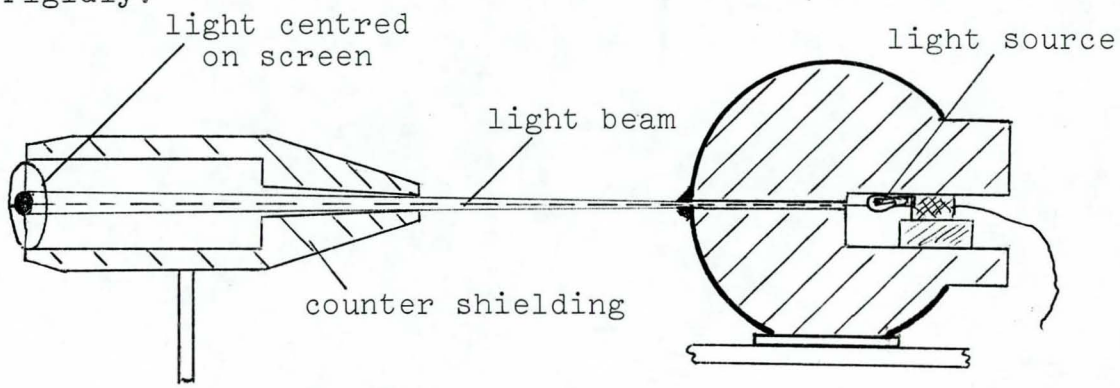

Figure 4.27. Alignment of Scintillation Counter and Caesium 137 Collimator.

4.2.5. Setting up H.V. Unit, Pulse Height Analyser and Ratemeter

With the "threshold" setting at 40% of its total range and the "gate width" fully open, the H.V. was slowly increased until a count was indicated by the ratemeter. The H.V. reading was then noted for subsequent setting-up. The "threshold" was then increased in sets of five volts, from 0 to 60, for different discriminator widths; and the Caesium spectrum obtained for the beam passing through the maximum quantity of sand. The spectrum obtained for one discriminator

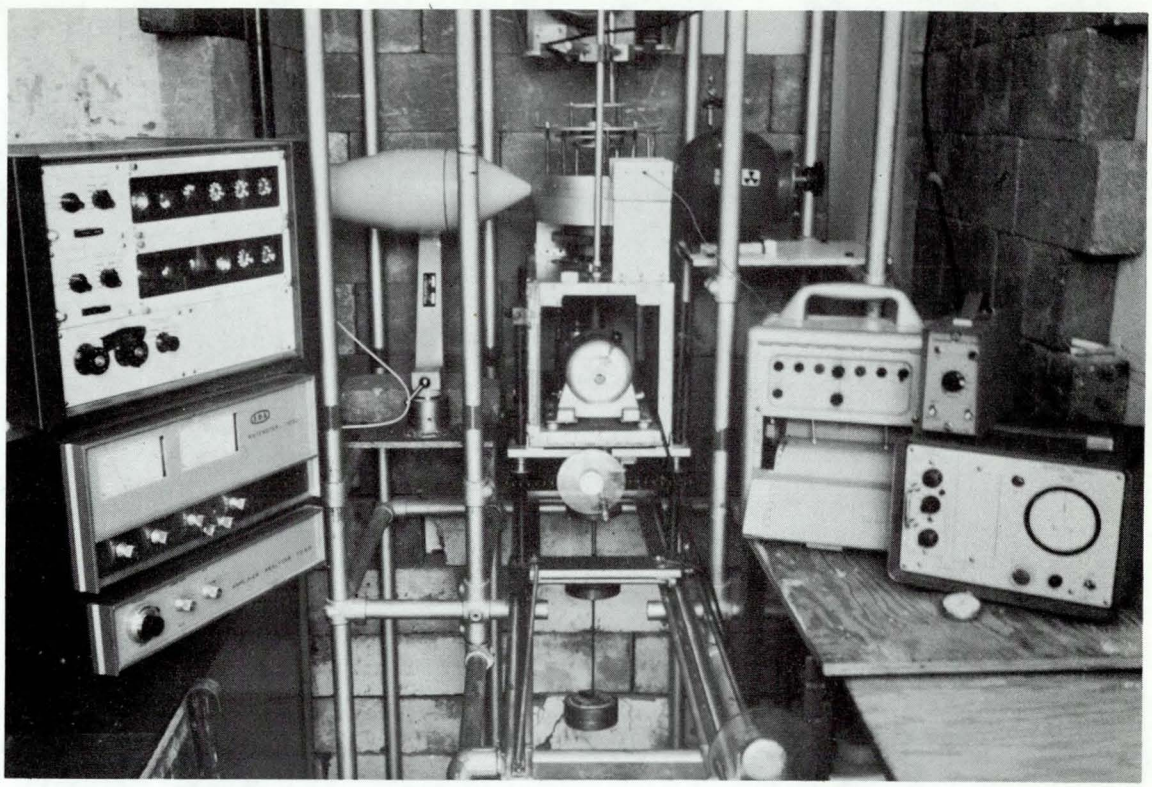

Figure 4.28. Photograph of Shear Cell, source container and scintillation counter arrangement.

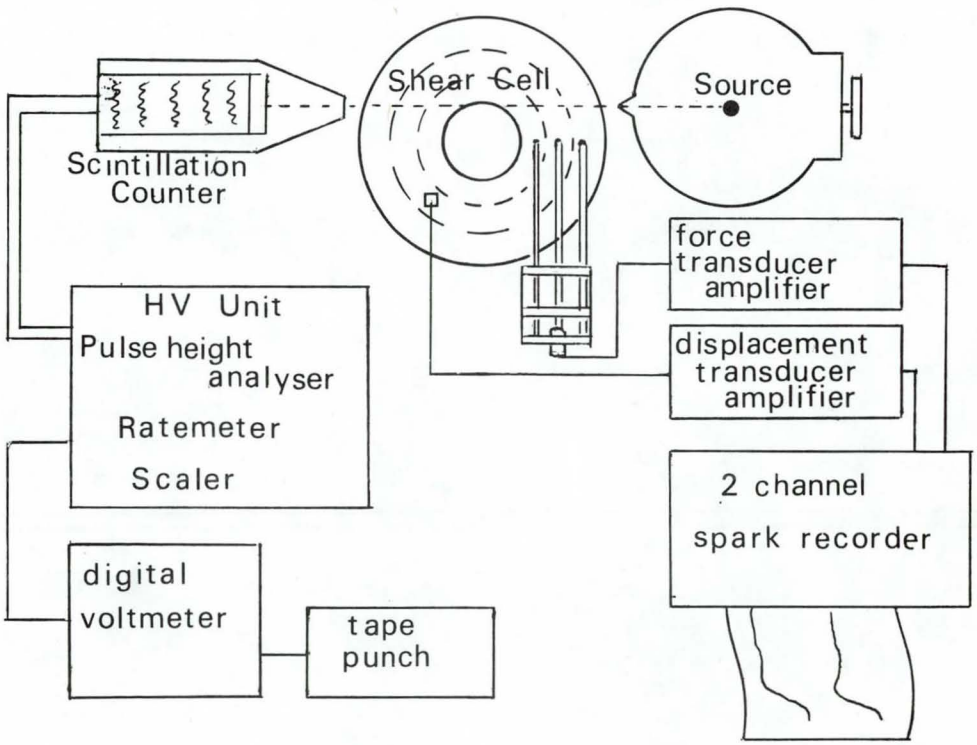

Figure 4.29. Block diagram of apparatus arrangement.

width is shown in figure 4.30.

The limiting factor of the system was the ratemeter, in that the maximum allowable count was 10,000 counts per second. The "threshold" and "gate width" were so set that the maximum count rate was no more than the limit of the ratemeter and so that only the peak area was counted to eliminate backscatter detection.

4.2.6. Determination of Mass Absorption Coefficient

To determine the mass absorption coefficients for the sand used, it was necessary to determine the attenuation for known quantities of sand. For this purpose a calibration box was built which consisted of five sections of known dimensions, each section being separated by thin pieces of aluminium. This box was fitted, in place of the shear cell, between the source and the detector so that the beam passed through its centre. (Figure 4.31).

The count was taken with and without the box and also when the box contained a "standard" piece of lead, which was used for setting up the equipment each day. The sand sample was poured lightly into the centre section 3, and the count measured. The box was vibrated, more sand added to section 3 and again vibrated until no more sand could be added, and the count measured. The operation was repeated through all the sections 2, 4, 1 and 5 until all the boxes were filled. The weight of sand added to each section was noted and from the dimensions of each section the bulk density determined. Using this bulk density value and the length of absorber per section, the total mass per square centimetre in the beam direction was determined and plotted against the $\log_e$ of the count per second. Figures 4.32 - 4.34 give the plots for each of the sand samples from which the mass absorption coefficients were determined.

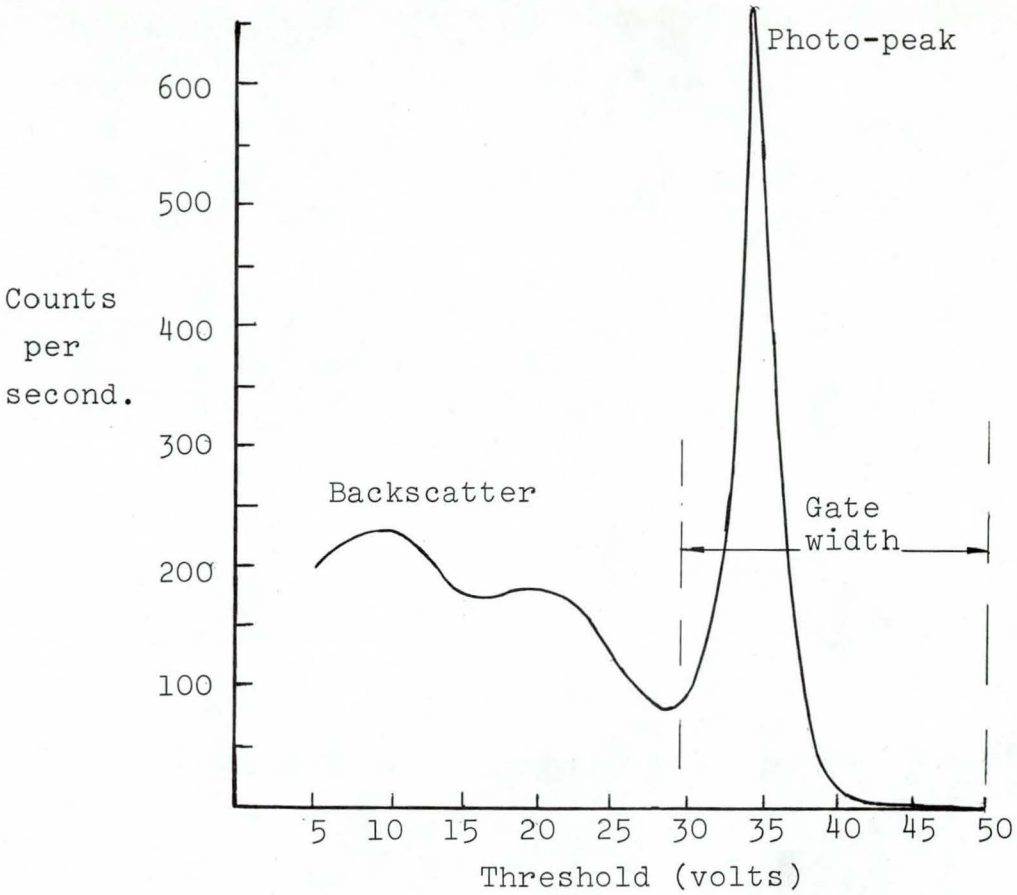

Figure 4.30. Caesium 137 spectrum, showing photopeak over which the gamma attenuation was measured.

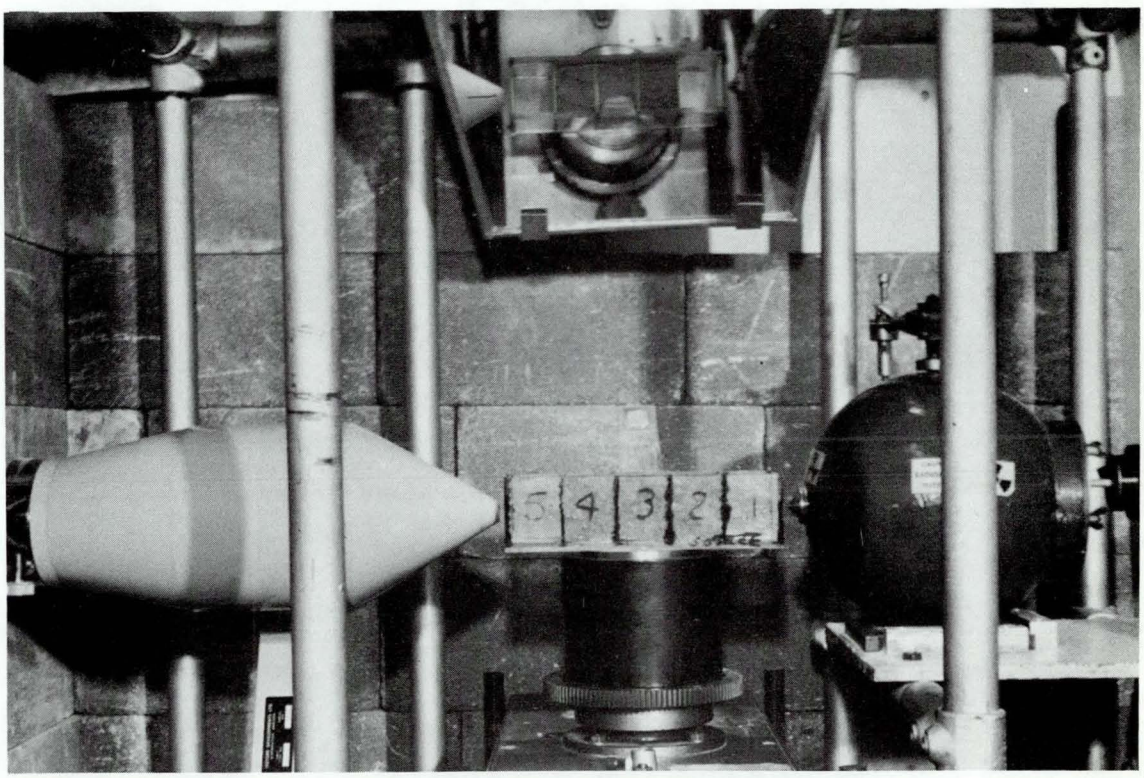

Figure 4.31. Photograph of calibration box between source and detector, for the determination of the mass absorption coefficient.

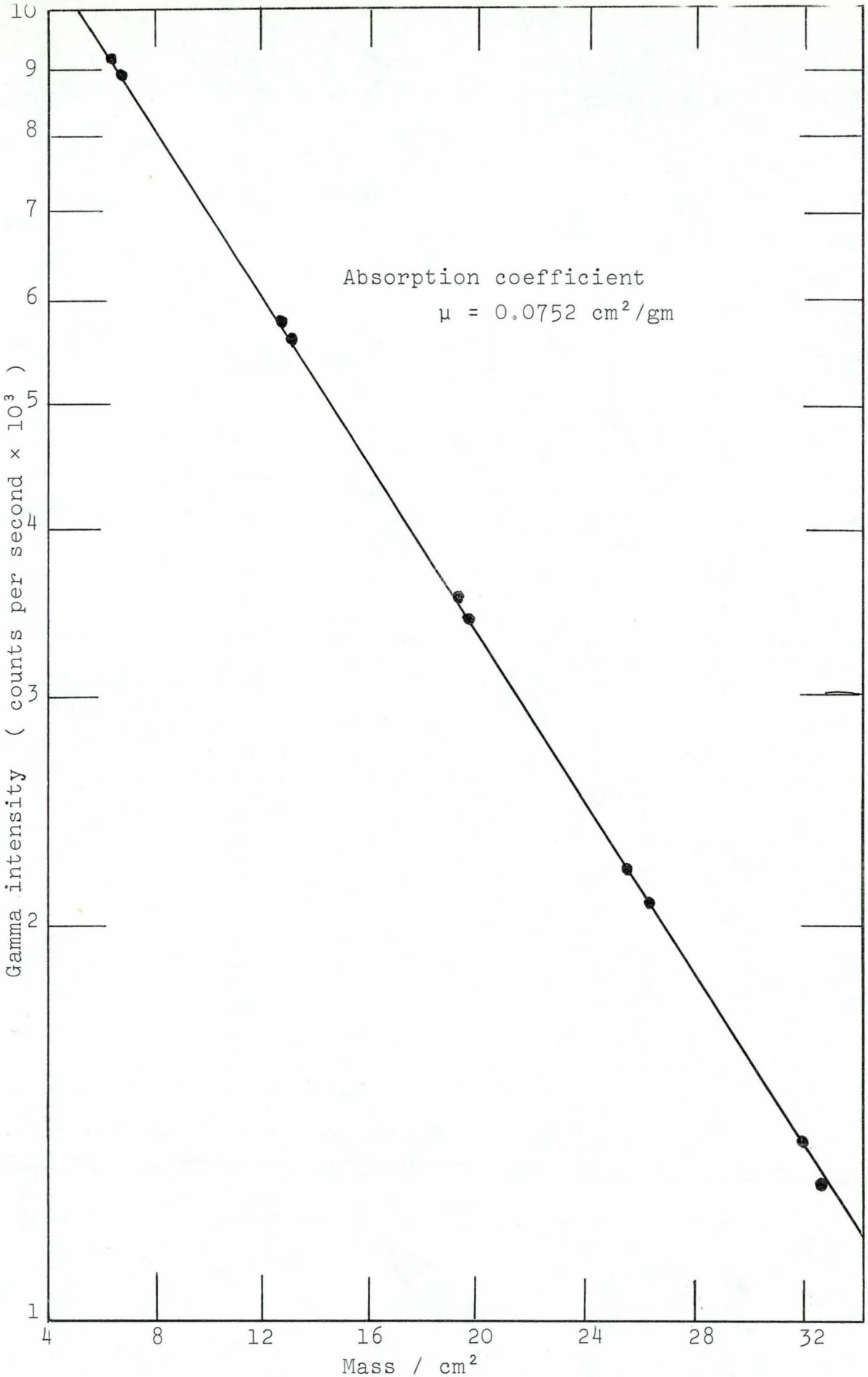

Figure 4.32. Semi-log plot of gamma intensity versus gm/cm² for 14-18 B.S.S. mesh sand

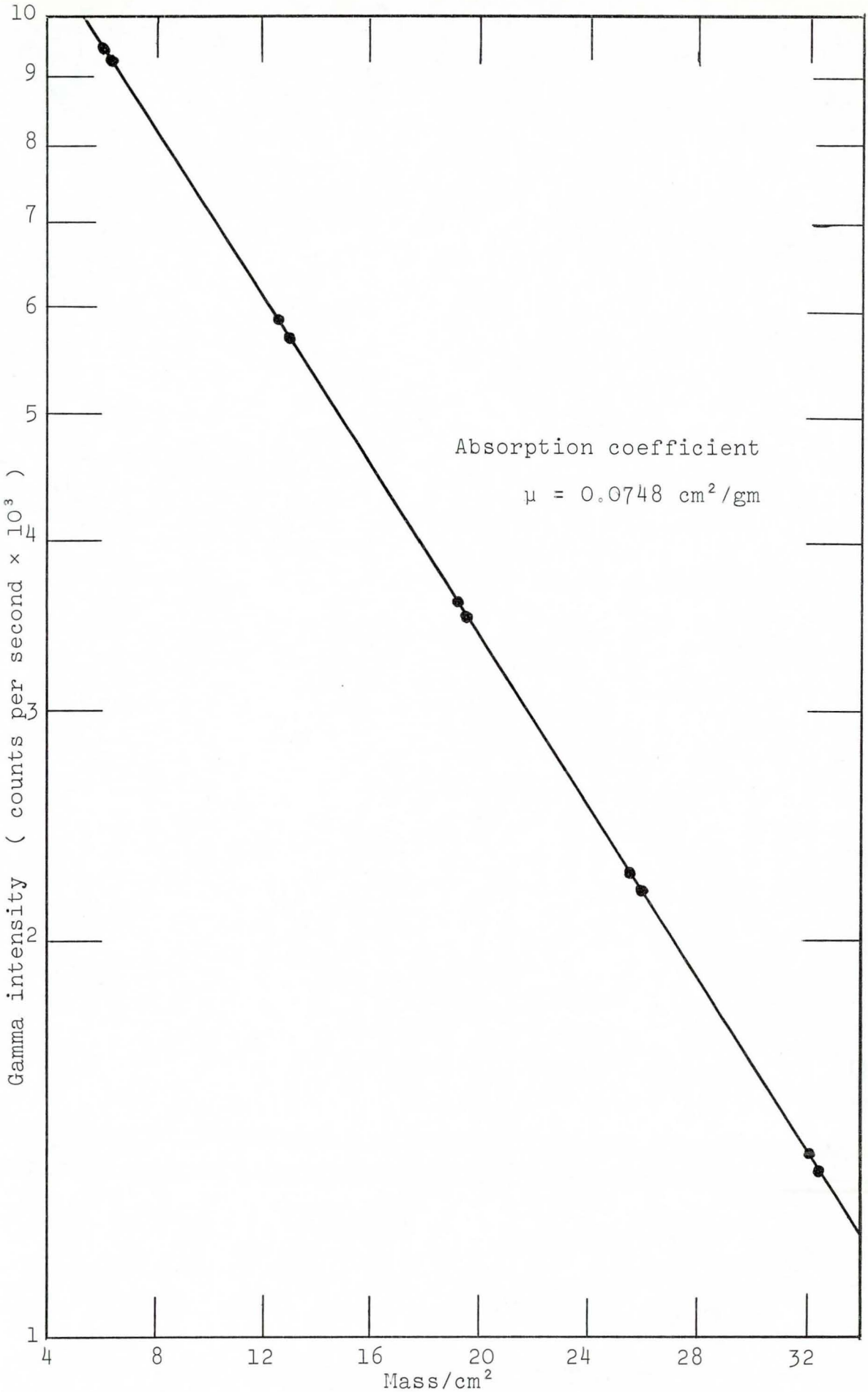

Figure 4.33. Semi-log plot of gamma intensity versus gm/cm for 36-52 B.S.S. mesh sand.

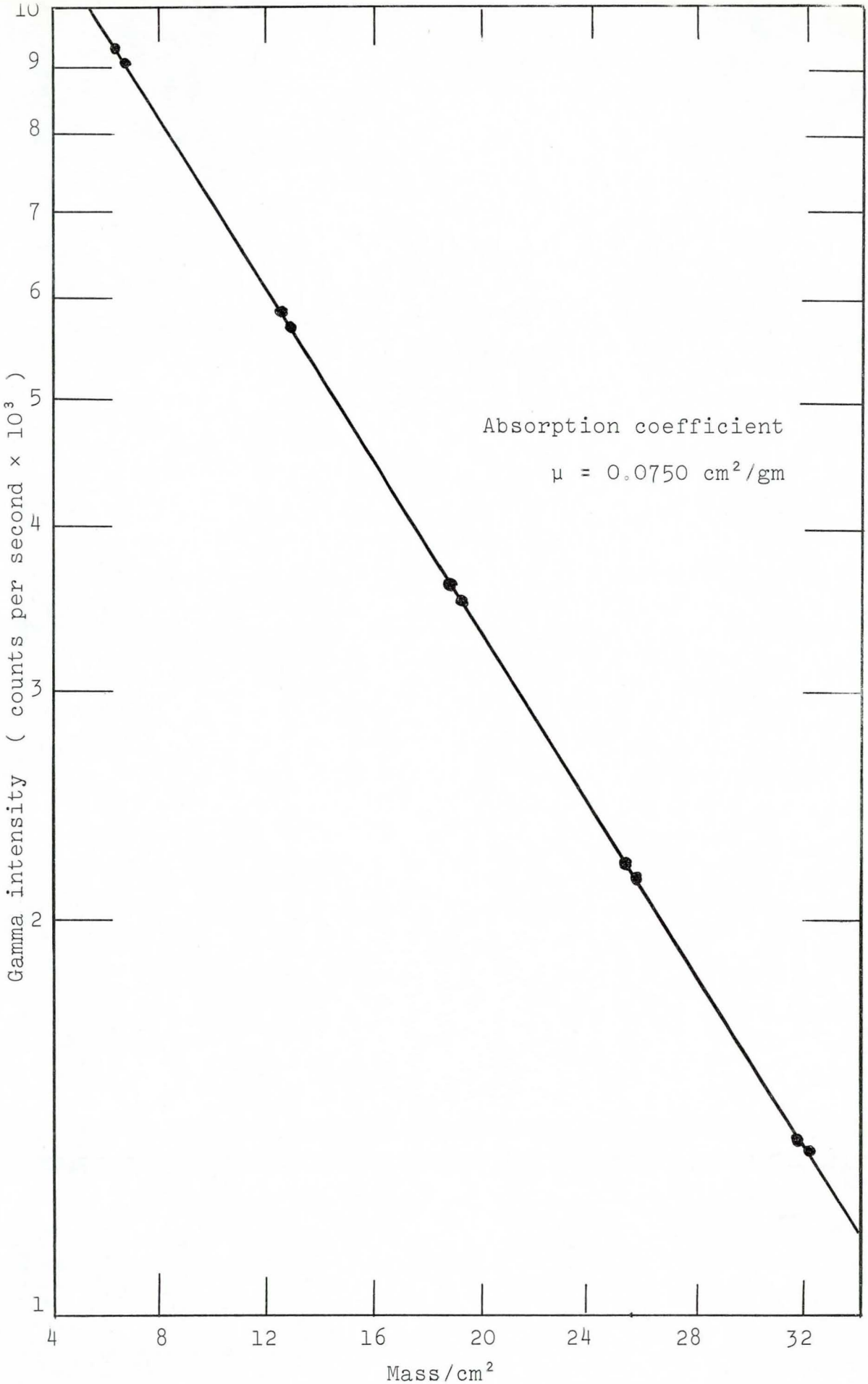

Figure 4.34. Semi-log plot of gamma intensity versus gm/cm² for 60-85 B.S.S. mesh sand

CHAPTER 5

EXPERIMENTAL MEASUREMENTS

CHAPTER 5:- EXPERIMENTAL MEASUREMENTS

5.1. Evaluation of Split Ring Annular Shear Cell

5.1.1. Influence of Wall Friction

One of the reasons for using a Split Ring Annular Shear Cell was to avoid the measurement of the stress concentrations at the walls of the cell.

Tests were conducted to examine if there was any difference in the shear stress measurement when the apparatus was used in the conventional form, compared to that obtained when it was used in the "Split Ring" form. To convert the apparatus into a conventional annular shear cell, the split ring plates were strapped together and the lid was constrained from rotation by the centre rod, only, bearing against the force transducer.

The tests were conducted on a sample of sand of 30-36 B.S.S. mesh and at one normal stress.

The cell was prepared in the same way for each series of tests. The sample was poured into the cell, tapped down on the bench and then scraped level. The shearing plate was then fitted to the cell, the whole transferred to the annular shear cell drive unit and the weights added.

For each mode of operation (that is the plates unlocked and locked) a number of runs were made at the same normal load and a trace taken of the torque necessary to retain the shearing plate while the base of the cell rotated.

An example of the trace of the torque for the shear cell in the conventional form and for the shear cell in the Split Ring form is given in figure 5.1.

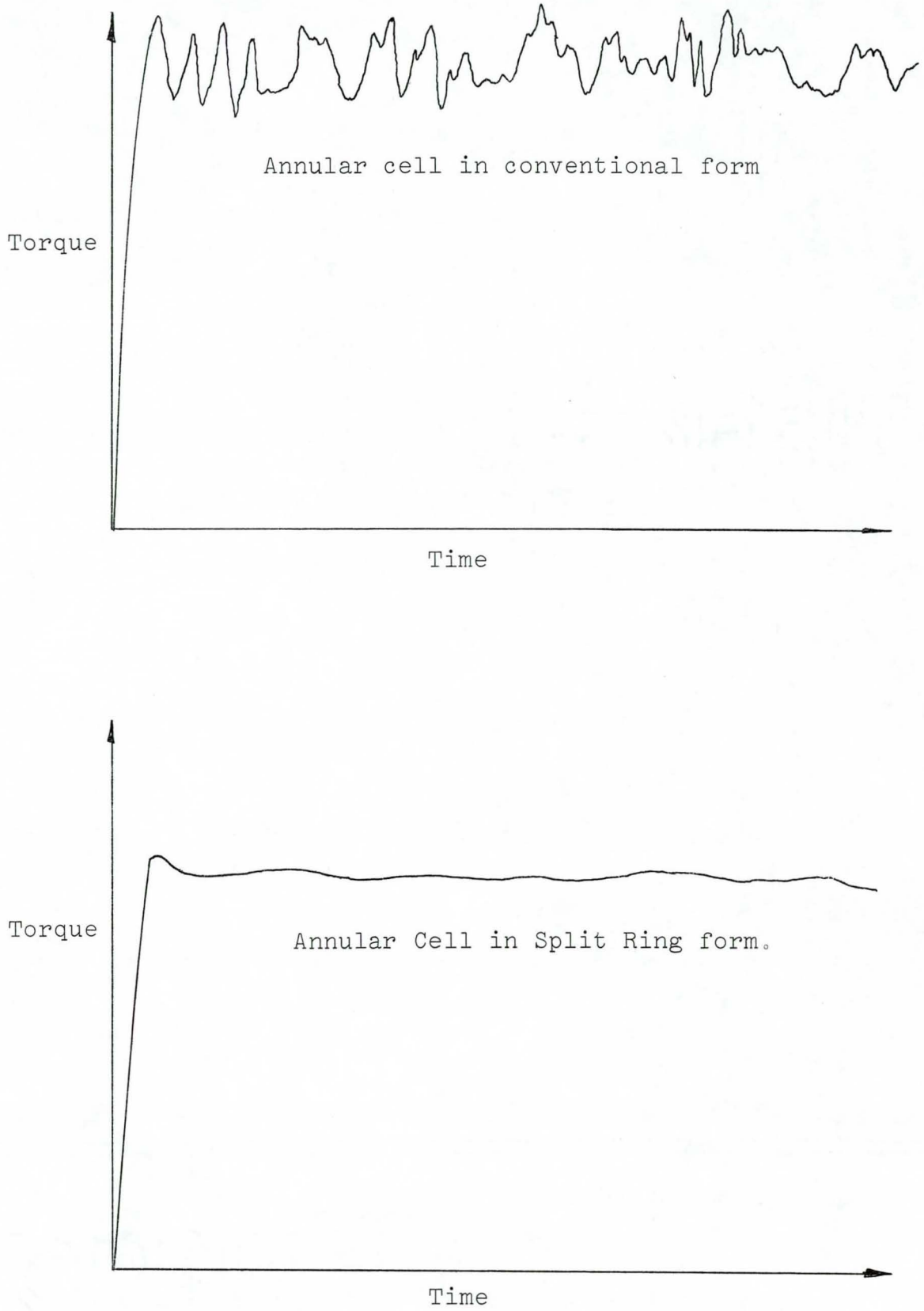

Figure 5.1. Traces obtained from wall friction test

The table of results is given in table T.1.*

5.1.2. Surface Contact Test and Horizontal Flow Profile Examination

To ensure that there was good contact between the shearing plate and the material contained in the cell, a visual examination was made of the form of the material bed after having sheared for approximately one third of a revolution.

The material used for the test was sand, a portion of which had been dyed. When making up the bed of material in the cell a vertical layer of dyed tracer sand was also added. A photograph was taken of the bed, with the shearing plate removed, both before and after shear. These photographs are shown in figure 5.2.

5.1.3. Comparison of Jenike, "Portishead" and Split Ring Annular Shear Cells

By arrangement with I.C.I. Dyestuffs Division, a comparison was made of a modified "Portishead" Annular Shear Cell, a Jenike Shear Cell and the Split Ring Annular Shear Cell. The tests on the "Portishead" Shear Cell were made by I.C.I. Dyestuffs Division.

The material used for the test was a sample of adipic acid as supplied by I.C.I.

The procedure as required for the formation of yield loci for design purposes was used. The same consolidation loads were used for each type of cell.

*The tables of all the results are given in appendix A.3.

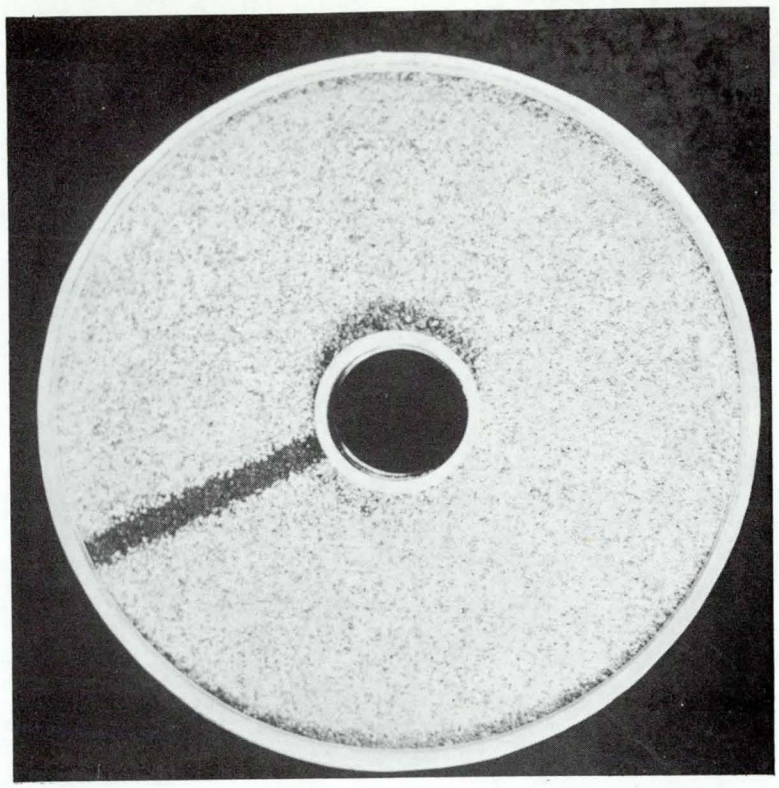

Figure 5.2a. Dyed tracer showing horizontal profile before shear.

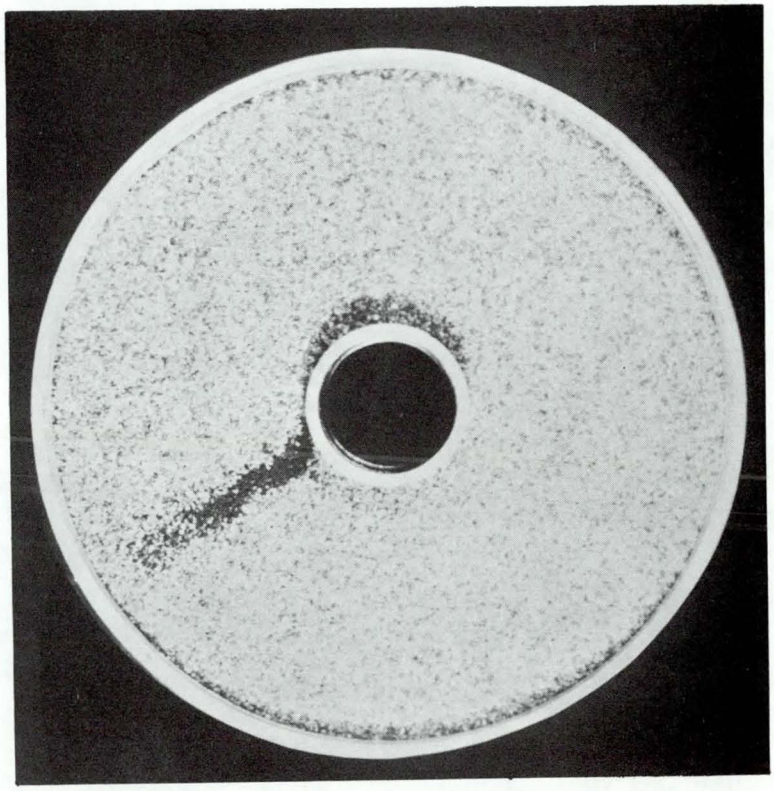

Figure 5.2b. Dyed tracer showing horizontal profile after shear, indicating the stress concentration at the walls of the cell.

The procedure for the Jenike test was as follows. Material was poured into the Jenike cell (with a mould ring attached), pressed down with the fingers and scraped level. The consolidation load was added, and approximately thirty twists applied to the cover. The mould ring was removed and the top surface again scraped level. After the shearing cover had been applied, together with the consolidation load, shear force was applied. When a steady shear stress had been reached, the shear force was removed, and the consolidation load replaced by a lower load. Shear force was again applied and the peak shear stress noted. For each point on the yield locus this procedure was carried out, emptying and repacking the cell each time.

The procedure for the Split Ring Annular Shear Cell tests was as follows. The material was poured into the cell which was then tapped on the bench and the surface levelled. The shearing plate was fixed and the cell mounted on the drive unit. A consolidation load was added to each of the three annuli; and torque applied. When a steady state had been reached, indicated by a steady torque value, the torque was retracted, the consolidation loads were replaced by normal loads (of lower value than the consolidation loads) and the torque reapplied. The peak shear stress was then noted. This procedure was repeated for a number of normal loadings for each of a series of consolidation loads. The whole test was completed without emptying the cell.

The procedure for the "Portishead" cell, as carried out by I.C.I., was similar to that for the Split Ring Annular Shear Cell given above.

The results obtained from all three types of cell were

plotted on τ, σ plots. The peak values for the normal loads and consolidation loads and the steady state consolidation value for the annular cells were plotted. A significant point is that the steady state value for the Jenike cell is the failure value as the material is packed so that the shear stress does not go over a peak for the consolidation condition. In the annular cell the steady state value was lower than the peak consolidation value in all cases. The results, in graphical form, for all the cells are given in figures 5.3.a-f.

5.2. Shear Studies on the Split Ring Annular Shear Cell

5.2.1. Introduction

Three size fractions of sand were used for these studies, the nominal size ranges being 14-18 B.S.S. mesh, 36-52 B.S.S. mesh, and 60-85 B.S.S. mesh.

Before considering the specific parameters measured, a general description of the test will be given.

The samples in the cell were prepared by pouring the sand into the cell and forming in it a thin vertical layer of coloured dyed tracer sand of the same size fraction. This layer was formed by placing two thin pieces of metal across the radius of the cell and pouring the dyed sand between them. When the cell had been filled with the rest of the sand, the metal pieces were removed. After tapping the cell and its contents on the bench, the surface was levelled and the depth of the bed was measured by using a thin "dip stick". Before placing the shearing plate on to the sand the dyed tracer position was noted.

The cell and its contents were transferred to the

Yield loci obtained from comparison tests

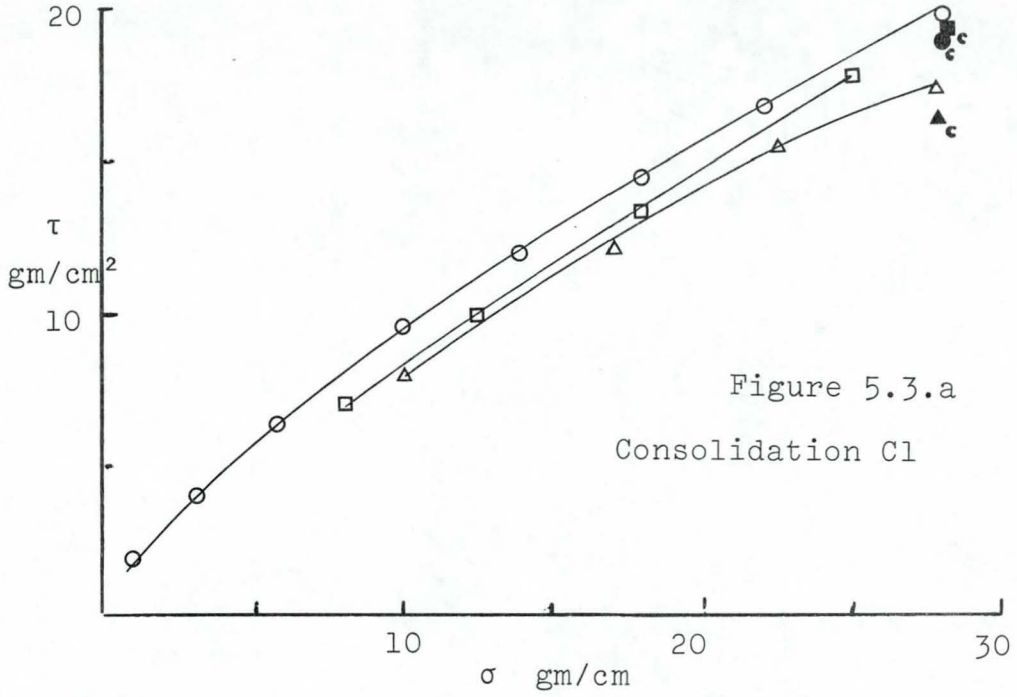

Figure 5.3.a

Consolidation C1

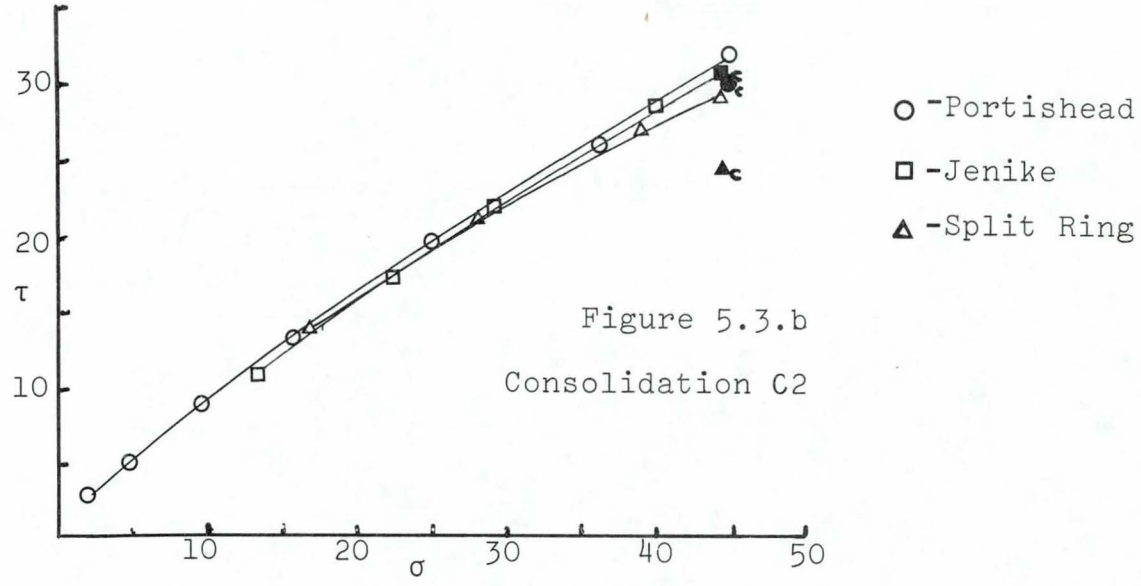

Figure 5.3.b

Consolidation C2

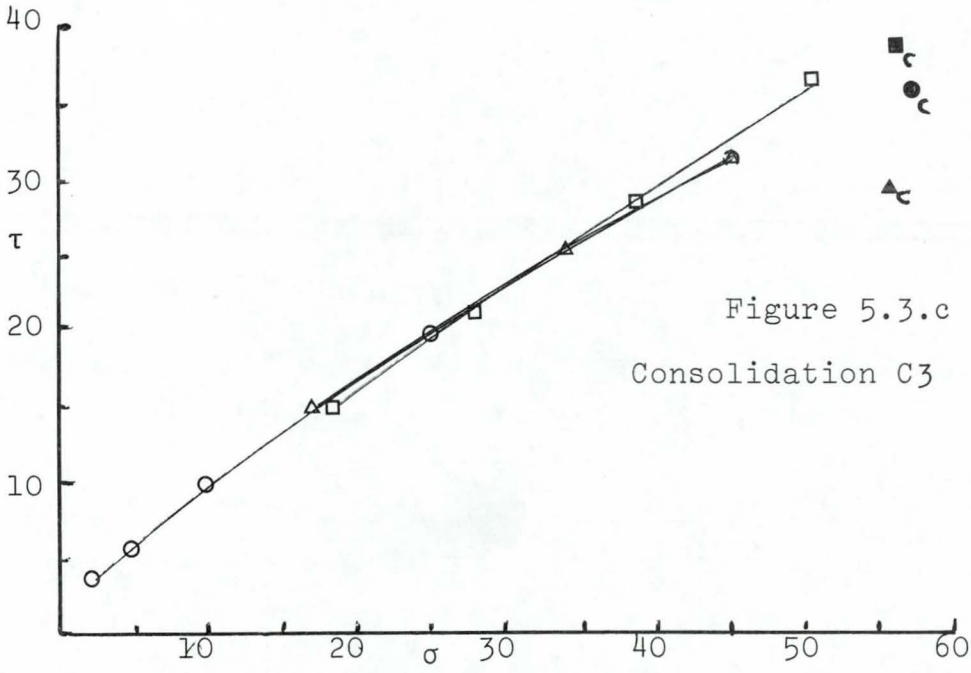

Figure 5.3.c

Consolidation C3

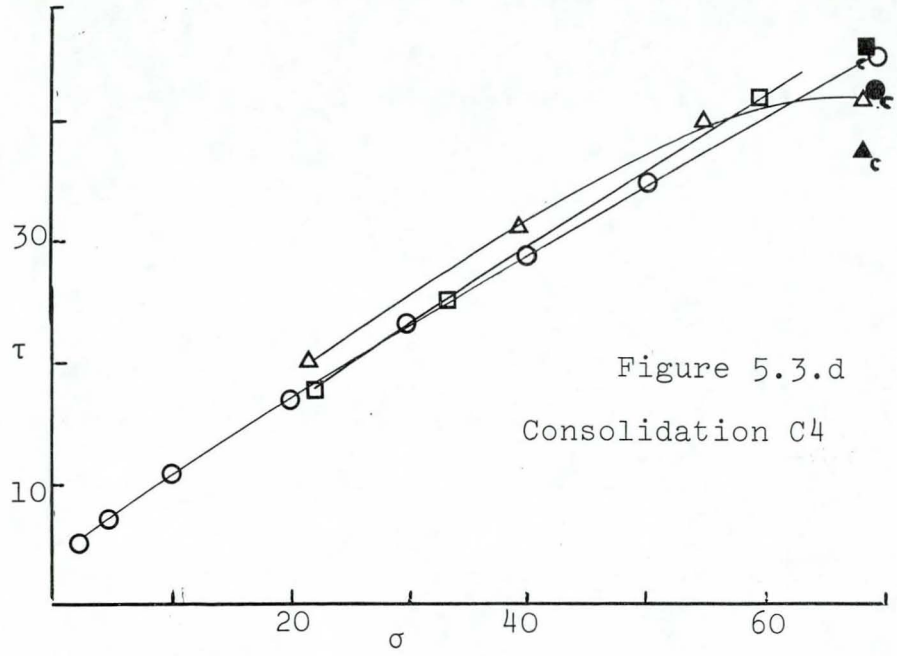

Figure 5.3.d

Consolidation C4

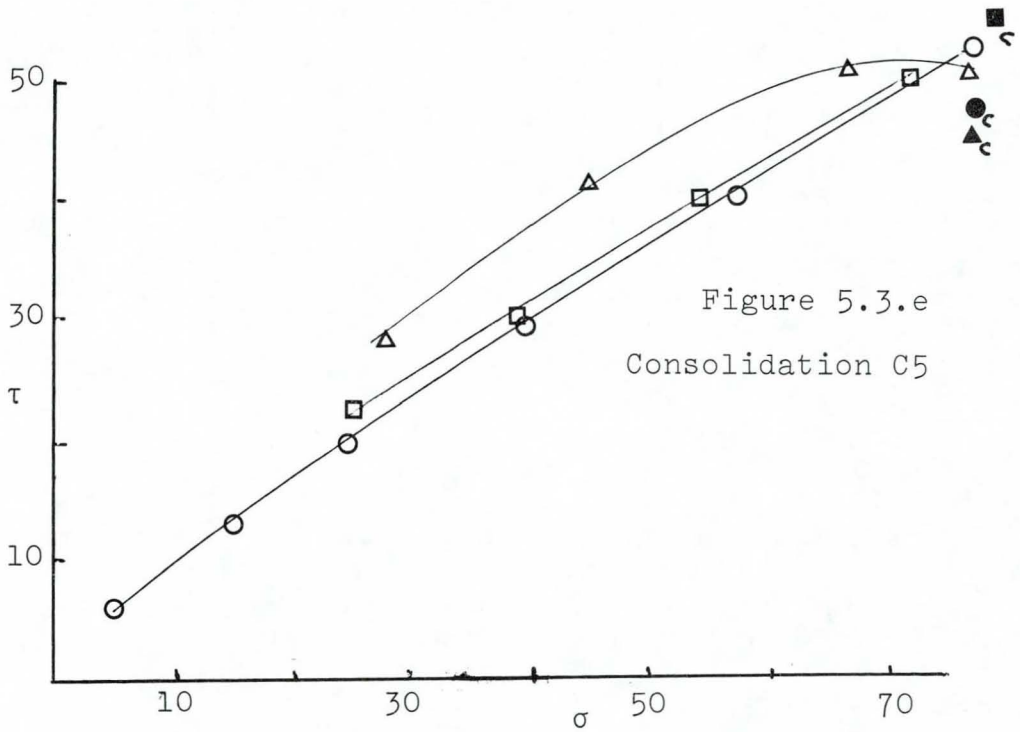

Figure 5.3.e

Consolidation C5

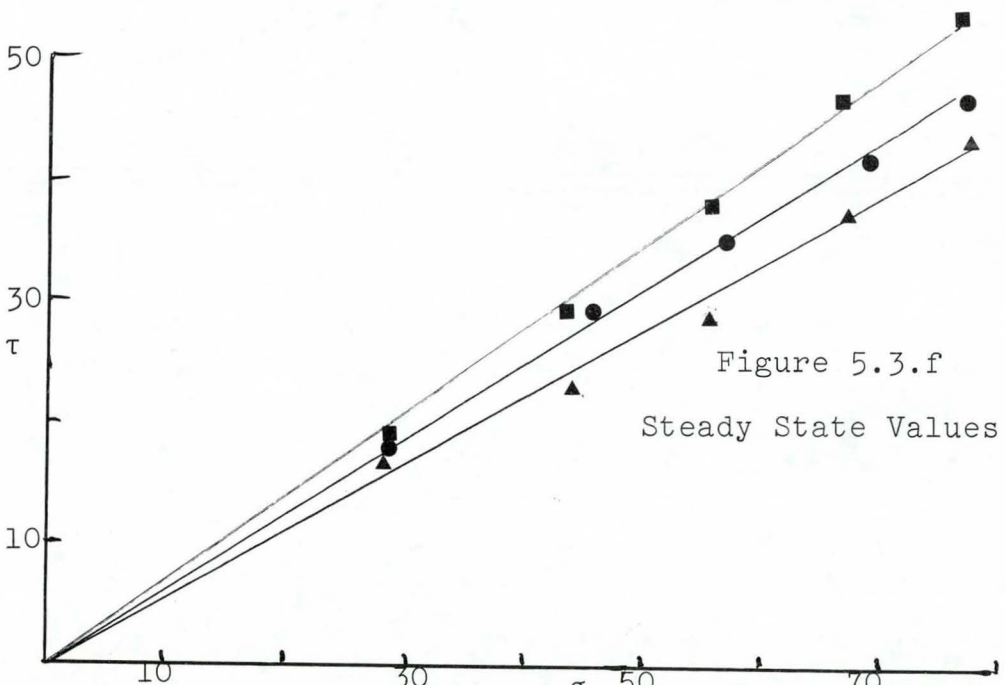

Figure 5.3.f

Steady State Values

drive unit mounted on the gamma attenuation scanning trolley. Although the split ring annuli were aligned when the shearing plate was placed in the cell, to make sure that perfect alignment was obtained, the restraining rods were placed in the plate and shear applied for a very short interval. The plate was then tapped down.

The normal loads were then applied, and the vertical displacement transducer fitted above the middle annulus. The normal loads chosen were 33.33gm/cm^2, 55.09gm/cm^2, and 76.86gm/cm^2 since this was the region of maximum variation of critical porosity as found by Roscoe, Schofield and Wroth.[140]

Before commencing shear, the cell was scanned with the gamma beam in both a vertical and a horizontal direction. The vertical scan gave an indication of the variation in porosity over the depth of the bed and the best position to scan in the horizontal direction. The horizontal scan was taken at fixed radii and the readings noted on a ratemeter coupled to a digital voltmeter driving a tape punch unit. A photograph of the cell being scanned is shown in figure 5.4.

The data from the punch tape was later fed into a computer and the mean and standard deviation for 100 seconds was determined. At a later stage the ratemeter was read directly when it had been found that the standard deviation was not too great; and at an even later stage the scaler was used for these readings.

When the vertical and horizontal scans had been completed the cell was sheared for four revolutions, and a continuous recording taken of the dilation and shear force necessary to restrain the lid. An example of a typical trace is given in figure 5.5.

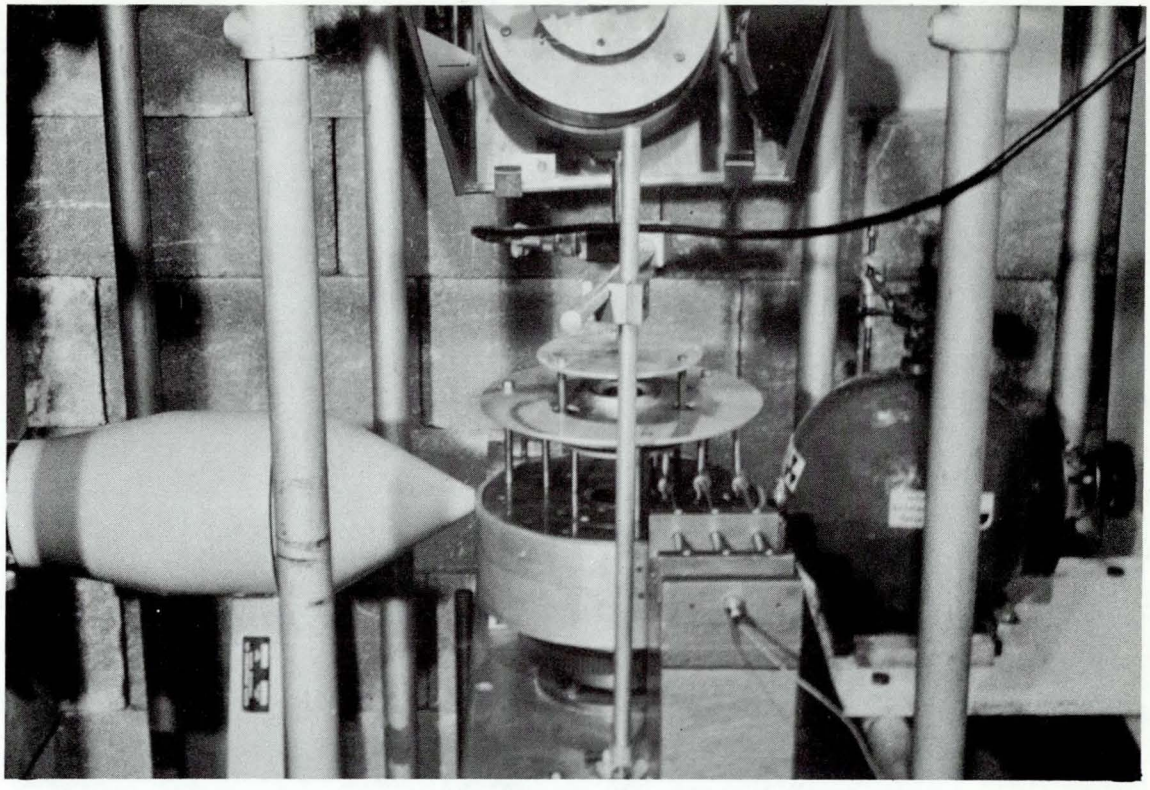

Figure 5.4. Photograph of Split Ring Annular Shear Cell in gamma beam.

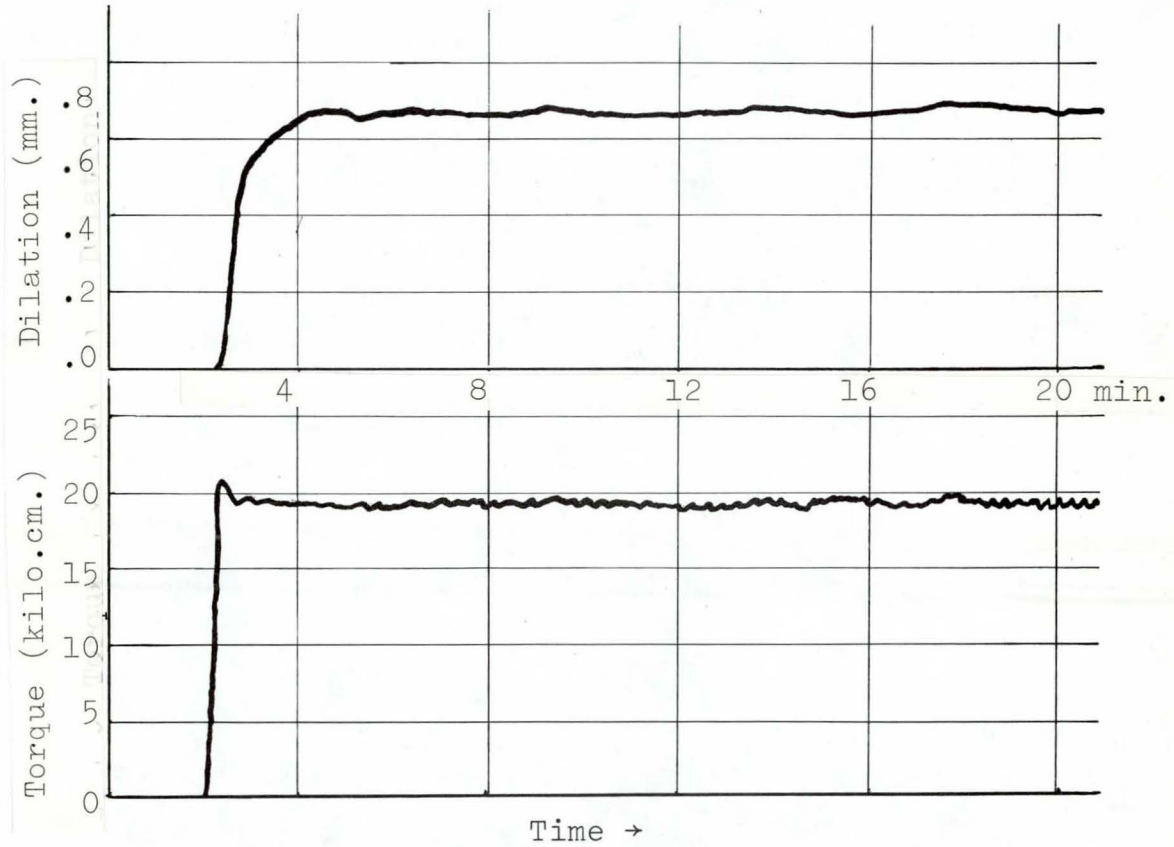

Figure 5.5. Typical stress/strain and dilation/strain output trace from spark recorder for Split Ring Annular Shear Cell measurements.

After four revolutions of the cell, the torque was removed and the cell scanned again in a vertical direction to detect the sheared zone. The cell was then scanned in a horizontal direction in the same position as before, to detect the porosity in the region of shear.

Figure 5.6 a.-c. shows, for each size fraction, one of the vertical gamma attenuation scans before and after shear had taken place.

A matrix of twelve separate tests were carried out on each sample, at three normal loads and for four shear rates. To examine the effect of shear rate it was varied from 1.26 radians per minute to 5.1 radians per minute.

After the scanning operation the loads were removed and the split ring annulus was carefully lifted from the cell and, by carefully removing successive layers of sand in the region where the dyed tracer was placed, the point where the tracer had been undisturbed was reached. The depth of this undisturbed layer was measured using the "dip stick".

Having completed all these measurements the weight of sand contained in the cell was measured.

The following information from each test was punched on to computer cards for processing:- density and size of sand; standard count (this being the gamma count through a piece of lead to enable the initial count to be determined); depth and weight of the bed; depth of the sheared zone; total dilation; shear rate; normal load on the centre annulus; and the steady state shear value.

A series of twelve runs on the 36-52 B.S.S. mesh sample at the same normal load and shear rate were also made to check the reproducibility of the runs.

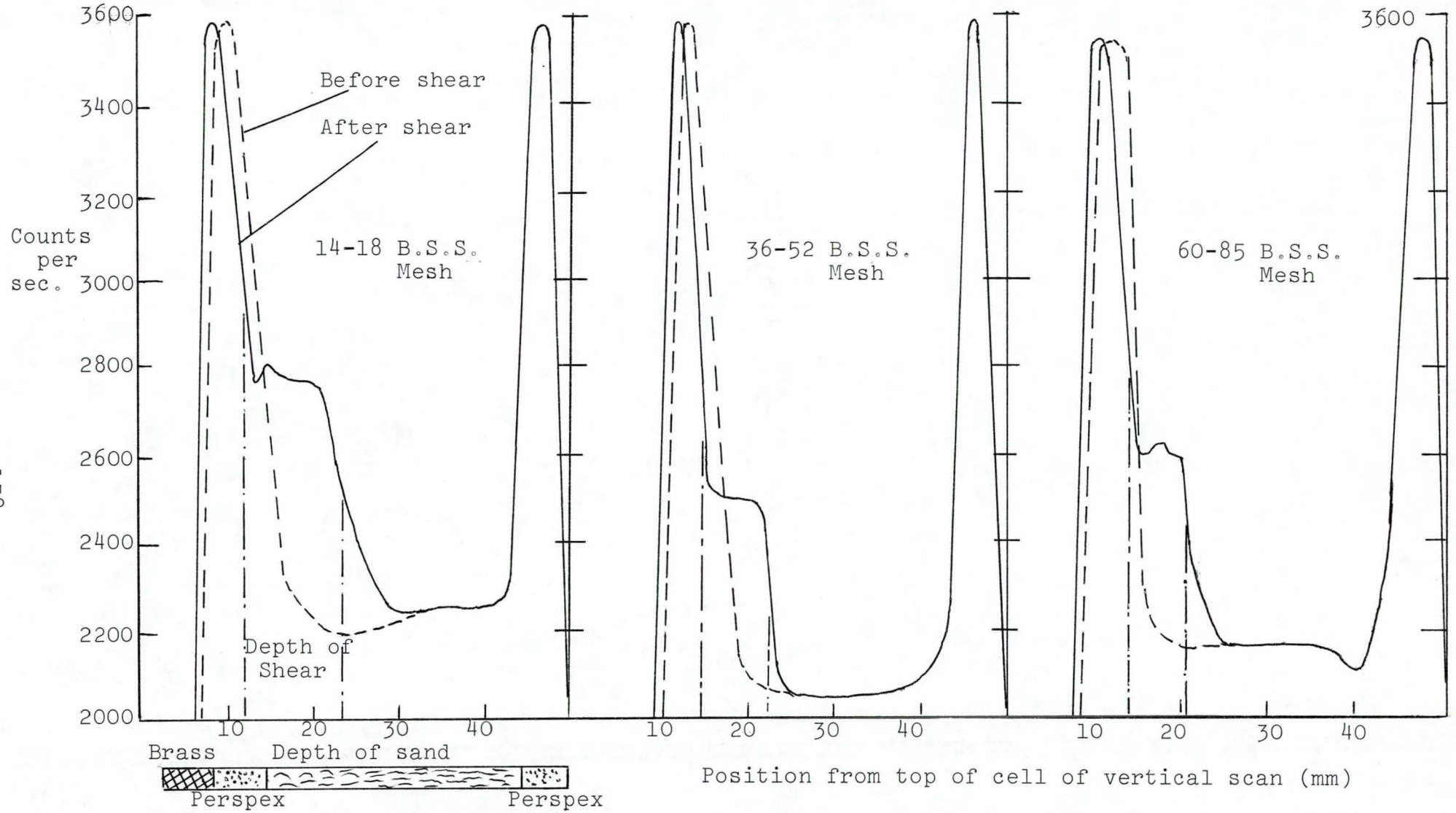

Figure 5.6. Density Profiles from Vertical Gamma Scans.

5.2.2. Measurement of the Critical Porosity

Two methods were used for measuring the porosity of the bed before and after shear. The first method was by weighing the sample of sand contained in the cell and measuring its depth in the cell, from which an estimate of the initial porosity of the sand could be determined. The critical porosity was then calculated by using the depth of shear measurement and the dilation which had taken place in the sheared zone. The results of these measurements are given in tables T.2.-T.5. The second, and more reliable, technique used for measuring the porosity of the sand was the gamma attenuation technique.

An allowance was made for the attenuation of the aluminium walls of the shear cell, by checking the attenuation caused by the cell when it was empty. The attenuation was measured at the same radii settings as were used for the horizontal scans.

The vertical scans over the depth of the cell were used to give an indication of the changes in the density of the bed rather than a specific value. From the vertical scans, taken after shear had taken place, a clear indication was given of the region in which the particles had been sheared and where steady state conditions existed. It was in this region that the horizontal scan was taken for the determination of the critical porosity. The attenuation of the gamma beam was noted at the same position as for the horizontal scan before shear.

The gamma attenuation values were processed by a computer and the porosity obtained by calculating the mass per cm^2 at each horizontal scan position and dividing by the length

through which the beam had passed.

A check was also made on the possible variation of the critical porosity with the radial position. Considering figure 5.7:-

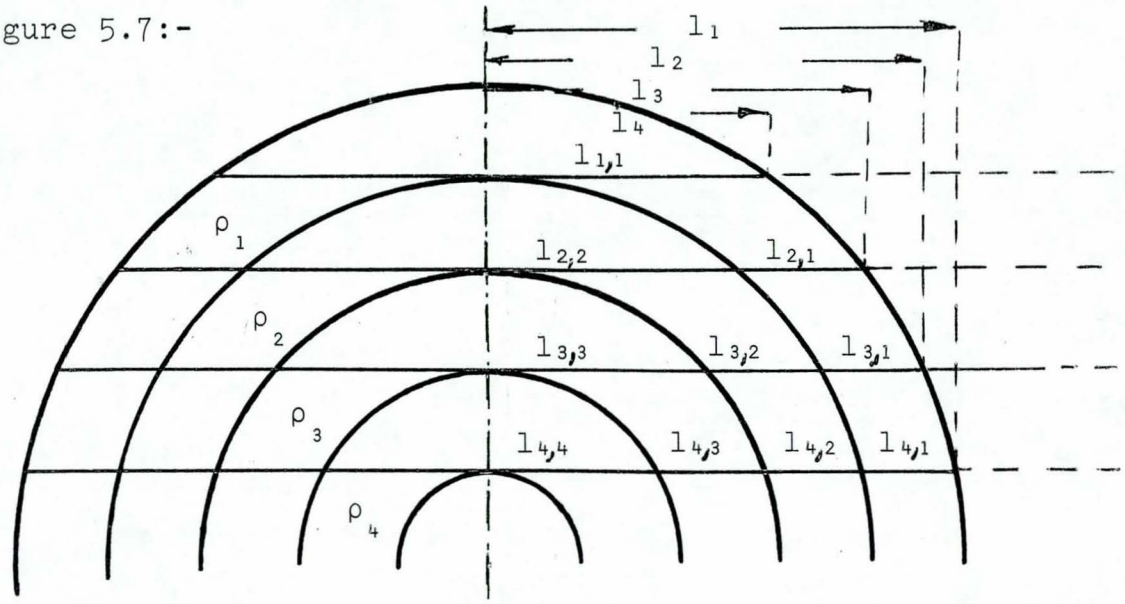

Figure 5.7. Calculation of porosity with radial position.

$$m_i = \frac{\log_e I_o - \log_e I}{\mu}$$

where: i = radial position

m = mass per cm^2

I_o, I = incident and attenuated gamma intensity

μ = mass absorption coefficient

ρ_i = radial density value

$$\rho_1 = \frac{m_1}{2 l_{1,1}} \quad , \qquad \rho_2 = \frac{m_2 - 2\, l_{2,1} \rho_1}{2\, l_{2,2}}$$

$$\rho_3 = \frac{m_3 - (2\, l_{3,1} \rho_1 + 2\, l_{3,2} \rho_2)}{2\, l_{3,3}}$$

Therefore, in general:-

$$\rho_i = \frac{m_i - (2\, l_{i-1} \rho_i + 2\, l_{i-2} \rho_2 + \cdots + 2\, l_{ii-1} \rho_{i_1})}{2\, l_{ii}}$$

It was found that there was no radial change in

porosity and so it was assumed that the density of the sand was constant throughout the shear zone region. Table T.6. gives the critical porosity values from a radial position calculation and from a direct average, that is:-

$$\rho = \frac{\frac{m_1}{l_1} + \frac{m_2}{l_2} \cdots \frac{m_i}{l_i}}{i}$$

i = number of radial scan positions

ρ = average density

The critical porosity and initial porosities are given for three sand samples and for the twelve identical runs in tables T.7. - T.10.

5.2.3. Measurement of the Depth of Shear

The depth of shear (that is the depth to which the material in the cell was disturbed) was determined by three independent methods:

i. By gradually removing the surface of the sample until the original dyed material was exposed and then measuring the depth of the undisturbed layer with the "dip stick". The difference between this value and the original depth, plus the dilation, gave a depth of shear value.

ii. On the vertical gamma attenuation plots, (examples of which are given in figure 5.6.a-c), a plateau is formed which has a density intermediate between the density of the shearing lid and the portion of the bed which has not been sheared. An estimate of the length of the straight portion gives a value of the depth of shear.

iii. An extrapolated measurement of the depth of shear was determined by using the critical porosity and initial porosity

given by the gamma attenuation technique and the total dilation of the sample. The depth of shear was calculated from the equation:-

$$\frac{H - h}{H} = \frac{1 - \varepsilon_c}{1 - \varepsilon_i}$$

H = depth of shear

h = dilation

ε_c & ε_i = critical and initial porosity, respectively

Tables T.11 - T.14 give the three values of the depth of shear for the three sand samples and the twelve identical runs.

5.2.4. Measurement of the Steady State Friction

After the shear cell had been rotating for a short interval a reasonably steady value of torque was obtained, giving a measure of the steady state friction which exists once the dilation is complete.

The angle of friction ϕ was calculated according to the equations given in table T.1. The steady state friction values in terms of $\tan\phi$ and ϕ are given in tables T.15-T.16 for each sample and for the twelve identical runs.

5.3. Investigation of Shear Stress and Dilation at Different Initial Porosities Using the Jenike Shear Tester

An investigation was made of the effect of the state of the sand, that is its initial porosity, on the stress and dilation of the three sands, using the Jenike Shear Cell.

The Jenike Shear Cell was the same as used for conventional design studies, although the design shear strength

procedure was not carried out. The pneumatic transducer and circular recorder as supplied with the instrument were not used, the former being replaced by the piezo-electric force transducer as used in the Split Ring Annular Shear Cell. A displacement transducer was fitted on to the machine, to rest on the load arm on the shearing plate, so measuring the vertical dilation. The output from the two transducers were continuously recorded on the two channel spark recorder. The total horizontal strain was measured by a dial gauge fitted against the shear cell ring. The samples were prepared by pouring the sand into the cell with the mould ring in place and scraping level after removing the mould ring. Different initial porosities were obtained by preparing the sand samples in different ways:- the loosest by gently pouring in the sand and the tightest by pressing the sand in the cell tightly with a plunger and tapping on the bench. A photograph of the apparatus is shown in figure 5.9.

The procedure for shearing the sample was as prescribed by Jenike; although the shear was not removed when a peak had been reached but was allowed to continue until the drive was automatically switched off when the limit of horizontal strain possible with the cell had been reached.

A number of tests were carried out for each of three normal loads over a range of initial porosities. The tests were made on the same samples as in the Split Ring Annular Shear Cell tests. A typical stress/strain and dilation plot obtained from the tests is given below. (Figure 5.8.) From these plots the following were tabulated:- the peak shear stress; the angle of friction at the peak stress; the dilation; the total shear strain; the ratio of the maximum rate of normal

strain to the rate of shear strain; the residual angle of friction from the equation given by Skempton and Bishop; the initial porosity ε_i and $(1 - \varepsilon_i)^{-1}$. (Tables T.17-T.25)

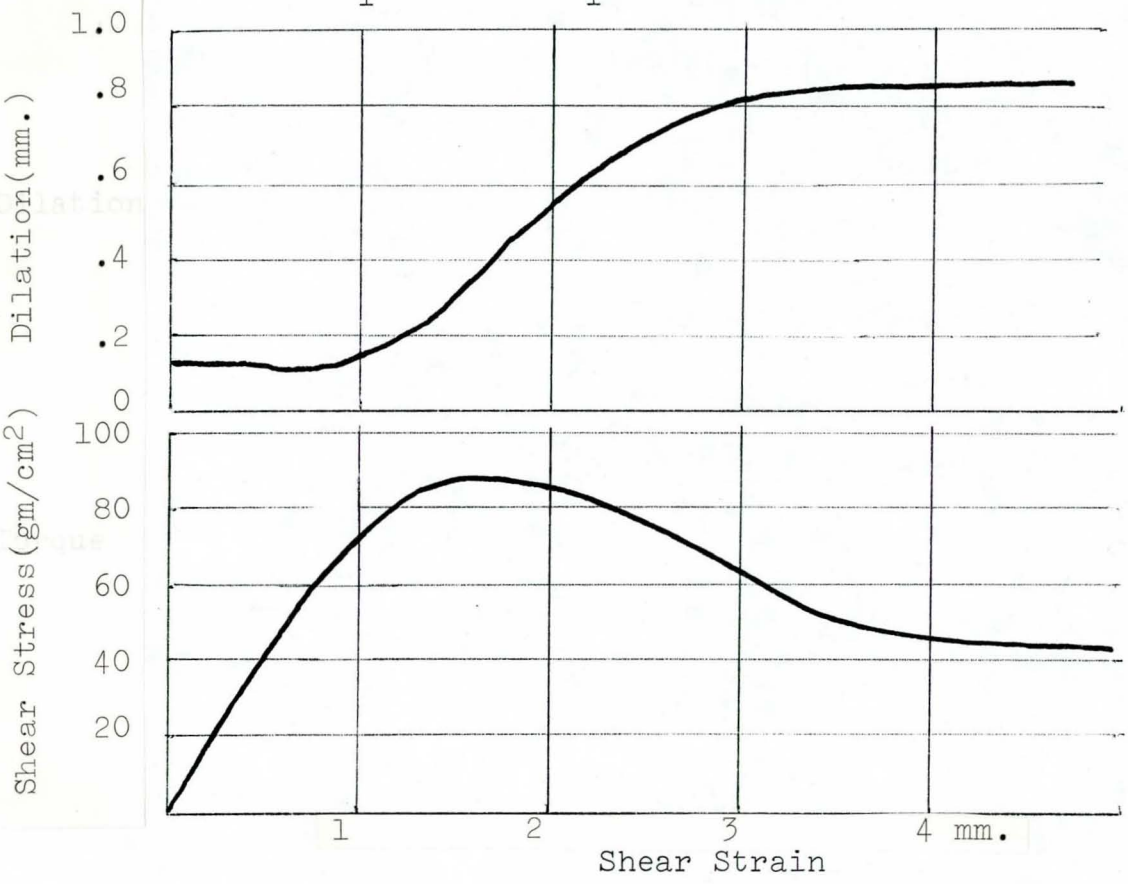

Figure 5.8. Typical output from stress/strain and dilation/strain tests in Jenike shear cell.

For the 36-52 B.S.S. mesh sample the same test as described above had previously been carried out using the Jenike cell fitted with the pneumatic force transducer and the vertical dilation being measured by a dial gauge. (Tables T.26-T.27). During this set of tests three widely spaced initial porosities were scanned in the gamma beam, vertically, before and after the shear test, to give an indication of the zone of shear. A photograph of the arrangement is shown in figure 5.10 and figure 5.11 shows the vertical gamma attenuation scans through the Jenike shear cell at the three initial porosities.

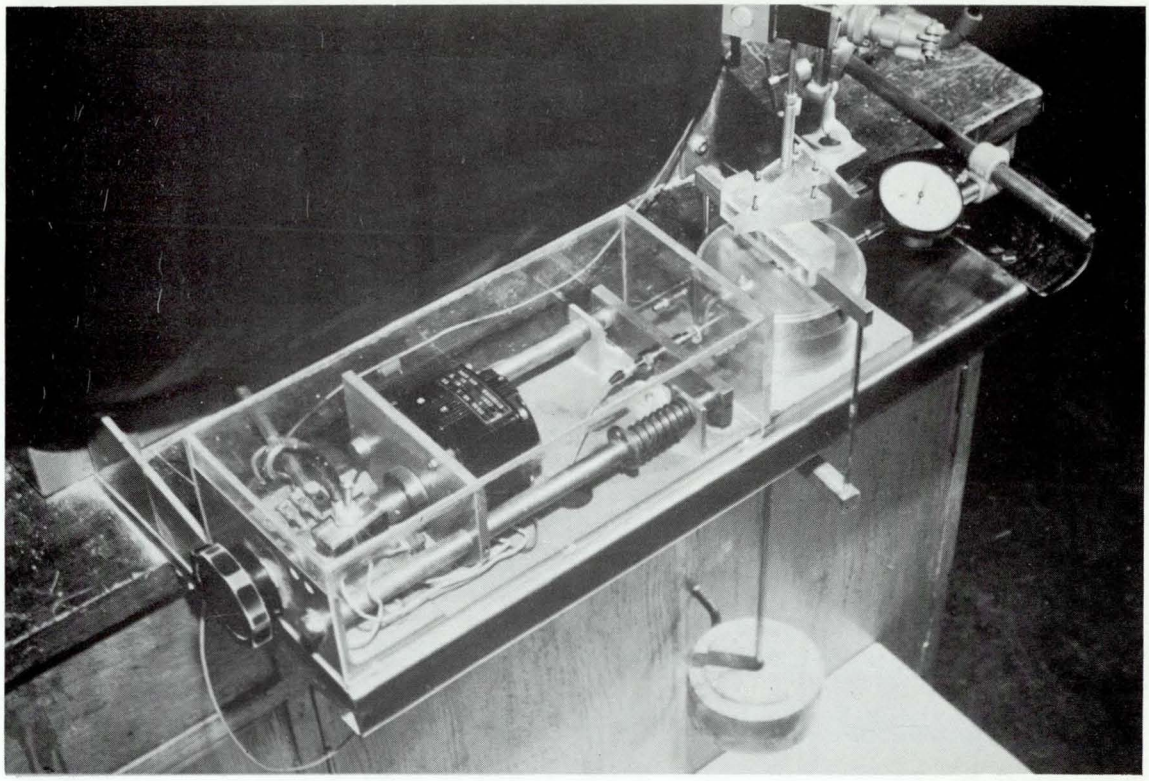

Figure 5.9. Photograph of arrangement for tests in Jenike shear cell.

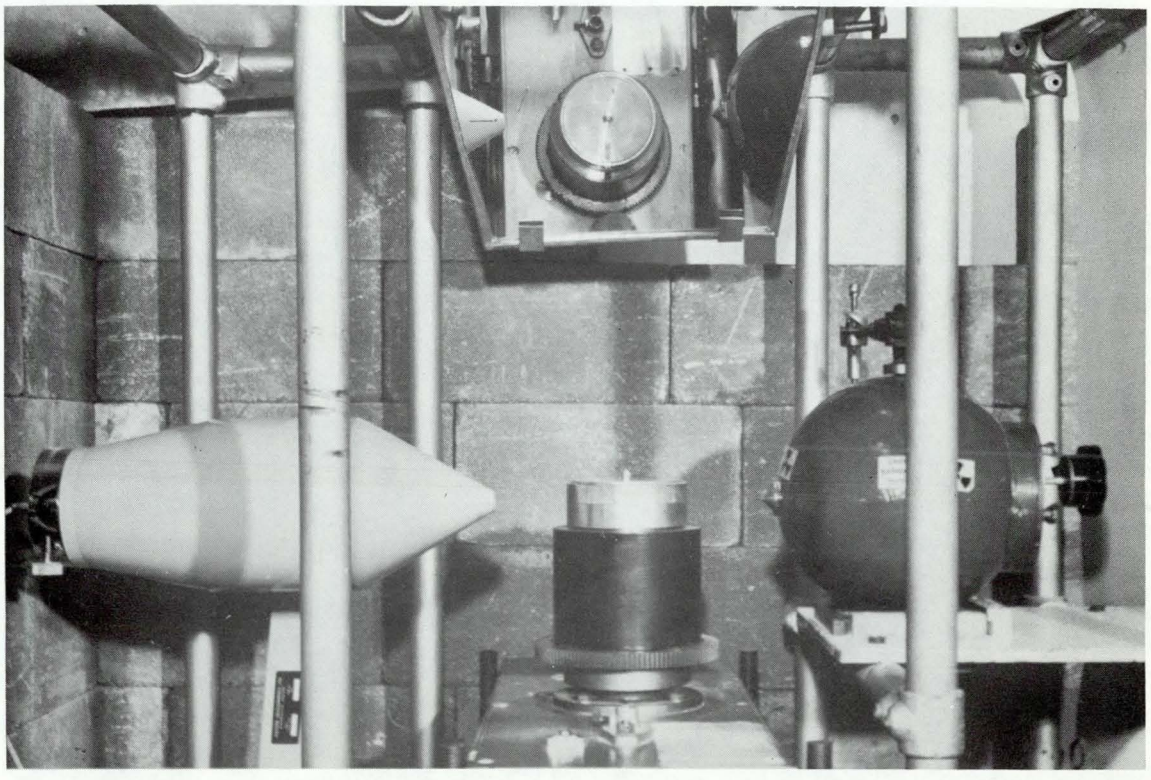

Figure 5.10. Photograph of arrangement for Jenike shear cell in gamma beam.

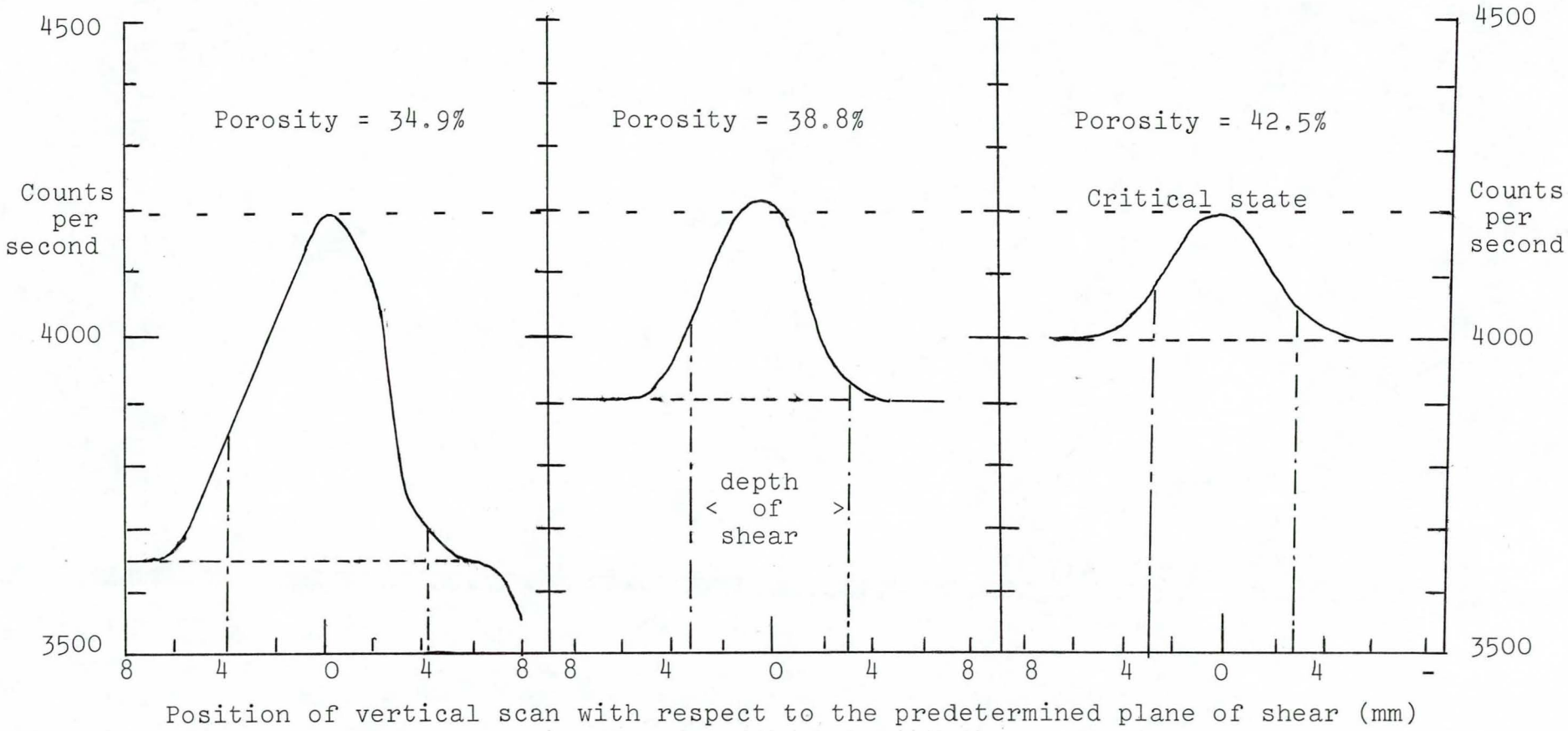

Figure 5.11. Density profiles from vertical gamma scans of three initial densities in Jenike shear cell (36-52 B.S.S. Mesh)

5.4. Particle Characterisation

5.4.1. Material Investigated

The free flowing material chosen for the investigations was "Hoveringham Zone 2" sand. It had the characteristics of being irregular in shape and hard, so that particle breakdown during shear did not occur.

The different size fractions were obtained from a general supply by sieving a number of times on British Standard sieves. After obtaining a reasonable quantity of each sample, the samples were washed and dried.

A small portion of each sample was dyed, using a scarlet fabric dye. Although the technique was such that a permanent colour was not obtained, the dyed sand was adequate to act as a tracer in the shear cell experiments.

To give an indication of the shape of the particles used, a series of "Stereoscan" photographs were taken of each sample.

The particle size distributions of the samples were obtained from a microscopic analysis of the image shearing diameters.

5.4.2. Measurement of the Chord Size Distribution

Chord size distributions were obtained initially by the following relatively simple technique.

Representative samples were obtained from the sand samples by riffling and then a number of microscope slides were made up. The chord size distributions were obtained by traversing the microscope in a straight line across the field of view and each time the horizontal cross wire intersected a

particle, the length of the intersection was recorded.

In this technique approximately 625 chords were measured, one chord per particle.

It was obvious from this method that, at its best, the chord size distribution obtained was approximate. It is known that a particle will sit on a microscope slide in its most stable position; and that the chords obtained from a profile measurement will give a distribution with more larger chords than obtained from particle sections. A true chord size distribution could only be obtained by studying the transections from two dimensional sections of the material.

There follows an account of the methods used to prepare sections of the material; and a description of the methods used to determine the chord size distributions therefrom.

5.4.2.1. Preparation of Particle Sections

To obtain particle cross-sections a method was devised for fixing a bed of particles. A number of techniques were investigated.

One technique attempted was to evacuate the air from a small tube containing a sample of the sand and then inject into the sample an epoxy resin. This technique had the advantage that all the voids in the bed were filled with the resin and it also eliminated air bubbles. When the sample had been cured the fixed sample was cut into a number of slices on a diamond impregnated cutter. One very thin slice was cut, about .5mm. thick. The slices were then polished and examined under a microscope.

Due to the limitations of microscope counting and the need to count many more than 625 chords, the samples were

examined under the microscope with the view of measuring them automatically. The method used, which will be described in more detail later, needed a high contrast between the particles and the resin in which they were to be bonded. In view of this high contrast required the use of a very thin slice using transmitted light was unsuitable, in that the sand being opaque, although giving a clear picture of the section outlines, was not in contrast enough for the automatic system to be used.

Another technique investigated was the use of a thermoplastic . The sample of sand was mixed with the black thermoplastic powder and then poured into the die of a press. Heat and pressure were then applied for a short time. After cooling, the fixed sample was removed from the die and cut into slices on a diamond impregnated saw.

On examination under the microscope it was initially felt that this technique would be suitable, in that good contrast was obtained between the thermoplastic and the sand. However, on closer examination of the slices it was found that, in cutting the sample, the sand tended to pull out of the plastic leaving a number of voids. It was decided that this technique was unsuitable, as in the cutting operation the majority of the small sections would be lost, giving a biased chord size distribution.

From the previous trial it was shown that the material for fixing the bed needed to be such that the particles were actually bonded to the resin.

Another resin was used, which was dyed a deep red to give a good contrast with the sand. In this case, the sand sample was added to the liquid resin in a mould, stirred and tapped on the bench to remove air bubbles and allowed to cure.

Slices, about 3 to 4mm. thick were cut on the diamond wheel and then polished on a series of papers and with a diamond impregnated cloth.

Under the microscope it was shown that the contrast was much better, reflected light being used. On using a blue filter with the reflected light it was found that the contrast was even better but not suitable for the automatic system.

To overcome this high contrast problem, selected polishing was introduced. After curing the sample and cutting the slices the sections were polished only on the first two emery papers, to remove the majority of the cutting marks. A "perspex" polish was then used to finally polish the samples, which had the effect of leaving the particle sections "etched" and the resin highly polished. Under the microscope, with blue light, the "etched" particles reflected sufficient light to give a good contrast.

Photographs were taken of the sections using a high contrast, safety positive film, which was insensitive to red light. 35mm. slides were made up from the photographs.

A portion of the section photograph used for the automatic system, together with "Stereoscan" photographs of the particles and particle sections for each sample are shown in figures 5.12 - 5.14.

5.4.2.2. Automatic Scanning of Particle Sections for the Determination of the Chord Size Distributions

Owing to the tedium involved in counting the chords for about 625 particles and the need for more to be counted, it was obvious an automatic measuring process would be required.

Figure 5.12a.

"Stereoscan" photograph of sand particles 14-18 B.S.S. mesh. (magnification × 13½)

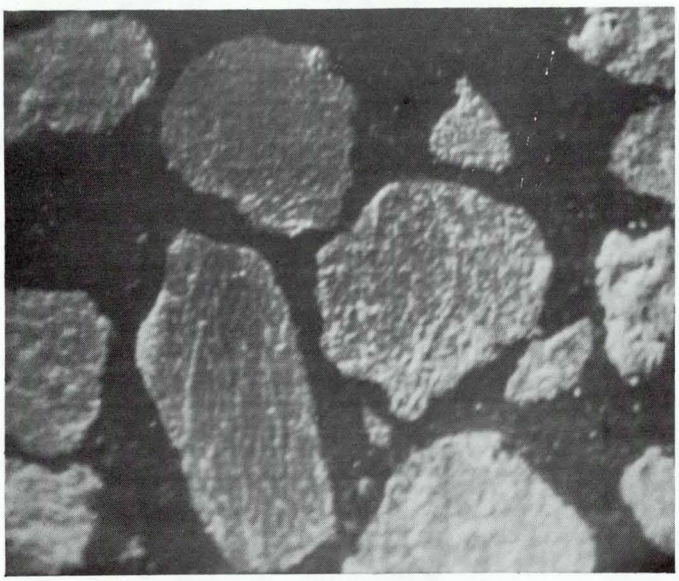

Figure 5.12b.

"Stereoscan" photograph of sand sections 14-18 B.S.S. mesh

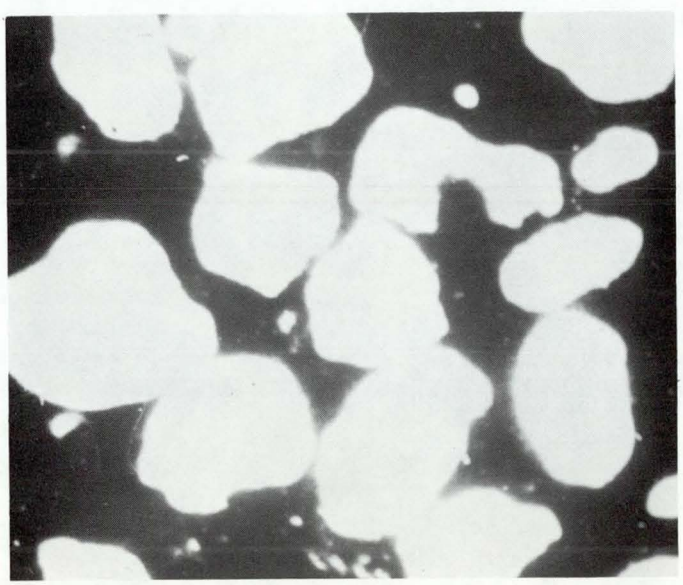

Figure 5.12c.

Section of image used in automatic scanning system.

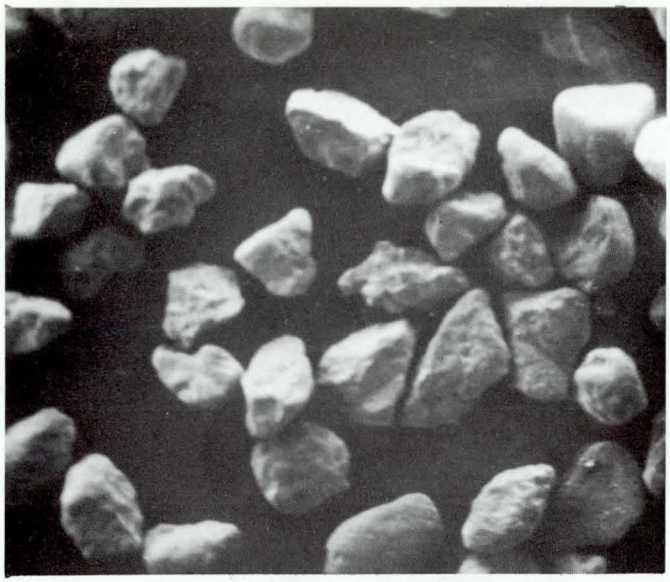

Figure 5.13a.

"Stereoscan" photograph
of sand particles
36-52 B.S.S. mesh
(magnification × 25)

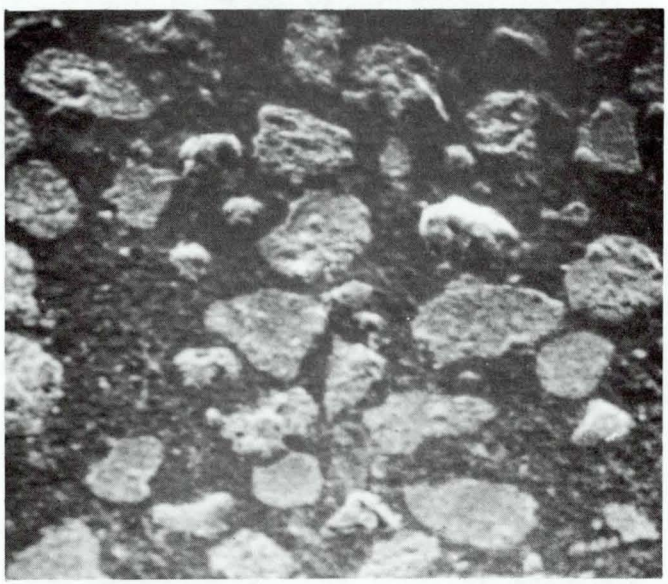

Figure 5.13b.

"Stereoscan" photograph
of sand sections
36-52 B.S.S. mesh

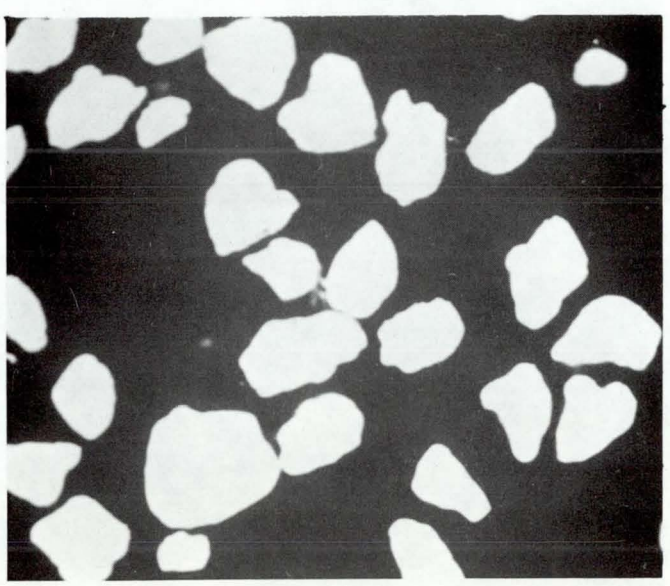

Figure 5.13c.

Section of image used in
automatic scanning system

Figure 5.14a.

"Stereoscan" photograph
of sand particles
60-85 B.S.S. mesh
(magnification × 73)

Figure 5.14b.

"Stereoscan" photograph
of sand sections
60-85 B.S.S. mesh

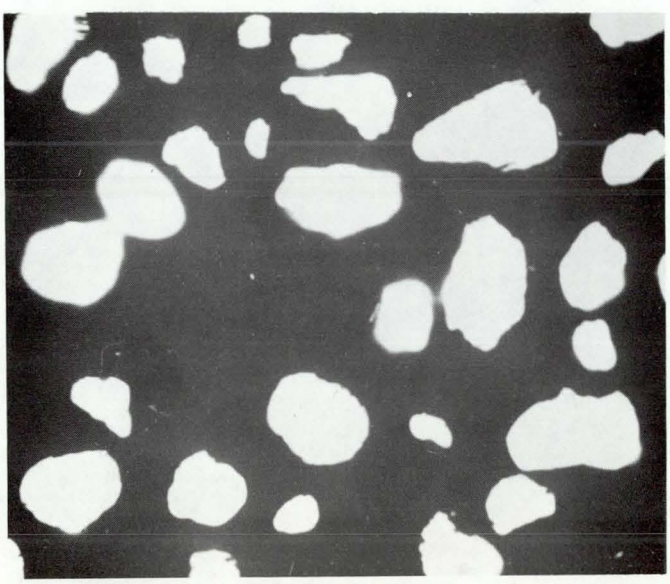

Figure 5.14c.

Section of image used in
automatic scanning system

Before discussing the system used, a review of automatic measuring and scanning devices will be given.

The examination of particles or sections of particles which are randomly distributed in a field of view by a microscope is probably one of the most direct methods of measuring particles and sections. The major disadvantages with it, are that the time required to count a comparatively small number of particles is considerable, and the unreliability of manual counts and the fatigue caused to the operator. It is for these reasons and for the techniques that Stereology demands that semi-automatic and automatic measuring and scanning devices have been developed.

Rather than do a complete review of the methods developed and available, reference will be made to two fairly complete reviews on the subject; those of Fisher[49] and Fischmeister[48].

Some of the mechanical systems have been mentioned while discussing the application of the Stereological principles, particularly those of Delesse[41] and Rosiwal.[144]

Several automatic particle counters have been developed and they all basically measure the intensity of a light beam which may be intercepted by the particle or specimen to be measured. The pulses produced from a photocell are proportional to the size of the particle and these pulses are then discriminated and counted electronically. There are two basic types of scanning counter, the slit scanning counter and the spot scanning counter.

The slit scanning microscope is a statistical method which makes some assumption on the special distribution of the specimen over the microscope slide. A photocell measures

the light passing through a slit and registers when it is partially obscured by a particle. The height of the signal from the feature passing across the slit will be proportional to its longest dimension in the direction parallel to the slit. Similarly the projected area of the particle or section will be proportional to the area under the electrical impulse curve and, again, the length of the particle in a direction perpendicular to the slit is proportional to the length of electrical pulse.

The two major problems associated with this type of counting are that a particle which only partially lies in the light beam is counted as a smaller particle, and two particles lying simultaneously in the light beam are counted coincidently as one large particle (figure 5.15). Both these errors can be corrected on a statistical basis by a manipulation of the results, but this reduces the accuracy.

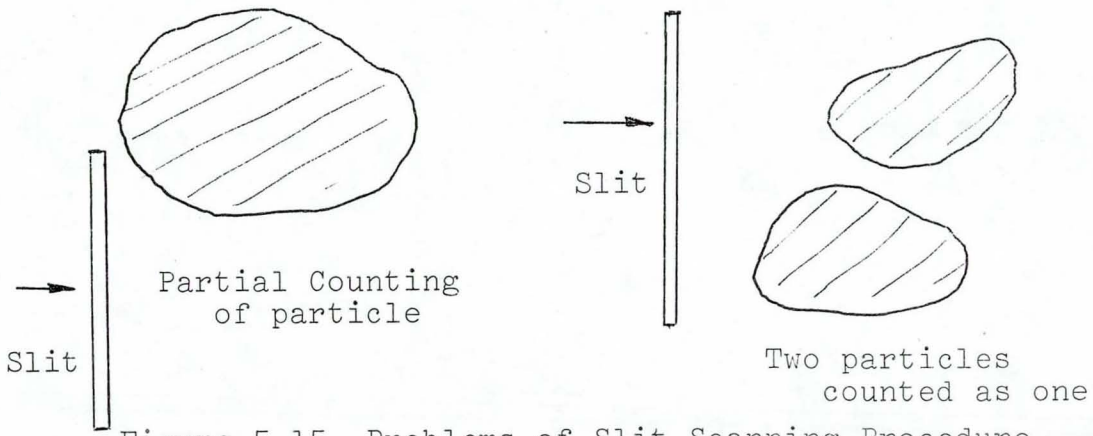

Figure 5.15. Problems of Slit Scanning Procedure

The spot scanning technique required more complex electronics and logic. Fisher has noted that there are many versions of this method, including systems which use up to twenty-three different spots, and even "seeking" spots which when they find a particle explore it thoroughly before passing

on to find another. In this technique the field of view is scanned with a spot which is very much smaller than the particles, in much the same way as a television picture is formed. Again, however, there are two particular problems associated with this type of counting. Firstly, two particles which are touching may be counted coincidently as one particle, and, secondly, a particle whose profile is re-entrant may be counted twice or more. Figure 5.16.

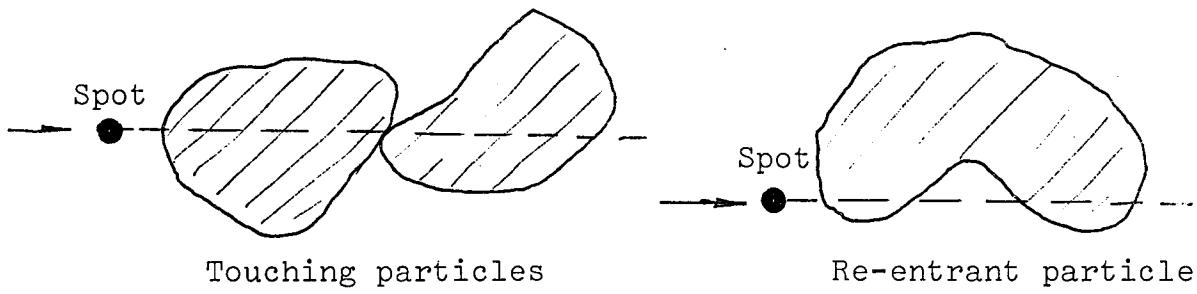

Figure 5.16. Problems of Spot Scanning Procedures

There have been suggestions as to the possible solutions to these problems. Firstly, a system may be given a line-to-line memory; for example, the position of a pulse may be stored in some way and compared with the succeeding line, or it may be a double spot system in which adjacent lines are scanned by two similar spots.

One of the most up-to-date methods available is the "Quantimet Image Analysing Computer" but this suffers from the problem of re-entrance and counting touching particles as one. The complete size distribution, total projected area, total particle number, total particle length and the total particle chord size distribution are obtained by setting different acceptance widths on the instrument and scanning at these

settings. A computer is used in conjunction with the instrument.

The other major difficulty which applies to both the slit and spot scanning methods is the focussing. For high resolution a microscope of large numerical aperture must be used, which necessarily has a small depth of focus. A human microscopist constantly adjusts the focus to accommodate this, which cannot be done with an automatic microscope. The problem can often be alleviated by the use of intermediate photography.

The method used, as part of a wider research programme, was to scan, automatically, an image of the section and measure the image density at any point fixed by its X and Y co-ordinates.

This method can be divided into the three following sections:-

i. Obtaining an image of the section. Due to the fact that the system used was to detect particles by the image density, the need for high contrast between particle and background was vital. It was found that the ideal of black against white was difficult to obtain.

The photographs taken of the sections were projected on to the measuring plane of the image scanner.

ii. The scanning equipment. A block diagram of the system and a diagram of the equipment is shown in figures 5.17-5.18.

A digital computer was linked to a large modified X-Y plotting table, fitted with a photocell instead of a pen. The scanning motion was made up of a series of parallel straight lines that covered the field of view projected on to the plotting table.

The computer, via the motors driving the X and Y axis

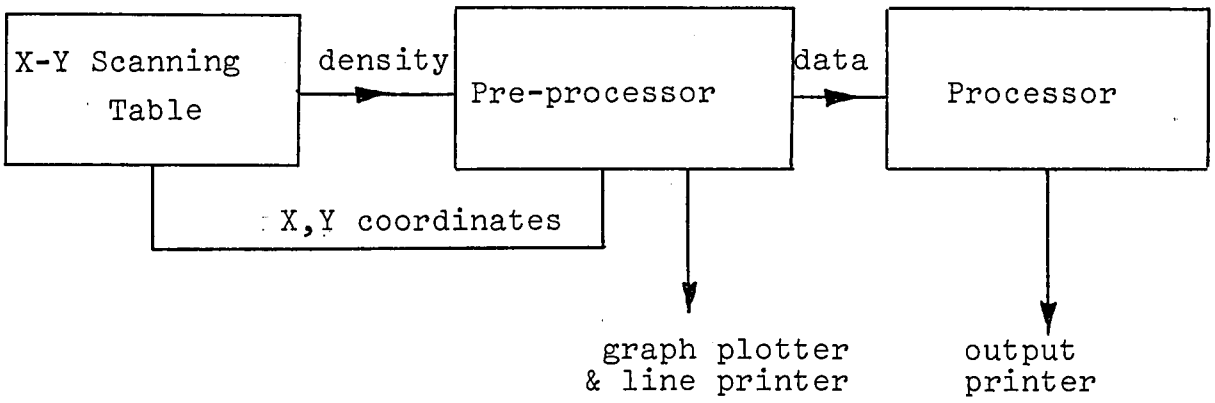

Figure 5.17. Functional Blocks of the Automatic Image Analyser

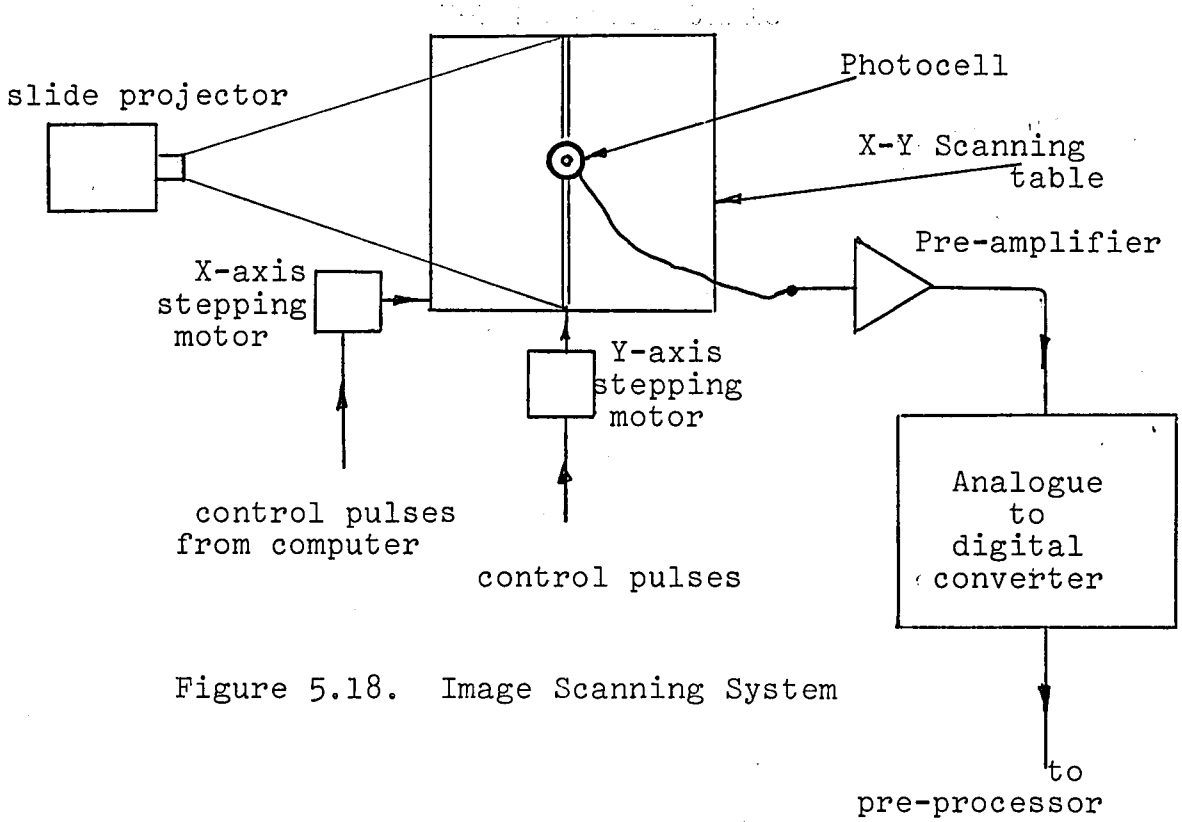

Figure 5.18. Image Scanning System

pens, moved the photocell over the table in one direction in pulsed movements. When the end of the scan line was reached the other axis was advanced a little and the scan restarted. As the photocell moved over the field measuring the intensity, a pre-processing routine detected the particle edges and when the photocell had traversed the particle, the X,Y co-ordinates of its initial intersection with the line of scan were recorded together with the length of the intersection. The output from the computer was punched out on to paper tape so that it could be processed later. At the initial stages of the scan the output from the photocell was printed out on to a line printer so that the density levels for detection could be set directly to ensure that only the particles were counted. A section of typical output from the computer and the line printer are shown in figure 5.19.

With this system, because the line of scan intersected the particles a number of times, not only was it possible to obtain the chord size distribution, but also the area size distribution as the perimeter of each particle had been defined in the scanning process.

iii. The processor. The output data from the computer contained the lengths and the X,Y co-ordinates of the particle cross-sections which could be later fed into the computer and, using the main processing programmes, a number of relevant parameters obtained. Of particular interest was the chord size distributions of the total section.

A more detailed description of the system and its use in particle size analysis is given in reference (1).

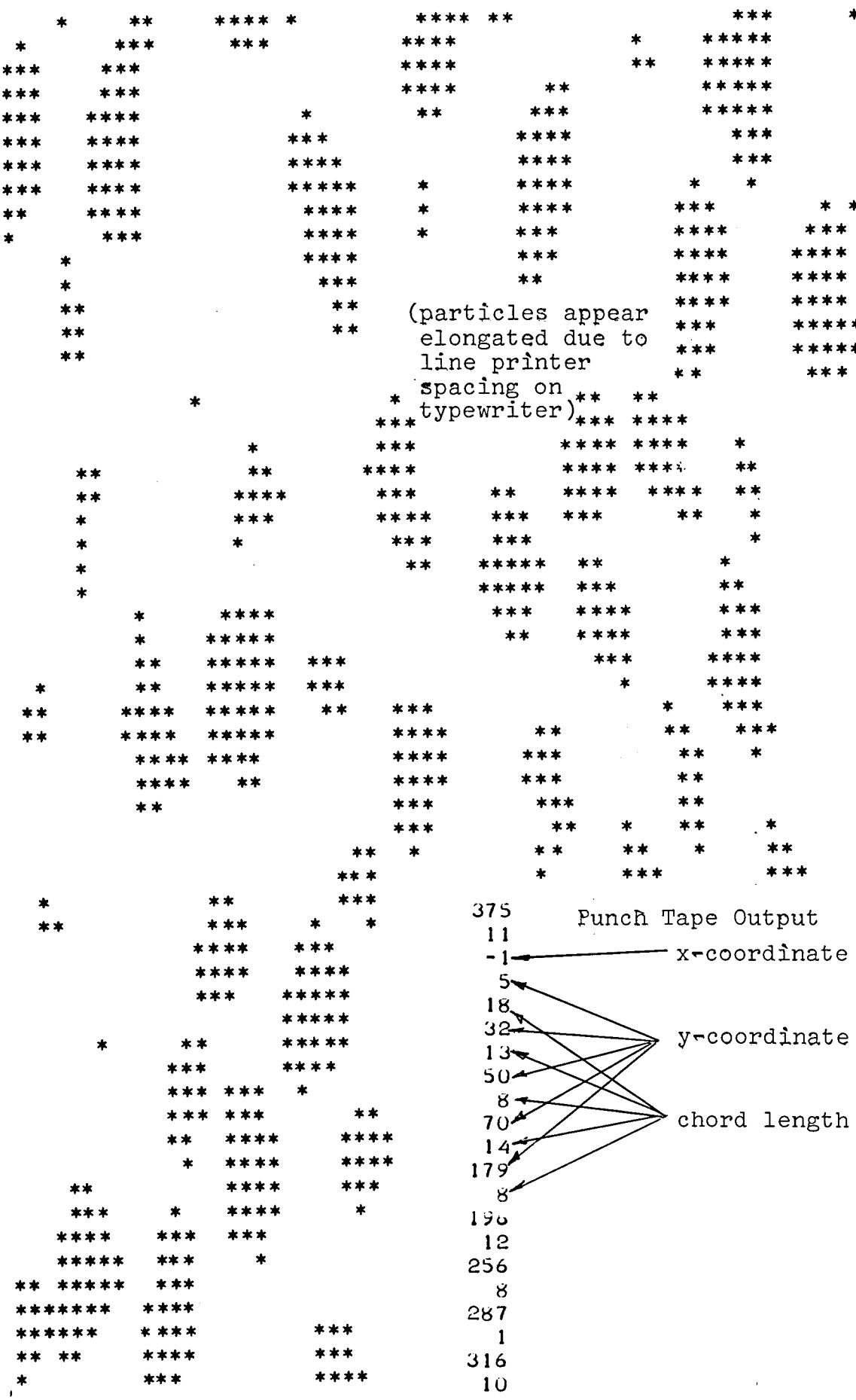

Figure 5.19. Typical output from line printer, showing particle sections measured, and tape output giving coordinates and lengths of the measured chords.

5.4.2.3. Section Counting by Hand

As a check against the automatic system a hand counting method was used. Large size photographic prints of each section were made and the prints mounted under a"perspex" sheet scribed with lines every $\frac{1}{10}$". Using a ruler, the lengths of the transections of the particles lying under the etched lines were measured.

A semi-automatic system was later devised for this hand counting technique. A caliper unit fitted on to a potentiometer was linked to a digital voltmeter and tape punch. The caliper was placed over the particle transection, a foot switch depressed and the length of the chord punched out on the computer tape, which could be later processed.

For the three sand samples the cumulative chord size distributions obtained from the above methods, together with the particle size distribution are given in figures 5.20-5.22.

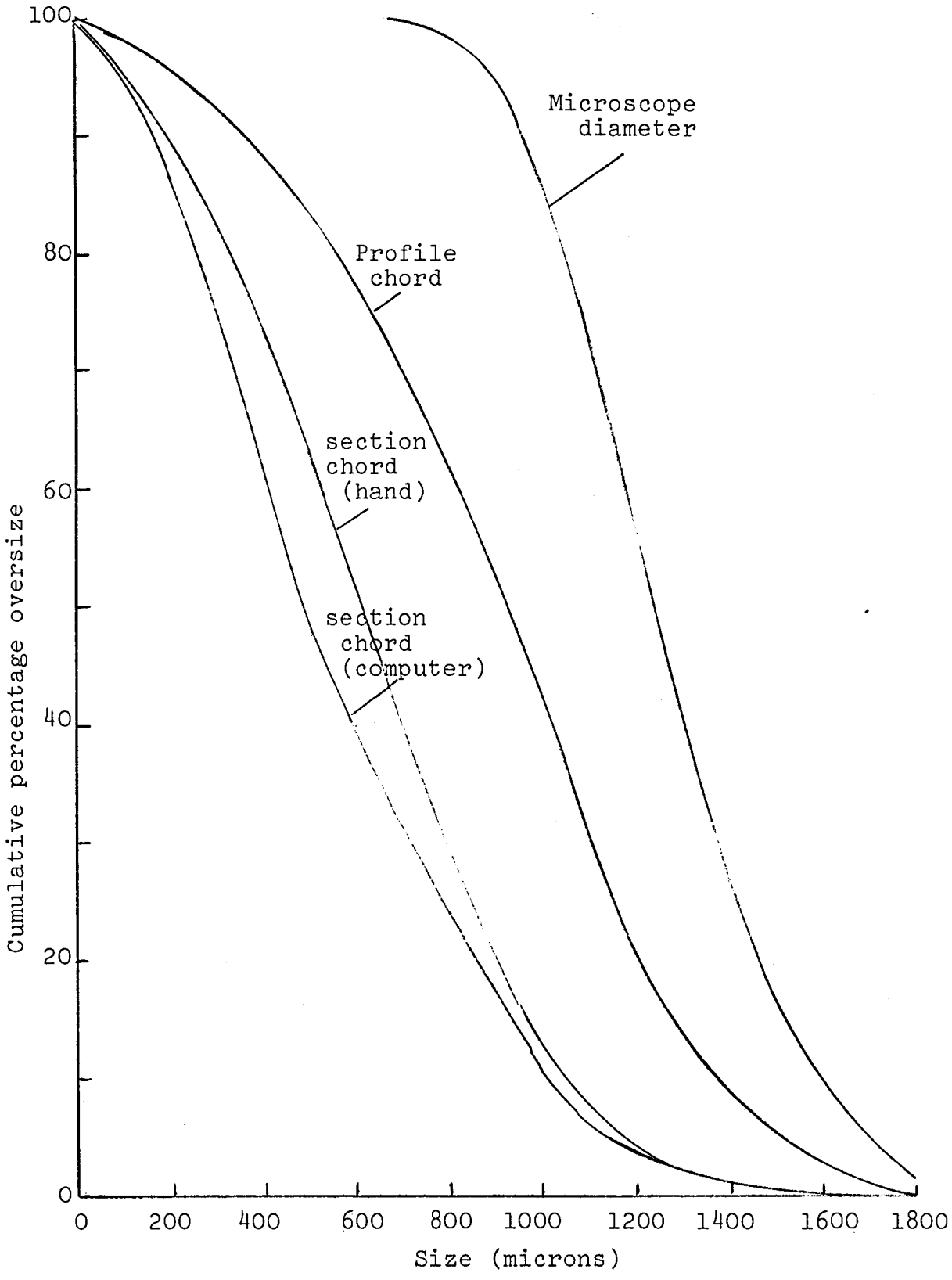

Figure 5.20. Size Distributions for 14-18 B.S.S. Mesh Sand

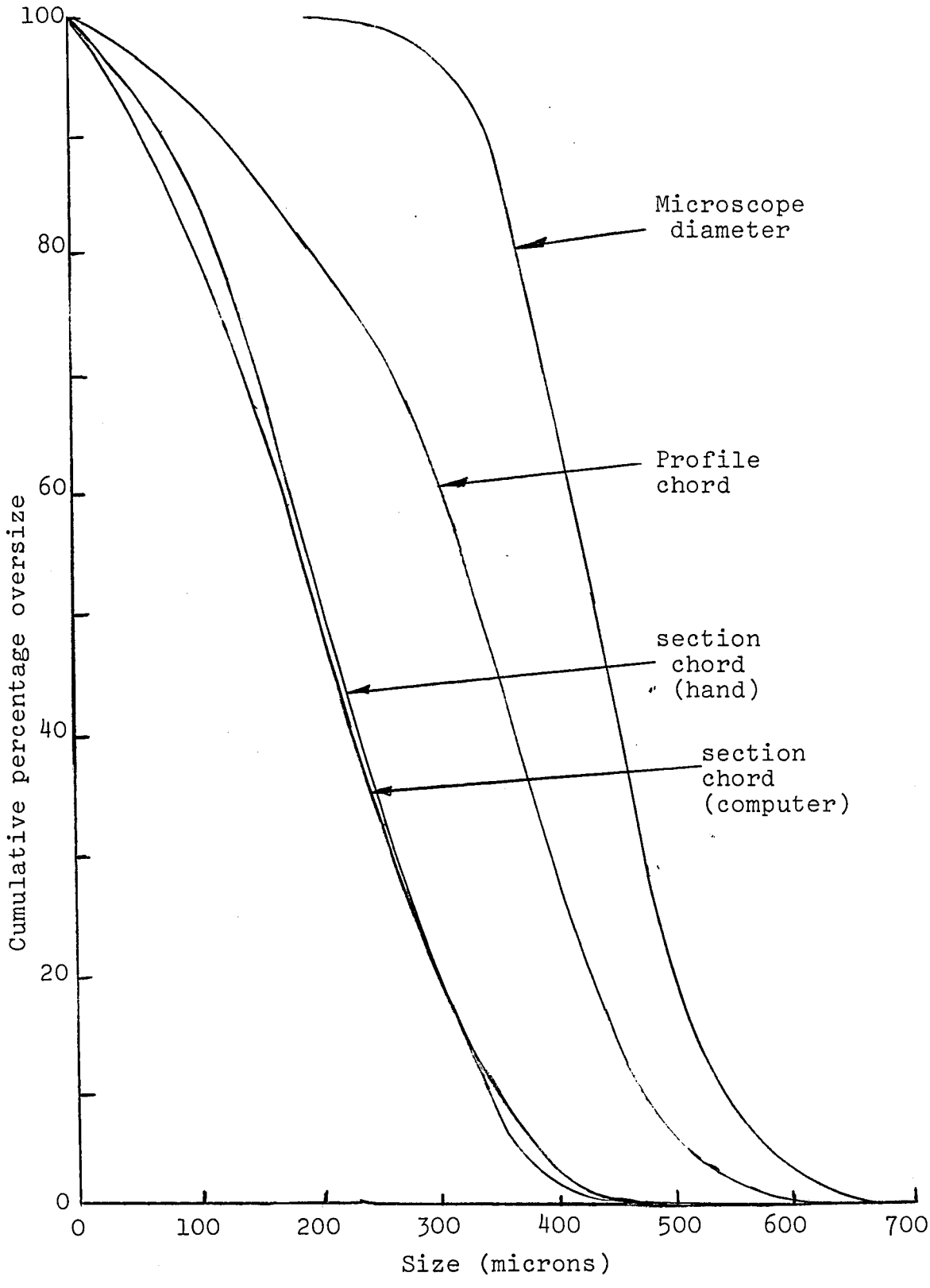

Figure 5.21. Size Distributions for 36-52 B.S.S.Mesh Sand

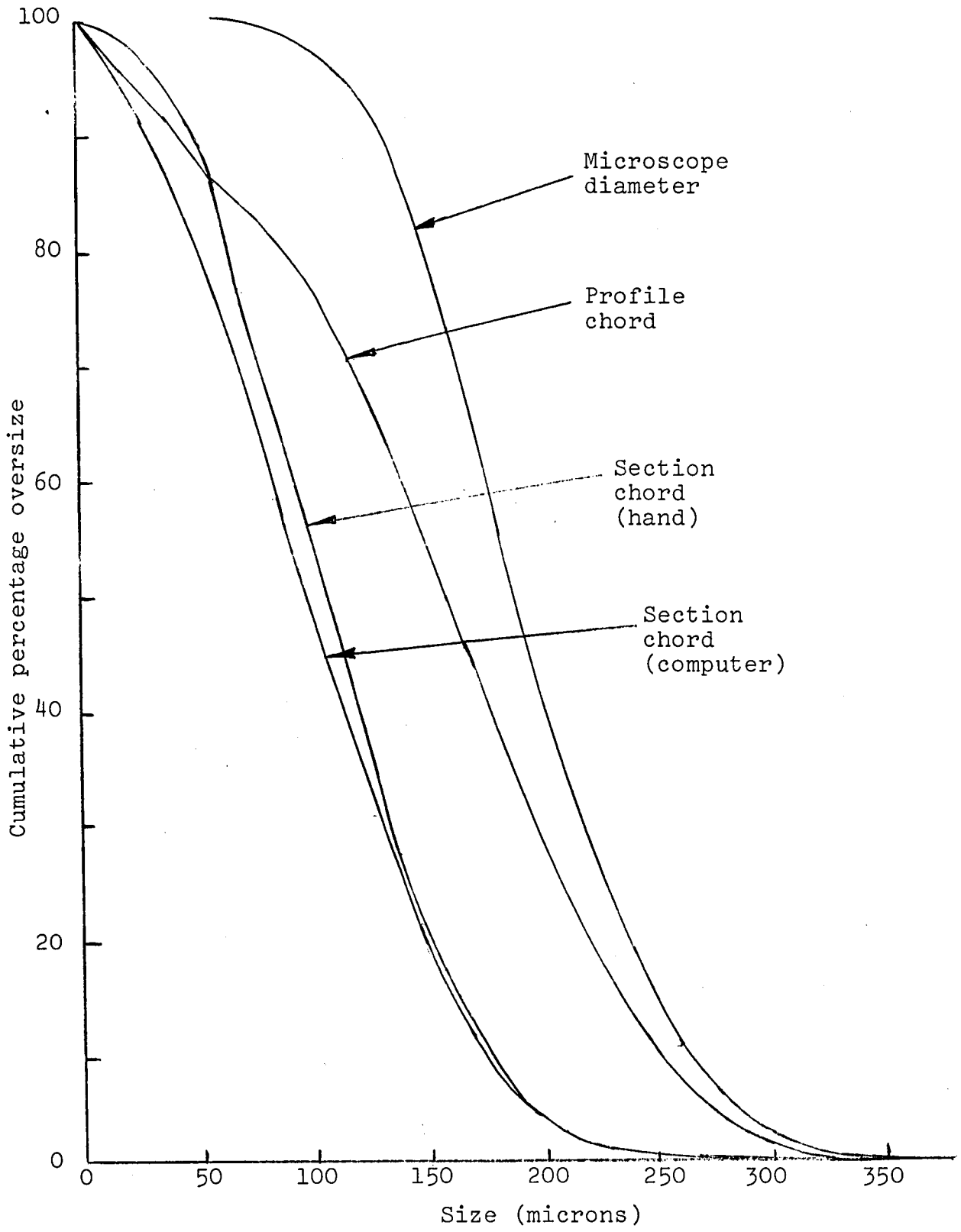

Figure 5.22. Size Distributions for 60-85 B.S.S.Mesh Sand

CHAPTER 6

DISCUSSION OF RESULTS

CHAPTER 6:- DISCUSSION OF RESULTS

6.1. Evaluation of the Split Ring Annular Shear Cell

6.1.1. Elimination of Wall Friction

Comparing the results (Table T.1.) from the annular shear cell used in its conventional form with those from it used in the Split Ring form, it is evident that the wall friction evident in the former was eliminated in the latter. The steady state value for the conventional form was 43.8° with a range of $\pm 6^{\circ}$. The traces obtained were very erratic; and this accounts for a maximum, minimum and average value being given. From the test in its designed, Split Ring, form the steady state value was $32.8^{\circ} \pm 2.4^{\circ}$, a lower and less spread value than for the other tests.

Besides eliminating wall friction measurement it is also evident that such a design also eliminated fluctuations that can arise due to material binding between the walls of the cell and the shearing annulus.

6.1.2. Surface Contact and Horizontal Profile Examination

The photographs (figure 5.2., page 150) indicated by the intact layer of sand over the centre annulus, after shear had taken place, show the good contact that existed between the top surface of the sand and the base of the shearing plate. However, over the region covered by the outer annulus the dyed tracer had been disturbed giving visual evidence of the stress concentration at the walls of the cell. Disturbance of the tracer for the region covered by the inner annulus can also be seen.

6.1.3. Vertical Dilation of Each Annulus

In order to detect any possible migration of particles from one annulus to another, a test was conducted in which the annuli were clamped together and the vertical dilation measured. The dilation of the total bed was found to correspond to that of the centre annulus for the same sample and packing.

With the plates in the designed form it was found that the overall dilation for each ring was the same. However, there was evidence that during the initial stages of the shear, there was greater dilation at the outer annulus.

6.1.4. Comparison of the "Portishead", Split Ring and Jenike Shear Cells

Considering the results of the comparison test as given in graphical form in figure 5.3., pages 153-154, five consolidation loads were used for all the tests and on each graph is drawn the yield locus for each of the three cells.

The results of the tests have shown one major limitation in the particular design of the Split Ring Annular Shear Cell. This is the inability to load the cell to low normal stresses. The "Portishead" cell as used by I.C.I. had a counterbalance system fitted, enabling stresses down to 1.5gm/cm^2 to be applied. The lowest stress for the Split Ring cell was 10gm/cm^2.

This limitation shows itself in the plotting of the flow function where it is necessary to extrapolate the Split Ring results to give an indication of the shear stress values at low normal stresses. The Jenike shear cell also has the same limitation.

Considering the yield loci for consolidations C1 - C5, the agreement for C2 and C3 is good, although the Jenike cell

at the higher end of the yield loci gives larger peak stresses than the two annular cells. For consolidation C1 the "Portishead" cell gives higher peak values than the Jenike cell which is slightly higher than the Split Ring cell. For consolidations C4 and C5 the differences are reversed and the Split Ring values are higher than the other two. As indicated in section 4.1.1.2. during the review of annular shear cells, they are not well suited for the measurement of peak shear values. However, neglecting consolidation C1, it appears there is a significant difference between the three methods when measuring peak values. It is to be expected that, due to the spreading of the peak stress in an annular cell, the annular cells would give lower yield loci than the direct shear test. The reason for the Split Ring loci being higher than the others could be due to the sand roughened shearing surface, giving an uneven surface with the very fine adipic acid. However, this needs to be investigated further.

Considering figure 5.3e, which gives the steady state consolidation values for the tests, the results are more significant than the peak stress values. The steady state angles of friction are as follows. (Table 6.1.)

Table 6.1. Steady State Angles of Friction

Consolidation	Jenike	Portishead	Split Ring
27 gm/cm^2	35.0	35.0	30.0
44	34.0	35.0	28.5
56	35.0	32.5	28.0
67	35.0	31.5	29.0
75	35.0	31.5	29.5
Mean	35.0	33.1±2	29.0±1

The table shows the difference between the two annular

shear cells which is due, probably, to the elimination of wall friction in the Split Ring Annular Shear Cell. A comparison between the higher values from the Jenike cell and the lower values from the annular cells is probably rendered invalid because it is doubtful if the steady state condition does prevail in the Jenike cell with such material and small shear strain.

The material tested was relatively free flowing and an evaluation using a more cohesive powder may give more definite results.

6.2. Particle Characterisation

6.2.1. Measurement of the Chord Size Distribution

Figures 5.20-22 (pages 182-184) give the cumulative distribution for the chord size measurements obtained by each of the three methods of measurement, together with the particle size distribution for each sample.

As expected, the profile microscopic technique gave a distribution with a greater proportion of longer chords than the other two methods. This emphasises the need to obtain chords from transections rather than from particle profiles.

The distribution obtained from the hand counting of the chords and those obtained from computer scanning of the sections agree closely, although at the small size there appears to be some difference. Great difficulty was experienced using the computer system for, even with the photographic technique used, the computer found it difficult to distinguish some particles from the background. It was decided to make large prints of the 35mm. slides and to colour in the particles which

were rather indistinct and then to rephotograph the print. This proved to be successful.

The number of chords counted by hand and those from the computer scan were approximately 1800 and 7000 respectively. As the distributions were almost the same the distributions obtained from the computer scan were used in the determination of the sectioned filament distribution for the particles.

6.2.2. Determination of Sectioned Filament Distribution from Chord Size Distribution Measurement

The sectioned filament distribution was determined by a numerical method of solving equation (1):-

$$g(y) = \int_{x=y}^{x=x_{max}} \frac{f(x)dx}{x}$$

where g(y) is the number distribution of sectioned filaments of length y

f(x) is the number distribution of filaments of length x

This method is laid out in appendix A.2. together with the method used to calculate the median value, the critical porosity and the mean filament length.

Table 6.2., below, gives a summary of the above values obtained from the computer scan chord size distributions; and figures 6.1-3 give the cumulative sectioned filament distributions and the measured cumulative distributions of the chords from which they were determined.

Table 6.2. Results Obtained from Chord Size Measurement

Sample Size B.S.S. Mesh	Mean Filament Length $\bar{x}$ (microns)	Median Sectioned Filament y_m (microns)	Critical Porosity ε_c (%)
14-18	556	507	45.2
36-52	192	182	44.4
60-85	98	91	44.3

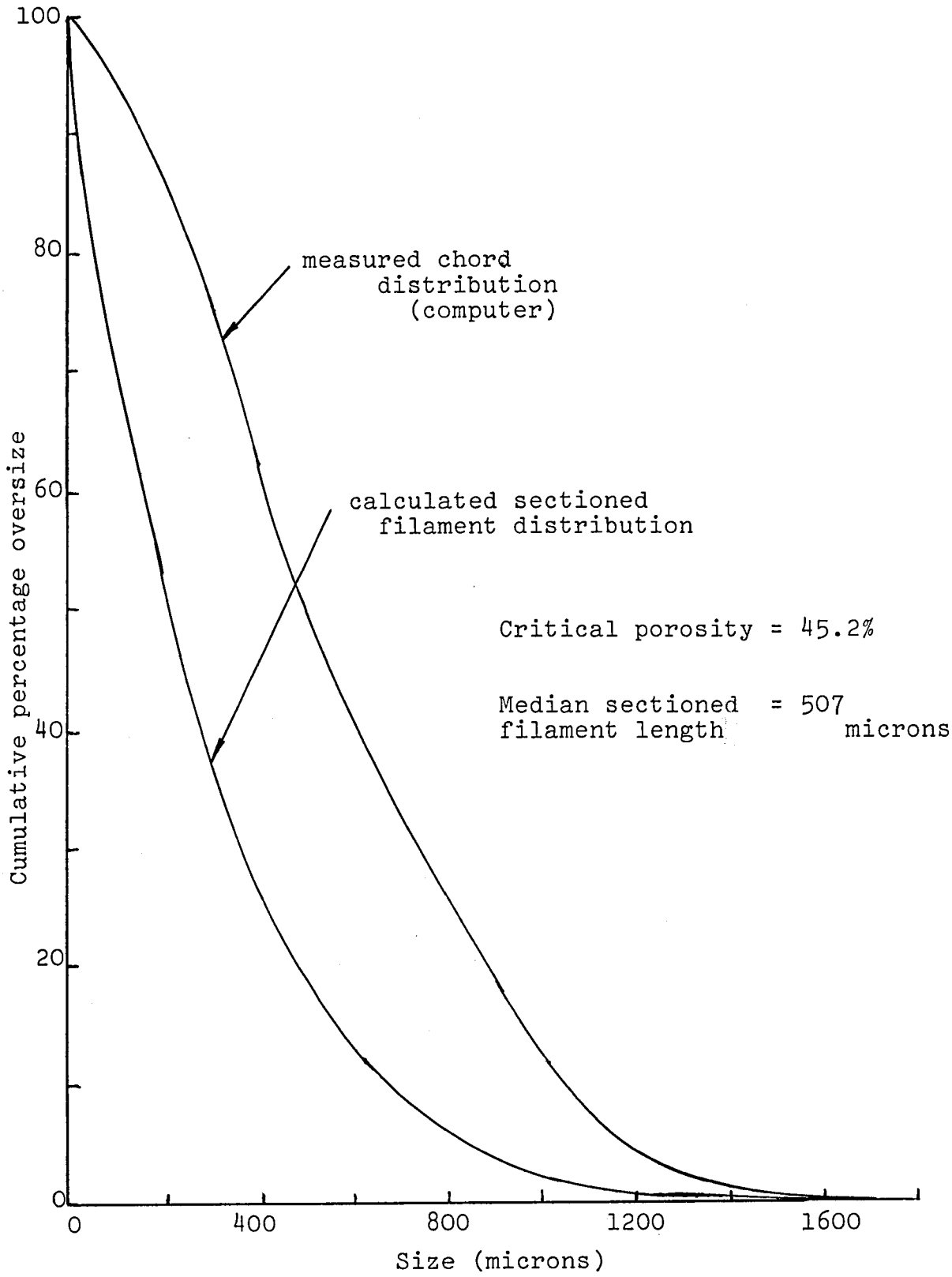

Figure 6.1. Calculated sectioned filament distribution and measured chord distribution from which it was determined for sand size 14-18 B.S.S. mesh sand.

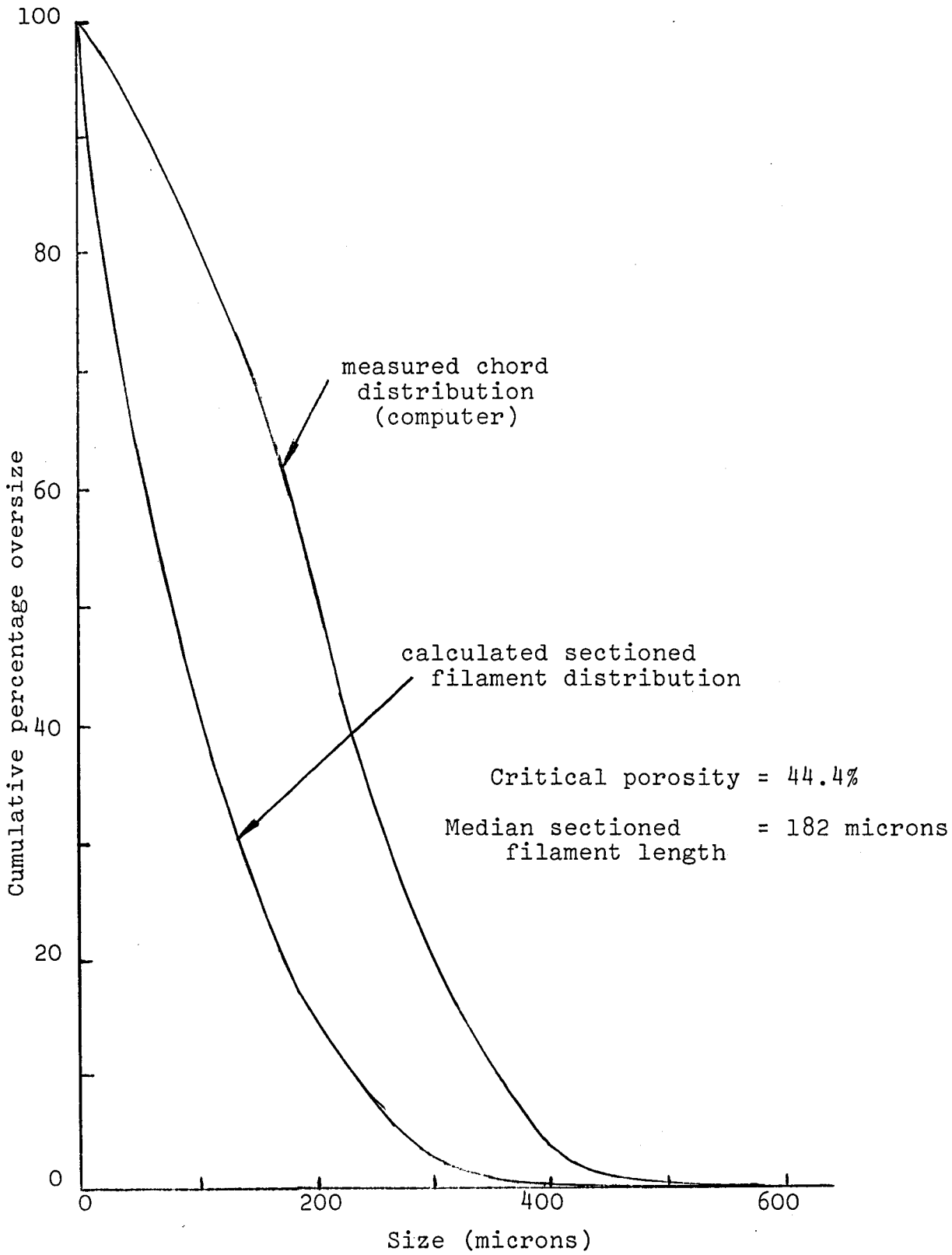

Figure 6.2. Calculated sectioned filament distribution and measured chord distribution from which it was determined for sand size 36-52 B.S.S. mesh sand.

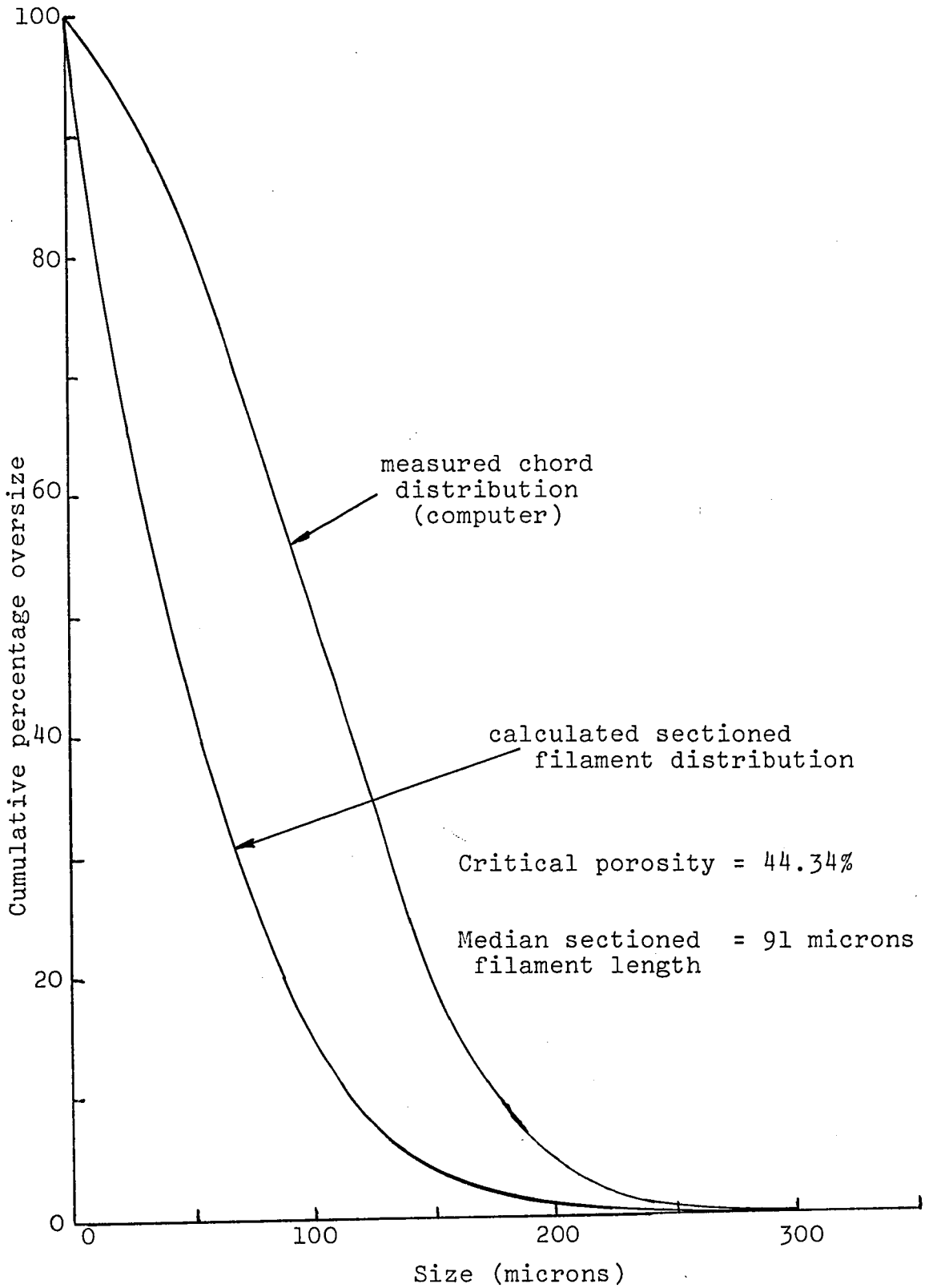

Figure 6.3. Calculated sectioned filament distribution and measured chord distribution from which it was determined for sand size 60-85 B.S.S. mesh sand.

6.3. Shear Studies on the Split Ring Annular Shear Cell

6.3.1. Measurement of the Critical Porosity

The results obtained from the measurement of the critical porosity, using the gamma attenuation technique and the indirect method of measuring the dilation and depth of shear, differ widely. The results obtained from the latter, which are given in detail in tables T.2-5, are considered suspect for two reasons. Firstly, they were based on the depth of shear as measured by the dyed tracer technique and it is felt that this depth of shear measurement is an over-estimate. This is discussed more fully in section 6.3.2., below. Secondly, the results from this technique have a much wider scatter than those from the gamma attenuation technique. This is best indicated in tables T.5 and T.10 for the twelve identical runs on the 36-52 B.S.S. sample. For the gamma attenuation technique the mean critical porosity value was 44.97% with a standard deviation of .27%, compared with the other technique of 42.26% with a standard deviation of 1.4%. In some cases, from the results from the matrix of tests at four shear rates and three normal loads, the standard deviation for the indirect technique was up to 2.94%.

Before considering in more detail the critical porosity measurements obtained from the gamma attenuation technique, the gamma absorption coefficient used in these measurements will be discussed.

6.3.1.1. Absorption Coefficient and the Accuracy of Measurement

The semi-log plots of figures 4.32-34 (pages 143-145) indicate the justification for using the equation, $I = I_o e^{-\mu m}$.

However, although the sand at different thicknesses and bulk densities appeared to obey this relationship, it was noticed that only a small difference in the mass absorption coefficient from, for example, .0750 - .0748 changed the porosity measurements by .16%. The mass absorption coefficient values varied by $\pm .0002 cm^2/gm$.

The count rates as obtained from the horizontal scans had a standard deviation around 15 counts per second. This was equivalent to ±.6% in the porosity value for 99.5% confidence, ± .4% for 90% confidence and ±2% for 66.6% confidence. The results as given were based on ratemeter readings using a 10 second time constant. Greater accuracy could have been obtained if a scaler had been used over a longer counting period.

It is suggested, also, that the accuracy of the gamma attenuation values could have been increased by using a more sophisticated technique in the determination of the mass absorption coefficient.

Roscoe[135], whilst reporting on the work of Coumoulos[36], has suggested that the direct use of the Beer-Lambert Law is open to some errors. Coumoulos found that, due to the scattering effect, the attenuation of the material altered for different packings. He noticed a variation in the absorption coefficient of 4%. In the present work such a difference was not noticed. However, it is wondered whether in Coumoulos' work the attenuation of the whole spectrum was measured or only the attenuation over the photopeak using a discriminator. By counting over the photopeak most of the scattering effects are not detected, which may be a reason for the smaller variation in the absorption coefficient than indicated by Coumoulos. However, this needs further investigation.

6.3.1.2. Critical Porosity as a Function of Normal Load.

As indicated by Roscoe[140], the work of Wroth[199] showed that the greatest change in critical void ratio with normal stress, as experienced in the Simple Shear Apparatus, occurs at low normal stresses. The tests on steel balls gave a greater change than did those for glass beads, but in both cases the void ratio became constant as the normal stress increased.

If there is a significant difference in the critical porosity due to normal stress the values measured on the Split Ring Annular Shear Cell should indicate it. Table 6.3. below gives a summary of tables T.7-9 for all the samples of the critical porosity values at the three normal stress conditions. The values given are means of the four shear rate runs at the particular normal stress.

Table 6.3. Critical Porosity as a Function of the Normal Load

Sample B.S.S. Mesh	Critical Porosity %	Normal Stress gm/cm^2	Student "t" Values Calculated	Tabulated $_{95\%}$	Tabulated $_{90\%}$
	48.1	33.3			
14-18	47.5	55.1	2.25 (6)	2.447 (6)	1.943 (6)
	47.2	76.9			
	45.5	33.3			
36-52	45.2	55.1	1.94 (6)	1.943 (6)	1.440 (6)
	44.6	76.9			
	45.9	33.1			
60-85	45.8	55.1	2.34 (6)	2.447 (6)	1.943 (6)
	45.4	76.9			

Figures in parenthesis denote degrees of freedom.

A student "t" test on the results at the three normal

stresses does indicate a significant variation between the mean value of critical porosity taken at 33.3gm/cm^2 and 76.9gm/cm^2. The indicated trend is in the direction of decreasing critical porosity with increasing normal stress; and this agrees with Wroth. The values of student "t" are shown with the tabulated values and the confidence limits.

One possible explanation of the variation of critical porosity with normal load is that it is due to the fracturing of the particles. According to Roscoe[140], Wroth experienced fracturing of sand particles causing a scatter in his results. From the stresses experienced in the Split Ring Cell, however, it appears that particle fracture is unlikely to occur. Another, and more likely, explanation is the increase in the order of the bed with increase in normal stress. In the case of sand, this probably means preferential orientation of the particles, that is the bed becomes anisotropic.

6.3.1.3. Critical Porosity as a Function of the Shear Rate

Table 6.4. below, gives the mean critical porosity measurements for the same shear rates over the three normal stresses.

Table 6.4. Critical Porosity as a Function of Shear Rate

Sample B.S.S. Mesh	Critical Porosity % Shear Rate rad/min.			
	1.37	2.33	3.97	4.44
14-18	$46.97_{1.52}$	$47.86_{.175}$	$47.47_{1.17}$	$48.33_{.92}$
36-52	$45.78_{.47}$	$45.76_{.30}$	$45.53_{.66}$	$45.71_{.26}$
60-85	$44.83_{.64}$	$45.03_{1.16}$	$44.98_{.52}$	$45.59_{.54}$

small figures denote standard deviations.

Considering table 6.4., there appears to be no significant change in the critical porosity with increasing shear rate. This is in agreement with other researchers[194] who have found no significant change in the angle of friction with increasing shear rate. However, if there is an effect of shear rate, which could be the case if an inertia parameter was present in the behaviour of the bulk material, then this change is likely to be too small to be detected within the limits of accuracy of the measurements made.

6.3.1.4. Comparison of Measured and Theoretical Values of Critical Porosity

The values of the critical porosity as measured by the gamma ray attenuation and those calculated from the measured chord size distribution are shown below in table 6.5.

Table 6.5.

Comparison of Measured and Theoretical Values of Critical Porosity

Sample B.S.S. Mesh	Experimental Normal Load gm/cm^2 33.3	50.1	76.9	Mean	Theoretical from computer Chord Size
14-18	48.1 (.27)	47.5 (.53)	47.2 (.73)	47.6	45.2
36-52	45.5 (.26)	45.2 (.68)	44.6 (.74)	45.1	44.4
60-85	45.9 (.27)	45.8 (.31)	45.4 (.43)	45.7	44.4
	140.	700.	4900.		
Monosize Spheres[140]	40.0	39.5	38.5	39.4	33.3

Figures in parenthesis denote standard deviations.

The measured and calculated values for the sand samples

agree quite well. It is unfortunate, however, that the measured values of critical porosity for the three grades of sand which were arbitrarily prepared do not show much variation. To test the theory more rigorously, samples with more widely varying values of the critical porosity will need to be examined.

Also shown in table 6.5. is the calculated value of critical porosity 33.3% for a set of monosized spheres. This is seen to compare badly with a value of 39.35% which is the mean value of the critical porosity as reported by Roscoe[140]. The critical porosity for spheres which he reported ranged from 40% at 2lb/in^2 to 38.5% at 70lb/in^2. The theoretical value of 33.33% does not depend on any measurements of chord size; and this illustrates, as an extreme case, why the simple theory which has been proposed will have to be elaborated to take account of the state of order of the bed. The theory assumes that the bed is perfectly random and that the filaments are free to interchange positions. It is doubtful whether any packed bed of particles, as opposed to a system of particles which are dispersed, can be completely random. The order of packing is likely to increase if the particles are regular in shape or if they are monosized. A set of particles which have a large aspect ratio is likely to show preferential alignment when flow occurs. In the case of monosized spheres, if the possible forms of regular packing are considered, it is seen that the system can flow if the packing is orthorhombic, or as it is sometimes termed, cubical tetrahedral[42,175]. This packing does have a porosity of 39.54%. Figure 6.4. below, illustrates three modes of packing for monosize spheres.

Thus, although the theory may work well for a system of irregular particles of varying particle size in which the motion

is irregular, it does not work well for a completely ordered system in which the chord size distribution in a random line varies with the position of the line. The greater the state of order in a bed the more the relative positions of the filaments and laminae become fixed; and the more complicated the statistical theories become. By a strange paradox, therefore, the most complicated case to describe by a statistical theory may be that of a system of monosized spheres.

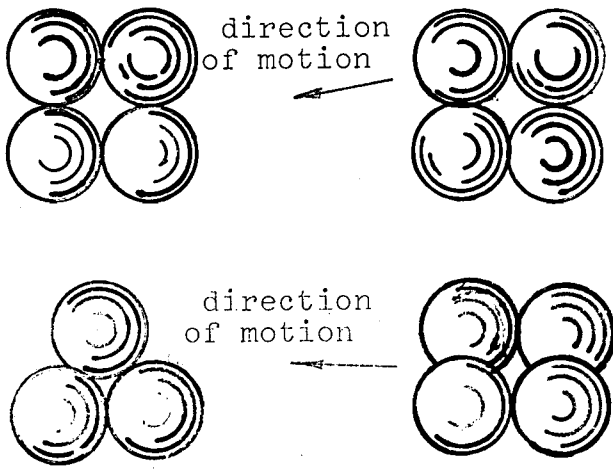

Packings for Monosize Spheres

Loose packing

Porosity 47.64%

Critical packing

Porosity 39.54%

Dense packing

Porosity 25.95%

Figure 6.4.

6.3.2. Measurement of the Depth of Shear

In table 6.6., which is a summary of tables T.11-13, is given the depth of shear as determined by the three independent methods described in section 5.2.3.

Each individual value of shear depth is the mean of four runs at different shear rates. The actual depths of the shear zone are seen to be small. Rowe[142] has pointed out that shear occurs in a narrow region of a bed, this region being too

weak to propagate the shear stress to a greater depth and itself absorbing all the energy put into the system. Thus it is very difficult to propagate flow to a great depth in a bed of particles by applying a shear stress at the surface.

Table 6.6. Depth of Shear for the Three Sand Samples

Sample B.S.S. Mesh	Normal Stress gm/cm^2	Scraping Technique		Calculated from h and ε_c		Density Profile from γ Plot	
		D.o.S.(cm)	HN	D.o.S.(cm)	HN	D.o.S.(cm)	HN
	33.3	1.06	10.4	0.53	5.2	0.89	8.8
14-18	50.1	1.26	12.4	0.65	6.4	0.92	9.1
	76.9	1.22	12.0	0.67	6.6	1.01	10.0
	Mean	1.18	11.6	0.61	6.0	0.94	9.3
	33.3	0.69	20.0	0.45	13 0	0.62	18.0
36-52	50.1	0.69	20.0	0.37	10.7	0.64	18.6
	76.9	0.71	20.3	0.51	14.8	0.65	18.9
	Mean	0.69	20.0	0.44	12.7	0.64	18.6
	33.3	0.52	29.5	0.25	14.2	0.41	23.3
60-85	50.1	0.52	29.5	0.25	14.2	0.50	28.5
	76.9	0.53	30.0	0.31	17.6	0.50	28.5
	Mean	0.52	29.7	0.27	15.7	0.47	26.7

D.o.S. = Depth of Shear HN = Number of Particle Layers

Measurement of the depth of shear by both scraping and gamma density measurement were effected by the nature and depth of the roughening on the shearing plate. With the scraping technique there was the additional possibility of disturbing the sand whilst making the examination. Plots of the density distribution as determined by gamma ray absorption (figures 5.6a-c, page 158) show the shear zone to have a constant density and a sharp interface with the undisturbed material. However, the diameter of the gamma beam was larger than would have been liked. Another reason for the difference in the depth

determined by the scraping technique and the calculated value may be due to the possibility of the depth of shear during dilation being greater than that which exists when the critical porosity is attained.

There was no large variation of the depth of shear with either the normal load or the shear rate. However, a comparison of the mean values at different normal loads by a student "t" test indicates that there may be some tendency for the depth of shear to increase with normal load. The values of student "t" are given in the table 6.7. below.

Table 6.7. Student "t" Test on Depth of Shear Values

Sample B.S.S. Mesh	Depth of Shear(cm)	Normal Stress gm/cm^2	Student "t" Values Calculated	Tabulated	
Scraping Technique:-					
14-18	1.06	33.3	36.0 (6)	99% 3.707 (6)	99.9% 5.959 (6)
	1.22	76.9			
36-52	0.69	33.3	.495 (6)	30% .404 (6)	40% .553 (6)
	0.71	76.9			
60-85	0.52	33.3	1.0 (6)	60% .906 (6)	70% 1.134 (6)
	0.53	76.9			
Calculated from h and ε_c:-					
14-18	0.53	33.3	1.86 (6)	80% 1.440 (6)	90% 1.943 (6)
	0.67	76.9			
36-52	0.45	33.3	1.05 (6)	60% .906 (6)	70% 1.134 (6)
	0.51	76.4			
60-85	0.25	33.3	1.37 (6)	70% 1.134 (6)	80% 1.440 (6)
	0.31	76.9			
Density Profile from λ Plot:-					
14-18	0.89	33.3	3.88 (6)	99% 3.707 (6)	99.9% 5.959 (6)
	1.01	76.9			
36-52	0.62	33.3	.95 (6)	60% .906 (6)	70% 1.134 (6)
	0.65	76.9			
60-85	0.41	33.3	3.46 (6)	98% 3.143 (6)	99% 3.707 (6)
	0.50	76.9			

Figures in parenthesis denote degrees of freedom.

Using the filament size distribution as described in section 3.2.4. to determine the mean filament length, the number of particle layers, HN, which have been disturbed are also given in table 6.7. There is a clear tendency for the shear strain to be propagated through an increasing number of particles as the particle size decreases. The depth of shear is obviously a complicated function of particle size and packing, and needs further investigation.

6.3.3. Shear Strength

The values of the dynamic angle of friction at the steady state condition as given in table T.15 are summarised below in table 6.8.

Table 6.8. Steady State Angles of Friction

Sample B.S.S. Mesh	Normal Stress gm/cm^2	Angle of Friction(^{o})
	33.3	35.9
14-18	50.1	35.6
	76.9	34.8
	33.3	36.3
36-52	50.1	34.6
	76.9	32.6
	33.3	29.7
60-85	50.1	31.1
	76.9	34.1

These results may be compared with the value for massive rose quartz, dried and air equilibrated, of approximately 10^o, [75] and 26^o for fine sand on a quartz block.[142] They illustrate the fact that the angle of dynamic friction is greater for the bulk material than for the material in the massive state. From the twelve identical runs (table T.16) the reproducibility of

the steady state values is disappointing with a standard deviation in tan ϕ of .036.

6.4. Shear Studies on the Jenike Shear Cell

6.4.1. Depth of Shear Measurement

The results obtained from the tests conducted at different initial porosities in the Jenike shear cell are disappointing, in that considerable scatter was experienced when plotting the results.

It is considered that the depth of shear could be determined from these results by considering the mass balance equation:-

$$\frac{H - h}{H} = \frac{1 - \varepsilon_c}{1 - \varepsilon_i}$$

where H = depth of shear

h = dilation

ε_c = critical porosity

ε_i = initial porosity

By rearrangement, this equation becomes:-

$$h = H - \frac{H(1 - \varepsilon_c)}{(1 - \varepsilon_i)}$$

If it is assumed that the depth of shear is independent of the geometry of any equipment, which applied a simple shear force, and is only a function of the material properties, the depth of shear can be determined by plotting h vs. $(1 - \varepsilon_i)^{-1}$. This should give a straight line whose slope is $-H(1 - \varepsilon_c)$ and which intersects the axis at a value of $(1 - \varepsilon_c)^{-1}$.

The data obtained for all the samples, which is given in detail in tables T.17-27 are plotted in the above way.(Figs.6.5-8)

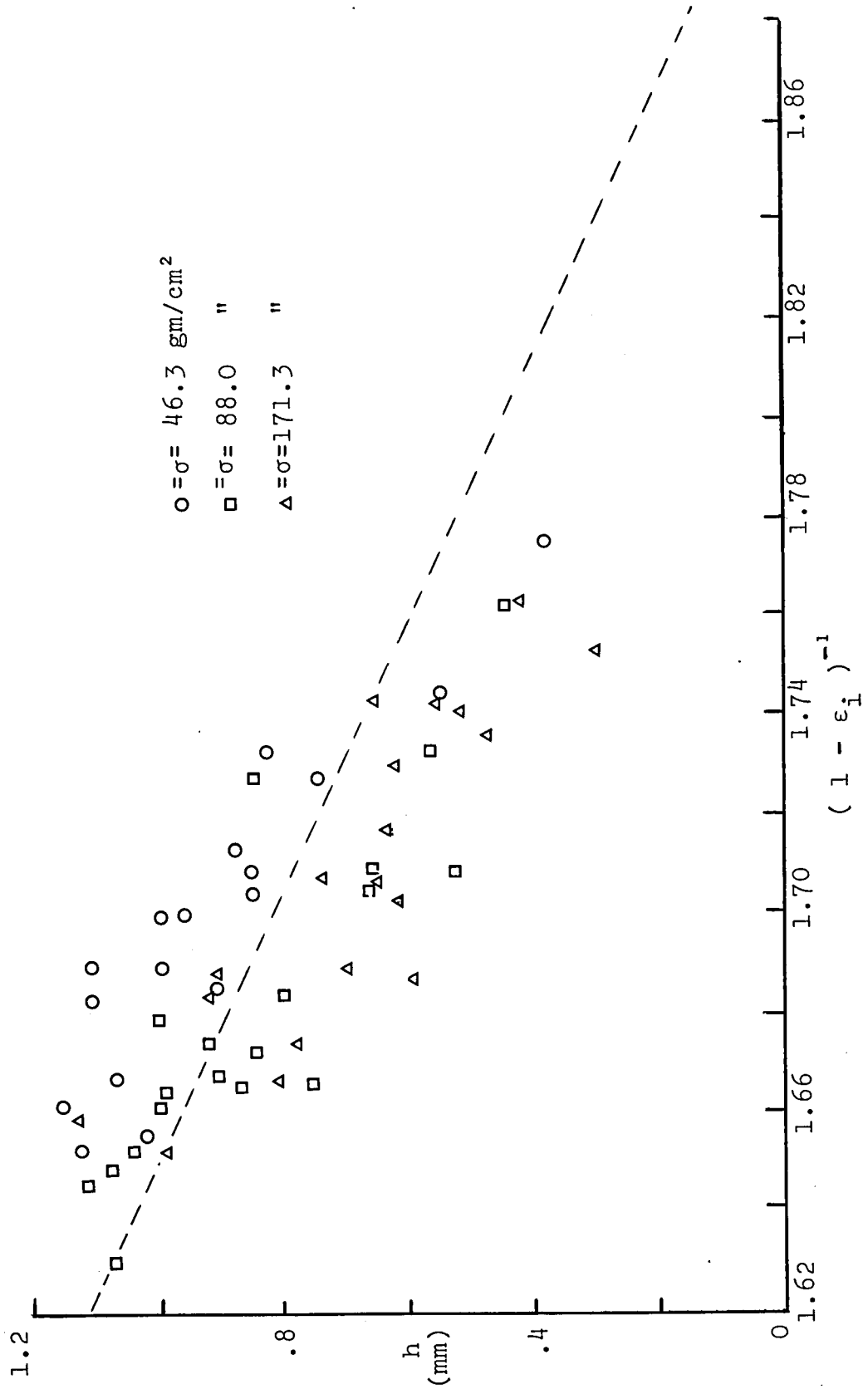

Figure 6.5. Plot of dilation against $(1-\varepsilon_i)$ for Jenike cell (A) results for 14-18 B.S.S. mesh sand

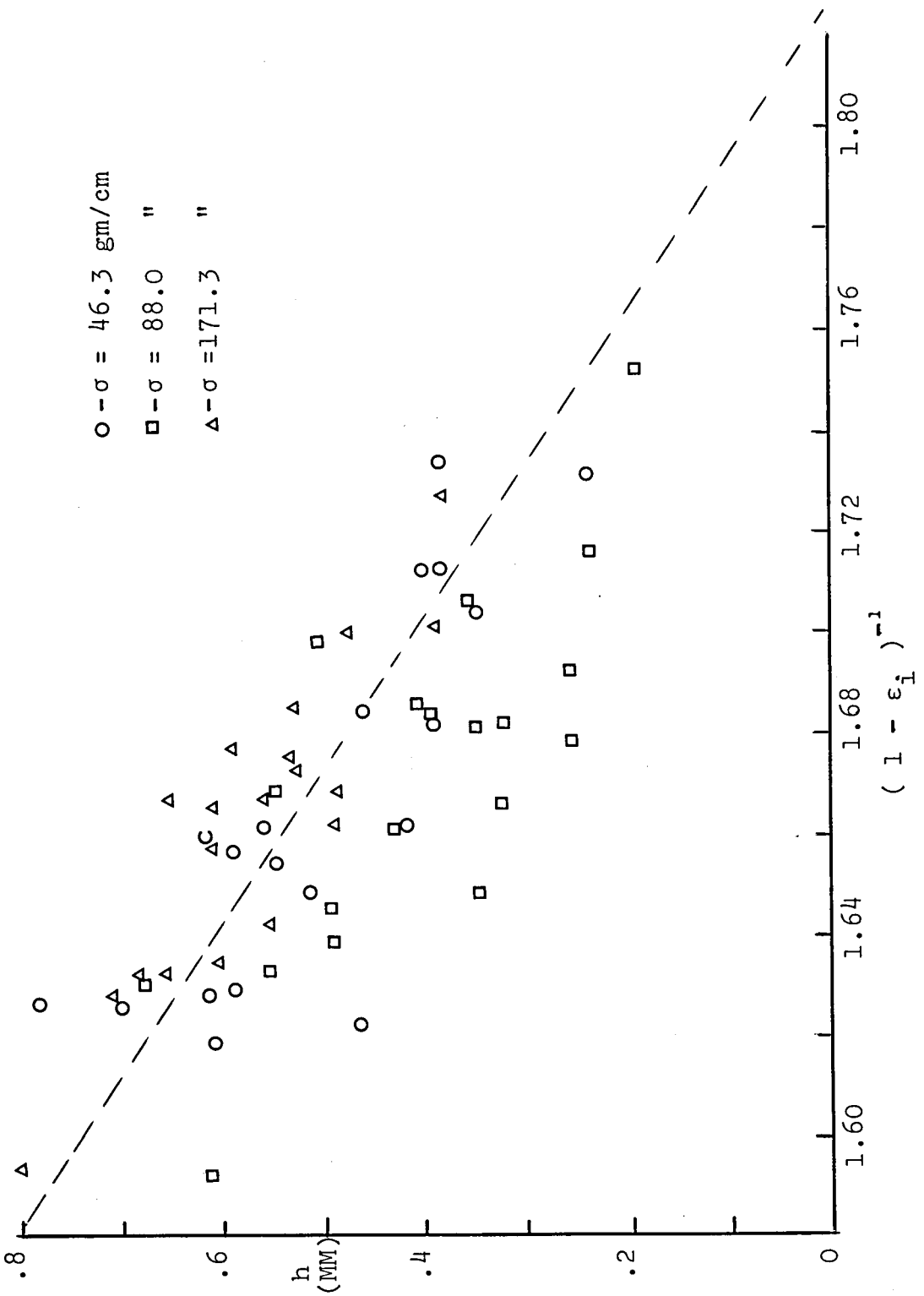

Figure 6.6. Plot of dilation against $(1-\varepsilon_i)^{-1}$ for Jenike cell (A) results for 36-52 B.S.S. mesh sand.

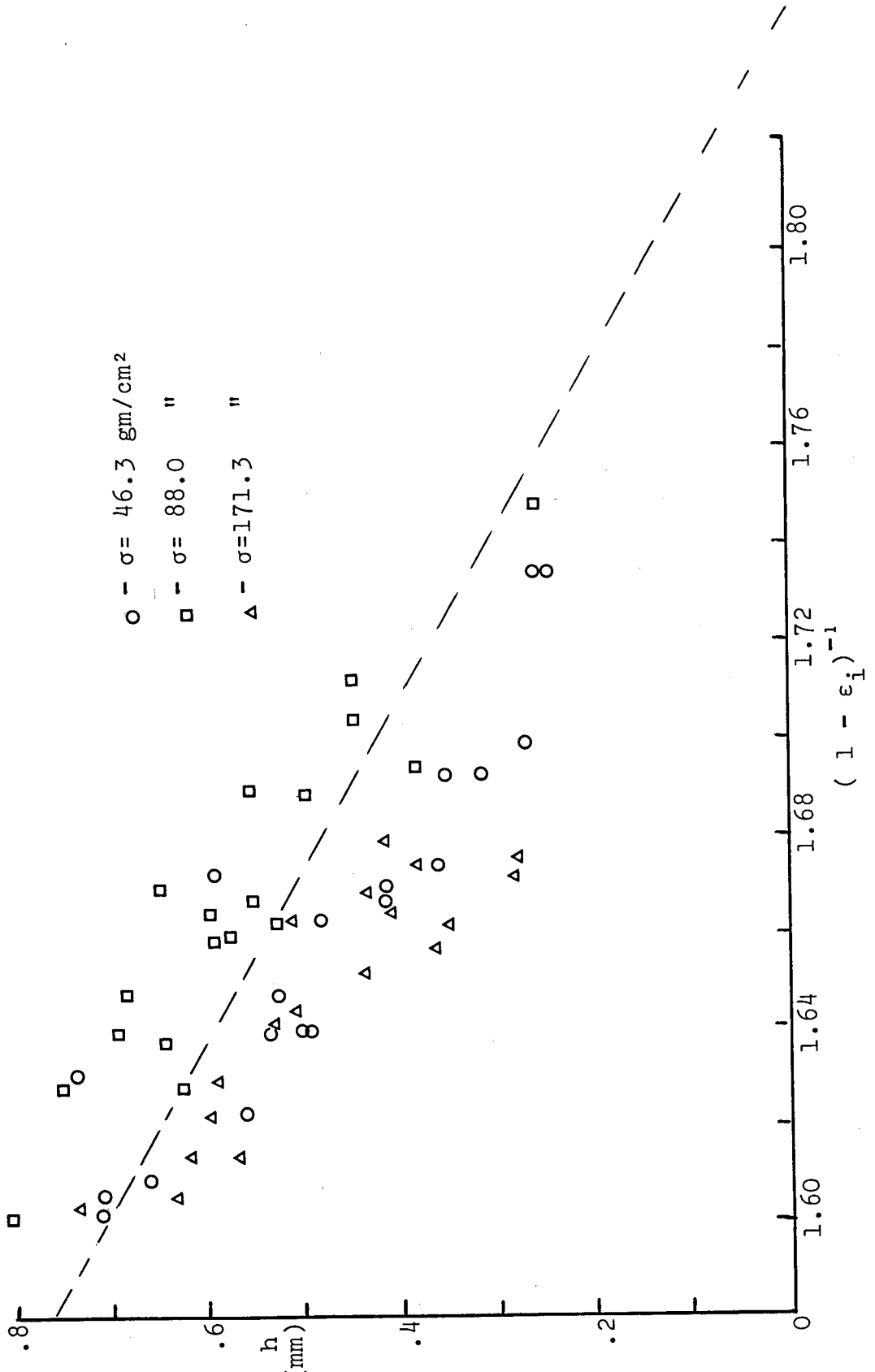

Figure 6.7. Plot of dilation against $(1-\varepsilon_i)^{-1}$ for Jenike cell (A) results for 60-85 B.S.S. mesh sand.

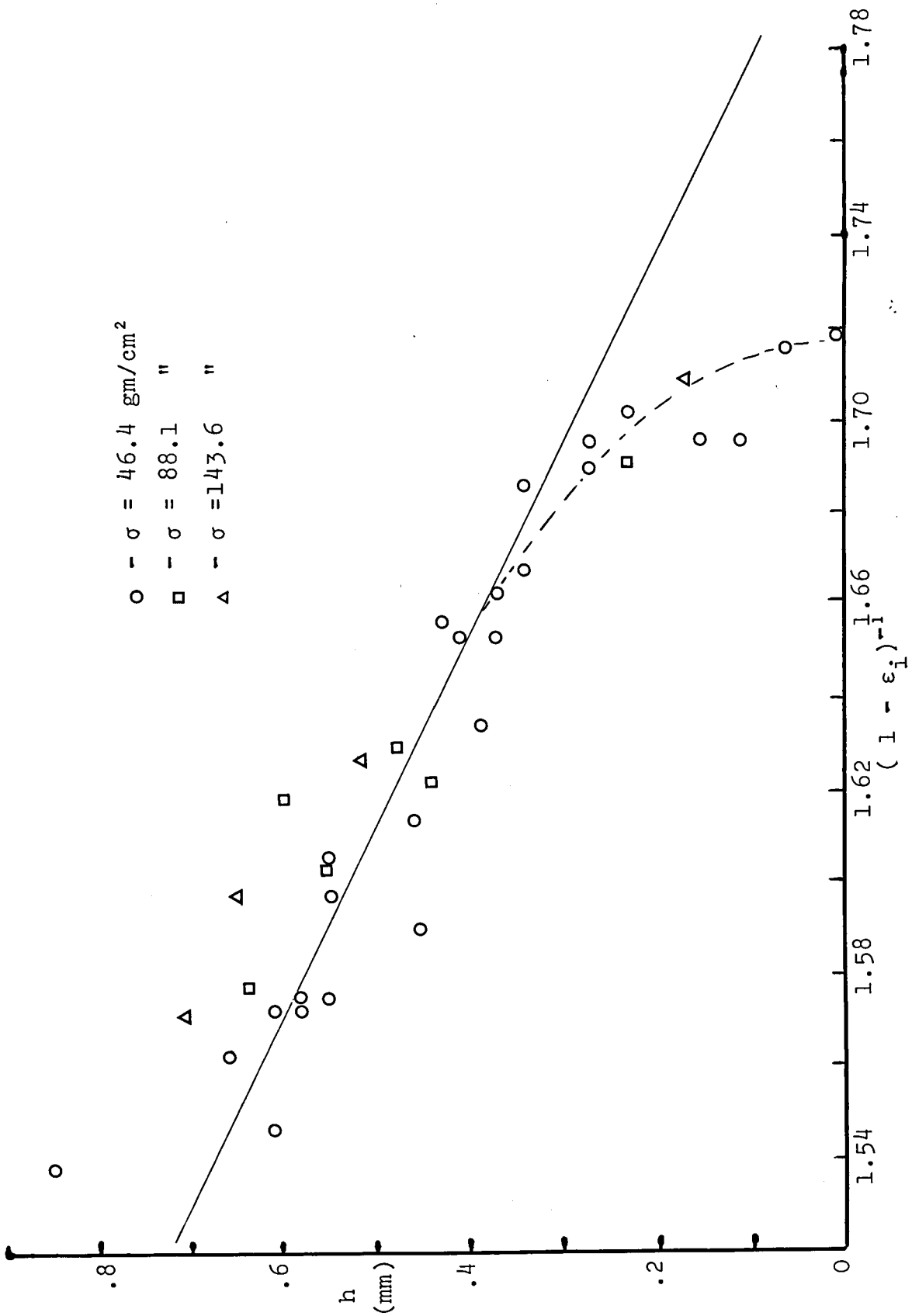

Figure 6.8. Plot of dilation against $(1 - \varepsilon_i)^{-1}$ for Jenike cell (B) results, for 36-52 B.S.S. mesh sand

Apart from figure 6.8., there appears to be little linear relationship; but this figure does appear to indicate a linear relationship at the low porosity end. At the larger values of initial porosity there is a tendency for the portion of the bed, which does not shear after large strain, to pack and to reduce the expansion. However, if the linear portion of the graph is extrapolated it is seen to predict a value for the depth of shear of .425cm. and a critical porosity of 45%. This depth of shear value compares well with the values measured in the annular shear cell based on the dilation and critical porosity measurements. With the critical porosity measurement there also appears to be good agreement. Using figures 6.5-7, however, it is not possible to extrapolate the results to obtain the same information. To determine an order of depth of shear values, a straight line was drawn through the points based on the critical porosity measurements as measured in the Split Ring Annular Shear Cell. Table 6.9., below, gives these depth of shear values and those determined from the annular shear cell measurements.

Table 6.9. Calculated Depth of Shear

Sample B.S.S. Mesh	Depth of Shear (cm) Jenike Cell	Annular Cell Calc.h&ε_c	Annular Cell λ Profile	Annular Cell 'Scraping'
14-18	0.77_{8}	$0.61_{6.2}$	$0.94_{9.3}$	$1.18_{11.6}$
36-52	0.61_{18}	$0.44_{12.8}$	$0.64_{18.6}$	0.69_{20}
60-85	0.52_{30}	0.27_{15}	$0.47_{26.7}$	$0.52_{29.7}$

Small figures denote values for HN (number of particle layers)

The Jenike cell values for the depth of shear lie between the depths measured by the "tracer" scraping technique and gamma density profile plot and those calculated from the dilation and

critical porosity. However, any conclusions from these Jenike cell measurements must be speculative only.

6.4.2. Peak Angle of Friction Measurements

Due to the considerable scatter of these results not a great deal of information can be obtained from them. The ratio of peak shear stress to normal stress is plotted against the initial porosity in figures 6.9-11. Also plotted on these graphs are; the steady state angle of friction values obtained using the annular shear cell and the average residual angle of friction, using the equation given by Skempton and Bishop[159]:-

$$\tan \phi_r = \tan \phi_m - \frac{\delta V}{\delta \Delta}$$

where ϕ_r = residual angle of friction

$\tan \phi_m = \frac{\tau_m}{\sigma_n}$

δV = maximum rate of dilation

$\delta \Delta$ = rate of shear strain

For the 36-52 B.S.S. and 60-85 B.S.S. samples the residual angle of friction is virtually the same as the steady state angle of friction. For the 36-52 B.S.S. sample the value as obtained from the 12 identical runs was chosen, as the value obtained from the other tests seemed high.

Considering the Jenike tests at the lowest normal load, a straight line drawn through the peak shear stress points appears to intersect the residual angle and critical state angle at around the critical porosity. For the higher normal loads straight lines can only be drawn speculatively, but they do indicate a tendency for the critical porosity to decrease with increasing normal load.

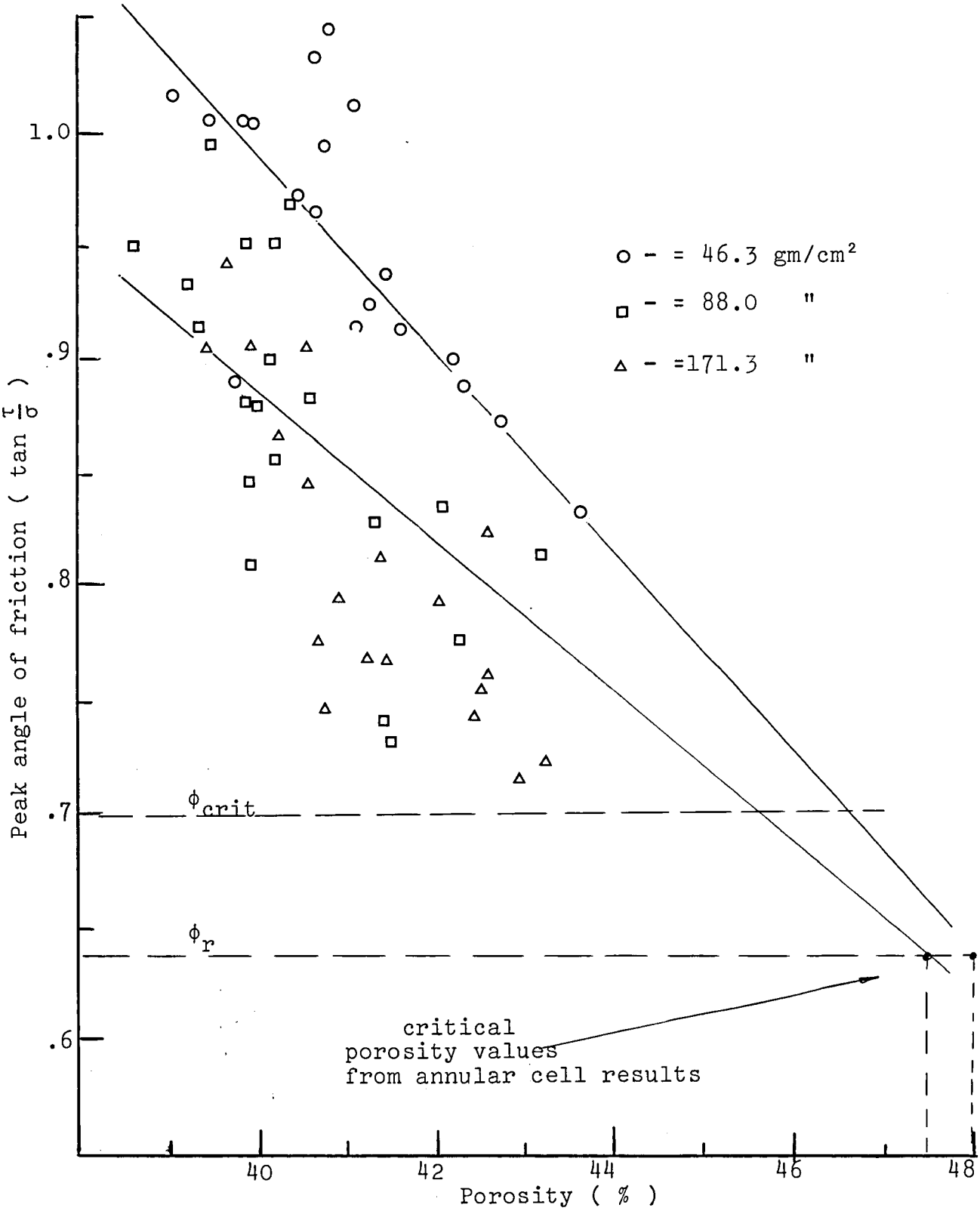

Figure 6.9. Peak stress values against porosity for Jenike cell (A) results for 14-18 B.S.S. mesh sand

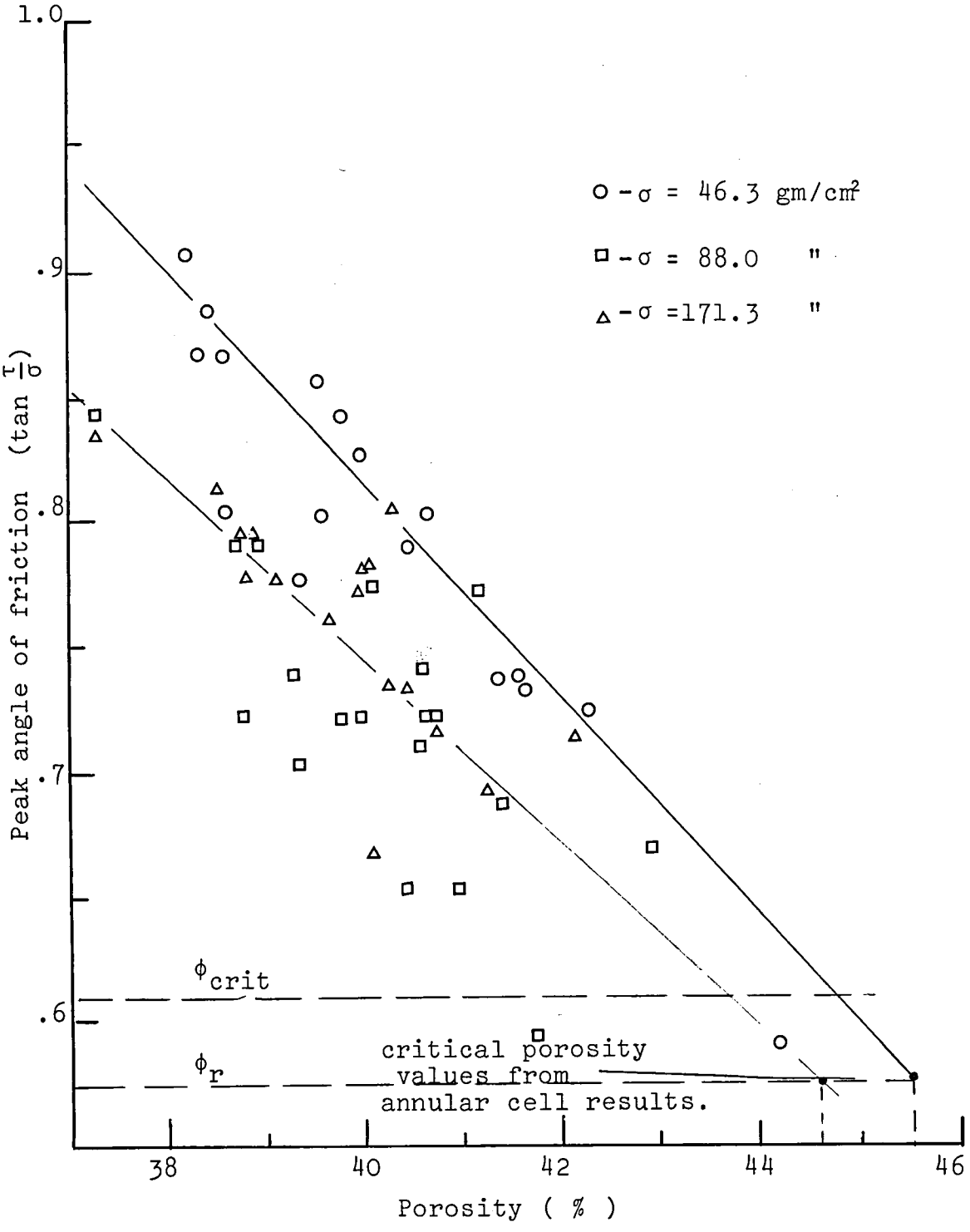

Figure 6.10. Peak stress values against porosity for Jenike cell (A) results, for 36-52 B.S.S. mesh sand.

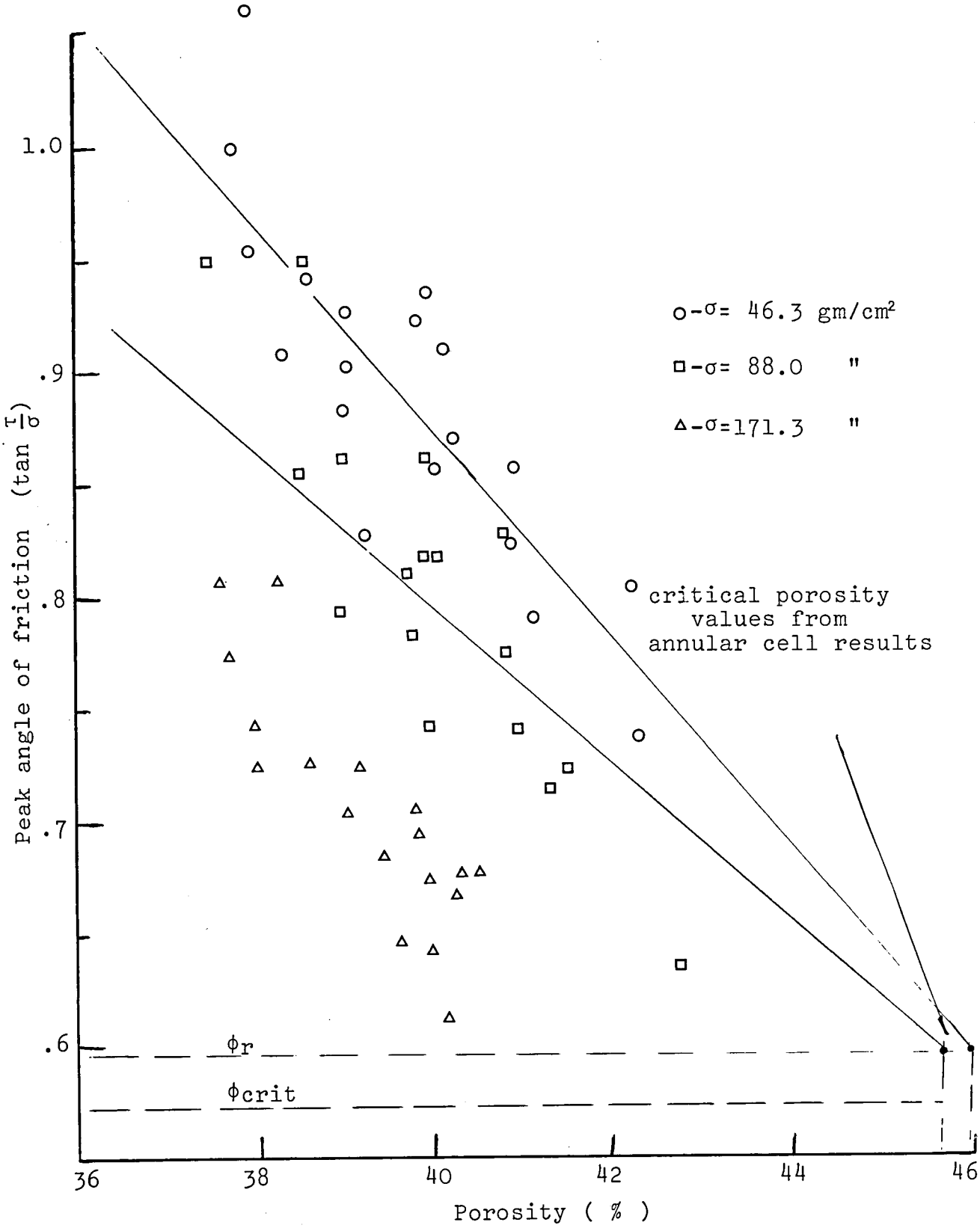

Figure 6.11. Peak stress values against porosity for Jenike cell (A) results, for 60-85 B.S.S. mesh sand.

The possible reason for such disappointing results from the Jenike cell experiments is the uneven state of packing obtained during the experiments. It is possible that parts of the cell were packed to a greater density than others. Also the stress pattern produced in the Jenike cell is probably unsuitable for such tests and a cell of square cross-section, or a Simple Shear Apparatus would be preferable. The main limitation, however, of the Simple Shear Cell is that it is difficult to study the propagation of shear stress through the bed.[135]

6.4.3. Density Profile Measurements

Considering figure 5.11. (page 166); the gamma attenuation density profile plots through the Jenike shear cell, there is a clear indication of the final state of the bed, at the steady state condition, being independent of the initial packing of the material. However, due to Compton scattering the actual measured density was found to be different from the density determined by weighing. To determine actual density values through the Jenike cell, the collimation of the source and detector will need to be brought closer to the cell. This will reduce the scattering effect. From the density profiles an indication is given of the depth of shear at the steady state condition. The depths of shear for the three initial porosities of 34.9% and 42.5% were .8cm., .65cm. and .63cm. respectively, agreeing closely with those determined from the dilation vs. $(1 - \varepsilon_i)^{-1}$ plots.

CHAPTER 7

SUGGESTIONS FOR FURTHER WORK

CHAPTER 7:- SUGGESTIONS FOR FURTHER WORK

The present work has revealed a number of factors which need further investigation. In general, the suggestions can be considered from two aspects, firstly, the improvement in experimental measurements and techniques; and, secondly, in experimental examination of some of the theoretical propositions made in chapter 3.

7.1. Experimental Measurements and Techniques

7.1.1. Redesign of the Split Ring Annular Shear Cell

It was considered in section 5.1.3., when comparing the different shear cells, that although an annular shear cell gives a lower and broader peak shear stress measurement, the use of a Split Ring Cell could reduce this error. The following suggestions, therefore, take into consideration the possible application of it for use in the design of bunkers, the annular shear cell measurements being less tedious to carry out than the present Jenike cell procedure.

i. The present design does not allow shear stress measurements to be made at low normal stresses, unlike the "Portishead" cell, due to the weight of the shearing plate. To enable normal stresses to be reduced it will be necessary to use a counterbalance system to load the annuli. In the conventional annular shear cell this is a relatively simple task, but the shearing plate is made up of thin separate annuli in the Split Ring form. A counterbalance system for each annulus, therefore, will have to be used, which will be more complicated.

ii. The present drive system is too fast, with a lower limit of about 1rad/min. Although this is siutable for steady state measurements, lower speeds are necessary for peak stress determinations. For bunker design purposes, probably a low constant speed drive of about 2rev/hr. would be the best compromise between cost and versatility.

iii. At present the apparatus is only suitable for studying the failure surface and critical state condition in the constant σ plane. It would be advantageous to have a system whereby σ can be varied during the test. In this case, instead of a "dead" weight loading system a hydraulic system linked to the displacement transducer, measuring the dilation of the bed, could be used. This would enable the test to be conducted at constant porosity; and to include variation of both load and porosity.

iv. Although it has been shown that the instrument eliminates the detection of the wall friction, there is more scatter on the steady state angle of friction values than would have been desired. To improve the torque measurement, a system could be devised where the cell is restrained on diametrically opposite sides of the top shearing plate rather than only on the one side as at present. This would also enable the cell to operate at higher normal stresses, which is precluded at present due to tilting of the cell.

v. For the purposes of the measurements on the sand, the roughened sand surface was found to be suitable. For general use, however, another method for giving good powder-to-powder contact is necessary, to prevent the powder under examination from being contaminated with sand. A series of radial vanes might be more satisfactory.

vi. The present design only measures the torque required

to restrain the centre annulus. For a more detailed investigation for research purposes, all three restraining torques could be measured using three load cells. The measurement of the dilation on each annulus would also be useful.

vii. An important part in the bunker design procedure is the measurement of the friction of the powder against the bunker construction material. For this reason the top Split Ring annulus will need to be made up of these construction materials, and the design such that quick changing of these "wall friction" plates is possible.

viii. The present cell, with a diameter of approximately 22cm., is too large for work on costly pharmaceutical powders etc; but a smaller unit could be designed for this purpose.

It is suggested that the principle of the guard ring as used in the Split Ring Annular Shear Cell could also be applied to linear types of direct shear cells. The shearing plate over which the measurement of shear stress is determined, could be made of separate parts, to cover the regions affected by complicated stress distributions and those regions where the stress distribution is more simple.

7.1.2. The Use of the Gamma Attenuation Technique for Determination of Critical Porosity

Further work is necessary in examining this method for the measurement of porosity. In the present work Caesium 137 was used but other sources are available and an examination of their use with respect to various powders could result in greater accuracy in the measurement.

The absorption coefficient needs to be more accurately

determined. By measuring the gamma attenuation at different orientations through a particle bed under shear, a measure of the order of the bed could be obtained. Probably this would involve the simultaneous use of more than one source mounted at different positions with respect to the shear cell.

Reference has been made to the use of X-ray films to study the density profiles in hoppers. The use of gamma ray attenuation techniques may well be an even more useful tool in the study of the porosity in flowing particulate material. Although no specific references are given it is known that the technique is used for examining fluidised systems, such as measuring the porosity in fluidised beds, on air slides, and for the determination of solids concentrations in pneumatic conveying systems. Two further possible applications are:-

i. The measurement of the porosity within a hopper. Using a hopper section with plane sides, the different regions of flow and the porosity in each region could be determined. It would be useful to see where the packing of the material changed to the critical state, and how much above this value the porosity varied. The method would also give an indication of the position and porosity value of the dynamic arch.[156]

ii. The different density regions in a drum mixer have been indicated by Lloyd and Yeung.[110] By measuring the attenuation of a gamma beam along the drum the value of these density regions could be determined as well as the state and mode of packing in the drum.

7.1.3. Automatic Measurement of the Chord Size Distribution

The system used for the determination of the chord size

distribution had several limitations, namely:-

i. The system needed very high contrast photographs of particle sections, which were very difficult to obtain. To overcome this, new techniques in obtaining the photographs of the sections need to be developed; or an automatic system used which does not need such high contrast photographs. It is realised that opaque sand is a difficult material for such an automatic system and a material more reflecting or absorbant to light would be better.

ii. The present system is such that it takes approximately 15 hours to scan a 35mm. slide enlarged to 35in. Although this is an automatic system, needing no person present, it is too expensive on computer time. A faster system is required with, ideally, a television camera to do the scanning. However, the use of a television camera at present would be unsuitable, in that the computer would be too slow to process the results, and so keep up with the camera.

iii. The present theories show the large influence of the small chords on the prediction of the macroscopic properties. The system as used to measure the chord lengths is less accurate as these lengths get shorter. Although the photographs of smaller particle sections could be enlarged, the problem would not be solved as even the large particles have chords down to zero length. A suitable technique needs to be developed, perhaps using an indirect method.

iv. The preparation of particle sections is a tedious process and so the examination of chords and section areas of particles necessitates one further step than the usual form of particle sizing by microscopic methods. If a relationship could be found between the profile chord size distribution and the section

chord size distribution, the need for measuring chords from particle sections would be unnecessary.

Clearly if the concept of Stereology for the prediction of bulk particulate properties and for microscopic properties comes into favour many of the above problems will be overcome.

7.2. Theoretical Concepts

7.2.1. The Examination of Anisotropy

It is clear from the literature that the existance of anisotropy has largely been neglected in studying the behaviour of particulate material. It is suggested, therefore, that a closer investigation of this concept is necessary. The suggested application of the theory in chapter 3 needs verifying for anisotropic cases.

The measurement of anisotropy in such a situation as a shear cell would probably involve the "fixing" of the particle bed and examining sections of the bed cut in different orientations. By "fixing" at various normal stresses and for different stages of the test a much clearer picture would be obtained of the parameters effecting the state of anisotropy in a bed of irregular particles.

The effect of particle shape on anisotropy would also be a valuable study.

7.2.2. The Prediction of Segregation

In section 3.2.3.3. it was proposed that the model described for the prediction of the critical porosity will also predict segregation for certain particle size distributions.

This proposal needs experimental examination. The filament size distributions for samples which are known to segregate during shear will need to be determined and compared with figure 3.17 (page 88). Also, samples could be made up in a predictable way to give a sectioned filament distribution as shown in figure 3.17. This distribution could then be examined in the annular shear cell to see if segregation occurs during flow.

7.2.3. The Prediction of Steady State Friction from Microscopic Properties

It was suggested in section 3.2.3. that a Stereological method could be used in predicting the difference between the steady state friction and the mineral friction. As pointed out in that section it is likely that an understanding of the number of point contacts, as a function of the packing, would be necessary before such a prediction could be evolved. The number of particle contacts could be determined from the "fixed" sections obtained from the proposed anisotropy studies.

For these studies a hard bulk material with a known mineral friction, such as quartz, would be necessary.

7.2.4. Stress/Strain Relation

Having determined the steady state stress value from microscopic measurements, the next logical step would be to describe the stress/strain relation from a similar standpoint, by relating the predicted shear stress to packing through the stages of shear. This, however, would also require a deeper understanding of the relation between dilation and horizontal strain for different particle size distributions. Ultimately, bulk stress behaviour may be determined by simple microscopic

measurements, with the possible elimination of intermediate shear strength measurements.

7.3. The Study of Cohesive Systems

This thesis has centred around free flowing material and the theory predicts the behaviour for such a material. It is realised, however, that most of the "difficult" powders are cohesive in nature.

From a brief examination of the literature it appears that the basic ideas of cohesion and the effect of moisture on the strength of particulate material are vague. It is suggested, therefore, that alongside the proposed free flowing experiments a study of the same parameters for cohesive material should be made.

In concluding this chapter, it is suggested that by considering the behaviour of bulk material from a particulate basis a much deeper and more useful knowledge of the behaviour of particulate material will be obtained when used alongside the present continuum theories.

CHAPTER 8:- CONCLUSIONS

1. It is possible to characterise a packed particle system by the consideration of the four characterisations of microscopic, state, macroscopic and behavioural properties.

2. The particle is not the primary unit of a particulate system. A particulate system can be characterised by a filament size distribution and by a lamina size distribution, both of which can be obtained from an analysis of particle sections.

3. The porosity of a random, isotropic bed of particles due to shear deformation, at the steady state condition, is independent of the initial packing conditions. This porosity, the critical porosity, can be related to the microscopic property of particle size using the sectioned filament size distribution, by the relation:-

$$1 - \varepsilon_c = \frac{\int_0^{x_{max}} g(y)ydy}{y_m}$$

where ε_c = critical porosity

$g(y)$ = number distribution of sectioned filaments of length y

y_m = median sectioned filament length

x_{max} = maximum filament length

The median sectioned filament length, y_m, is given by the relation:-

$$\int_0^{y_m} g(y)ydy = \int_{y_m}^{x_{max}} g(y)ydy$$

The critical porosity is independent of the geometry of a shear cell but variation will be caused by increasing the state of order of the bed which is, itself, a function of the normal stress. The model can be altered to account for anisotropy.

4. If direct shear is applied to a bed of free flowing particles, flow will occur in a region of definite depth which is a function of the properties of the material. The depth of shear tends to increase with normal stress and also as the particle size increases.

5. A particulate material attains a definite value of its angle of friction after the steady state has been reached. It is higher than the pure material mineral friction, and appears to be a function of the particle size distribution of the bed.

6. The steady state flowing condition can be successfully obtained in a Split Ring Annular Shear Cell. This shear cell obviates the detection of the stress concentration at the walls of an annular shear cell; and limits the shear stress measurement to a narrow annulus. The cell may also be used to measure peak shear stress values, as this measurement is not taken over the whole annulus width, as is the case with the conventional annular cell.

7. The porosity and density profiles of a bed of particles in a shear cell may be successfully obtained using a gamma ray attenuation technique.

APPENDIX A.1.

A.1. Justification of the Use of Stereology

A.1.1. Proof that a three dimensional system can be represented in composition by a two dimensional sample

Delesse [41] 1842:-

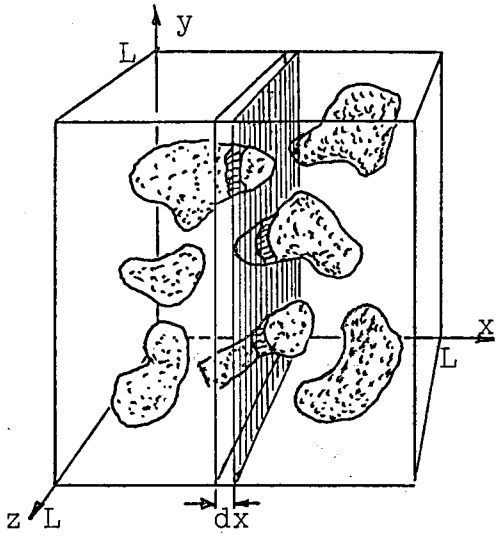

Figure A.1.

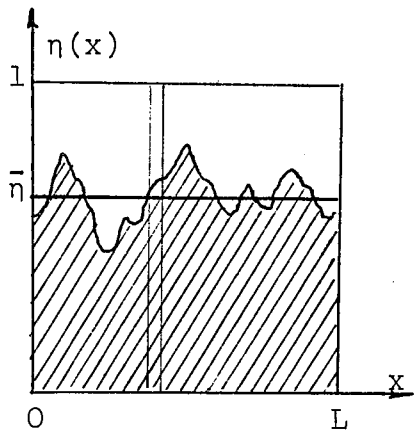

Figure A.2.

Suppose that a cube, figure A.1., with volume:

$$V = L^3 \quad . \quad . \quad . \quad . \quad . \quad (A.1.)$$

contains granules of shape and size which together have a volume:

$$v = \Omega V \quad . \quad . \quad . \quad . \quad . \quad (A.2.)$$

Consider now a thin slice of this cube of thickness dx parallel to the (z,y) plane having a volume:

$$dV = L^2 dx \quad . \quad . \quad . \quad . \quad . \quad (A.3.)$$

In this slice a volume:

$$dv = \eta(x)dV = \eta(x)L^2 dx \quad . \quad . \quad (A.4.)$$

will contain segments of the granules. L and dx are constant wherever we place the slice but $\eta(x)$ will vary with x, as is indicated in figure A.2.

If $dx \to 0$ the total volume of the granules is:

$$v = \int_0^L dv = L^2 \int_0^L \eta(x)dx = \Omega L^3 \quad . \quad . \quad (A.5.)$$

But:

$$\frac{1}{L} \int_0^L \eta(x)dx = \bar{\eta} \quad . \quad . \quad . \quad (A.6.)$$

is the average value of the coefficient $\eta(x)$ between 0 and L so that it follows from equations A.3. and A.6. that:

$$\bar{\eta} L^3 = \Omega L^3$$

or:

$$\bar{\eta} = \Omega \quad . \quad . \quad . \quad . \quad (A.7.)$$

Equation A.7. means that the volumetric frequency Ω of a given component is reflected on sections of the component in occupying a corresponding fraction η of the sectioned area. In more practical terms, an average fractional coefficient $\bar{\eta}$ determined on sections through a volume represents an estimator of the volumetric frequency Ω of the component under investigation. From this it follows that: a section is a quantitatively representative two dimensional sample of a three dimensional system of randomly distributed structures.

A.1.2. Proof that a three dimensional system can be represented in composition by a one dimensional sample

Rosiwal[144] 1892:

Let a square area $S=L^2$ be covered by spots (transections of the structure G under investigation) as illustrated in figure A.3 over an area:

$$s_G = \eta_G S \quad . \quad . \quad . \quad . \quad . \quad (A.8.)$$

and consider a strip of width dx and area:

$$dS = Ldx \quad . \quad . \quad . \quad . \quad . \quad (A.9.)$$

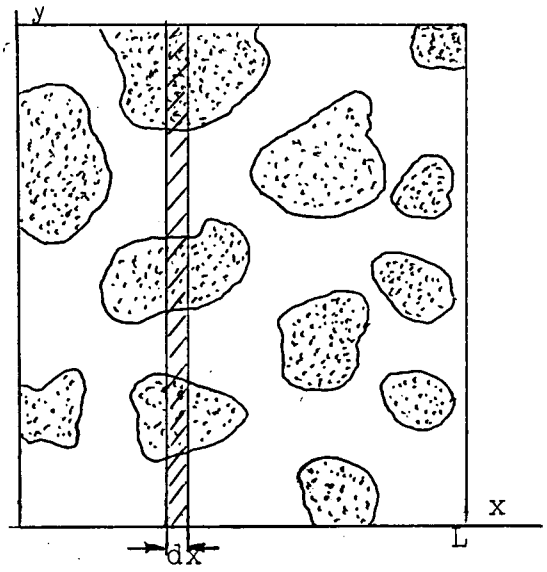

Figure A.3.

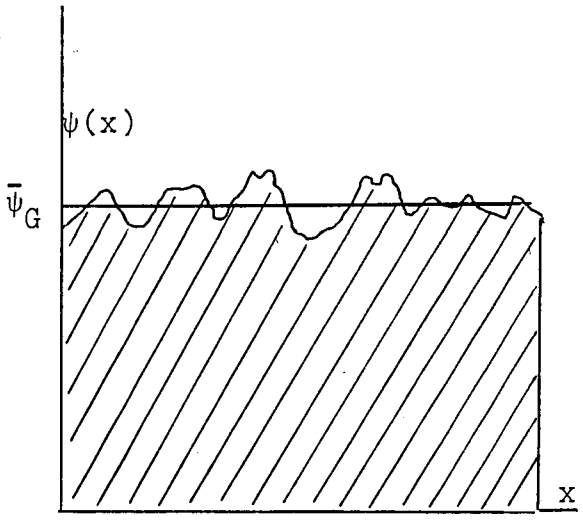

Figure A.4.

A fraction:

$$ds_G = \psi_G dS = \psi_G L dx \quad . \quad . \quad . \quad . \quad (A.10.)$$

of this strip will be covered by spots. Considering figure A.4. $\psi_G(x)$ varies with x. If $dx \to 0$:

$$s_G = L \int_0^L dx \psi_G(x) = \eta_G L \quad . \quad . \quad . \quad (A.11.)$$

But since:

$$\frac{1}{L} \int_0^L dx \psi_G(x) = \bar{\psi}_G \quad . \quad . \quad . \quad . \quad (A.12.)$$

is the average value of $\psi_G(x)$ between 0 and L, it follows that:

$$\bar{\psi}_G = \eta_G \quad . \quad . \quad . \quad . \quad (A.13)$$

In deriving Delesse's principle it was shown that the average value of η_G is an estimator of the volumetric fraction Ω_G occupied by the structures under investigation. It is, therefore, found that

$$\Omega_G = \bar{\eta}_G = \bar{\psi}_G \quad . \quad . \quad . \quad . \quad (A.14.)$$

Rosiwal also demonstrated that the line along which ψ_G is determined need not be straight but may have any shape so long as its course is not biased by the underlying array of transections.

A.1.3. Proof that a three dimensional system can be represented in composition by a zero dimensional (points) system

Weibel [187] 1963:-

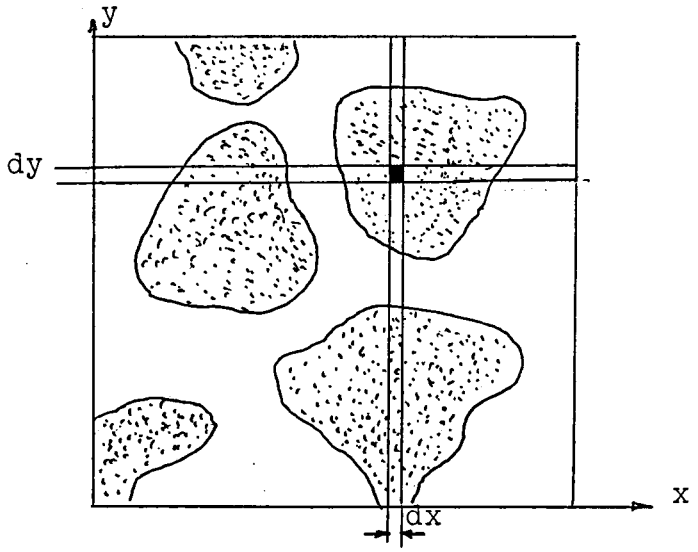

Figure A.5.

Let the probability of a point lying on transections of G:

$$\text{Probability (point lying on G)} = P_s^G$$

Let a point be a very small square of area dy dx. The total number of squares in the area S, figure A.5., is

$$n_s = \frac{S}{dxdy}$$

Of these squares a total number of:

$$n_G = \frac{S_G}{dxdy} = \frac{n_G S}{dxdy}$$

will lie on granules where $S_G = n_G S$ is the area covered by transections of G. It follows that the probability of a point lying on a granule is:

$$P_s^G = \frac{n_G}{n_s} = \frac{S_G}{S} = n_G$$

By a similar procedure it is evident that the probability of a point lying in a granule contained in a three dimensional system of volume, V, is:

$$P_v^G = \frac{n_G}{n_v} = \Omega_G$$

since:

$$n_v = \frac{V}{dv}$$

and

$$n_G = \frac{\Omega_G V}{dv}$$

where dv is the shrinking volume of the point. Since in equation A.7. it was shown that

$$\bar{n}_G = \Omega_G$$

it follows that:

$$P_s^G = P_v^G = \Omega_G$$

which indicates that the average probability of a point falling on to a transection of the component G on a section is given by the volumetric fraction Ω_G of the component occupied by G.

APPENDIX A.2.

Calculation of $\bar{x}$, y_m and ε_c from the number chord size distribution, f(x)

1. The number size distribution for x, f(x), is normalised so that:

$$\int_0^{x_{max}} f(x)dx = 1$$

2. The area under the curve $\int_0^{x_{max}} f(x)dx$ vs. x is equal to $\int_0^{x_{max}} f(x)xdx$ therefore:

$$\bar{x} = \frac{\int_0^{x_{max}} f(x)xdx}{\int_0^{x_{max}} f(x)dx}$$

that is: $\bar{x}$ = Area $\int_x^{x_{max}} f(x)dx$ vs. x

3. From equation (1):

$$g(y)dy = \int_{x=y}^{x=x_{max}} \frac{f(x)dx}{x}.dy$$

$\int_{x=y}^{x=x_{max}} \frac{f(x)dx}{x}$ is equal to the cumulative area in the curve $\int_{x=y}^{x_{max}} f(x)dx$ vs. $\frac{1}{x}$. Considering figure A.6., a plot of $\frac{f(x)dx}{x}$ vs. x.

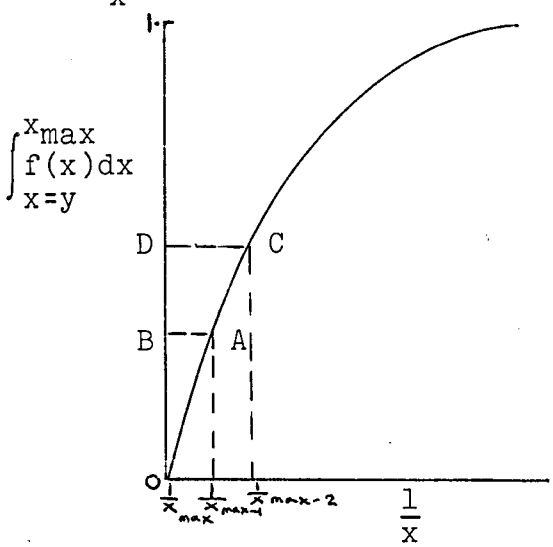

$g_{\left(\frac{x_{max} + x_{max-1}}{2}\right)}$ = Area OAB

$g_{\left(\frac{x_{max-1} + x_{max-2}}{2}\right)}$ = Area OCD

and so on, which gives g(y).

Figure A.6.

4. The median chord, y_m, is determined by:

$$\sum_{i=1}^{n} \frac{g(y_i)y_i}{2} = g(y_m)y_m$$

where n is the number of increments in y.

5. The critical porosity, ε_c, is given by equation (5)

$$1 - \varepsilon_c = \frac{\int_0^{x_{max}} g(y)y\,dy}{y_m}$$

The number sectioned filament distribution obtained in (3) is normalised such that:

$$\int_0^{x_{max}} g(y)\,dy = 1$$

In a similar manner as for $\bar{x}$, the equation is solved by measuring the area under the cumulative sectioned chord distribution vs. x curve. That is:

$$\int_0^{x_{max}} g(y)y\,dy = \text{Area under, } \int_y^{x_{max}} g(y)\,dy \text{ vs. } y \text{ curve.}$$

APPENDIX A.3.

Tables of Results

TABLE T.1.

Evaluation of Split Ring Annular Shear Cell

Influence of Wall Friction Results

Sand Size = 30-36 B.S.S. Mesh

Loads on annuli :- Inner = 2.531 Kilo

Centre = 5.063 Kilo

Outer = 10.126 Kilo

Shear torque = M Normal load = N

r_1 = inner radius of annulus

r_2 = outer radius of annulus

r_2 = 10.45cm. shear cell in conventional form

r_2 = 7.1cm. shear cell in split ring form

r_1 = 2.5cm. shear cell in conventional form

r_1 = 4.6cm. shear cell in split ring form

$$\text{shear stress} = \tau = \frac{3M}{2\pi(r_2^3 - r_1^3)}$$

$$\text{normal stress} = \sigma = \frac{N}{\pi(r_2^2 - r_1^2)}$$

$$\tan\phi = \frac{\tau}{\sigma} = \frac{M3(r_2^2 - r_1^2)}{N2(r_2^3 - r_1^3)}$$

$$\tan\phi = \frac{M}{Nr^*}$$

$$\text{where } r^* = \frac{2}{3}\,\frac{r_2^3 - r_1^3}{r_2^2 - r_1^2}$$

TABLE T.1. (cont.)

	M	N	Nr*	tanϕ	ϕ°
Annular Shear Cell in Conventional Form					
	kilo.cm.	kilo	kilo.cm.		
Maximum	157.82	17.76	127.26	1.2487	50.3
Minimum	104.72	"	"	0.8228	39.7
Average	126.36	"	"	0.9920	44.7
Maximum	136.88	"	"	1.0755	47.0
Minimum	99.77	"	"	0.7839	38.1
Average	120.36	"	"	0.9457	43.4
Maximum	131.57	"	"	1.0338	46.0
Minimum	110.33	"	"	0.8669	41.0
Average	120.95	"	"	0.9500	43.6
Maximum	131.57	"	"	1.0330	46.0
Minimum	105.31	"	"	0.8270	39.6
Average	120.95	"	"	0.9500	43.6
				Mean	$43.8^{\circ} \pm 6^{\circ}$
Annular Shear Cell in Split Ring Form					
	21.07	5.063	29.85	0.7050	35.2
	19.09	"	"	0.6394	32.5
	19.75	"	"	0.6615	33.5
	19.75	"	"	0.6615	33.5
	19.78	"	"	0.5957	30.8
	18.45	"	"	0.6175	31.7
				Mean	32.8 ± 2.4

TABLE T.2.

Split Ring Annular Shear Cell Results

Density Measurements from Weight and Dilatancy Measurements

Sand Size - 14-18 B.S.S. Mesh

	Before Shear			After Shear		
Shear Rate (rad/min)	Bulk Density	Void Ratio	Porosity %	Bulk Density	Void Ratio	Porosity %
Normal Stress = 33.33gm/sq.cm						
1.37	1.537	.723	41.97	1.452	.825	45.21
2.33	1.568	.690	40.85	1.475	.796	44.33
3.93	1.521	.792	42.60	1.444	.836	45.53
4.48	1.553	.706	41.40	1.466	.807	44.66
					Mean	44.93
					S.D.	.47
Normal Stress = 55.09gm/sq.cm						
1.57	1.555	.704	41.32	1.470	.803	44.53
2.81	1.556	.703	41.28	1.485	.785	43.98
3.97	1.550	.710	41.54	1.450	.827	45.29
4.44	1.553	.707	41.41	1.461	.814	44.86
					Mean	44.66
					S.D.	.55
Normal Stress = 76.86gm/sq.cm						
1.27	1.591	.665	39.95	1.472	.800	44.45
2.28	1.592	.664	39.91	1.493	.775	43.67
3.31	1.574	.684	40.61	1.464	.809	44.74
5.10	1.591	.665	39.95	1.494	.774	43.63
					Mean	44.12
					S.D.	.56
				Overall Mean		44.57

TABLE T.3.

Split Ring Annular Shear Cell Results

Density Measurements from Weight and Dilatancy Measurements

Sand Size - 36-52 B.S.S. Mesh

	Before Shear			After Shear		
Shear Rate (rad/min)	Bulk Density	Void Ratio	Porosity %	Bulk Density	Void Ratio	Porosity %
Normal Stress = 33.33gm/sq.cm						
1.56	1.614	.642	39.09	1.511	.754	43.00
2.76	1.607	.648	39.34	1.508	.757	43.07
3.97	1.589	.667	40.03	1.519	.744	42.67
4.28	1.584	.672	40.20	1.444	.835	45.50
					Mean	43.56
					S.D.	1.30
Normal Stress = 55.09gm/sq.cm						
1.57	1.502	.764	43.31	1.406	.885	46.96
2.90	1.621	.635	38.83	1.561	.697	41.09
4.05	1.626	.630	38.64	1.579	.678	40.42
4.19	1.602	.654	39.53	1.510	.755	43.02
					Mean	42.87
					S.D.	2.94
Normal Stress = 76.86gm/sq.cm						
1.32	1.603	.653	39.49	1.508	.757	43.10
2.00	1.608	.648	39.32	1.522	.740	43.55
3.34	1.592	.665	39.94	1.514	.750	42.86
4.71	1.608	.648	39.32	1.497	.775	43.51
					Mean	43.00
					S.D.	.41
				Overall Mean		43.15

TABLE T.4.

Split Ring Annular Shear Cell Results

Density Measurements from Weight and Dilatancy Measurements

Sand Size - 60-85 B.S.S. Mesh

	Before Shear			After Shear		
Shear Rate (rad/min)	Bulk Density	Void Ratio	Porosity %	Bulk Density	Void Ratio	Porosity %
Normal Stress = 33.33gm/sq.cm						
1.46	1.621	.635	38.83	1.515	.749	42.82
2.83	1.617	.639	38.99	1.514	.750	42.88
3.62	1.626	.630	38.66	1.567	.691	40.88
4.44	1.614	.636	38.89	1.555	.704	41.31
					Mean	41.97
					S.D.	1.03
Normal Stress = 55.09gm/sq.cm						
1.41	1.612	.644	39.16	1.522	.741	42.55
2.73	1.624	.631	38.72	1.562	.696	41.04
3.59	1.612	.644	39.17	1.578	.723	41.97
4.28	1.618	.637	38.92	1.523	.740	42.52
					Mean	42.02
					S.D.	.71
Normal Stress = 76.86gm/sq.cm						
1.43	1.630	.625	38.47	1.527	.736	42.39
2.22	1.617	.639	38.97	1.540	.721	41.89
3.36	1.606	.650	39.41	1.524	.739	42.50
4.83	1.607	.649	39.36	1.525	.737	42.45
					Mean	42.31
					S.D.	.28
				Overall Mean		42.10

TABLE T.5.

Split Ring Annular Shear Cell Results

Density Measurements from Weight and Dilatancy Measurements

Sand Size - 36-52 B.S.S. Mesh

12 Identical Runs
(normal stress and shear rate constant)

	Before Shear			After Shear		
Shear Rate (rad/min)	Bulk Density	Void Ratio	Porosity %	Bulk Density	Void Ratio	Porosity %
Normal Stress = 55.09gm/sq.cm						
2.75	1.673	.584	36.88	1.552	.707	41.42
2.75	1.637	.619	38.23	1.575	.683	40.58
2.75	1.630	.625	38.48	1.501	.765	43.34
2.75	1.621	.634	38.82	1.521	.742	42.59
2.75	1.668	.588	37.05	1.585	.672	40.18
2.75	1.652	.604	37.64	1.570	.687	40.74
2.75	1.623	.632	38.74	1.509	.756	43.05
2.75	1.643	.613	37.99	1.541	.720	41.85
2.75	1.629	.626	38.52	1.533	.728	42.14
2.75	1.579	.677	40.39	1.478	.793	44.24
2.75	1.618	.654	39.56	1.470	.802	44.52
2.75	1.615	.641	39.05	1.525	.737	42.44
					Mean	42.26
					S.D.	1.40

TABLE T.6.

Comparison of Critical Porosity Values Calculated as a Function of the Radius A and as an Average at the Radial Position B

Sand Size = 36-52 B.S.S. Mesh

Normal Stress = 55.09 gm/sq.cm.

Shear Rate = 4.19 rad/min.

Order of Scan	Radius of Scan. cm.	Bulk Density	Void Ratio	Critical Porosity
A - As a function of the radius				
1	9.4	1.465	.809	44.72
2	8.4	1.452	.825	45.20
3	7.4	1.462	.812	44.81
4	6.4	1.452	.825	45.21
5	5.4	1.444	.836	45.51
6	4.4	1.451	.826	45.25
7	3.4	1.474	.798	44.36
				Mean = 45.08
				S.D. = .195
B - As an average at radial position				
1	9.4	1.465	.809	44.72
2	8.4	1.466	.820	45.05
3	7.4	1.460	.815	44.88
4	6.4	1.456	.820	45.05
5	5.4	1.452	.825	45.19
6	4.4	1.453	.824	45.16
7	3.4	1.460	.815	44.91
				Mean = 49.94
				S.D. = .03

TABLE T.7.

Split Ring Annular Shear Cell Results

Gamma Attenuation Density Measurements Before and After Shear

Sand Size - 14-18 B.S.S. Mesh

	Before Shear			After Shear		
Shear Rate (rad/min)	Bulk Density	Void Ratio	Porosity %	Bulk Density	Void Ratio	Porosity %
Normal Stress = 33.33gm/sq.cm						
1.37	1.532	.730	42.20	1.374	.929	48.16
2.33	1.569	.689	40.80	1.386	.912	47.69
3.93	1.549	.710	41.54	1.373	.930	48.19
4.48	1.554	.705	41.34	1.369	.935	48.32
					Mean	48.09
					S.D.	.27
Normal Stress = 55.09gm/sq.cm						
1.57	1.588	.669	40.08	1.451	.827	45.26
2.81	1.563	.696	41.03	1.391	.905	47.50
3.97	1.553	.706	41.39	1.376	.925	48.04
4.44	1.556	.703	41.26	1.344	.970	49.26
					Mean	47.51
					S.D.	.53
Normal Stress = 76.86gm/sq.cm						
1.27	1.604	.652	39.46	1.391	.905	47.50
2.28	1.607	.649	39.34	1.382	.917	47.83
3.31	1.577	.680	40.49	1.426	.863	46.17
5.10	1.599	.660	39.66	1.393	.901	47.41
					Mean	47.22
					S.D.	.73
				Overall Mean		47.61

TABLE T.8.

Split Ring Annular Shear Cell Results

Gamma Attenuation Density Measurements Before and After Shear

Sand Size - 36-52 B.S.S. Mesh

	Before Shear			After Shear		
Shear Rate (rad/min)	Bulk Density	Void Ratio	Porosity %	Bulk Density	Void Ratio	Porosity %
Normal Stress = 33.33gm/sq.cm						
1.56	1.610	.646	39.25	1.440	.837	45.57
2.76	1.594	.663	39.86	1.450	.827	45.28
3.97	1.600	.656	39.62	1.459	.816	44.93
4.28	1.615	.641	39.06	1.427	.856	46.13
					Mean	45.47
					S.D.	.51
Normal Stress = 55.09gm/sq.cm						
1.58	1.589	.668	40.04	1.474	.798	44.36
2.90	1.616	.639	39.00	1.430	.854	46.05
4.05	1.613	.643	39.16	1.44	.835	45.53
4.19	1.603	.653	39.51	1.456	.820	45.04
					Mean	45.24
					S.D.	.69
Normal Stress = 76.86gm/sq.cm						
1.32	1.544	.663	39.86	1.468	.805	44.58
2.00	1.599	.657	39.64	1.490	.778	43.77
3.34	1.605	.651	39.42	1.471	.802	44.49
4.71	1.594	.663	39.85	1.442	.838	45.58
					Mean	44.60
					S.D.	.74
				Overall Mean		45.10

TABLE T.9.

Split Ring Annular Shear Cell Results

Gamma Attenuation Density Measurements Before and After Shear

Sand Size - 60-85 B.S.S. Mesh

	Before Shear			After Shear		
Shear Rate (rad/min)	Bulk Density	Void Ratio	Porosity %	Bulk Density	Void Ratio	Porosity %
Normal Stress = 33.33gm/sq.cm						
1.46	1.597	.659	39.73	1.424	.860	46.24
2.83	1.616	.640	39.01	1.430	.853	46.03
3.62	1.584	.673	40.22	1.434	.849	45.89
4.44	1.611	.645	39.20	1.442	.838	45.59
					Mean	45.94
					S.D.	.27
Normal Stress = 55.09gm/sq.cm						
1.41	1.592	.665	39.93	1.450	.828	45.30
2.73	1.597	.659	39.71	1.436	.846	45.81
3.59	1.596	.660	39.78	1.433	.850	45.94
4.28	1.603	.653	39.49	1.431	.852	46.00
					Mean	45.76
					S.D.	.32
Normal Stress = 76.86gm/sq.cm						
1.43	1.620	.635	38.85	1.436	.845	45.80
2.22	1.610	.646	39.24	1.446	.833	45.44
3.36	1.578	.679	40.43	1.463	.811	44.78
4.83	1.587	.669	40.10	1.443	.836	45.53
					Mean	45.39
					S.D.	.43
				Overall Mean		45.69

TABLE T.10.

Split Ring Annular Shear Cell Results

Gamma Attenuation Density Measurements Before and After Shear

Sand Size - 36-52 B.S.S. Mesh

12 Identical Runs
(normal stress and shear rate constant)

	Before Shear			After Shear		
Shear Rate (rad/min)	Bulk Density	Void Ratio	Porosity %	Bulk Density	Void Ratio	Porosity %
Normal Stress = 55.09gm/sq.cm						
2.75	1.681	.576	36.55	1.455	.820	45.07
2.75	1.621	.634	38.78	1.471	.801	44.47
2.75	1.659	.597	37.38	1.458	.818	44.99
2.75	1.638	.618	38.19	1.464	.809	44.73
2.75	1.656	.600	37.49	1.454	.822	45.12
2.75	1.659	.597	37.39	1.453	.823	45.16
2.75	1.631	.625	38.47	1.458	.817	44.98
2.75	1.643	.612	37.98	1.457	.818	45.02
2.75	1.623	.633	38.75	1.450	.828	45.30
2.75	1.600	.657	39.63	1.455	.821	45.10
2.75	1.611	.644	39.20	1.455	.821	45.10
2.75	1.632	.624	38.42	1.473	.800	44.42
					Mean	44.97
					S.D.	.27

TABLE T.11.

Split Ring Annular Shear Cell Results

Depth of the Region of Shear at Critical State

Sand Size = 14-18 B.S.S. Mesh

Shear Rate (rad/min)	Depth of Region of Shear (cm) Dyed Tracer	Critical Porosity and Dilation	Vertical γ Plot
Normal Stress = 33.33gm/sq.cm			
1.37	1.06	0.57	0.95
2.33	1.06	0.54	0.90
3.93	1.06	0.53	0.85
4.49	1.06	0.50	0.85
	Mean 1.06	0.53	0.89
	HN*10.4	5.2	8.8
Normal Stress = 55.09gm/sq.cm			
1.57	1.38	0.87	0.90
2.81	1.36	0.57	0.95
3.99	1.23	0.69	0.90
4.44	1.06	0.46	0.95
	Mean 1.26	0.65	0.92
	HN 12.4	6.4	9.1
Normal Stress = 76.86gm/sq.cm			
1.26	1.24	0.70	1.00
2.28	1.17	0.52	1.05
3.31	1.24	0.90	1.00
5.10	1.23	0.58	1.00
	Mean 1.22	0.67	1.01
	HN 12.0	6.6	10.0
Overall Mean	1.18	0.61	0.94
	HN 11.6	6.0	9.2

* HN = number of particle layers given by equation (14).

TABLE T.12.

Split Ring Annular Shear Cell Results

Depth of the Region of Shear at Critical State

Sand Size = 36-52 B.S.S. Mesh

Shear Rate (rad/min)	Depth of Region of Shear (cm) Dyed Tracer	Critical Porosity and Dilation	Vertical γ Plot
Normal Stress = 33.33gm/sq.cm			
1.56	0.64	0.40	0.62
2.76	0.64	0.44	0.65
3.97	0.73	0.37	0.60
4.28	0.77	0.58	0.60
	Mean 0.69	0.45	0.62
	HN 20.0	13.0	18.0
Normal Stress = 55.09gm/sq.cm			
1.58	0.66	0.59	0.60
2.90	0.73	0.23	0.65
4.05	0.62	0.20	0.67
4.19	0.74	0.46	0.65
	Mean 0.69	0.37	0.64
	HN 20.0	10.7	18.6
Normal Stress = 76.86gm/sq.cm			
1.32	0.69	0.52	0.67
2.00	0.74	0.57	0.65
3.34	0.75	0.43	0.65
4.71	0.75	0.54	0.62
	Mean 0.71	0.51	0.65
	HN 20.3	14.8	18.9
Overall Mean	0.69	0.44	0.64
	HN 20.0	12.7	18.6

TABLE T.13.

Split Ring Annular Shear Cell Results

Depth of the Region of Shear at Critical State

Sand Size = 60-85 B.S.S. Mesh

Shear Rate (rad/min)	Depth of Region of Shear (cm) Dyed Tracer	Critical Porosity and Dilation	Vertical γ Plot
Normal Stress = 33.33gm/sq.cm			
1.46	0.53	0.32	0.45
2.83	0.53	0.30	0.40
3.62	0.52	0.20	0.37
4.44	0.52	0.20	0.42
Mean	0.52	0.25	0.41
HN	29.5	14.2	23.3
Normal Stress = 55.09gm/sq.cm			
1.41	0.53	0.33	0.47
2.73	0.52	0.20	0.55
3.59	0.52	0.24	0.47
4.28	0.53	0.30	0.52
Mean	0.52	0.25	0.50
HN	29.5	14.2	28.5
Normal Stress = 76.86gm/sq.cm			
1.43	0.53	0.30	0.55
2.22	0.53	0.25	0.50
3.36	0.53	0.37	0.47
4.83	0.53	0.27	0.57
Mean	0.53	0.31	0.50
HN	30.0	17.6	28.5
Overall Mean	0.52	0.27	0.47
HN	29.5	15.7	26.7

TABLE T.14.

Split Ring Annular Shear Cell Results

Depth of the Region of Shear at Critical State

Sand Size = 36-52 B.S.S. Mesh

12 Identical Runs
(normal stress and shear rate constant)

Shear Rate (rad/min)	Depth of Region of Shear (cm) Dyed Tracer	Critical Porosity and Dilation	Vertical γ Plot
Normal Stress = 55.09gm/sq.cm			
2.75	0.72	0.34	0.65
2.75	0.71	0.29	0.70
2.75	0.76	0.50	0.70
2.75	0.72	0.42	0.70
2.75	0.68	0.28	0.65
2.75	0.68	0.28	0.75
2.75	0.70	0.46	0.75
2.75	0.66	0.36	0.75
2.75	0.64	0.35	0.70
2.75	0.75	0.53	0.75
2.75	0.76	0.64	0.70
2.75	0.74	0.42	0.65
Mean	0.71	0.40	0.70
S.D.	0.039	0.112	0.039
HN	20.7	11.6	20.4

TABLE T.15.

Split Ring Annular Shear Cell Results

Steady State Shear Stress Measurements

$$\tan \phi = \frac{\tau}{\sigma}$$

Shear Rate (rad/min)	Steady State Shear Stress					
	tan ϕ	ϕ^0	tan ϕ	ϕ^0	tan ϕ	ϕ^0
σ =	33.33gm/cm^2		55.09gm/cm^2		76.86gm/cm^2	
Sand Size = 14-18 B.S.S. Mesh						
1.33	.715	35.6	.724	35.9	.727	36.0
2.45	.715	35.6	.676	34.0	.683	34.3
3.70	.715	35.6	.712	35.4	.683	24.3
4.70	.747	36.7	.712	35.4	.692	24.7
Mean	.723		.706		.696	
S.D.	.042		.020		.082	
Sand Size = 36-52 B.S.S. Mesh						
1.50	.636	32.5	.483	25.8	.623	31.9
2.50	.795	38.5	.693	34.7	.657	33.3
3.60	.715	35.6	.676	34.0	.657	33.3
4.40	.790	38.5	.720	35.9	.623	31.9
Mean	.734		.643		.640	
S.D.	.074		.086		.019	
Sand Size = 60-85 B.S.S. Mesh						
1.43	.572	29.8	.627	32.1	.675	34.0
2.55	.508	27.0	.676	34.0	.675	34.0
3.55	.604	31.1	.579	30.1	.692	34.7
4.50	.620	31.8	.531	28.0	.666	33.6
Mean	.576		.603		.677	
S.D.	.049		.062		.010	

TABLE T.16

Split Ring Annular Shear Cell Results

Steady State Shear Stress Measurements

$$\tan \phi = \frac{\tau}{\sigma}$$

Sand Size = 36-52 B.S.S. Mesh

12 Identical Runs
(normal stress and shear rate constant)

Shear Rate (rad/min)	tan ϕ	ϕ^0
Normal Stress = 55.09gm/sq.cm		
2.75	.531	28.0
2.75	.555	29.0
2.75	.603	31.1
2.75	.531	28.0
2.75	.555	29.0
2.75	.579	30.1
2.75	.531	28.0
2.75	.579	30.1
2.75	.579	30.1
2.75	.639	33.0
2.75	.579	30.1
2.75	.627	32.1
Mean	.574	
S.D.	.036	

TABLE T.17

Jenike Shear Cell Results - A

Stress/Dilatancy Measurements at Different Initial Porosities

Sand Size = 14-18 B.S.S. Mesh

$^*\varepsilon_i$	τ_m	$\frac{\tau_m}{\sigma_n}$	h	Δ	$\left(\frac{\delta V}{\delta \Delta}\right)_{max}$	$\frac{\tau_r}{\sigma_n}$	$\frac{1}{1-\varepsilon_i}$
Normal Stress = σ_n = 46.2-46.4 gm/cm^2							
43.61	38.8	0.84	0.38	4.54	0.15	0.69	1.773
42.68	40.3	0.87	0.55	4.83	0.15	0.72	1.744
42.27	41.0	0.89	0.83	4.96	0.23	0.66	1.732
42.14	41.5	0.90	0.75	4.60	0.20	0.70	1.728
41.59	42.2	0.91	0.88	5.01	0.25	0.66	1.712
41.46	43.4	0.94	0.86	4.65	0.24	0.70	1.708
41.31	42.8	0.92	0.85	3.89	0.27	0.65	1.704
41.17	42.3	0.91	0.96	4.87	0.25	0.66	1.700
41.16	46.8	1.01	0.99	4.99	0.26	0.75	1.700
40.82	48.4	1.04	1.03	4.81	0.29	0.75	1.689
40.78	45.9	0.99	0.99	4.45	0.29	0.70	1.689
40.77	47.7	1.03	1.10	4.79	0.30	0.73	1.688
40.68	44.6	0.96	0.92	4.24	0.28	0.69	1.686
40.49	45.0	0.97	1.10	4.96	0.32	0.65	1.680
40.01	46.5	1.00	1.07	4.46	0.29	0.71	1.667
39.81	46.5	1.00	1.14	4.70	0.32	0.68	1.661
39.57	41.2	0.89	1.01	4.73	0.27	0.62	1.655
39.50	46.5	1.00	1.12	4.76	0.33	0.67	1.653
39.08	47.1	1.02	1.14	4.91	0.32	0.70	1.641

$^*\varepsilon_i$ = initial porosity (%)

τ_m = peak shear stress (gm/cm^2)

h = dilation (mm)

Δ = total horiz'l strain(mm)

$\left(\frac{\delta V}{\delta \Delta}\right)_{max}$ = dilation/strain at τ_n

$$\frac{\tau_r}{\sigma_n} = \frac{\tau_m}{\sigma_n} - \left(\frac{\delta V}{\delta \Delta}\right)_{max}$$

TABLE T.18

Jenike Shear Cell Results - A

Stress/Dilatancy Measurements at Different Initial Porosities

Sand Size = 14-18 B.S.S. Mesh

ε_i	τ_m	$\frac{\tau_m}{\sigma_n}$	h	Δ	$\frac{\delta V}{\delta \Delta_{max}}$	$\frac{\tau_r}{\sigma_n}$	$\frac{1}{1-\varepsilon_i}$
Normal Stress = σ_n = 87.9-88.1 gm/cm^2							
43.18	71.3	0.81	0.44	4.44	0.15	0.66	1.760
42.25	68.2	0.78	0.57	4.71	0.16	0.62	1.732
42.12	74.4	0.85	0.85	4.83	0.20	0.64	1.728
41.50	64.3	0.73	0.66	4.87	0.18	0.55	1.709
41.45	65.1	0.74	0.53	5.36	0.13	0.61	1.708
41.35	72.9	0.83	0.66	4.68	0.19	0.63	1.705
40.58	77.5	0.88	0.79	4.54	0.24	0.64	1.683
40.38	85.3	0.97	0.99	4.54	0.30	0.67	1.677
40.22	75.2	0.85	0.92	4.72	0.27	0.58	1.673
40.15	79.2	0.90	0.85	4.48	0.27	0.63	1.671
40.01	77.5	0.88	0.90	4.91	0.25	0.63	1.667
39.95	71.3	0.81	0.75	4.28	0.25	0.56	1.665
39.94	74.4	0.85	0.86	4.62	0.27	0.58	1.665
39.83	83.7	0.95	0.99	4.67	0.28	0.67	1.662
39.83	77.5	0.88	0.99	4.62	0.28	0.60	1.662
39.49	87.6	0.99	1.05	4.65	0.34	0.66	1.653
39.36	80.6	0.92	1.07	4.93	0.32	0.60	1.649
39.24	82.2	0.93	1.10	4.75	0.33	0.60	1.646
38.58	83.7	0.95	1.07	4.87	0.30	0.65	1.628

TABLE T.19

Jenike Shear Cell Results - A

Stress/Dilatancy Measurements at Different Initial Porosities

Sand Size = 14-18 B.S.S. Mesh

ε_i	τ_m	$\frac{\tau_m}{\sigma_n}$	h	Δ	$\frac{\delta V}{\delta \Delta}_{max}$	$\frac{\tau_r}{\sigma_n}$	$\frac{1}{1-\varepsilon_i}$
Normal Stress = σ_n = 171.2-171.4 gm/cm^2							
43.20	123.5	0.72	0.40	4.43	0.12	0.60	1.760
42.94	122.5	0.72	0.29	4.48	0.11	0.61	1.752
42.65	130.2	0.76	0.55	4.41	0.18	0.58	1.743
42.64	141.1	0.82	0.65	4170	0.19	0.64	1.743
42.53	129.4	0.76	0.51	4.74	0.15	0.60	1.740
42.37	127.1	0.74	0.46	4.07	0.14	0.61	1.735
42.17	136.4	0.80	0.62	4.85	0.19	0.61	1.729
41.75	127.9	0.75	0.63	4.52	0.17	0.58	1.717
41.41	139.5	0.81	0.74	4.79	0.19	0.62	1.707
41.41	131.8	0.77	0.64	4.76	0.18	0.59	1.707
41.23	131.8	0.77	0.61	4.57	0.17	0.60	1.70
40.82	136.4	0.80	0.70	4.63	0.21	0.59	1.689
40.72	133.3	0.78	0.59	4.74	0.17	0.61	1.687
40.67	155.3	0.91	0.90	4.38	0.29	0.62	1.685
40.55	144.9	0.85	0.92	4.44	0.29	0.56	1.682
40.23	148.8	0.87	0.76	4.15	0.24	0.62	1.673
39.95	155.0	0.90	0.81	4.20	0.21	0.69	1.665
39.69	161.2	0.94	1.13	4.56	0.32	0.62	1.658
39.44	155.0	0.90	0.99	4.34	0.30	0.60	1.651

TABLE T.20

Jenike Shear Cell Results - A

Stress/Dilatancy Measurements at Different Initial Porosities

· Sand Size = 36-52 B.S.S. Mesh

ε_i	τ_m	$\frac{\tau_m}{\sigma_n}$	h	Δ	$\frac{\delta V}{\delta \Delta}_{max}$	$\frac{\tau_r}{\sigma_n}$	$\frac{1}{1-\varepsilon_i}$
Normal Stress = σ_n = 46.2-46.4 gm/cm^2							
44.17	27.3	0.59	0.00	4.43	0.00	0.59	1.791
42.31	40.3	0.87	0.39	4.86	0.12	0.75	1.733
42.24	33.5	0.72	0.24	4.95	0.07	0.66	1.731
41.63	33.5	0.72	0.39	5.20	0.12	0.60	1.713
41.60	34.1	0.74	0.40	4.88	0.12	0.62	1.712
41.34	34.1	0.74	0.35	4.88	0.14	0.59	1.705
40.63	37.2	0.80	0.46	4.91	0.16	0.65	1.684
40.49	36.6	0.79	0.40	4.97	0.14	0.65	1.680
39.82	35.3	0.76	0.42	4.75	0.23	0.53	1.661
39.80	38.4	0.83	0.55	4.58	0.24	0.59	1.661
39.75	39.1	0.84	0.62	4.76	0.28	0.56	1.651
39.63	37.2	0.80	0.59	4.51	0.29	0.52	1.656
39.57	39.7	0.86	0.54	4.52	0.30	0.56	1.655
39.34	36.0	0.78	0.51	4.82	0.19	0.58	1.649
38.64	37.2	0.80	0.58	5.07	0.26	0.54	1.629
38.58	40.3	0.87	0.61	4.87	0.28	0.59	1.628
38.41	40.9	0.88	0.78	4.73	0.26	0.62	1.623
38.35	40.3	0.87	0.46	4.73	0.21	0.66	1.622
38.20	42.2	0.91	0.61	4.56	0.21	0.69	1.618

TABLE T.21

Jenike Shear Cell Results - A

Stress/Dilatancy Measurements at Different Initial Porosities

Sand Size = 36÷52 B.S.S. Mesh

ε_i	τ_m	$\frac{\tau_m}{\sigma_n}$	h	Δ	$\frac{\delta V}{\delta \Delta}_{max}$	$\frac{\tau_r}{\sigma_n}$	$\frac{1}{1-\varepsilon_i}$
Normal Stress = σ_n = 87.9-88.1 gm/cm^2							
42.94	58.9	0.67	0.19	4.99	0.08	0.59	1.752
41.75	52.2	0.59	0.23	4.70	0.12	0.48	1.717
41.39	60.3	0.69	0.36	4.97	0.12	0.57	1.706
41.13	68.2	0.78	0.51	4.75	0.22	0.55	1.698
40.91	57.4	0.65	0.26	4.05	0.11	0.55	1.692
40.67	63.6	0.72	0.40	4.57	0.13	0.59	1.686
40.56	65.1	0.74	0.40	4.96	0.16	0.58	1.682
40.55	63.6	0.72	0.32	5.00	0.14	0.58	1.682
40.53	62.5	0.71	0.34	4.66	0.16	0.55	1.681
40.41	57.4	0.65	0.26	4.23	0.10	0.55	1.678
40.04	68.2	0.77	0.54	4.55	0.19	0.58	1.667
40.00	62.0	0.70	0.32	3.56	0.18	0.53	1.667
39.83	62.0	0.70	0.42	4.96	0.14	0.57	1.661
39.29	62.0	0.70	0.35	4.80	0.13	0.57	1.647
39.24	65.1	0.74	0.50	4.67	0.15	0.59	1.646
38.94	69.8	0.79	0.50	4.88	0.15	0.64	1.638
38.75	63.6	0.72	0.55	4.54	0.19	0.54	1.632
38.67	69.8	0.79	0.68	4.95	0.24	0.56	1.630
37.25	74.4	0.84	0.61	4.52	0.21	0.64	1.593

TABLE T.22

Jenike Shear Cell Results - A

Stress/Dilatancy Measurements at Different Initial Porosities

Sand Size = 36-52 B.S.S. Mesh

ε_i	τ_m	$\frac{\tau_m}{\sigma_n}$	h	Δ	$\frac{\delta V}{\delta \Delta}_{max}$	$\frac{\tau_r}{\sigma_n}$	$\frac{1}{1-\varepsilon_i}$
Normal Stress = σ_n = 171.2-171.4 gm/cm^2							
42.12	122.5	0.72	0.39	4.86	0.13	0.58	1.727
41.24	126.3	0.74	0.39	4.78	0.18	0.56	1.702
41.21	118.6	0.69	0.47	4.39	0.19	0.51	1.700
40.68	122.5	0.71	0.53	4.62	0.17	0.54	1.686
40.38	125.6	0.73	0.59	4.64	0.20	0.53	1.677
40.31	138.0	0.81	0.53	4.54	0.22	0.58	1.675
40.25	125.6	0.73	0.53	4.86	0.20	0.53	1.674
40.07	114.7	0.67	0.49	4.65	0.21	0.45	1.668
40.05	134.1	0.78	0.55	4.94	0.20	0.58	1.668
40.03	134.1	0.78	0.66	4.67	0.22	0.56	1.667
39.97	134.1	0.78	0.61	4.60	0.21	0.58	1.666
39.86	132.5	0.77	0.50	4.45	0.21	0.56	1.662
39.65	130.2	0.76	0.62	4.79	0.21	0.55	1.657
39.10	133.3	0.78	0.56	4.80	0.23	0.55	1.642
38.78	136.4	0.80	0.60	4.74	0.27	0.53	1.633
38.74	136.4	0.80	0.67	4.94	0.27	0.53	1.632
38.74	133.3	0.78	0.67	4.79	0.21	0.56	1.632
38.54	139.5	0.81	0.71	4.95	0.24	0.57	1.627
37.25	143.4	0.84	0.80	4.64	0.29	0.54	1.593
37.25	143.4	0.84	0.80	4.64	0.29	0.54	1.593

TABLE T.23

Jenike Shear Cell Results - A

Stress/Dilatancy Measurements at Different Initial Porosities

Sand Size = 60-85 B.S.S. Mesh

ε_i	τ_m	$\frac{\tau_m}{\sigma_n}$	h	Δ	$\frac{\delta V}{\delta \Delta}_{max}$	$\frac{\tau_r}{\sigma_n}$	$\frac{1}{1-\varepsilon_i}$
Normal Stress = σ_n = 46.2-46.4 gm/cm^2							
42.29	34.1	0.74	0.25	5.01	0.11	0.63	1.733
42.30	37.2	0.80	0.26	4.70	0.11	0.70	1.733
41.13	36.6	0.79	0.27	4.42	0.12	0.67	1.698
40.91	39.7	0.86	0.31	4.84	0.19	0.67	1.692
40.87	38.1	0.82	0.34	4.95	0.16	0.67	1.691
40.25	40.3	0.87	0.35	4.71	0.20	0.67	1.673
40.18	42.2	0.91	0.59	4.75	0.24	0.67	1.672
40.08	39.7	0.86	0.41	4.34	0.19	0.67	1.669
39.96	43.4	0.94	0.41	4.90	0.24	0.70	1.665
39.82	42.8	0.92	0.48	4.50	0.24	0.68	1.662
39.27	38.4	0.83	0.52	4.59	0.29	0.54	1.647
39.02	41.9	0.90	0.49	4.63	0.29	0.62	1.640
39.00	40.9	0.88	0.50	4.73	0.23	0.65	1.639
39.00	43.1	0.93	0.53	4.69	0.28	0.65	1.639
38.64	43.7	0.94	0.74	5.01	0.31	0.63	1.629
38.33	42.2	0.91	0.57	4.91	0.24	0.67	1.621
37.95	44.3	0.95	0.71	4.87	0.32	0.63	1.611
37.85	49.3	1.06	0.66	4.84	0.35	0.71	1.609
37.72	46.5	1.00	0.70	4.82	0.29	0.71	1.606

TABLE T.24

Jenike Shear Cell Results - A

Stress/Dilatancy Measurements at Different Initial Porosities

Sand Size = 60-85 B.S.S. Mesh

ε_i	τ_m	$\frac{\tau_m}{\sigma_n}$	h	Δ	$\frac{\delta V}{\delta \Delta}_{max}$	$\frac{\tau_r}{\sigma_n}$	$\frac{1}{1-\varepsilon_i}$
Normal Stress = σ_n = 87.9-88.1 gm/cm^2							
42.76	55.8	0.63	0.27	4.74	0.08	0.56	1.747
41.53	63.6	0.72	0.44	4.55	0.16	0.56	1.710
41.31	62.8	0.71	0.45	4.57	0.18	0.54	1.704
40.94	65.1	0.74	0.38	4.88	0.17	0.57	1.693
40.82	72.9	0.83	0.55	4.26	0.19	0.64	1.690
40.77	68.2	0.78	0.50	4.34	0.19	0.59	1.688
40.01	72.1	0.82	0.64	4.47	0.24	0.58	1.667
39.95	65.1	0.74	0.55	4.04	0.24	0.50	1.665
39.89	72.1	0.82	0.60	4.87	0.24	0.57	1.663
39.80	76.0	0.86	0.52	4.61	0.19	0.67	1.661
39.73	69.0	0.78	0.57	4.77	0.20	0.58	1.659
39.71	71.3	0.81	0.58	5.00	0.26	0.55	1.658
39.26	72.9	0.83	0.68	4.76	0.27	0.56	1.646
38.91	69.8	0.79	0.64	4.64	0.24	0.56	1.637
39.00	76.0	0.86	0.69	4.58	0.25	0.61	1.639
38.62	83.7	0.95	0.74	4.85	0.28	0.67	1.629
38.56	75.2	0.85	0.63	4.67	0.24	0.62	1.627
37.50	83.7	0.95	0.80	4.69	0.29	0.65	1.600

TABLE T.25

Jenike Shear Cell Results - A

Stress/Dilatancy Measurements at Different Initial Porosities

Sand Size = 60-85 B.S.S. Mesh

ε_i	τ_m	$\frac{\tau_m}{\sigma_n}$	h	Δ	$\frac{\delta V}{\delta \Delta}_{max}$	$\frac{\tau_r}{\sigma_n}$	$\frac{1}{1-\varepsilon_i}$
Normal Stress = σ_n = 171.2-171.4 gm/cm^2							
40.45	116.3	0.68	0.41	4.66	0.13	0.55	1.679
40.33	116.3	0.68	0.28	4.75	0.10	0.58	1.656
40.23	114.7	0.67	0.38	4.56	0.16	0.51	1.673
40.18	104.6	0.61	0.28	4.72	0.10	0.51	1.671
40.04	110.1	0.64	0.42	4.61	0.15	0.49	1.668
39.92	116.3	0.68	0.40	4.58	0.12	0.56	1.664
39.86	136.4	0.80	0.35	4.59	0.17	0.63	1.663
39.84	120.9	0.71	0.51	4.46	0.13	0.58	1.662
39.62	110.8	0.65	0.37	4.43	0.12	0.53	1.657
39.44	117.0	0.68	0.43	4.52	0.14	0.54	1.651
39.17	124.0	0.72	0.51	4.94	0.19	0.54	1.644
39.08	120.1	0.70	0.52	4.13	0.19	0.51	1.641
38.60	124.0	0.72	0.58	4.94	0.24	0.48	1.628
38.28	138.7	0.81	0.60	4.98	0.23	0.58	1.620
37.99	124.0	0.72	0.62	4.41	0.24	0.49	1.612
37.99	127.1	0.74	0.57	4.72	0.19	0.55	1.612
37.67	132.5	0.77	0.63	4.78	0.22	0.55	1.604
37.57	138.0	0.80	0.73	4.50	0.26	0.55	1.600

TABLE T.26

Jenike Shear Cell Results - B

Stress/Dilatancy Measurements at Different Initial Porosities

Sand Size = 36-52 B.S.S. Mesh

Porosity(ε_i) %	Peak Stress (gm/cm^2)	Peak Angle of Friction ($\frac{\tau}{\sigma}$)	Dilation (mm)	$\frac{1}{(1-\varepsilon_i)}$
Normal Stress = 46.3→46.5 gm/cm^2				
35.0	48.8	1.051	0.85	1.538
35.3	42.8	0.923	0.61	1.546
36.0	43.1	0.926	0.66	1.562
36.4	45.0	0.968	0.61	1.572
36.4	44.3	0.955	0.58	1.572
36.5	39.7	0.856	0.58	1.575
37.1	43.1	0.929	0.45	1.590
37.4	38.1	0.824	0.55	1.597
37.7	43.8	0.942	0.55	1.605
38.0	40.4	0.874	0.46	1.613
38.8	34.8	0.752	0.39	1.634
39.5	35.2	0.758	0.41	1.653
39.5	33.4	0.721	0.37	1.653
39.6	34.0	0.735	0.43	1.656
39.8	35.0	0.755	0.37	1.661
40.0	32.6	0.705	0.34	1.667
40.7	34.7	0.748	0.34	1.686
40.8	31.7	0.684	0.27	1.689
41.0	33.3	0.719	0.27	1.695

TABLE T.27

Jenike Shear Cell Results

Stress/Dilatancy Measurements at Different Initial Porosities

Sand Size = 36-52 B.S.S. Mesh

Porosity(ε_i) %	Peak Stress (gm/cm^2)	Peak Angle of Friction ($\frac{\tau}{\sigma}$)	Dilation (mm)	$\frac{1}{(1-\varepsilon_i)}$
Normal Stress = 46.3-46.5 gm/cm^2				
41.2	33.5	0.723	0.23	1.701
41.7	30.5	0.661	0.06	1.715
41.8	29.9	0.647	0.00	1.718
41.0	31.4	0.677	0.12	1.695
41.0	31.9	0.690	0.15	1.695
Normal Stress = 88.0-88.2 gm/cm^2				
36.6	84.3	0.956	0.64	1.577
37.6	67.5	0.766	0.56	1.603
38.2	74.7	0.848	0.60	1.618
38.3	80.5	0.914	0.44	1.621
38.6	67.0	0.761	0.48	1.629
40.9	77.2	0.876	0.23	1.692
Normal Stress = 143.5-143.7 gm/cm^2				
36.4	119.5	0.835	0.71	1.572
37.4	114.3	0.796	0.66	1.597
38.5	105.0	0.715	0.52	1.626
41.5	91.0	0.635	0.17	1.709

NOMENCLATURE

The following are the principal symbols used; all the symbols used are explained in the text.

C - cohesion

CVR - critical voids ratio

CP - critical porosity

e - voids ratio

f_c - unconfined yield stress

h - dilation

H - depth of region of shear at critical state

M - slope of critical state line in σ, τ plane

N - number of particles cut by a line of unit length

T - tensile stress

x - length of chord (filament)

f(x) - number distribution of chords (filaments) of length x

y - length of sectioned filament

g(y) - number distribution of sectioned filaments of length y

x_{max} - maximum chord (filament) length

y_m - median sectioned filament

y_{sep} - separation for anisotropic case

α - geometrical angle of packing (Rowe)

δ - effective angle of friction

$\dot{\varepsilon}$ - rate of change of strain

ε_c - critical porosity

ε_i - initial porosity

μ - mass absorption coefficient

ρ - bulk density

σ, σ' - normal stress

τ - shear stress

τ_m - peak shear stress

ϕ - angle of friction

ϕ_{crit} - angle of friction at critical state

ϕ_f - angle of internal friction

ϕ_r - residual angle of friction

ϕ_μ - angle of sliding friction

Ω - volume fraction of component (appendix A.1.)

η - area fraction " " "

ψ - length fraction " " "

BIBLIOGRAPHY

1. ALLEN, P: "Automated Particle Size Analysis Using a Digital Computer". Symp. Recent Advances in Powders, I.Chem.E., 1969.

2. ALLEN, T. "Particle Size Measurement", Powder Technology Series. Chapman & Hall, Ltd., London, 1968.

3. AMONTONS."De la resistance causée dans les machines".Academie Royale des Sciences, Paris. Histoire avec les Memoires de Mathematique et de Physique. 206-227, 1699.

4. ARTHUR, J.R.F. "Strains and Lateral Force in Sand". Ph.D. Thesis, Cambridge Univ., 1962.

5. A.S.C.E. "Progress report of the special committee to codify present practise on the bearing value of soils for foundations". Proc.A.S.C.E., Aug., 1174, 1917.

6. ASHTON, M.D.,FARLEY, R.,VALENTIN,F.H.H. "An improved apparatus for the measuring of the tensile strength of powders". J.Sci.Inst., 41, 763-765, 1964.

7. ASHTON, M.D.,FARLEY, R.,CHENG, D.C-H.,VALENTIN, F.H.H. "Some investigations into the strength and flow properties of powders" Rheol.Acta., 4, 206, 1965.

8. BACH, G. "Size distribution of particles derived from the size distribution of their sections". Proc.2nd.Int.Cong. Stereology, Chicago. 174-186, 1967.

9. BELCHER, D.J.,CUYKENDALL, T.R.,SACK, H.S. "The measurement of soil moisture and density by neutron and gamma ray scattering". C.A.A.Tech.Rept., 127, Oct., 1950.

10. BENARIE, M.M. "Rheology of granular material II - A method for the determination of the intergranular cohesion". Brit.J.Appl.Phys., 12, 514-518, 1961.

11. BERNHARD, R.K.,CHASEK, M. "Soil determination by means of radioactive isotopes". Non-destruct.Test., 11, (8), 1953.

12. BISHOP, A.W. "Correspondence on shear characteristics of a saturated silt measured in triaxial compression". Geotechnique, 4, 43-45, 1954.

13. BISHOP, A.W. "A large shear box for testing sands and gravels". Proc.2nd.Int.Conf.S.M.&F.E., 1, 207-211, 1948.

14. BISHOP, A.W.,HENKEL, D.J. "The measurement of soil properties in the triaxial test". Arnold, London. (2nd.ed. 1962).

15. BJERRUM, L.,KRINGSTAD, S.,KUMMENEJE, O. "The shear strength of a fine sand". Proc.5th.Int.Conf.S.M.&F.E., 29-37, 1961.

16. BLUM, F.H.,WILHELM, R.H. "A statistical geometric approach to random packed beds". A.I.Ch.E.&Chem.E.Symp.Series, Symp. on the application of mathematical models in chemical engineering., 20-25, 1966.

17. BO,M.K. "Fundamentals of flow through packed beds". Ph.D. Thesis, Loughborough Univ. of Tech., 1968.

18. BOWDEN,F.P., TABOR,D. "The friction and lubrication of solids". Oxford Univ. Press, London, 1950.

19. BROWN,R.L. "Powders in industry". S.C.I.Monograph, 14, 150-164, 1961.

20. BURMISTER,D.M. "The importance and practical use of relative density in soil mechanics". Proc.A.S.T.M., 48, 1249-1268, 1948.

21. BURMISTER,D.M. "Investigations on the shearing resistance of cohesionless and cohesive materials". Proc.A.S.T.M., Symp. on shear testing of soils, 39, 1071-1083, 1932.

22. CAQUOT,A., KERISEL,J. "Traite de mecanique des sols". 3rd.ed. Gauthier-Villiers, Paris, 1956.

23. CARR,J.F. WALKER,D.M. "An annular shear cell for granular materials". 5th. West Reg. C.E.G.B. Report SSD/SU/N 157, Dec., 1967.

24. CASAGRANDE,A. "Characteristics of cohesionless soils affecting the stability of slopes and earth fills". J.Boston Soc. Civil Engs. 23, (1), 13-32, 1936.

25. CHALKLEY,H.W. "Method for quantitative morphologic analysis of tissues". J.nat.Cancer Inst., 4, 47, 1943.

26. CHALKLEY,H.W., CORNFIELD,J., PARK,H. "A method for estimating volume surface ratios". Science, 110, 295, 1949.

27. CHEN,L.S. "An investigation of the stress-strain and strength characteristics of soils by triaxial compression". Proc. 2nd. Int. Conf. S.M.&F.E., 5, 35-48, 1948.

28. CHENG,D.C-H. "Some preliminary results on the measurement of powder properties under torsional tests". Warren Spring Internal Report LR 49(CE), May, 1967.

29. CHENG,D.C-H. "The tensile strength of powders". Chem.Eng.Sci., 23, 1405-1420, 1968.

30. CHENG,D.C-H., FARLEY,R., VALENTIN,F.H.H. "The effect of particle size and inter-particle forces on the flow properties of powders". Proc. Tripartite Chem. Eng. Conf., Montreal, 1968.

31. CHENG,D.C-H., VALENTIN,F.H.H. "Some fundamental aspects of powder behaviour". Chem.Eng.Sci., 23, 723-738, 1968.

32. CLAYTON,D. "An introduction to boundary and extreme pressure lubrication". Brit.J.Appl.Phys., Suppl. 1., 25-32,

33. COOLING,L.F., SMITH,D.B. "The shearing resistance of soils". Proc. Int. Conf. S.M.&F.E., 1, 37, 1936.

34. COULOMB,C.A. "Essai sur une application des regles des maximis et minimis à quelques problèms de statique relatifs à d'Architecture". Memoires de Mathematique et de Physique, Paris, 343-381, 1773.

35. COULOMB,C.A. "Theorie des machines simples en ayant égard au froitement de leurs parties et a la roideur des cordages". Academie Royale de Sciences, Paris. Mémoires de Mathematique et de Physique, 10, (2), 161-332, 1785.

36. COUMOULOS,D.G. "A radiographic study of soils". Ph.D. Thesis Cambridge Univ., 1967.

37. CUTTRESS,J.O., PULFER,R.F. "X-ray investigations of flowing powders". Powder Technology, 1, 213-220, 1968.

38. DANTU,P. "Etude mechanique d'un milieu pulverulent forme de spheres egales de compacite maximis". Proc. 5th. Int. Conf. S.M.&F.E., 1, 61-70, 1961.

39. DAWES,J.G. "Dispersion of dust deposits by blasts of air". Pt.1. Safety in Mines Research Establishment Research Rept., 36, May, 1952.

40. DEHOFF,R.T. "Sampling of material and statistical analysis in quantitative stereology". Proc. 2nd. Int. Cong. Stereology, 119-130, 1967.

41. DELESSE,M.A. "Procédé méchanique pour determiner la composition des roches". Compt. Rend. Acad. Sci., 25, 544-547, 1847.

42. DERESEIWICZ,M. "Mechanics of granular matter". Adv.Appl.Mechs. 5, 233-303, 1958.

43. ELIAS,H. Editor. Proc. 2nd. Int. Cong. Stereology, Chicago. Springer-Verlag. 1967.

44. EISNER,H., FOGG,G., TAYLOR,T.W. "Cohesion of powders and the effect of atmospheric moisture". Untergruppe B/111/1, 57, 3rd. Int. Cong. Surface Activity, Cologne, 2, Sect. B, 378-382, 1960.

45. EYRING,H., POWELL,R.E. "Rheological properties of simple and colloidal systems". Alexander's Colloid Chemistry, 5, 236-252, 1944.

46. FARLEY,R., VALENTIN,F.H.H. "Effect of particle size upon the strength of powders". Powder Technology, 1, 344-354, 1967/68.

47. FAROUKI,O.T., WINTERKORN,H.F. "Mechanical properties of granular systems". Highway Res. Record, No.52, 10-52, 1960.

48. FISCHMEISTER,H.F. "Automatic measuring and scanning devices in stereology". Proc. 2nd. Int. Cong. Stereology, Chicago. 263-274, 1967.

49. FISHER,C. "The metals research image analysing computer". Particle Size Analysis Conf., 1966.

50. FOWLER,R.T., CHODZIESNER,W.D. "Influence of variables upon the angle of friction of granular materials". Chem.Eng. Sci., 10, 157-162, 1959.

51. FRANZIUS, STRECK, HINDERKS. "The experiment institute for hydraulics and foundations at the Technical University at Hanover". Hydraulic Laboratory Practise, 599-601, A.S.M.E., 1929.

52. FRASER,H.J. "Experimental study of porosity and permeability of clastic sediments". J.Geol. 43, 910-1010, 1935.

53. FURNAS,C.C. "Grading aggregates. Mathematical relations for beds of broken solids of maximum density". Ind.Eng.Chem., 23, 1052-1058, 1931.

54. GARDNER,G.C. "Limiting conditions for flow of a cohesive granular material down an inclined plane (chute) or between parallel inclined walls". Chem.Eng.Sci., 17, 1079-1086, 1962.

55. GERSTAL,G. "Uber die moglichkeiten exakter bestimmung der relation zwischen gewebsbestandteilen".(Relatwe histometrie mit dem heitzschen integrationstisch). Kerh. dtsch.Ges.Path., 32, 140-142, 1950.

56. GIBSON,R.E., MORGENSTERN,N.R. "Stress-dilatancy, earth pressures and slopes", (by) Rowe,P.W. (discussion). Proc.A.S.C.E.,J.Soil Mechs.& Founds. Div., 89, SM.6, 127-129, 1963.

57. GLAGOLEFF,A.A. "On the geometrical methods of quantitative mineralogic analysis of rocks". Trans. Inst. Econ. Min. Moskau., 59, 1933.

58. GRATON,L.C., FRASER,H.J. "Systematic packing of spheres with particular relation to porosity and permeability". J.Geol., 43, 785-909, 1935.

59. GRODSTEIN,G.W. "X-ray attenuation coefficients from 10KeV to 100MeV". U.S. Dept. Commerce N.B.S. Circular 583, 1957.

60. GRUNER, HAEFLI. "Beitrag zur untersuchung des physikalischen und statischen verhattens koharenter boden". Schweizer Bauzeitung, 103, 171-174, 1934.

61. HANDLEY,M.F., PERRY,M.G. "Stresses in granular materials flowing in converging hopper sections". Powder Technology, 1, (5), 245-251, 1968.

62. HARLAND,D.G., URKAN,S.R. "Effect of soil type on the single probe gamma transmission method for measuring in-situ densities". Road Research Lab. Report, No.52, 1-21, 1966.

63. HAUG,H. "Die treffermethode ein verfahren zur quantitativen analyse im histologischen schnitt". Z.Anat.Entwickl.-Gesch., 118, 302-312, 1955.

64. HAUSNER,H.H. "Characterisation of powder particle shape". Particle Size Analysis Conf., 1966.

65. HAYTHORNTHWAITE,R.M. "Mechanics of the triaxial test for soils". Proc.A.S.C.E., J.Soil Mech.& Found. Eng. Div.,SM5, 35-62, Oct., 1960.

66. HENNES,R.G. "The strength of gravel in direct shear". A.S.T.M. Symp. on Direct Shear Testing of Soils, 1953.

67. HENNIG,A. "Bestimmung der oberfluche beliebig geformter korper mit besonderer anwendung auf korperhaufen im mikroskopischen berich". Mikroskopie, 11, 1-20, 1956.

68. HERDAN,G. "Small particle statistics". Elsevier Publ. Co., Amsterdam. 1953.

69. HERWOOD,C.F., PILPEL,N. "Measurement of flow properties of powders". Chem.& Process Eng., July, 92-96, 1968.

70. HEYWOOD,H. "The evaluation of powders". J.Pharm.Pharmacol., Suppl., 15, 56T, 1963.

71. HILLIARD,J.E. "Determination of structural anisotropy". Proc. 2nd. Int. Cong. Stereology, 219-227, 1967.

72. HOLMES,A.H. "Petrographic methods and calculations". Murby & Co., London. 1927.

73. HOLTZ,W.G. Discussion of "Effect of particle shape texture on the strength of non-cohesive aggregates", (by) H.C. Morris. A.S.T.M.Spec.Tech.Publn. 254, 363-364, 1959.

74. HOLTZ,W.G., GIBBS,H.J. "Triaxial shear test on pervious gravelly soils". Proc.A.S.C.E.,J.Soil Mech.& Found.Div., 82, SM1, 22, 1956.

75. HORN,H.M., DEERE,D.U. "Frictional characteristics of minerals". Geotechnique, 12, 319, 1962.

76. HORNE,M.R. "The behaviour of an assembly of rotund, rigid, cohesionless particles, 1". Proc. Royal Soc. London, Series A, 286, 62-78, 1965.

77. HORNE,M.R. "The behaviour of an assembly of rotund, rigid, cohesionless particles, 2". Proc. Royal Soc. London, Series A, 286, 79-97, 1965.

78. HOROJEFF,R., GOLDBERG,I. "Field measurements of soil moisture and density with radioactive materials". Proc. Highway Research Board, 32, 500-511, 1953.

79. HORSFIELD,H.T. "The strength of asphalt mixtures". J.Soc. Chem.Ind., 53, 107T-115T, 1934.

80. HOUGH,B.K. "An analysis of the effect of particle interlocking on the strength of cohesionless soil". A.S.T.M.Bull., No.176, 55-60, Sept, 1951.

81. HOUSEL,W.S. "Internal stability of granular materials". Proc.A.S.T.M., 36, II, 426-468, 1936.

82. HVORSLEV,M.J. "A ring shearing apparatus for the determination of the shearing resistance and plastic flow of soil". Proc. Int. Conf. S.M.& F.E., 2, 125, 1936.

83. HVORSLEV,M.J. "Uber die festigkeitseigenschaften gestorter bindiger boden." ("On the physical properties of disturbed cohesive soils"). Ingenioroidenskabelige Skriffer, A, No.45, 159, 1937.

84. HVORSLEV,M.J. "Torsion shear tests and their place in the determination of the shearing resistance of soils". Proc.A.S.T.M., 39, 999-1022, 1939.

85. HVORSLEV,M.J. "Torsion shear apparatus and testing procedures". Bull. No.38, Waterways Expt. Stn.,U.S.Army, May, 1952.

86. IDEL,K. "Die scherfestigkeit rolliger erdstoffe". Veroffent. des Inst. fur Bodenmechanick und Grundbau der T.H. Fridericiana in Karlsruhe, 2, 1960.

87. JENIKE,A.W. "Gravity flow of bulk solids". Bull. 108, Utah Eng.Expt.Station, Oct., 1961.

88. JENIKE,A.W. "Gravity flow of solids". I.Chem.E. Symp. on Handling of Solids, 30-37, 1962.

89. JENIKE,A.W. "Storage and flow of solids". Bull. 123, Univ. Utah Eng.Expt.Station, Nov., 1964.

90. JENIKE,A.W. "Quantitative design of mass-flow bins". Powder Technology, 1, 237-244, 1967.

91. JENIKE,A.W., ELSEY,P.J., WOOLEY,R.H. "Flow properties of bulk solids". Proc.A.S.T.M., 60, 1168-1190, 1960.

92. JENIKE,A.W., JOHANSON,J.R. "Bin loads". Proc.A.S.C.E., J. Structural Div., April, 1011-1041, 1968.

93. JENIKE,A.W., LESSER,T. "A flow-no-flow criterion in the gravity flow of powders in converging channels". Proc. 4th. Int. Cong. Rheology., Pt.3, 125-140, 1965.

94. JENIKE,A.W., SHIELD,R.T. "On the plastic flow of coulomb solids beyond original failure". J.Appl.Mech.,Paper No. 59-A-7, Dec., 1959.

95. KAYE,B.H. "Some aspects of efficiency of statistical methods of particle size analysis". Powder Technology, 2, 97-110, 1968/69.

96. KETCHUM,M.S. "The design of walls, bins and grain elevators". McGraw-Hill Book Co.Inc., New York, 1909.

97. KJELLMAN,W. "Testing the shear strength of clay in Sweden". Geotechnique, June, 225-235, 1951.

98. KIRKPATRICK,W.M. "Effects of grain size and grading on the shearing behaviour of granular materials". Proc. 6th. Int. Conf. S.M.& F.E., 1, Div.2, 2T-273-277, 1965.

99. KODOCIKOV,P.N., JURJEV,K.V. "K. opredeleniju plotnosti grunt prosvecivaniem gamma-lucami". Isvestija Akademii Nauk S.S.S.R., No.8, 1955.

100. KOLBUSZEWSKI,J.J. "An experimental study of the maximum and minimum porosities of sands". Proc. 2nd. Int. Conf. S.M.& F.E., 1, 158-165, 1948.

101. KOLBUSZEWSKI,J.J., FREDERICK,M.R. "The significance of particle shape and size on the mechanical behaviour of granular materials". European Conf. on Soil Mech. & Found. Eng. (Wiesbaden)., Sect.4, Paper 9, 1953.

102. KREY,H. "Erddruck. erdwiderstand und tragfahigkeit des baugrundes". Ernst, Berlin, 5th. ed., 1936.

103. KUNO,H., KURIHARA,K. "Rheological behaviour of a powder in a rotational viscometer". Rheologica Acta, 4, (1), 73-74, 1965.

104. LANE,D.A., TORCHINSKY,B., SPINKS,J.W.T. "Determining soil moisture and density by nuclear radiations". Eng.J., 1-7, 1953.

105. LANGER,C. "Propriétés mécaniques et physiques des terrains cohèrents". Laboratories du Batiment et des Travaux Publics, Paris, Compte Rendu des Recherches Effectuées durant l'Annee 1938, 19-27, 1938.

106. LAWRENCE,L.R., BEDDOW,J.K. "Some effects of vibration upon powder segregation during die filling". Powder Technol., 2, 125-130, 1968/69.

107. LEE,K.L. "Drained strength characteristics of sands". Proc. A.S.C.E., J.Soil Mech.& Found. Div., 93, SM6, 117-141, 1967.

108. LENZ,F. "Zur grobenverteilung von kugelschnitten". Z.wiss. Mikr., 63, 50-56, 1955.

109. LEWIS,W.A. "Nuclear apparatus for density and moisture measurements - study of factors affecting accuracy". Roads & Road Construction, 43, No.516, 37-43, 1965.

110. LLOYD,P.J., YEUNG,P.C.M. "Mixing of powders". Chem. & Proc. Eng., 48, (10), 57-61, 1967.

111. MACCURDY,E. "The notebook of Leonardo da Vinci". 1, Reynal & Hitchcock, New York, 1938.

112. MACKEY,R.D. "The shearing resistance of granular soils". Civil Eng. & Public Works Rev., Sept., 1085-1089, 1964.

113. MEIGH,A.C., SKIPP,B.O. "Gamma-ray and neutron methods of measuring soil density and moisture". Geotechnique, 10, 110-126, 1960.

114. MITCHELL,J.K. "Shearing resistance of soils as a rate process". Proc.A.S.C.E.,J.Soil Mech. & Found. Eng.,SM1, Jan., 29-61, 1964.

115. MOGAMI,T. "Statistical approach to mechanics of granular materials". Soil & Foundation, 5, No.2, 26-36, 1965.

116. MORRIS,H.C. "Effect of particle shape and texture on the strength of non-cohesive aggregates". A.S.T.M.Spec.Tech. Publ., 254, 350-363, 1959.

117. MYERS,E.J. "Size distribution of cubic particles". Proc.2nd. Int.Cong.Stereology, 187-188, 1967.

118. NASH,J.H., LEITER,G.G., JOHNSON,A.P., STENDER,D., ZELLER,H.W. Final Report - "Fundamental studies of the dispersibility of powdered materials". U.S.Defense Documentation Center, 1963.

119. NEWLAND,P.L., ALLELY,B.H. "Volume changes in drained triaxial tests on granular materials". Geotechnique, 7, 17-34, 1957.

120. NOVOSAD,J. "Studies on granular material, II, Apparatus for measuring the dynamic angle of internal and external friction of granular materials". Coll.Czech.Chem.Comms., 29, 2697-2701, 1964.

121. OKADA,J., ABE,T. "Measurement of the coefficient of friction and adhesion power of drug powders". Yakugaku Zasshi, 83, 39-44, 1963.

122. ORR,C., DALLAVALLE,J.M. "Fine Particle Measurement". MacMillan, New York, 1959.

123. OSTERMAN,J. "Influence of grain form on the behaviour of granular mass". Proc.Int.Conf.S.M.& F.E., 3, 67-70, 1961.

124. PARSONS,J.D. "Progress report on an investigation of the shearing resistance of cohesionless soils". Proc.Int. Conf.S.M.& F.E., Harvard, 2, 137, 1936.

125. PILPEL,N. "Cohesiveness of powders". Endeavour, 28, May, 73-76, 1969.

126. POKROVSKY,G.J. "The research on soil physics". Moscow, 1937.

127. PONTECORVO,B. "Neutron well logging". Oil & Gas J., 40, 32-33, 1941.

128. RALSTON,H.H., ANDAY,M.C. "Nuclear measurement of soil properties". Highway Res. Record., No.66, 15-33, 1965.

129. RENDULIC,L. "Der hydrodynamishe spannung sausgleich in zentral entwasserten tonzylindern". Wasserwirtsch.Tech. 2, 250-253, 269-273, 1935.

130. REYNOLDS,O. "On the dilatancy of media composed of rigid particles in contact". Phil.Mag., Ser.5, 20, 127, Dec., 1885.

131. RICHARDS,J.C. (Ed.) "The storage and recovery of particulate solids". I.Chem.E. Working Party Report, 1966.

132. RICHMOND,O. "Gravity hopper design". Mech.Eng., Jan.,46-49, 1963.

133. RICHMOND,O., GARDNER,G.C. "Limiting spans for arching of bulk materials in vertical channels". Chem.Eng.Sci., 17, 1071-1078, 1962.

134. ROSCOE,K.H. "An apparatus for the application of simple shear to soil samples". Proc.3rd.Int.Conf.S.M.& F.E., Zurich, 1, 186-191, 1953.

135. ROSCOE,K.H. "The critical state concept and the use of short wave length radiation to study the onset and maintenance of flow in granular materials". Proc.T.H.T.R. Symp. - Problems of the Pebble Bed and Granular Materials, Julich, Mar., 1968.

136. ROSCOE,K.H. "Some soil mechanics concepts and the possibility of their wider application". Bergbauwissenschaften, 14, (2), 464-472, 1967; 15, (1), 8-14, 1968, and Monograph, Cambridge Univ. Press, 81/1-27.

137. ROSCOE,K.H., ARTHUR,J.R.F., JAMES,R.G. "The determination of strains in soils by an X-ray method". Civil Eng. & Public Works Rev., July, 873-876, 1963; Aug., 1009-1012, 1963.

138. ROSCOE,K.H., POOROOSHASHB,H.B. "A theoretical and experimental study of strains in triaxial compression tests on normally consolidated clays". Geotechnique, 13, 12-38, 1963.

139. ROSCOE,K.H., SCHOFIELD,A.N. Discussion of "Stress-dilatancy, earth pressures and slopes". (by) Rowe,P.W., Proc. A.S.C.E.,J. Soil Mech. & Found Div., 90, SM1, 136-150, 1964.

140. ROSCOE,K.H., SCHOFIELD,A.N., WROTH,C.P. "On the yielding of soils". Geotechnique, 8, 22-52, 1958.

141. ROWE,P.W. Discussion closure of "Stress dilatancy, earth pressures and slopes". (by) Rowe,P.W. Proc.A.S.C.E., J. Soil Mech. & Found. Div., 90, SM4, 145-180, 1964.

142. ROWE,P.W. "The stress-dilatancy relation for static equilibrium of an assembly of particles in contact". Proc. Royal Soc. London, Ser. A, 269, 500-529, 1962.

143. ROWE,P.W. "Stress-dilatancy, earth pressures and slopes". Proc.A.S.C.E., J. Soil Mech & Found. Div., 89, SM3, 37-61, 1963.

144. ROSIWAL,A. "Uber geometrische gesteinsanalysen. Ein einfacher wer zur ziffermabigen fest stellung des quantitatsverhaltnisses der mineralbestandteile gementger gesteine". Verh.K.K.Geol.Reichsamt. Wien, 143, 1898.

145. RUMPF,H., DEBAS,S. "On the randomness of beds packed with spheres or irregular particles". Chem.Eng.Sci., 21, 583-607, 1966.

146. SALTIKOV,S.A. "Determination of size distribution of particles in an opaque material from a measurement of the size distribution of their sections". Proc. 2nd. Int. Cong. Stereology, 163-173, 1967.

147. SALTIKOV,S.A. "A stereological method for measuring the specific surface area of metallic powders". Proc. 2nd. Int. Cong. Stereology, 63-64, 1967.

148. SALTIKOV,S.A. "Stereometric Metallography". 2nd.ed. Metallurgizdat. Moscow, 446, 1958.

149. SCARLETT,B., EASTHAM,I.E. "Stresses in granular material due to applied vibration". Paper presented at Symp. on Behaviour of Granular Materials, Tripartite Chem. Eng. Conf., Montreal, 1968.

150. SCARLETT,B., HANSEN,R., BUXTON,R.E. "The electrical conductivity of powders and thermal conductivity of powders". Paper presented at Symp. Recent Advances in Powders, I.Chem.E., 1969.

151. SCOTT,R.F. "Principles of soil mechanics". Addison Wesley, Reading, Mass., 1963.

152. SCOTT,R.F. Discussion of "Stress-dilatancy, earth pressures, and slopes". (by) Rowe,P.W., Proc.A.S.C.E. J. Soil Mech. & Found. Div., 90, No.SM1, 133-135, 1964.

153. SCHUCHARDT,E. "Die gewebsanalyse mit dem integrationsolular". Z.wiss.Mikr., 62, 9-13, 1954.

154. SCHEUMANN,K.H. "Zwei hilfsapparaturen dur das petrographische mikroskop. II. Integrationstisch fur das shandsche analysenverfahen". Miner.Mitt.N.F. 41, 180-187, 1931.

155. SHAND,S.J. "A recording micrometer for geometrical rock analysis". J.Geol., 24, 394-404, 1916.

156. SHINOHARA,K., IDEMITSU,Y., GOTOH,K., TANAKA,T. "Mechanism of gravity flow of particles from a hopper". I.& E.C. Process Design & Dev., 7, (3), 378-383, July, 1968.

157. SJAASTAD,G.D. "The effect of vacuum on the shearing resistance of ideal granular systems". Ph.D. Thesis, Princeton Univ. Dept. of Civil Eng. June, 1963.

158. SKEMPTON,A.W., BISHOP,A.W. "The measurement of the shear strength of soils". Geotechnique, 2, 90-108, 1950.

159. SKEMPTON,A.W., BISHOP,A.W. Discussion of "Measurement of the shear strength of soils", by Bishop,A.W., Geotechnique 2, 113, 1950.

160. SLICHTER,C.S. "Theoretical investigation of the motion of ground waters". 19th. Ann.Rept., U.S. Geol. Survey, Pt.2, 295, 1897.

161. SMITH,C.S. "Sectioned textures in the decorative arts". Proc. 2nd. Int. Cong. Stereology, 33-48, 1967.

162. SMITH,W.O. "Capillary flow through an ideal uniform soil". Physics, 3, 139-146, 1932.

163. SMITH,W.O., FOOTE,P.D., BUSANG,P.F. "Packing of homogeneous spheres". Phys. Rev. 34, 1271-1274, 1929.

164. SOKOLOVSKI,V. "Statics of soil media". (Trans. by Jones,D.H. and Schofield,A.N.), Butterworths, London, 220, 1960.

165. STONE,J.R., KIRKHAM,D., READ,A.A. "Soil moisture determination by a portable neutron scattering moisture meter". J. Para.Mo.J. - 2641. Iowa.Agr.Exp.Sta., Ames, Iowa, Proj. No. 998, 1954.

166. TABOR,D. "Junction growth in metallic friction". Proc.Royal Soc. London, Ser.A, 251, 378-393, 1959.

167. TANEYA,S. "Flow properties of powder,I&II". Jap.J.Appl.Phys., 2, (11), 728-734, 1963; 4, (4), 297-307, 1965.

168. TAYLOR,D.W. "Fundamentals of soil mechanics". Wiley & Sons Inc., New York, 1948.

169. TAYLOR,D.W., LEPS,T.M. "Shearing properties of Ottawa standard sand as determined by the M.I.T. strain control direct shearing machine". Paper C, Proc. Soil & Foundation Conf., U.S. Eng.Dept., Boston, Mass.,June,1938.

170. TERZAGHI,K. "Old earth-pressure theories and new test results". Eng.Res.Record, 85, (14), 1920. (Reprinted - "From theory to practise in soil mechanics". J.Wiley & Sons, New York, 1960.).

171. TERZAGHI,K. "Erdbaumechanik auf bodenphysikalischer grundlage". F. Deuticke, Wien, Osterreish, 1925.

172. TERZAGHI,K., PECK,R.B. "Soil mechanics in engineering practice". Wiley & Sons, New York, 1948.

173. THEIMER,O.F. "Failures of reinforced concrete grain silos". Trans.A.S.M.E., J.Eng.Ind., 91, B, (2), 460-477, 1969.

174. THOUZEAU,G., TAYLOR,T.W. Safety in Mines Res. Report, No.197, 1961.

175. THURSTON,C.W., DERESEIWICZ,H. "Analysis of a compression test of a model of a granular media". J.Appl.Mech., A.S.M.E., 81, 251-258, 1959.

176. TIEDEMANN,B. "Uber die schubfestigkeit bindiger boden". Die Bautechnik, 15, (30), (33), 400-403, 433-435, 1937.

177. TINOCO,F.H. "Shear strength of granular materials". Ph.D. Thesis, Iowa Univ., 1967.

178. TOMKEIFF,S.I. "Linear intercepts, areas and volumes". Nature, (Lond.), 155, 24, 1945.

179. TRAIN,D. "Some aspects of the property of the angle of repose of powders". J.Pharm.Pharmacol. Suppl., 10, 127T-135T, 1958.

180. TROLLOPE,D.H., PARKIN,A.K. Discussion of "Stress-dilatancy, earth pressures and slopes" (by) Rowe,P.W. Proc.A.S.C.E. J. Soil Mech. & Found. Div., 89, (SM6), 129-133, 1963.

181. UNDERWOOD,E. "Quantitative evaluation of sectioned material". Proc. 2nd. Int. Cong. Stereology, 49-60, 1967.

182. UNDERWOOD,G.H.M., VAN BAVEL, SWANSON,R.W. "A portable rate-meter and a source counter assembly for measuring soil moisture content by neutron scattering". Dept.Agronomy State College, Raleigh. M.C. Lithoprint, 1955.

183. VAN DENBURG,J.F., BAUER,W.C. "Segregation of particles in the storage of materials". Chem.Engg., Sept.28, 135-142, 1961.

184. VOMOCIL,J.A. "In-situ measurement of soil bulk density". Agricultural Eng., Sept., 1954.

185. WALKER,D.M. "An approximate theory for pressures and arching in hoppers". Chem.Eng.Sci., 21, 975-997, 1966.

186. WALKER,D.M. "A basis for bunker design". Powder Technology, 1, (4), 228-236, 1967.

187. WEIBEL,E. "Morphometry of the human lung". Springer-Verlag, 9-39, 1963.

188. WEIBEL,E. "Structure in space and its appearance on sections". Proc. 2nd. Int. Cong. Stereology, Chicago, Springer-Verlag, 15-26, 1967.

189. WEIBEL,E., GOMEZ,D.M. "A principle for counting tissue structures on random sections". J.Appl.Physiol., 17, 343-348, 1962.

190. WENTWORTH,C.K. "An improved recording micrometer for rock analysis". J.Geol., 31, 228-232, 1923.

191. WESTERBERG,N. "Jordtryck i kohesionara jordarter". Tek. Tidskr., 51, 25-29, 1921.

192. WHITE,G.W., BELL,A.V., BERRY,G.K. "Measurement of the flow properties of powders". J.Food Technol., 2, 45-52, 1967.

193. WHITE,H.E., WALTON,S.R. "Particle packing and particle shape". J.Amer.Ceram.Soc., 20, 155-166, May, 1937.

194. WHITMAN,R.V. HEALEY,K.A. "Shear strength of sands during rapid loadings". Proc.A.S.C.E., J. Soil Mech. & Found. Div., Paper 3102, 99-132, April, 1962.

195. WICKSELL,S.D. "On the size distribution of sections of a mixture of spheres". Biometrika, 17, 84, 1925.

196. WILLIAMS,J.C., BIRKS,A.H. "The comparison of failure measurements of powders with theory". Powder Technology, 1, 199-206, 1967.

197. WINTERKORN,H.F. "Macromeritic liquids". A.S.T.M. Spec.Tech. Publ. No.156, 77-89, 1953.

198. WISE,M.E. "Dense random packing of unequal spheres". Philips Res. Rept., 7, 321-343, 1952.

199. WROTH,C.P. "The behaviour of soils and other granular media when subjected to shear". Ph.D. Thesis, Cambridge, 1958.

200. WROTH,C.P., BASSETT,R.H. "Shearing behaviour of sand". Geotechnique, 15, Mar., 32-55, 1965.

201. YONG,R.N., WARKENTIN,B.P. "Introduction to soil behaviour". MacMillan Co., New York, 1966.

202. ZENZ,F.A., OTHMER,D.F. "Fluidization and fluid-particle systems". Reinhold Publ. Corp., New York, 1960.